EVALUATION OF THE PALEOHYDRODYNAMIC CONDITIONS FOR THE DEPOSITON OF CAMPANO-MAASTRICHTIAN SEDIMENTS IN THE ANAMBRA BASIN, SE, NIGERIA

BY

AGBO, CHRISTIAN CHUKWUDI (B.Sc. UNN; M.Sc. UPH)

REG. NO. 20164067388

A DISSERTATION SUBMITTED TO THE DEPARTMENT OF GEOLOGY, POSTGRADUATE SCHOOL, FEDERAL UNIVERSITY OF TECHNOLOGY, OWERRI.

IN PARTIAL FULFILMENT OF THE REQUIREMENTS FOR THE AWARD OF THE DEGREE OF DOCTOR OF PHILOSOPHY, IN SEDIMENTARY/PETROLEUM GEOLOGY

NOVEMBER, 2025.

CERTIFICATION

This is to certify that this dissertation titled "Evaluation of Paleohydrodynamic conditions for the deposition of Campanian-Maastrichtian sediments in the Anambra Basin, Southeastern, Nigeria" was carried out by **Agbo, Christian Chukwudi (20164067388)** in partial fulfillment of the requirements for the award of the degree of Doctor of Philosophy (Ph.D) of the Department of Geology, School of Physical Sciences, Federal University of Technology, Owerri.

PROF. S.O. ONYEKURU
(Principal Supervisor)
07/04/2025
DATE

DR. D.O. IKORO
(Co-Supervisor)
07/04/2025
DATE

DR. T.C. ANYANWU
(Co-Supervisor)
07/04/2025
DATE

DR. MRS. B.O UBECHU
(Head of Department)
09/04/2025
DATE

PROF. MRS. C.E OGUKWE
(Dean School of Physical Sciences)
DATE

PROF. MRS. J.N NWOSU
(Dean Postgraduate School)
DATE

PROF. O.A. ANYIAM
(External Examiner)
26/11/2025
DATE

Scanned with CamScanner

DEDICATION

To my beloved father, Mr. Isaac Agbo, who selflessly dedicated his life to providing me with the best education. Your unwavering support and encouragement throughout my studies, from BSc to PhD, have been the driving force behind my academic achievements. I am forever grateful for the sacrifices you made to ensure that I had every opportunity to succeed. This PhD is as much yours as it is mine, for without your wisdom, guidance and belief in me, I would not be where I am today. Thank you, Daddy, for being an exceptional role model and for instilling in me the values of hard work, integrity and perseverance. This dissertation is humbly dedicated to you.

ACKNOWLEDGMENTS

I am profoundly grateful to all who supported my doctoral journey. My deepest appreciation goes to my principal supervisor, Prof. S.O. Onyekuru, whose visionary guidance from project conception to completion shaped this research. His expertise, critical feedback, and unwavering commitment to excellence were instrumental to my academic growth.

I deeply appreciate my co-supervisors, Dr. D.O. Ikoro and Dr. T.C. Anyanwu, for their invaluable guidance and critiques. My thanks also go to Prof. C.N. Okereke and incoming Postgraduate Coordinator Dr. Amadi C. C. for fostering a culture of academic excellence

I acknowledge Dr. Ijeoma Okiyi for her intellectual partnership during this research's formative stages, and my colleagues—Dr. Kelechi Opara**,** Dr. Temple Dikeogu**,** Dr. JohnKennedy Agubom, and Dr. Paul Brown Onyeanwu—for their camaraderie and shared insights that enriched my doctoral experience.

I thank the entire Geology Department, especially HOD Dr. Mrs. B. O. Ubechu, for fostering a stimulating academic environment. The department's wisdom and the staff's unwavering support greatly enriched my growth. My appreciation also extends to the technical and administrative teams for their invaluable behind-the-scenes contributions

I sincerely appreciate the Postgraduate School's support, particularly Dean Prof**.** J.N**.** Nwosu, the Associate Dean, and Mr**.** Nwafor Ebere, the schedule officer, whose administrative diligence ensured smooth progress throughout my program. Their commitment to student success created an enabling framework for scholarly achievement.

To my extended family—uncles, aunts, and mentors—thank you for your prayers and words of wisdom that kept me motivated during challenging moments. Your belief in my potential helped sustain my focus through this demanding process.

Finally, I thank my parents, Mr. and Mrs. Isaac Agbo, and my siblings and family for their lifelong encouragement and emotional support. Their sacrifices and steadfast belief in education laid the foundation for this achievement. This milestone is as much theirs as it is mine.

TABLE OF CONTENTS

CONTENTS		PAGE NUMBERS
Title Page		i
Certification		ii
Dedication		iii
Acknowledgements		iv
Table of Contents		v
List of Tables		ix
List of Figures		xi
List of Plates		xiv
Abstract		xv
CHAPTER ONE – INTRODUCTION		
1.1	Background Information	1
1.2	Statement of the Problems	4
1.3	Objectives of the Study	5
1.4.	Justification of the Study.	5
1.5	Scope of the Study	5
1.6	Limitations of the Study	6
CHAPTER TWO - LITERATURE REVIEW		
2.1	Literature Insight on Depositional System	8
2.2	Regional Geology of Anambra Basin	9
2.3	Tectonic Setting	10
	2.3.1 Pre- Albian Tectonics	11
	2.3.2 Albian to Tertiary Tectonics	11
2.4	Stratigraphy.	14
	2.4.1 Nkporo Group and Owelli Sandstone	18
	2.4.2 Mamu Fm.	18
	2.4.3 Ajali Fm.	19
	2.4.4 Nsukka Fm.	20
2.5	Depositional Environments	22
2.6	Provenance Studies.	23

2.7 The Paleo-Hydrodynamic Conditions 24
2.8 Hydrocarbon Potential 26

CHAPTER THREE - MATERIALS AND METHODS

3.1 Materials 28
3.1.1 Study Area 28
3.1.2 Data Sets 30
3.2. Methods 31
3.2.1 Work Flow 31
3.2.2 Desk Studies 33
3.2.3 Reconnaissance Studies 33
3.2.4 Field Mapping/Investigation 34
. 3.2.4.1 Facies Analysis 35
3.2.5 Laboratory Analysis 38
3.2.5.1 Grain Size Sieve (univariate) Analysis 38
3.2.5.1.1 Graphic Mean 39
3.2.5.1.2 Inclusive Standard Deviation 39
3.2.5.1.3 Inclusive Graphic Skewness 39
3.2.5.1.4 Inclusive Graphic Kurtosis 40
3.2.5.2 Multivariate and Bivariate Analysis 40
3.2.5.3 Quantitative Methods of Paleohydrodynamics 43
3.2.5.3.1 Bedform Height (Hm) and the Paleo-Channel Depth (Dc) 43
3.2.5.3.2 Paleo-Channel Slope 43
3.2.5.3.3 Boundary Shear Stress 44
3.2.5.3.4 Critical Shear Stress 44
3.2.5.3.5 Paleoflow Velocity 45
3.2.5.3.6 Darcy-Weisbach Friction Factor 45
3.2.5.3.7 Rouse Number (Z) for Sediment Transport 46
3.2.5.3.8 Sediment Settling Velocity 46
3.2.5.3.9 Boundary Shear Velocity 46
3.2.5.3.10 Reynolds Particle Number (Rep) 46
3.2.5.3.11 Froude Number (Fr) 47

CHAPTER FOUR - RESULTS AND DISCUSSION

4.1 RESULTS

4.1.1 Lithostratigraphic Studies
4.1.1.1 Litho Desc. of Nsukka Fm Section at Isukwato Valley 50
4.1.1.2 Litho. Desc. of Nsukka Fm. at Akara Junction Section, Isukwato 54
4.1.1.3a Litho. Desc. of Ajali Fm. Section at Onyekaba Mine 58
4.1.1.3b Litho. Description of Modern Alluvial Fan in Onyekaba Mine 60
4.1.1.4 Litho. Desc. of Ajali Fm. Section at Uturu (Near ABSU) 66
4.1.1.5 Litho. Desc. of Mamu Fm. Section at Ohafia 68
4.1.1.6 Litho. Desc. of Mamu Fm. Section at Ihube 71
4.1.1.7 Litho. Desc. of Owelli Sandstone Section at Agbogugu Village 76
4.1.1.8 Litho. Desc. of Owelli Sandstone Section at Agbogugu Junction 80

4.1.2 Lithofacies
4.1.2.1 Interbedded Calcareous Mudstone/Shale Facies (FA) 84
4.1.2.2 Plane and Cross-Stratified Sandstone Facies (FB) 84
4.1.2.3 Heterolithic Shale and Siltstone Facies (FC) 84
4.1.2.4 Imperfectly Stratified Sandstone Facies (FD) 85
4.1.2.5 Reddish Brown Sandstone Facies (FE) 85
4.1.2.6 Oolitic Sandstone Facies (FF) 85

4.1.3 Univariate Grain Size Analysis
4.1.3.1 Graphic Mean Size (Mz) 127
4.1.3.2 Inclusive Graphic Standard Deviation (σi) 127
4.1.3.3 Inclusive Graphic Skewness (Ski) 127
4.1.3.4 Graphic Kurtosis (KG) 127

4.1.4 Bivariate Grain Size Parameters
4.1.4.1 Mz vs. σi 129
4.1.4.2 Mz vs. Ski 129
4.1.4.3 Mz vs. KG 129
4.1.4.4 σi vs. Ski 130

4.1.5 Grain size Parameters (Multivariate Analysis)
4.1.5.1 Function Plots of Y2 against Y1 138
4.1.5.2 Function Plots of Y2 against Y3 138

4.1.6 Log probability Plots
4.1.6.1 Samples Having one Saltation Subpopulation 143
4.1.6.2 Samples Having two Saltation Sub Population 143

4.1.7 Percentage Distribution of Quartz, Feldspar, and Lithic Fragments 149

4.1.8 Quantitative Paleo-Hydrodynamic Conditions 156

4.2 Discussions
4.2. 1 Flow Energy Conditions 159
4.2.2 Grain Size vs. Transport Mechanism 164
4.2.3 Bedform Development 168
4.2.4 Sediment Settling Velocity Impact 171
4.2.5 Depositional Models 173

CHAPTER FIVE CONCLUSION AND RECOMMENDATION

5.1 Conclusion 179

5.2 Recommendations for Further Studies 180

5.3 Contribution to Knowledge 181

REFERENCES 182

APPENDIX 200

LIST OF TABLES

Table		Page
3.1	Facies Association vs. Facies: a Tabular Comparison	37
3.2	Hydrodynamic Parameters, Empirical Formulae and Citations	49
4.1	Lithostratigraphic Desc. and Comments of Nsk Fm. at Isukwato	51
4.2	Lithostratigraphic Desc. and Comments of Ajali Fm. at Onyekaba	59
4.3	Lithostratitigraphic Desc. of Mamu Fm. Exposed at Ihube	73
4.4	Lithostratitigraphic Desc. of Owelli Sandstones at Agbogugu Junction	81
4.5.	Facies classification and Characteristics	86
4.6	The Percentile Values of Nsukka Fm. and AjaliSst. Samples	119
4.7	The Percentile Values of Mamu Fm.and Owelli SSt Samples	120
4.8	Calculated Grain-Size Parameters and Description for Nsukka Fm.	122
4.9	Calculated Grain-Size Parameters and Description for Ajali Fm.	123
4.10	Calculated Grain-Size Parameters and Description for Mamu Fm.	124
4.11	Calculated Grain-Size Parameters and Description for Owelli Sandstone	125
4.12	Interpretation for Sieve parameters	126
4.13	Mean, Kurtosis, Sorting and Skewness of Formations	128
4.14	Interpretation Plot Table of Standard Deviation Vs Mean	131
4.15:	Interpretation plot table of Graphic mean VS standard Deviation	132
4.16	Interpretation Graph of Graphic Mean Size Vs Graphic Skewness	133
4.17	Interpretation for Plotting Graph of Graphic Mean Size Vs Graphic Skewness	134
4.18	Interpreted Data Obtained from Analyses Based On Linear Discriminant Fun	140
4.19	Phi Value of Coarse Truncation Point (C.T.) and Fine Truncation Point (F.T) 1	146
4.20	Phi Value of Coarse Truncation Point (C.T.) and Fine Truncation Point (F.T.) 2	147
4.21	Comparism of Sediment Transport Mechanisms and Hydrodynamic Conditions	148
4.22	Percentage Distribution of Quartz, Feldspar, and Lithic Fragments	150
4.23	Quantitative Hydrodynamics and Sediment Transport Characteristics	156
4.24	Flow Regime Standardization Using Reynolds Number Range	157

4.25 Reynolds Number Values and Paleohydraulic Interpretation 158

5.1 Summary of Grain Size and Petrographic Data for Anambra Basin Formations 163

LIST OF FIGURES

Figure		Page
2.1	Models for RRR-Rift Origin of Benue Trough of Nigeria.	12
2.2	Tectonic Map of Southeastern Nigeria During Albian-Tertiary	13
2.3	Tectonic Map of Southeastern Nigeria During Campanian-Eocene	16
2.4	Geologic Map of Nigeria Showing the Location of Anambra Basin	17
2.5	Stratigraphic Succession in Anambra Basin and Outcropping Niger Delta	21
3.1	Location and Accessibility Map of the Study Area	29
3.2	Workflow of Methodological Approach for Paleohydrodynamic Analysis	32
4.1	Lithostratigraphic log of Nsukka Fm. in Umuasua Outcrop	53
4.2	Lithostratigraphic log of NsukkaFm in Akara Junction Outcrop	57
4.3	Lithostratigraphic Log of Ajali Sandstone Fm. at Onyekaba Mine	64
4.4	Lithostratigraphic Log of Ajali Sandstone Fm. Near ABSU	67
4.5.	Lithostratigrapic Log of Mamu Fm. Exposed at Ohafia	70
4.6	Lithostratigraphic Log of Mamu Fm. Exposed at Ihube Section	75
4.7	Lithostratigraphic Log of Owelli Sandstone at Agbogugu Village Section	78
4.8	Lithostratigraphic Log of Owelli Sandstone at Agbogugu Junction	83
4.9	Cumulative Log-Probability Plots of Nsukka Fm. Sample 1(Inset: Bar Chart)	88
4.10:	Cumulative Log-Probability Plots of Nsukka Fm. Sample 2(Inset: Bar Chart)	89
4.11	Cumulative Log-Probability Plots of Nsukka Fm. Sample 3 (Inset: Bar Chart)	90
4.12	Cumulative Log-Probability Plots of NsukkaFm.Sample 4(Inset: Bar Chart)	91
4.13	Cumulative Log-Probability Plots of Nsukka Fm. Sample 5 (Inset: Bar Chart)	92
4.14	Cumulative Log-Probability Plots of Nsukka Fm. Sample 6 (Inset: Bar Chart)	93
4.15	Cumulative Log-Probability Plots of Nsukka Fm. Sample 7(Inset: Bar Chart)	94
4.16	Cumulative Log-Probability Plots of Nsukka Fm. Sample 8(Inset: Bar Chart)	95
4.17	Cumulative Log-Probability Plots of Ajali Fm. Sample 1 (Inset: Bar Chart)	97
4.18	Cumulative Log-Probability Plots of Ajali Fm. Sample 2 (Inset: Bar Chart)	98
4.19	Cumulative Log-Probability Plots of Ajali Fm. Sample 3 (Inset: Bar Chart)	99
4.20	Cumulative Log-Probability Plots of Ajali Fm. Sample 4 (Inset: Bar Chart)	100
4.21	Cumulative Log-Probability Plots of Ajali Fm. Sample 5 (Inset: Bar Chart)	101
4.22	Cumulative Log-Probability Plots of Mamu Fm. Sample 1(Inset: Bar Chart)	103

4.23 Cumulative Log-Probability Plots of Mamu Fm. Sample 2 (Inset: Bar Chart) 104
4.24 Cumulative Log-Probability Plots of Mamu Fm. Sample 3 (Inset: Bar Chart) 105
4.25 Cumulative Log-Probability Plots of Mamu Fm. Sample 4(Inset: Bar Chart) 106
4.26 Cumulative Log-Probability Plots of Mamu Fm. Sample 5 (Inset: Bar Chart) 107
4.27 Cumulative Log-Probability Plots of Mamu Fm**.** Sample 6 (Inset: Bar Chart) 108
4.28 Cumulative Log-Probability Plots of Mamu Fm. Sample 7 (Inset: Bar Chart) 109
4.29 Cumulative Log-Probability Plots of Mamu Fm.Sample 8 (Inset: Bar Chart) 110
4.30 Cumulative Log-Probability Plots of OwelliSst. Sample 1 (Inset: Bar Chart) 111
4.31 Cumulative Log-Probability Plots of OwelliSst.Sample 2 (Inset: Bar Chart) 117
4.32 Cumulative Log-Probability Plots of OwelliSst.Sample 3 (Inset: Bar Chart) 113
4.33 Cumulative Log-Probability Plots of OwelliSst.Sample 4 (Inset: Bar Chart) 114
4.34 Cumulative Log-Probability Plots of OwelliSst.Sample 5 (Inset: Bar Chart) 115
4.35 Cumulative Log-Probability Plots of OwelliSst.Sample 6 (Inset: Bar Chart) 116
4.36 Cumulative Log-Probability Plots of OwelliSst.Sample 7 (Inset: Bar Chart) 117
4.37 Values and Generated plot of Graphic mean VS standard Deviation 131
4.38 Values and Generated plot of Graphic mean VS standard Deviation 132
4.39 Values and Graph of Graphic Mean Size Vs Graphic Skewness 133
4.40: Values and Graph of Graphic Mean Size Vs Graphic Skewness 134
4.41 Graphic Skewness Vs Graphic Standard Deviation 135
4.42. Graphic Standard Deviation Vs Skewness(AfterMoiola And Weiser, 1968) 136
4.43 Graphic Standard Deviation Vs Graphic Skewness (After Friedman, 1967) 137
4.44 Function Plots of Y2 against Y1 for Sandstone Samples (After Sahu, 1964) 141
4.45 Function Plots of Y2 Against Y3 For Sandstone Samples (After Sahu,1964) 142
4.46 Textural Classification of Sandstones of Nsukka Fm. 151
4.47 Textural Classification of Sandstones of Ajali Fm. 152
4.48 Textural Classification of Sandstones of Mamu Fm. 153
4.49 Textural Classification of Sandstones of Owelli Sandstone 154
4.50 Hjulström Diagram Showing the Grain Sizes Vs Flow Velocity of Sediments 162

4.51 Bed from Stability Diagram in Relation to Grain Sizes against Flow Velocity 170

4.52 3-D Depositional Model for Nsukka Fm. 175

4.53: 3-D Depositional Model for Ajali Sandstone Fm. 176

4.54: 3-D Depositional Model for Mamu Fm. 177

4.55: 3-D Depositional Model for Owelli Sandstone Fm. 178

LIST OF PLATES

Plates		Page
4.1.	Isukwato Outcrop Section at Junction Along Ohafia – Umahia Road	52
4.2	Outcrop section at Akara Junction along Ohafia – Umahia Rd	56
4.3	Outcrop of Ajali Sandstone exposed at Onyeama Mine	61
4.4.	Modern Alluvial Fan, Onyeama Mine, Anambra Basin, Nigeria	62
4.5	Alternating Sandstone and Clay Drapes, Ajali Fm. at Onyekaba	63
4.6.	A Close-Up of an Outcrop with Multiple Sets	66
4.7	Ihube Section Outcrop	74
4.8	Panoramic Outcrop View of Agbogugu village	79
4.9	Outcrop View of Agbogugu Junction Outcrop along Enugu PH Road	82

ABSTRACT:

This study evaluates the paleohydrodynamic conditions governing the deposition of Campanian–Maastrichtian sediments in the Anambra Basin, southeastern Nigeria. The formations studied include the Owelli Sandstone, Mamu Formation, Ajali Sandstone, and Nsukka Formation. A total of 68 representative samples were subjected to sieve analysis, moment statistical calculations, petrographic evaluation, and paleohydraulic modeling to reconstruct the depositional environments, flow dynamics, and sediment transport mechanisms. Grain size analysis revealed that mean grain sizes ranged from 1.10 φ (coarse sand) in the Owelli Sandstone to 3.50 φ (fine sand) in the Mamu Formation. Standard deviation values (sorting) ranged from 0.46 to 1.59, indicating a transition from well-sorted to poorly sorted sediments. Skewness values varied from -0.32 (strongly coarse-skewed) to +0.45 (fine-skewed), suggesting bidirectional transport and channel-floodplain interactions. Kurtosis values ranged between 0.75 (platykurtic) and 1.98 (leptokurtic), reflecting both steady and fluctuating energy regimes. Quartz content ranged from 68% to 85%, feldspar from 10% to 22%, and lithic fragments from 5% to 13%, indicating mixed provenance. Observed sedimentary structures included planar cross-bedding, ripple marks, mud drapes, and climbing ripples, characteristic of fluvial-tidal interactions. Calculated channel slopes ranged from 0.12 to 0.18, while flow depths varied from 6.12 m in the Mamu Formation to 15.05 m in the Nsukka Formation. Corresponding flow velocities ranged from 0.62 m/s to 1.45 m/s, and sediment settling velocities ranged between 0.016 m/s and 0.082 m/s, supporting variable hydraulic conditions. Bedform analysis identified ripple, dune, and upper plane beds, while probability curves showed suspension and saltation as key transport modes, notably in the Ajali and Owelli Formations. Depositional models indicate braided fluvial systems for the Owelli and Ajali Formations, vegetated delta plain to tidal flat settings for the Mamu Formation, and delta-front to prodelta transitions for the Nsukka Formation.The study enhances understanding of paleoflow regimes and depositional architecture in the Anambra Basin, offering a quantified sedimentological framework for petroleum reservoir prediction and Late Cretaceous environmental reconstruction in West Africa.

Keywords: Paleohydrodynamic conditions; Textural characteristics; Sandstones; Depositional conditions; Rouse Number.

CHAPTER ONE
INTRODUCTION

1.1 Background Information

The Anambra Basin, a prominent geological feature in southeastern Nigeria, has been the subject of extensive research due to its significant hydrocarbon potential and complex depositional history (Nwajide, 2013; Okoro, Igwe & Eze, 2016). The basin's formation is intricately linked to the Santonian tectonic event, which resulted in the inversion of the Abakaliki Anticlinorium and the subsequent development of the Anambra Basin as a depression to the southwest (Murat, 1972; Nwajide and Reijers, 1996; Benkhelil, 1989). This tectonic reorganization played a crucial role in shaping the basin's stratigraphic architecture and sediment distribution patterns (Obi and Okogbue, 2004).The Late Cretaceous sedimentary sequences within the Anambra Basin, particularly the Mamu, Ajali, and Nsukka formations, have been extensively studied for their stratigraphic relationships, depositional environments, and petroleum system elements (Kogbe, 1989; Nwajide, 2005; Onyekuru & Iwuagwu, 2010; Dim, Egbai, & Omosanya 2019). These formations represent a diverse range of depositional settings, from coastal plain and deltaic environments to shallow marine conditions, reflecting the dynamic nature of sedimentation during this period (Egbu, Onwuemesi, & Chinwuko, 2009; Akande, Adeigbe & Salifu., 2012).

Traditionally, facies analysis has been the primary approach in understanding these formations, focusing on lithological characteristics, sedimentary structures, and fossil content (Hoque and Ezepue, 1977; Amajor, 1984; Nwajide, 1980). This approach has provided valuable insights into the depositional environments and stratigraphic evolution of the basin. However, recent advancements in sedimentological research have highlighted the importance of integrating quantitative paleohydrodynamic analysis with qualitative observations to develop more comprehensive and accurate depositional models.

The application of paleohydrodynamic analysis to the Anambra Basin sediments offers a novel and powerful approach to unraveling the complex interplay between sediment supply, basin subsidence, and sea-level changes during the Late Cretaceous (Nichols, 2009; Leeder, 2011). This method involves the use of hydrodynamic equations and principles, such as the Shields diagram for initiation of sediment motion, Froude number analysis for flow regime determination, and bedform stability diagrams, to reconstruct flow conditions and sediment

transport mechanisms (Leeder, 1999; Allen, 2009; Bridge and Demicco, 2008). By applying these quantitative techniques, researchers can gain deeper insights into the physical processes that controlled sedimentation in the basin.Understanding the paleohydrodynamics of the Owelli, Mamu, Ajali, and Nsukka formations is crucial for several reasons. Firstly, it provides insights into the basin's response to regional tectonic events and global climate changes during the Late Cretaceous (Petters, 1995; Oboh-Ikuenobe, Obi, & Jaramillo, 2005). This information is vital for reconstructing the paleoenvironmental and paleogeographic evolution of the basin within a broader regional context..

Secondly, it aids in predicting variations in reservoir properties, which is essential for hydrocarbon exploration and production strategies in the basin (Weber & Daukoru ,1975; Dim Onwuka & Egbu, 2019; Mode, Okpara & Dim, 2013). Through comprehensive analysis of hydrdynamic conditions controlling sediment deposition, geologists can accurately predict the spatial distribution and quality of reservoir facies. Moreover, the integration of paleohydrodynamic analysis with traditional sedimentological approaches aligns with the growing trend in geosciences towards multidisciplinary research (Nichols & Fisher, 2007; Miall, 2014). This comprehensive methodology not only enhances our understanding of the Anambra Basin's depositional history but also has broader implications for studying similar sedimentary basins worldwide.

Moreover, Paola, Straub, Mohrig, & Reinhardt, (2009). emphasize the role of hydrodynamic modeling in elucidating sedimentary distributions, showcasing the potential for numerical simulations to refine depositional interpretations. Moreover, the integration of paleohydrodynamic analysis with traditional sedimentological approaches aligns with the growing trend in geosciences towards multidisciplinary research (Nichols and Fisher, 2007; Miall, 2014). This comprehensive methodology not only enhances our understanding of the Anambra Basin's depositional history but also has broader implications for studying similar sedimentary basins worldwide (Miall, 2010).

The Mamu Formation, which marks the base of the coal-bearing sequences in the Anambra Basin, has been interpreted as a product of deltaic to shallow marine environments (Nwajide & Reijers, 1996). However, detailed paleohydrodynamic analysis may reveal

more nuanced variations in depositional conditions, potentially identifying subtle changes in sea level or sediment supply that were not apparent through conventional facies analysis alone. The overlying Ajali Formation, characterized by its distinctive cross-bedded sandstones, has been traditionally interpreted as a fluvial to coastal deposit (Amajor, 1984; Nwajide, 2005). Paleohydrodynamic analysis of these sandstones could provide quantitative estimates of paleocurrent velocities, flow depths, and sediment transport modes, offering new insights into the depositional processes and paleogeography during this time (Bridge, 2003; Collinson Mountney & Thompson, 2006). The Nsukka Formation, which caps the sequence, represents a return to paralic conditions and has been less extensively studied compared to the underlying formations (Umeji, 2000; Dim, Egbai & Omosanya 2019). Applying paleohydrodynamic techniques to this formation could help elucidate the nature of the transition from the Ajali Formation and provide a more detailed understanding of the basin's evolution towards the end of the Cretaceous (Nwajide, 2013; Okoro, Igwe & Eze, 2014).

Furthermore, the application of paleohydrodynamic analysis to these formations also contributes to knowledge regarding the tectonic and eustatic controls on sedimentation in the Anambra Basin during the Late Cretaceous (Nwachukwu, 1972). By providing quantitative data on flow conditions and sediment transport, this approach can help distinguish between the effects of local tectonics and global sea-level changes on depositional patterns (Catuneanu, 2006; Miall, 2010).

The integration of paleohydrodynamic analysis with sequence stratigraphic concepts (Van Wagoner, Mitchum, Campion & Rahmanian, 1990; Catuneanu, 2006) offers a powerful tool for understanding the basin's evolution. This combined approach can provide insights into the relationship between changes in base level, sediment supply, and accommodation space, leading to a more robust stratigraphic framework for the Anambra Basin (Posamentier & Allen, 1999; Bhattacharya, 2006). In the context of petroleum geology, a detailed understanding of paleohydrodynamic conditions can significantly improve predictions of reservoir quality and distribution (Weber & Daukoru, 1975; Dim et al., 2019). For instance, variations in flow velocity and sediment transport modes can influence grain size distributions, sorting, and the preservation of porosity and permeability in potential reservoir rocks (Beard & Weyl, 1973; Morad, Al-Ramadan, Ketzer & DeRos 2010). This information is crucial for developing more accurate reservoir models and optimizing exploration and

production strategies in the Anambra Basin (Adedokun, Ladipo, Enu & Emofurieta, 2012; Mode, Opara & Dim., 2013). Additionally, the paleohydrodynamic approach can contribute to paleoclimatic reconstructions for the Late Cretaceous in this region. By providing quantitative estimates of flow conditions and sediment discharge, it becomes possible to infer aspects of the paleoclimate, such as precipitation patterns and seasonality (Miall, 1996; Nichols, 2009). This information can be integrated with paleontological and geochemical data to build a more comprehensive picture of the Late Cretaceous.

1.2 Statement of the Problem

The Anambra Basin's Cretaceous formations (Nsukka, Ajali, Mamu, and Owelli Sandstone) have been extensively studied, but critical uncertainties persist regarding their depositional environments, stratigraphic evolution, and resource potential. These knowledge gaps include:

1. Ambiguity in Depositional Models
    I. Existing studies present conflicting interpretations of the Nsukka Formation's depositional setting, with some emphasizing marine pelagic sedimentation (Reyment, 1965) and others favoring deltaic progradation (Umeji, 2005).
    II. The Ajali Formation's fluvial versus deltaic dominance remains debated, with limited consensus on the role of aeolian reworking (Nwajide, 2013) versus wave-influenced mouth bars (Amajor, 1987).
    III. Research Question: How do 3-D depositional models reconcile these conflicts and clarify facies distributions?
2. Poorly Constrained Hydrodynamic Regimes
    I. The energy conditions (low vs. high) of these formations are often over simplified, neglecting episodic high-energy events (e.g., storms in the Nsukka) or tidal modulation in the Mamu Formation.
    II. Research Question: What sedimentary structures and facies transitions reveal the true hydrodynamic variability in these systems?
3. Limited Applied Implications for Resource Exploration
    a. While the Ajali and Owelli Sandstones are known reservoirs, their heterogeneity (e.g., channel vs. floodplain facies) is poorly quantified.

b. The Mamu Formation's coal-bearing intervals lack detailed depositional controls, hindering source-rock assessments.

c. Research Question: How can depositional models improve predictions of reservoir, source, and seal distributions?

1.3 Objective of the Study

The main objective was to evaluate the paleohydrodynamic conditions for the deposition of Campano-Maastrichtian sediments in the Anambra Basin..

The specific objectives were to:

I. Analyze sedimentary structures, grain size and other physical parameters in order to reconstruct the energy regimes that prevailed during sediments deposition.

II. Establish relationships between grain size characteristics and the modes of sediment transport in order to investigate the influence of grain size on transport mechanisms:

III. Analyze preserved sedimentary structures and hydrodynamic conditions in order to reconstruct the formation and evolution of bedforms under varying flow conditions.

IV. Calculate sediment settling velocities for different formations in order to assess their influence on the vertical distribution of sediments during deposition.

V. Form the depositional models of Anambra Basin sediments

1.4. Justification of Study

The Anambra Basin is a significant geological feature in southeastern Nigeria, hosting important sedimentary successions, including the Nsukka, Mamu, Ajali, and Owelli formations. These formations are composed primarily of sandstones, which are crucial for understanding the basin's depositional history, paleogeography, and potential for hydrocarbon resources. However, a detailed understanding of the flow conditions and depositional environments that led to the formation of these sandstones remains relatively limited. This research aims to address this knowledge gap by reconstructing the paleoenvironmental and hydrodynamic conditions during the deposition of these formations through a detailed analysis of their sedimentary features and grain size characteristics.

1.5 Scope of the Study

This research will focus on the Nsukka, Mamu, Ajali, and Owelli Formations within the Anambra Basin of southeastern Nigeria. The study involved:

I. **Fieldwork:** Field investigations conducted at selected outcrops of these formations to document and measure sedimentary structures and collect representative rock samples. The choice of outcrop locations will be based on accessibility, exposure of key sedimentary features, and their relevance to the research objectives.

II. **Laboratory Analysis:** Collected rock samples to undergo grain size analysis to determine the mean grain size, sorting, and distribution characteristics of each formation. Additionally, detailed examination of sedimentary structures, particularly bedforms like cross-bedding, ripples, and planar beds, will be conducted using hand lenses, microscopes, and potentially thin sections.

III. **Data Interpretation:** The data collected from fieldwork and laboratory analyses are used to interpret the paleoenvironmental and hydrodynamic conditions during the deposition of each formation. This will involve applying principles of sedimentology, using the Hjulström diagram, and considering existing geological knowledge of the Anambra Basin.

IV. **Paleocurrent Reconstruction:** The study attempts to reconstruct paleocurrent patterns and inferred sediment transport pathways within the Anambra Basin during the deposition of these formations based on the orientations of sedimentary structures, such as cross-bedding.

V. **Comparison and Synthesis:** The inferred flow conditions and depositional environments for the different formations are compared and contrasted to identify similarities, differences, and potential relationships between them. The findings will be integrated with existing geological knowledge of the Anambra Basin to refine the understanding of its depositional history and paleogeography.

1.6 Limitations of Study

The scope of this research is limited to:

I. Geographic Area: The study focuses on the Anambra Basin within southeastern Nigeria.

II. Formations: The research is restricted to the Nsukka, Mamu, Ajali, and Owelli formations.

III. Data Collection: The extent of fieldwork and laboratory analyses is constrained by available resources and accessibility of outcrops.

IV. Interpretation: The interpretations of flow conditions and depositional environments are on the available data and may be subject to inherent uncertainties.

Despite these limitations, this research is expected to provide valuable insights into the depositional history and paleogeography of the Anambra Basin and contribute to a better understanding of sedimentary processes in rift basin settings.

CHAPTER TWO

LITERATURE REVIEW

2.1 Literature Insight on Depositional System

The evaluation of paleohydrodynamic conditions for the deposition of Campanian-Maastrichtian sediments in the Anambra Basin, Nigeria, has been addressed by several researchers who applied sedimentological and stratigraphic techniques to reconstruct the depositional settings, sediment dispersal, and flow regimes. Onyekuru & Iwuagwu (2010) studied dispersal patterns within these formations, highlighting the predominant paleocurrent directions indicative of fluvial to shallow marine depositional systems influenced by regional tectonics and sediment supply variations.

The Mamu Formation, Ajali Sandstone, and Nsukka Formation, which represent key sequences within the Anambra Basin, have been extensively analyzed for their lithofacies and paleoflow indicators. Nwajide (2005) and Reyment (1965) identified features such as cross-bedding, ripple marks, and grain size variations in these units, which suggest high-energy environments like braided rivers and deltas for the Ajali Sandstone and transitional settings for the Nsukka Formation. Additionally, the overlying Imo Shale marks a shift to quieter, marine conditions during the Paleocene.

Granulometric analyses, as detailed in studies such as Moiola and Weiser (1968), have employed bivariate plots to distinguish depositional processes in these formations. For example, sedimentary structures and grain-size trends in the Ajali Sandstone suggest a dominance of unidirectional flow associated with high-velocity currents. Similarly, the Mamu Formation's coal seams and fine-grained deposits point to periodic flooding and swampy conditions (Kogbe, 1989).

Studies using paleogeographic reconstructions have also indicated that sediment dispersal in the Anambra Basin was influenced by the structural framework of the Benue Trough and nearby basement complexes (Amajor, 1987). This structural control helped channel sediments into the basin, creating thick, laterally extensive sand bodies like the Ajali Sandstone, with significant hydrocarbon reservoir potential.

Recent work has integrated advanced techniques such as palynological analysis and provenance studies to better understand the source and depositional conditions of these sediments. For instance, Umeji (2005) utilized palynomorph marine indices to confirm the marginal marine settings of parts of the Ajali and Nsukka Formations. Provenance analysis has further linked sediment sources to continental basement rocks, indicating tectonic uplift and erosion during the Campanian-Maastrichtian (Onyekuru, 2009).

In summary, paleohydrodynamic conditions within the Anambra Basin reflect a dynamic interplay of tectonics, sediment supply, and paleoenvironmental shifts. The works of Onyekuru & Iwuagwu (2010) and Nwajide (2005) provide a summary of these processes, critical for evaluating the basin's petroleum system

2.2 Regional Geology of Anambra Basin

The Anambra Basin is an intracratonic Cretaceous sedimentary basin located in Nigeria, situated within the Benue Trough. This basin is of significant geological importance due to its substantial sediment thickness and diverse lithological heterogeneity, which spans both lateral and vertical extensions. The basin's geological history is closely tied to the tectonic events that occurred in the region, particularly the Santonian tectonics of the Abakaliki-Benue Basin, which led to the folding of the Abakaliki Anticlinorium and the subsequent deposition of sediments in the Anambra Basin (Akaegbobi, 2005; Obi, Okogbue & Nwajide, 1995).

The Anambra Basin is characterized by a cuesta topography, featuring an asymmetrical ridge that stretches from the western end of the River Niger at Idah to the northeastern direction, then turns southwards and terminates near Arochukwu at the right bank of the Cross-River. This unique topography is dominated by sigmoidal drainage divides between the Anambra River plain to the west and the cross catchment area to the east (Anakwuba, Onwuemesi, Chinweuko & Onu, 2018). The basin's sedimentary succession is composed of various lithostratigraphic units, including the Nkporo Group, Afikpo, Owelli, Enugu, Lafia, Nkporo Shale, Mamu Formation, and Ajali Formation. These units reflect a range of paleoenvironmental settings, from Campanian to Recent, and are believed to have been deposited under various conditions, including strong anoxic (euxinic) water conditions (Anakwuba et al., 2018; Onuoha, 2005).

The Anambra Basin has been the subject of ongoing research and exploration for commercial hydrocarbon resources. Despite initial efforts being unrewarding, the basin remains an economically viable hydrocarbon province due to its substantial sediment thickness and diverse lithological heterogeneity (Ikoro, Amajo, Iwuagwu, Ibechu, Israel & Onyekuru 2014; Onuoha, 2005).

The basin's sedimentary succession is characterized by a thick sequence of Cretaceous to Tertiary sediments, with a maximum thickness of approximately 3,000 meters (Onuoha, 2005). The lithostratigraphic units within the basin include the Asu River Group, Eze-Aku Formation, Awgu Formation, Nkporo Group, Mamu Formation, Ajali Formation, and Nsukka Formation (Anakwuba et al., 2018). These units represent a variety of depositional environments, ranging from fluvio-deltaic to shallow marine settings.

2.3 Tectonic Setting

The Anambra Basin is a Cretaceous sedimentary basin located in Nigeria, situated within the Benue Trough. The basin's geological setting is characterized by a complex tectonic history that is closely tied to the separation of Africa from South America and the opening of the South Atlantic Ocean.

The Anambra Basin is part of the Benue Trough, a major geological feature that trends in a northeast-southwest direction. The Benue Trough is a failed arm of the Cretaceous triple junction that formed during the separation of the African and South American plates (Murat, 1972). This event led to the formation of the South Atlantic Ocean and the subsequent rifting of the African and South American continents.

The Anambra Basin is situated within the southern part of the Benue Trough, which is characterized by a tripartite tectonic episode (Short and Stauble, 1967; Murat, 1972). The first phase of this episode involved pronounced subsidence in the Abakaliki domain of the Benue Trough, while the Anambra Basin remained a platform with mud and shallow marine deposits (Murat, 1972). The second phase saw the uplifting and folding of the Abakaliki-Benue Belt, leading to structural inversion and subsidence of the Anambra platform (Murat, 1972). The detritus generated during this phase is believed to have been the source of the Anambra lithic fills (Simpson, 1954; Short and Stauble, 1967).

The third phase of the sedimentary cycle initiated the southward progradation of the Niger Delta along the Anambra axis during the Late Eocene (Murat, 1972). This event led to the deposition of a wide range of sedimentary rocks, including coal-bearing sediments, sandstones, and shales (Nwajide, 2013; Onyekuru & Iwuagwu, 2014). The basin's sedimentary succession is composed of various lithostratigraphic units, including the Nkporo Group, Afikpo, Owelli, Enugu, Lafia, Nkporo Shale, Mamu Formation, and Ajali Formation (Anakwuba et al., 2018). These units reflect a range of paleoenvironmental settings, from Campanian to Recent, and are believed to have been deposited under various conditions, including strong anoxic (euxinic) water conditions (Nwachukwu, 1985).

2.3.1 Pre- Albian Tectonics

During the breakup of the continent, three divergent boundaries formed, radiating out from a central point – the triple junction. One of the three divergent plate boundaries failed, and formed the aulacogen (the failed arm of the triple junction). The N-E trending Benue Trough is the failed arm of the triple junction (Peters, 1978). The tectonic history of Southern Benue Trough, Southeastern Nigeria dates back to the Pre-Albian times. According to Burke et al. (1972), and Nwachukwu (1972), the Abakaliki Benue Trough originated as a failed arm of the tripple junction rift-ridge system, which led to the separation of Africa from South America during the Aptian/Albian (Fig. 2.1).The opening of these arms started in Mid Aptian in the Southern Atlantic by crustal stretching and downwarping, accompanied by the development of coastal evaporites basins.

2.3.2 Albian to Tertiary Tectonics.

Three main tectonic phases in the Benue Trough which controlled the basin filling were identified by Murat (1970). Phase one started during the Albian and featured movement along major NE-SW pointing, Benue-Abakiliki Trough. This culminated to the occurrence of two stable areas on either side of the Benue-Abakiliki Trough, called the Anambra Platform on the west and the Ikpe Platform on the East (Fig. 2.2). The NW-SE trending Ikang Trough, Ituk High and the Eket Platform are found on the eastern flank, and all persisted into the Tertiary without significant changes.

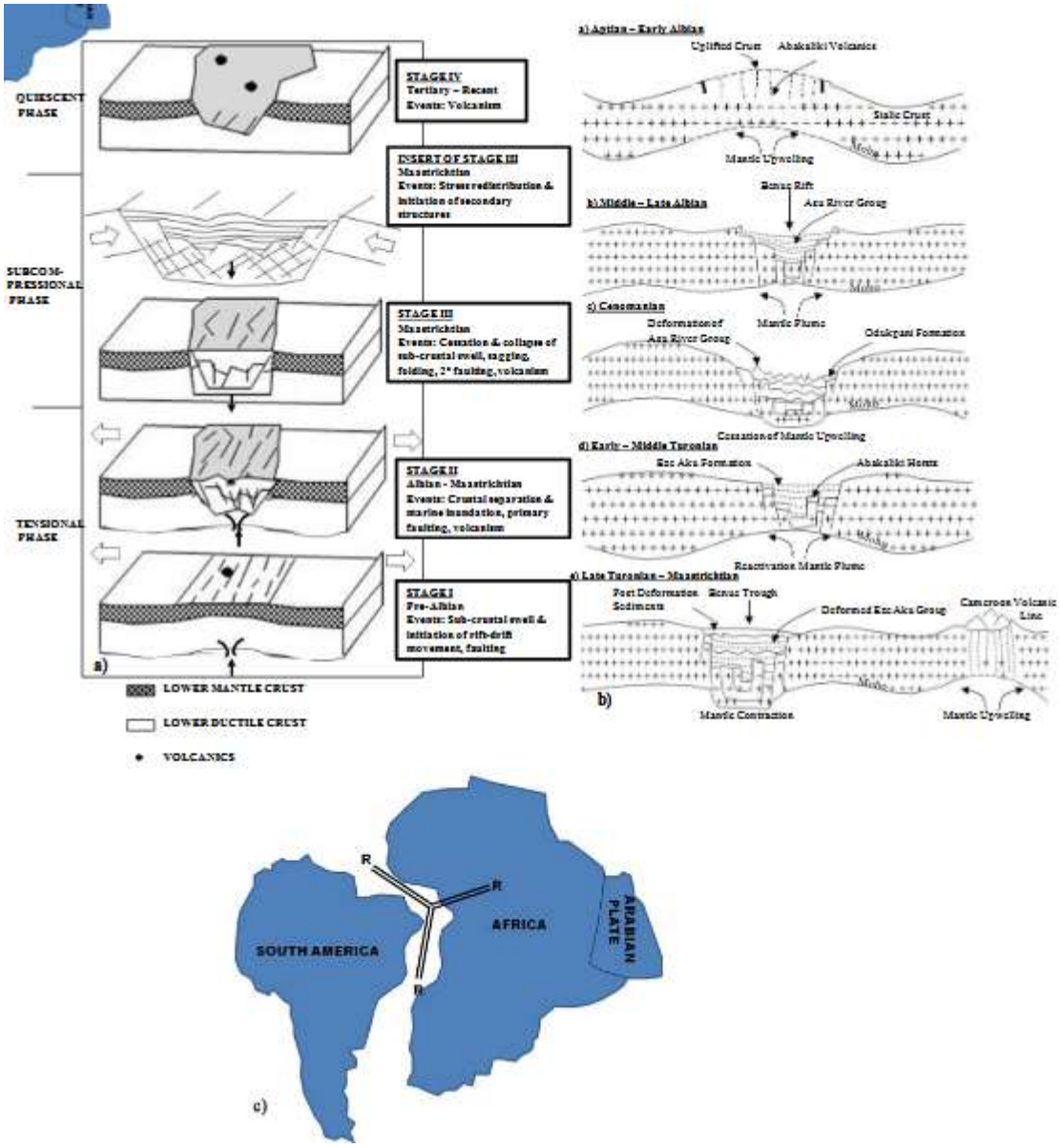

Figure. 2.1: Models for the RRR Rift origin of the Benue Trough of Nigeria. (a) Spreading Ridge Mode (from Avbovbo et al. 1986); (b) Aulacogen Model (from Olade, 1975); (c) RRF Model. (USGS, 1999)

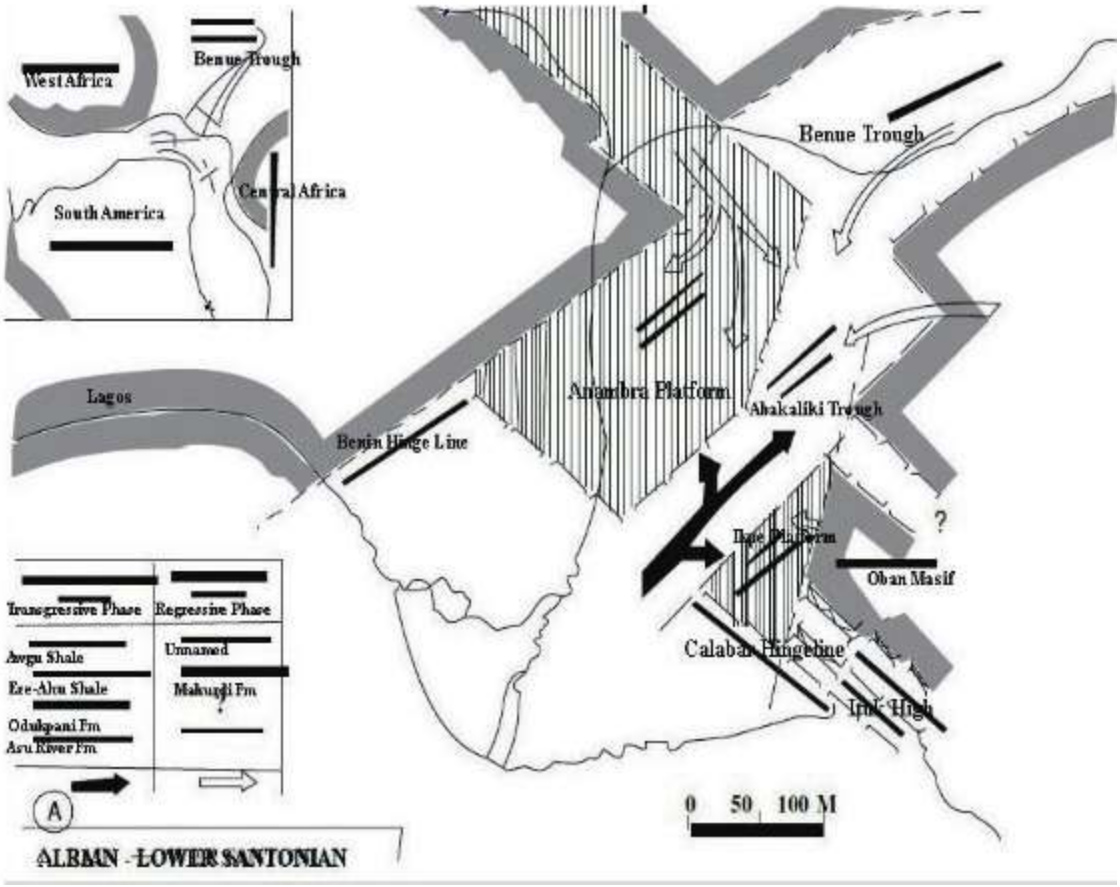

Figure 2.2: Tectonic Map of Southeastern Nigeria during Albian-Tertiary (adapted from Murat, 1970).

This led to a series of NE-SW trending folds that resulted in the Abakaliki Anticlinorium, and the subsequent downwarping of the Anambra Platform, to form the wide Anambra basin and the narrow Afikpo Synclinorium on the west and east of the Abakaliki Anticlinorium respectively, (Kogbe, 1976). The depressions became the main depositional axis from Campanian to Maastrichtian, (for Anambra Basin) and to Paleocene (for Niger Delta) getting sediments mainly from the bounding highlands. The beginning of this folding phase in the Late Santonian was accompanied by pronounced igneous activities, notably volacanism. These account for the occurrence of massive deposits of intermediate and basic intrusive rocks found at Abakaliki, Ishiagu, Lokpaukwu, Akpoha and some other localities within the region, (Onu, 2017). The curvature of the folding varies substantially from NE to SW and locally from the depositional axis towards the edges of the basin (Figure 2.3). The Niger Delta Basin which started in the Paleocene due to the tectonic movement was the result of the third sedimentary phase development (Ukpong & Anyanwu, 2018). This tectonism inverted the structure of the Abakiliki region and thus displaced the centre of deposition further toward the south of Anambra Basin.

2.4 Stratigraphy

The Anambra Basin, located in southeastern Nigeria, has been extensively studied for its stratigraphic framework, which spans from the Campanian to the Maastrichtian. Initial insights into the basin's stratigraphy were derived from regional geologic mapping efforts by the Geological Survey of Nigeria, which identified key lithostratigraphic units such as the Nkporo Group, Mamu Formation, Ajali Sandstone, and Nsukka Formation (Reyment, 1965). These formations, characterized by fluvial to deltaic and shallow marine facies, were linked to the basin's evolution as a depocenter during the Santonian tectonic inversion (Petters, 1982).

Detailed stratigraphic analysis began with sedimentological studies that focused on the facies distribution and depositional environments. Simpson (1954) was among the first to outline the stratigraphy of the Anambra Basin, correlating its units with similar deposits in adjacent basins. Later, Murat (1972) emphasized the role of tectonics in the deposition of the Nkporo Group and its transition to overlying units, highlighting the impact of eustatic sea-level changes.

The introduction of sequence stratigraphy in the 1980s refined the understanding of the basin's stratigraphic architecture. Nwajide and Reijers (1996) applied sequence stratigraphic techniques to identify systems tracts within the Ajali Sandstone and the Mamu Formation. This work revealed cyclic depositional patterns controlled by relative sea-level fluctuations, enabling the subdivision of these formations into transgressive and regressive sequences.

More recent studies have integrated geochronology, biostratigraphy, and petrography to refine the basin's stratigraphic framework. Umeji (2005) utilized palynological data to date key stratigraphic boundaries and reconstruct paleoenvironments, particularly emphasizing the coal-rich intervals of the Mamu Formation. Similarly, Onuoha and Egboka (2002) investigated the sediment provenance of the Ajali Sandstone, attributing its high quartz content to the reworking of older sedimentary rocks from the basement complex.

Advancements in sedimentological and geophysical methods have also enhanced understanding of the Anambra Basin's depositional history. Obi et al. (1995) incorporated subsurface data to establish depositional models for hydrocarbon exploration, recent works, such as those by Dim and Nwajide (2019), have combined grain-size analysis with paleohydraulic reconstructions to infer depositional energy and flow dynamics.

Today, the Anambra Basin (Figure 2.4) is recognized as a critical site for understanding Cretaceous paleoenvironments in West Africa. Its stratigraphic framework continues to evolve as new techniques, including high-resolution seismic data and geochemical analysis, are applied to refine its depositional history and resource potential (Amajor, 1987).

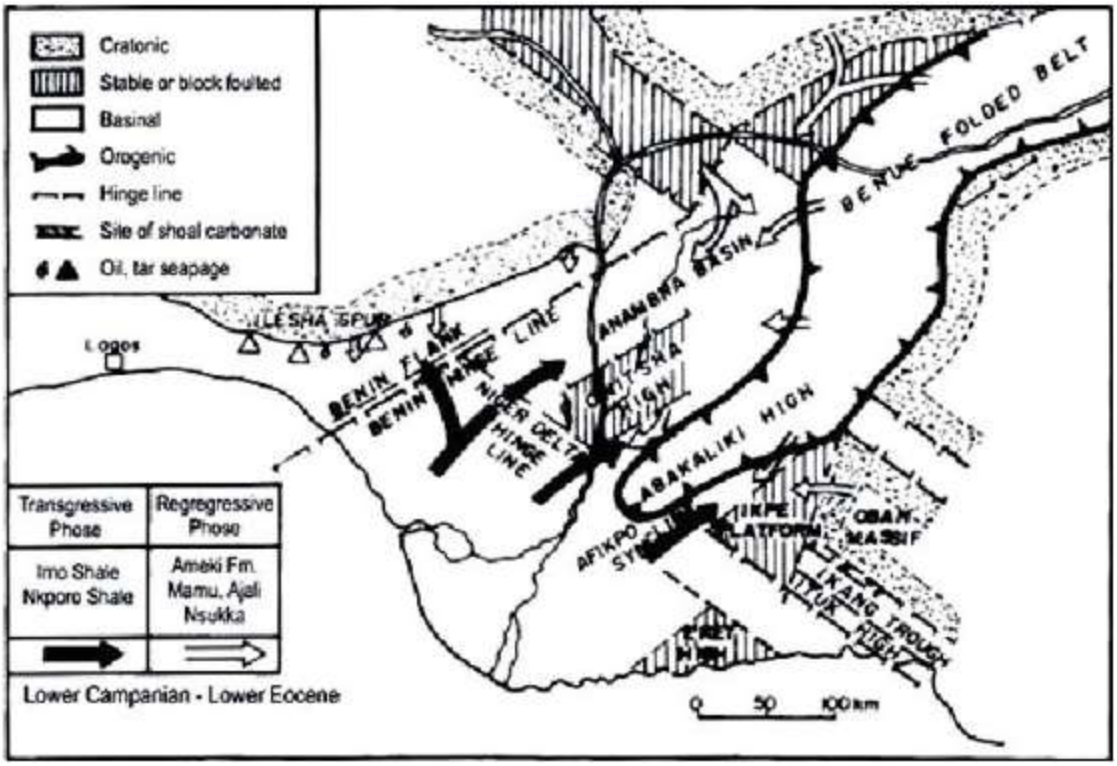

Figure 2.3 Tectonic map of southeastern Nigeria during the Campanian-Eocene (adapted after Murat, 1970)

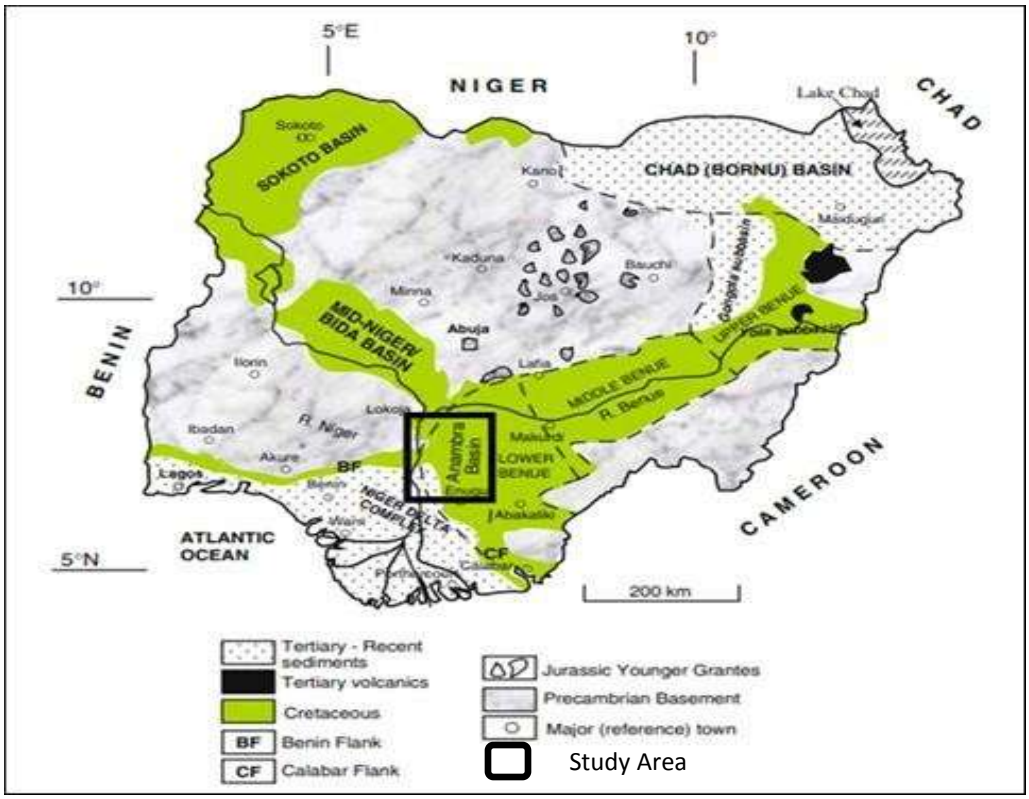

Figure 2.4: Geologic Map of Nigeria Showing the Location of Anambra Basin (Inset Africa Map, Modified after NGSA, 2001)

2.4.1 Nkporo Group and Owelli Sandstone

Subsequently and after the folding and the uplift that accompanied the Santonian Tectonism, sedimentation continued. Thus angular unconformity underlies the oldest sedimentary deposit in Anambra Basin. Deltiac sedimentation and the formation of coal swamps became prevalent during the final Campanian – Maastrichtian infilling of the basin. Three lithostratigraphic formations: the shaly Nkporo Formation, Owelli Sandstone and the Enugu Shale represent the Nkporo Group in the study area (Reyment, 1965). The arenaceous facies of the Afikpo and Owelli Sandstones are lateral equivalents to the Nkporo Formation in the Afikpo and Anambra Basins respectively. Nkporo Group (Nkporo shales and their lateral or stratigraphic equivalants) consist of the lowest stratigraphic unit of Anambra Basin. Nkporo Group is taken as the oldest sedimentary deposit in the area by earlier workers such as Nwajide (1997) and Nwachukwu (1972). Recent workers such as Ola-Buraimo and Akaegbobi (2012), however indicated the possibility of having pre-Santonian deposits especially at the northwestern part of the basin.

The Owelli Sandstone, a significant stratigraphic unit within the Campanian to Maastrichtian Anambra Basin in southeastern Nigeria, is notable for its sedimentological and petrological characteristics. It primarily consists of coarse to medium-grained sandstones, often displaying cross-bedding and other fluvial depositional features, suggesting deposition in high-energy environments such as river channels and deltaic systems (Nwajide & Reijers, 1996; Nwajide, 2013). Grain size analysis typically indicates poorly to moderately sorted sediments, reflective of variable energy conditions during deposition (Onyeagocha, 1980). Provenance studies reveal a predominance of quartz and feldspar, pointing to a continental block source and contributions from granitic and metamorphic terrains (Umeji, 2007). The Owelli Sandstone's reservoir potential is enhanced by its good porosity and permeability, making it an essential component of hydrocarbon exploration in the region (Nwajide & Reijers, 1996). Furthermore, its stratigraphic position above the Mamu Formation and beneath the Ameki Group provides valuable insights into the basin's evolutionary history and sedimentary dynamics (Akaegbobi et al., 2000).

2.4.2 Mamu Formation

The deposits of the transgressive Nkporo cycle is overlain by the Lower Maastrichtian sandstones, shales, siltstones and mudstones, and the interbedded coal seams of the deltaic

Mamu Formation in most parts of the Anambra Basin (Akande et. al 2011). A sharp contact with an underlying Enugu Shale has been identified by Agagu et al. (1985) behind the police Baracks in Agbani Road, Enugu. Rock types include very fine and fine- to medium-grained sandstone, siltstone, claystone, shale, silty-shale, black carbonaceous/coaly shale, coal and heteroliths at outcrop location. The logged sections are characterized by repeated cycles of sandstone, heterolith, carbonaceous shale and coal units(Dim, 2018; Ikoro et al. 2018).

Lateral extent and depth of sedimentary fill of Mamu Famation have been studied by earlier workers. Kogbe (1989) states that Mamu Formation is restricted to Anambra Basin and Afikpo Basin. An open-cast coal mine at Okaba, Benue State, was logged by Umeji (2005), where bituminous seam has over twenty (20) meters of overburden rocks. Reyment (1977) did a work in the area where he indicates that the sediment pile varies across the basin and ranges from 75 to over 1000 meters at different parts of the basin, and were deposited on estuarine floodplain, swamp and tidal flat floodplain.

Sedimentary structures are also reported in Mamu Formation. Slightly deformed primary sedimentary structures, such as hummocky and swaley cross-stratification, and fractures are seen occurring on the fine-grained sandstone units of the upper parts of the Mamu Formation (Dim, 2018). Parallel and wave-ripple laminations, tabular and trough cross-beds, with horizontal and vertical burrows of varying bioturbation intensities are other primary sedimentary structures observed in the area.

Biostratigraphy of Mamu Formation has been reported by earlier workers. Mebradu (1990) reported the following pollen marker species among others: Tricolpitestiebaensis; Retitrocolpitesclarensis and Staphanocolcostatus. Umeji (2000), reported freshwater pores and pollens and marine palynomorphs from the heteroliths directly overlying the Okaba coal seam and shale overlying the heteroliths respectively. This is a confirmation that the coal swamp was later submerged by marine incursion.

2.4.3 Ajali Sandstone

Ajali Sandstone, originally named by Reyment (1965) was formerly called Sandstone Series (Bain, 1924), False Bedded Sandstone (Tattan, 1944), Basal Sandstone and Shale Group

(Simpson, 1955) overlies the Mamu Formation (Obi, 2000). Ajali Sandstone is mainly unconsolidated, poorly sorted, coarse-fine grained sandstone, poorly cemented; mudstone and siltstone, and is dated Mid to Late Maastrichtian (Figure 2.5). The sandstone is typically white in colour but in some cases, iron-stained. Thin bands of white mudstone and shale in the Ajalli Formation occur at intervals and increases in number towards the base, (Onu, 2017). Most of the Ajali sandstone is composed of medium to coarse grained sub angular to angular quartz arenites. Exposed sections of Ajali Sandstone are made up of some sedimentary structures. Sandstone grain size varies from fine, medium, coarse, to partly pebbly, and are characterized by large-scale planar and herringbone cross-bedding with reactivation surfaces. Foresets of cross-beds laminae exhibit normal grading and are characterized by mud drapes.

Evidence of Several environmental interpretation have been suggested of Ajali Formation by many authors (Reyment, 1965; Murat, 1972; Agagu, 1978; Ladipo; 1986) based mainly on the predominance of coarse lithology, absence of marine fossils, unimodal paleocurrent, presence of plant indications and vertical association with coal formation.

2.4.4 Nsukka Formation

Nsukka Formation (Late Maastrichtian - Early Paleocene) which is also known as the "Upper Coal Measures" (Tattan, 1944) conformably overlies the Ajalli Sandstone (Reyment, 1965).The Formation lies directly on the Basement Complex in the Okitipupa area of southwestern Nigeria (Reyment, 1965) and could be the southwestern extremity of Anambra Basin in the area. In many locations within the basin, the lithological facies of Nsukka Formation are mainly sands, mudrocks (some mudrocks with coal) and limestone, often occurring as repetitions and alternations or in cyclic sedimentation.

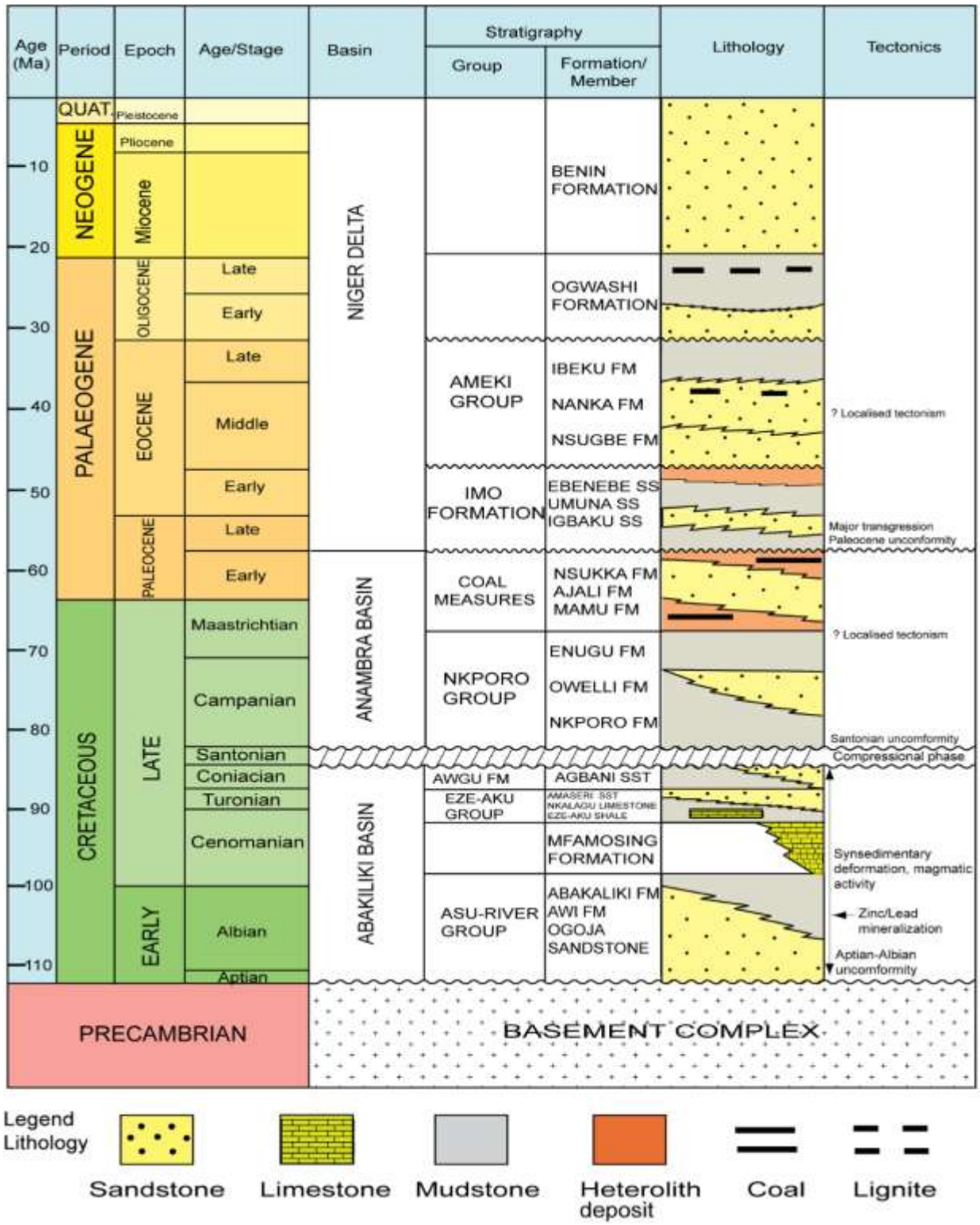

Figure 2.5: Stratigraphic Succession in the Anambra Basin and Outcropping Niger Delta (after Ekwenye and Nichols, 2016).

A prominent normal fault system is also exposed at Ikpankwo quarry showing the downthrown and upthrown blocks component (Dim, 2018). There are also primary sedimentary structures such as current-rippled surfaces and intensely bioturbated and burrowed sandstone units at Umuasua section of Nsukka Formation

2.5 Depositional Environments

Nsukka Formation

The Maastrichtian-Paleocene Nsukka Formation is dominated by fine-grained sandstones, shales, and occasional coal seams, indicating deposition in mixed fluvial to deltaic environments. Evidence such as fossil-rich shales, bioturbation, and rhythmic sedimentation suggests tidal and coastal swamp conditions. The formation is interpreted as representing a deltaic system with both freshwater and marine influences during sea-level fluctuations (Obi et al., 2020)

Ajali Sandstone

The Ajali Sandstone, formed during the Maastrichtian, is characterized by well-sorted medium to coarse-grained sandstones. Cross-bedding, ripple marks, and the absence of marine fossils suggest deposition in a high-energy braided river system transitioning into deltaic environments. The formation reflects a period of high fluvial input with the occasional marine influence in the form of storms and coastal conditions (Nwajide, 2021).

Mamu Formation

The Mamu Formation is best known for its coal deposits, which indicate deposition in a coastal swamp environment. The presence of estuarine sandstones and shales interbedded with coal and carbonaceous materials suggests periodic flooding and a shifting coastline. Its deposition in a deltaic to shallow marine environment with tidal and fluvial interactions is supported by sedimentological data (Nwajide, 2021).

Owelli Sandstones

The Owelli Sandstones are high-energy fluvial deposits characterized by coarse grain size, large-scale cross-bedding, and quartz-rich composition (>90%), consistent with a braided river system and minimal marine influence.

The lack of significant biotic content in the sandstones supports a predominantly terrestrial deposition, with periodic floodplain overbank deposition (Umeji 2000).

2.6 Provenance Studies

Provenance studies are crucial in understanding the sources of sediments in the Anambra Basin, as they provide insights into the geological history and evolution of the basin. These studies help identify the origin of sediments, the transport mechanisms, and the depositional environments, which are essential for reconstructing the paleogeographic and paleotectonic settings of the basin.

Despite the significance of provenance studies in the Anambra Basin, there is a notable lack of publications on this topic. Several authors have highlighted the need for further research to fill this gap and enhance our understanding of the sediment sources and the geological processes that have shaped the basin over time.

Nton and Bankole (2012) investigated the sedimentological characteristics, provenance, and hydrocarbon potential of post-Santonian sediments in the Anambra Basin. Their study revealed that the sandstone facies of the Nkporo, Owelli, Mamu, and Ajali Formations are cross-bedded, medium to coarse-grained, poorly sorted to moderately well-sorted, negatively skewed, and leptokurtic to platykurtic. Textural plots and multivariate parameters indicated a fluvial depositional environment for these sediments.

Obaje, Wehner, Scheeder, Abubakar, & Jibrin, 2020) and Waziri, Obaje, & Abaa (2020) conducted geochemical studies on the shales within the Lower Anambra Basin to unravel the depositional environment, provenance, maturity, and tectonic setting. Their findings suggest that detailed studies of the geochemistry and mineralogy of fine-grained clastic sedimentary rocks are valuable tools for determining provenance, tectonic setting, paleoweathering, and redox conditions of the basin.

In conclusion, provenance studies are essential for understanding the sources of sediments in the Anambra Basin, but there is a lack of publications on this topic. Further research is needed to address this knowledge gap and provide a more comprehensive understanding of the geological history and evolution of the basin. The studies by Nton and Bankole (2012), Obaje et al. (2020),

and Waziri et al. (2020) highlight the importance of provenance studies and the need for more detailed investigations in the Anambra Basin.

2.7 The Paleo-Hydrodynamic Conditions

The Anambra Basin, a significant sedimentary basin in southeastern Nigeria, has been the subject of numerous studies focusing on its stratigraphy, sedimentology, and depositional environments. However, specific research on the paleohydrodynamic conditions of its deposits has been relatively limited. This review synthesizes the available literature on the paleohydrodynamic aspects of the Anambra Basin deposits, with a focus on the Mamu, Ajali, Nsukka, and Owelli Sandstone Formations.

Nwajide (2005) provided a comprehensive overview of the Anambra Basin's geology, highlighting the diverse depositional environments represented by its formations. The author noted that the basin's sediments were deposited under varying hydrodynamic conditions, ranging from fluvial to deltaic and shallow marine environments. This work established a foundation for understanding the basin's depositional history but did not delve deeply into quantitative paleohydrodynamic analyses.

Egbu, Onwuemesi.and Chinwuko (2009) conducted a detailed sedimentological study of the Mamu Formation, employing grain size analysis and facies interpretation to infer depositional environments. Their findings suggested a transition from fluvial to estuarine conditions, implying changes in hydrodynamic regimes over time. The authors identified six lithofacies and interpreted them in terms of depositional processes, providing insights into the varying energy conditions during deposition.

The Ajali Sandstone, known for its distinctive cross-bedding, has been the subject of several studies. Amajor (1987) examined the formation's sedimentary structures and grain size characteristics, inferring a high-energy fluvial depositional environment. This work provided valuable data on paleocurrent directions and suggested that the Ajali Sandstone was deposited by braided streams flowing towards the southwest. While this study hinted at the potential for more detailed paleohydrodynamic analysis, it did not provide quantitative estimates of paleocurrent velocities or sediment transport modes.

Nwajide and Reijers (1996) conducted a comprehensive study of the Anambra Basin's stratigraphy and paleogeography. Their work touched on the hydrodynamic aspects of deposition, particularly for the Ajali and Mamu Formations. They suggested that the Ajali Sandstone was deposited in a braided river system characterized by high-energy flow conditions, while the Mamu Formation represented lower energy, tidally influenced environments. However, quantitative paleohydrodynamic parameters were not extensively explored in this study.

The Nsukka Formation, which overlies the Ajali Sandstone, has received less attention in terms of paleohydrodynamic analysis.. Ekwenye, Ukaegbu and Ofor (2015) studied its sedimentology and paleoenvironments, suggesting a transition from fluvial to estuarine conditions. The work identified nine lithofacies and interpreted them in terms of depositional processes, providing some insights into the hydrodynamic conditions during deposition. However, detailed quantitative analysis of paleohydrodynamic parameters was not a focus of this study.

The Owelli Sandstone Formation, being less extensively studied, presents a gap in the literature regarding its paleohydrodynamic conditions. Mode et al. (2013) briefly described its characteristics, suggesting a fluvial depositional environment based on sedimentological and petrographic analyses. However, detailed hydrodynamic analyses are lacking for this formation.

Recent advancements in paleohydrodynamic analysis techniques offer new opportunities for more quantitative assessments of the Anambra Basin's depositional conditions. For instance, Leclair and Bridge (2001) developed methods for estimating flow depths and velocities from cross-set thickness in fluvial deposits. Similarly, Bhattacharya and MacEachern (2016) demonstrated the use of clinoform geometries in deltaic deposits to infer paleohydrodynamic conditions. These methods have not yet been extensively applied to the Anambra Basin deposits but hold significant potential for enhancing our understanding of the basin's depositional history.

Oboh-Ikuenobe et al. (2005) conducted a palynological and sedimentological study of the Mamu Formation, providing insights into the paleoenvironment and sea-level changes. While this study did not focus specifically on paleohydrodynamic conditions, it offered valuable context for understanding the depositional setting and potential hydrodynamic variations over time.

In terms of modern analytical techniques, Dim et al. (2019) applied sequence stratigraphy and facies analysis to the Mamu Formation, integrating sedimentological data with well log

interpretations. Their work provided a more nuanced understanding of the depositional environments but stopped short of detailed paleohydrodynamic reconstructions.

The application of advanced statistical methods to grain size data, as demonstrated by Weltje and Prins (2007) in other sedimentary basins, has not yet been fully utilized in the Anambra Basin. Such methods could potentially reveal subtle variations in hydrodynamic conditions that are not apparent from traditional sedimentological analyses.

Umeji (2000) conducted a paleocurrent analysis of the Ajali Sandstone, providing valuable data on flow directions and suggesting a complex fluvial system. However, this study did not extend to quantitative estimates of flow velocities or sediment transport modes, leaving room for more detailed paleohydrodynamic investigations. The integration of multiple data types, including sedimentological, ichnological, and geochemical data, as demonstrated by MacEachern Bann, Gingras, and Zonneveld. (2010) in other basins, could provide a more comprehensive understanding of the paleohydrodynamic conditions in the Anambra Basin. Such an integrated approach has not yet been fully applied to the basin's formations.

In conclusion, while the Anambra Basin has been extensively studied in terms of its stratigraphy and general sedimentology, there remains a significant gap in the literature regarding detailed, quantitative paleohydrodynamic analyses. The existing studies provide a solid foundation for understanding the basin's depositional environments, but they generally lack the quantitative rigor that modern paleohydrodynamic techniques can offer. Future research employing these advanced methods could significantly enhance our understanding of the basin's depositional history, potentially improving predictions for hydrocarbon exploration and contributing to broader paleoenvironmental reconstructions of the Late Cretaceous in West Africa.

2.8 Hydrocarbon Potential:

The Anambra Basin in southern Nigeria is considered to have significant hydrocarbon potential due to the presence of Late Cretaceous-Paleocene deposits that represent prospective hydrocarbon resources. These deposits are characterized by the presence of organic-rich shales and coaly intervals that are capable of generating hydrocarbons (Akaegbobi, 2005; Nwachukwu, 1985; Obaje et al., 2020).

The Anambra Basin is a Cretaceous basin with a total sediment thickness of about 9km, which can present an ideal geo-reactor for all manner of complex chemical reactions that can lead to the generation of hydrocarbons (Akaegbobi, 2005). The basin is composed of several sedimentary formations, including the Nkporo Group, Mamu Formation, Ajali Sandstone, Nsukka Formation, Imo Formation, and the Ameki Group, which are primarily composed of sandstones, shales, and limestone (Nwachukwu, 1985; Obaje et al., 2020).

The hydrocarbon potential of the Anambra Basin is attributed to the presence of organic-rich shales and coaly intervals that are capable of generating hydrocarbons. These deposits are characterized by high total organic carbon (TOC) values, ranging from 0.31 to 3.51 wt% for the Nkporo/Enugu Formations, 0.82 to 6.10 wt% for the coaly shale of the Mamu Formation, and 30.80 to 60.80 wt% for the coals of the Mamu Formation and Nsukka Formation (Obaje et al., 2020).

The hydrocarbon generation potential of the Anambra Basin is further supported by the presence of potential reservoir rocks, including sandstone facies associated with the predominantly shale lithology of the basin (Obaje et al., 2020; Onyekuru et al., 2023). These reservoir rocks are capable of storing hydrocarbons generated from the organic-rich shales and coaly intervals

In summary, the Anambra Basin in southern Nigeria has significant hydrocarbon potential due to the presence of Late Cretaceous-Paleocene deposits that represent prospective hydrocarbon resources. These deposits are characterized by high TOC values and the presence of potential reservoir rocks, making them capable of generating and storing hydrocarbons.

CHAPTER THREE

MATERIALS AND METHODS

3.1 Materials.

3.1.1 Study Area

The study area for this paleohydrodynamic analysis encompasses a diverse range of outcrops across the Anambra Basin, focusing on the Mamu, Ajali, Nsukka, and Owelli Sandstone Formations. Eight key locations were selected for detailed examination, spanning a significant portion of the basin. These outcrops are distributed across southeastern Nigeria, with coordinates ranging from approximately 7.26632° to 7.83024° Longitude and 4.95264° to 6.2558° Latitude (Figure 3.1). The locations include Umuasua in Isukwato and Akara Junction, representing the Nsukka Formation; ABSU-Uturu Road and Onyekaba Mine, showcasing the Ajali Formation; Ohafia and Ihube, exposing the Mamu Formation; and Agbaogugu and Ikpankwu Ihube, featuring the Owelli Sandstone. This strategic selection of outcrops provides a comprehensive cross-section of the basin's stratigraphy, allowing for a thorough investigation of the paleohydrodynamic conditions that prevailed during the deposition of these important sedimentary units. The geographical spread of these locations enables researchers to capture potential lateral variations in depositional environments and hydrodynamic parameters across the

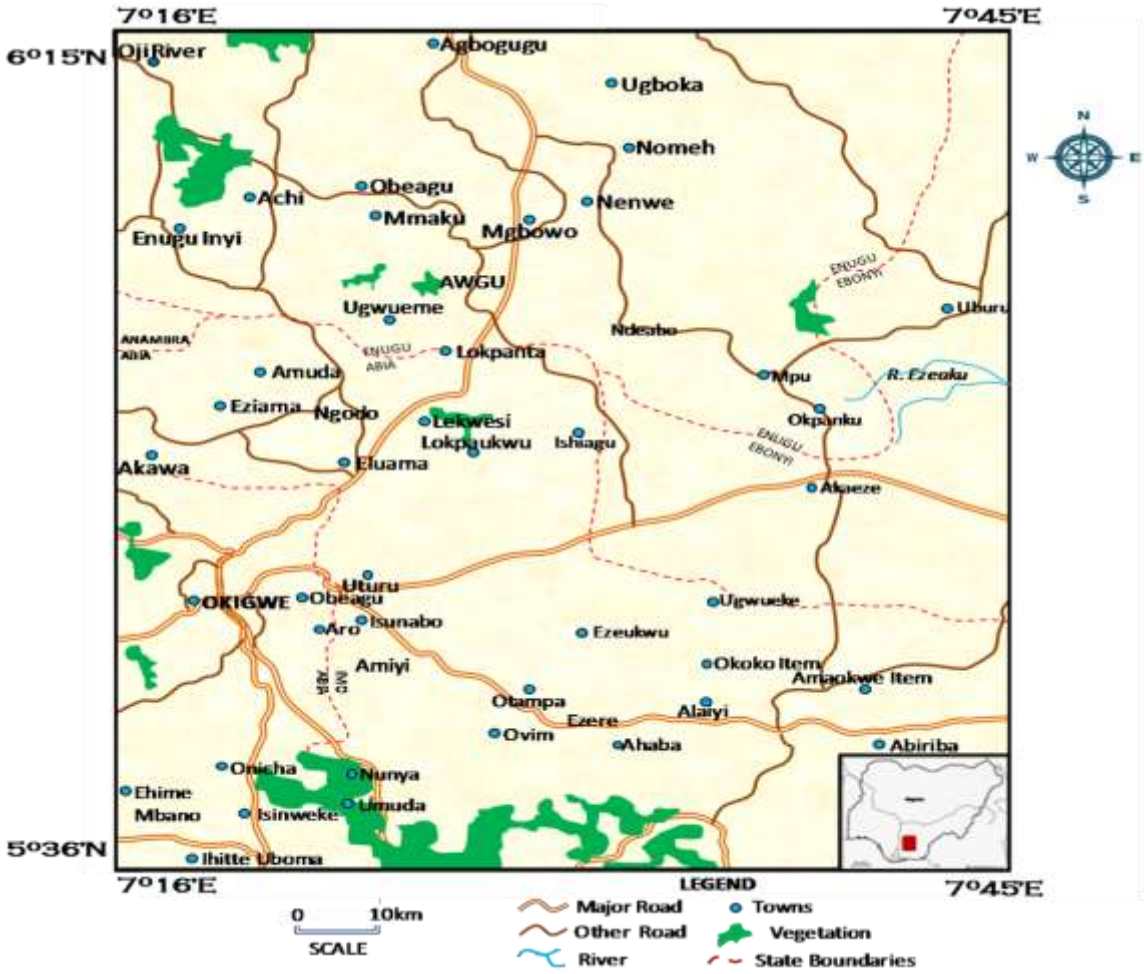

Figure 3.1 Location and Accessibility Map the Study Area (inset: Map of Nigeria)

The materials required for evaluating paleohydrodynamic conditions of the Campanian-Maastrichtian sediments in the Anambra Basin include field and laboratory equipment, reference materials, and sample storage tools. Key field materials involve topographic maps, GPS devices, hammers, sample bags, and notebooks for recording field observations. For sample collection, sieves of varying mesh sizes, dispersants like sodium hexametaphosphate, and airtight containers are essential to preserve sediment samples during transportation. Laboratory materials include microscopes for grain-size analysis, sedimentation tubes, calipers for particle measurement, and software tools like Excel for statistical analysis of sediment properties. Reference materials, such as geological atlases and sedimentological textbooks, provide a comparative framework for interpreting paleohydrodynamic features (Tucker, 2001). Additionally, petrographic thin-section slides, polarizing microscopes, and cameras for imaging grains are necessary for detailed analysis of sedimentary structures and textures. These materials collectively support comprehensive research into the basin's hydrodynamic and depositional conditions.

3.1.2 Data Sets

To conduct the research on sedimentary hydrodynamics deposition, the following datasets were required.

Grain Size Data: Sieve analysis data or laser particle size analysis data for sandstone samples from the Nsukka, Ajali, Mamu, and Owelli Formations in the Anambra Basin. The grain size data should include the weight percentages or volume percentages of sediment particles in various size classes or phi (ϕ) values. This data is essential for generating frequency distribution curves, calculating statistical parameters (mean, sorting, skewness, and kurtosis), and performing log-probability analysis.

Sedimentological Data: Textural descriptions of the sandstone samples, including information on grain sorting, grain roundness, and grain sphericity. Petrographic data from thin section analysis, providing information on the mineralogical composition and textural characteristics of the sandstones. Sedimentary structures and bedding features observed in outcrop or core samples, which can aid in interpreting depositional environments. Grain-size distribution and statistical parameters further constrain transport mechanisms and energy conditions.

Obtaining a comprehensive dataset that integrates these different types of data is crucial for conducting a robust sedimentological and paleoenvironmental analysis of the sandstone formations in the Anambra Basin. This data will enable the construction of detailed depositional models, reconstruction of paleoenvironmental conditions, and understanding of the hydrodynamic regimes that shaped these sedimentary successions.

3.2. Methods

The method integrates various analytical tools, including sieve analysis (Folk & Ward, 1957), facies analysis (Walker, 1992), paleocurrent analysis (Potter & Pettijohn, 1977), and optical microscopy (Mange & Maurer, 1992), to examine changes in texture, composition, and depositional processes. These analyses are complemented by quantitative evaluations of hydrodynamic parameters, such as energy of deposition (Hjulström, 1935), water depth (Allen, 1970), and temperature (Friedman & Sanders, 1978). The framework also considers porosity (Beard & Weyl, 1973), permeability (Krumbein & Monk, 1943), and grain characteristics (Sahu, 1964) to infer depositional environments ranging from low-energy settings to high-energy rivers and deltas (Reading, 1996). By synthesizing these diverse data sets, researchers can reconstruct ancient sedimentary hydrodynamic conditions (Visher, 1969; Passega, 1977), ultimately contributing to a more accurate paleogeographic interpretation and assessment of oil and gas potential (Selley, 1998; Slatt, 2006). This integrated methodology allows for a detailed reconstruction of depositional environments, providing valuable insights into the geological history and resource potential of sedimentary basins (Leeder, 2011; Miall**,** 2014).

3.2.1 Work Flow

Figure 3.2 presents a comprehensive methodological framework for reconstructing hydrodynamics in ancient sedimentary environments (Miall, 2013; Bridge, 2003). This multifaceted approach combines field-based outcrop analysis, laboratory techniques, and quantitative assessments to provide a holistic understanding of paleoenvironmental conditions (Nichols, 2009; Boggs, 2014).

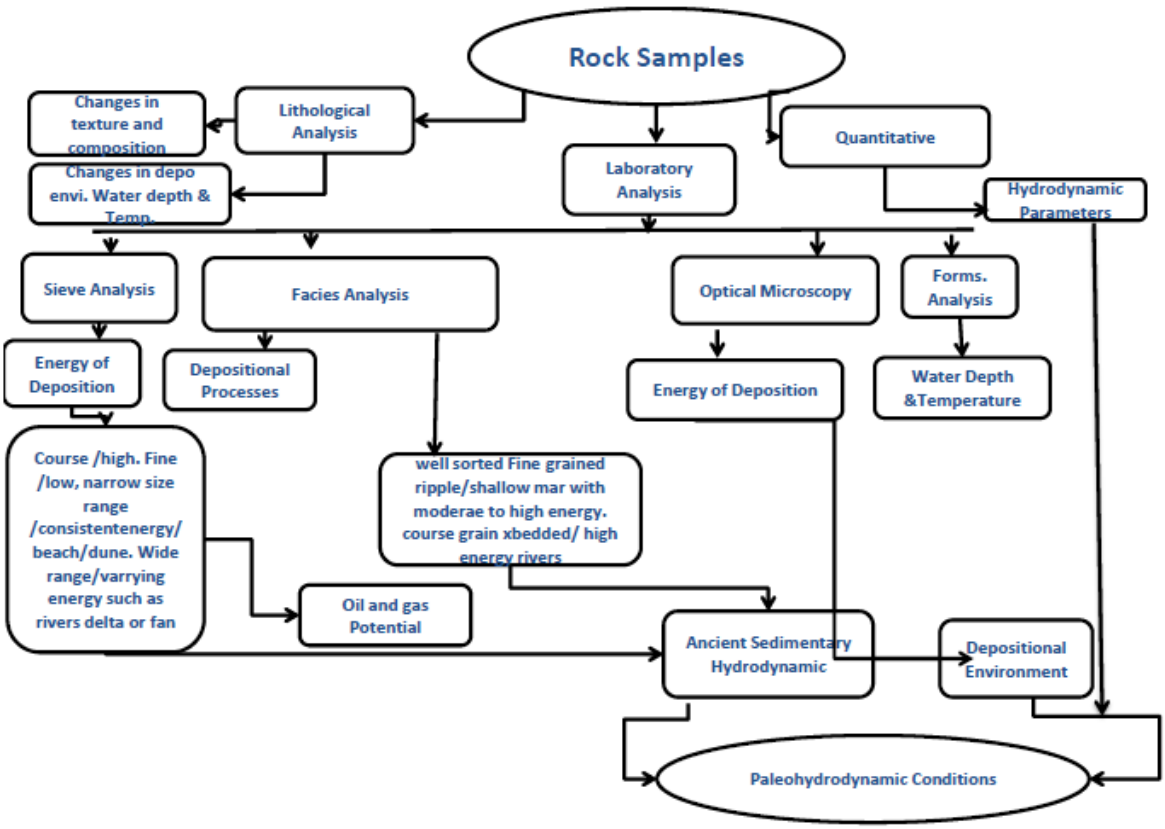

Figure 3.2 Workflow of Methodological Approach for Paleohydrodynamic Analysis in the Anambra Basin

3.2.2 Desk Studies

Desk studies play a foundational role in evaluating the paleohydrodynamic conditions of the Campanian-Maastrichtian sediments in the Anambra Basin by providing critical background information and contextual insights. This phase involves a detailed review of existing geological maps, reports, and previous studies to identify the spatial distribution of formations such as the Ajali Sandstone, Mamu Formation, and Nsukka Formation. It also involves accessing stratigraphic, sedimentological, and hydrodynamic data to assess depositional environments and sediment transport patterns. Key sources include works like Onyekuru et al. (2012) on sediment dispersal patterns and Reyment (1965), which provides regional stratigraphic insights into the Anambra Basin. These reviews help refine research objectives, identify knowledge gaps, and guide field and laboratory investigations.

Additionally, desk studies incorporate data from satellite imagery, borehole logs, and geophysical surveys to understand the basin's structural framework and sedimentation dynamics. Modern techniques, such as Geographic Information Systems (GIS), enhance spatial analysis, enabling the correlation of sedimentary facies and paleocurrent data (McManus, 1988; Nichols, 2009). Literature reviews also aid in selecting appropriate methods for grain-size analysis, hydrodynamic modeling, and paleoflow reconstructions, ensuring methodological rigor. By synthesizing regional and global studies, such as those by Tucker (2001) and Selley (1998), the desk study phase forms the scientific basis for reconstructing the paleohydrodynamic regimes in the Anambra Basin.

3.2.3 Reconnaissance Studies

Reconnaissance studies are a critical preliminary step in evaluating the paleohydrodynamic conditions of the Campanian-Maastrichtian sediments in the Anambra Basin. These studies involve field visits to identify accessible outcrop locations, assess lithological exposures, and document sedimentary structures indicative of depositional environments. During this phase, emphasis is placed on observing large-scale features such as cross-bedding, ripple marks, and erosional surfaces, which serve as direct indicators of paleoflow regimes and sediment transport dynamics (Nichols, 2009; Miall, 2016). Locations such as the Ajali Sandstone and Mamu

Formation are examined for their depositional patterns, grain size variations, and sedimentary architecture. Preliminary observations also include photographing outcrops, logging stratigraphic sections, and marking areas for detailed sampling and analysis (Onyekuru et al., 2012).

Moreover, reconnaissance studies help refine research plans by identifying potential challenges such as poor exposure, weathering, or anthropogenic impacts on outcrops. These initial surveys facilitate the collection of preliminary data on lithology, bed geometry, and paleocurrent directions. This information is vital for selecting sampling locations that best represent depositional environments and paleohydrodynamic conditions. For example, studies by Tucker (2001) and Selley (1998) emphasize the importance of observing sedimentary structures and facies transitions during reconnaissance to establish paleoenvironmental interpretations. Reconnaissance also includes engaging with local geological maps and consulting previous works, such as Reyment (1965), to corroborate field observations. This step ensures that the fieldwork and laboratory analyses that follow are both comprehensive and scientifically sound.

3.2.4 Field Mapping/Investigation

Field mapping and investigation are integral to the evaluation of paleohydrodynamic conditions in Campanian to Maastrichtian sediments of the Anambra Basin. This process begins with the systematic identification and logging of outcrop locations where sedimentary deposits are exposed, such as the Ajali Sandstone, Mamu Formation, and Nsukka Formation. Fieldwork focuses on documenting lithological variations, bed geometry, and sedimentary structures like cross-bedding, ripple marks, and mud cracks, which serve as indicators of flow regimes and depositional processes (Miall, 2016; Nichols, 2009). Essential tools such as Brunton compasses, measuring tapes, and field notebooks are employed to measure paleocurrent directions, stratigraphic thickness, and sedimentary architecture. Observations are supplemented by GPS coordinates to accurately locate sites, as demonstrated in studies by Onyekuru et al. (2012) and Reyment (1965).

During field investigations, special attention is given to sediment texture, grain-size variations, and bedform morphologies, as these provide insights into flow energy and sediment transport mechanisms (Tucker, 2001). Features like planar and trough cross-bedding in the Ajali

Sandstone may indicate high-energy fluvial environments, while laminated and ripple-marked facies in the Mamu Formation suggest lower-energy conditions typical of deltaic or coastal settings (Selley, 1998). The collection of sediment samples for laboratory analyses is guided by these field observations, ensuring that samples represent the full range of sedimentary facies present. For example, the work of Okogbue and Umeji (2005) highlights the importance of sampling across diverse depositional settings to reconstruct paleohydrodynamic regimes comprehensively.

Field mapping also involves detailed photo documentation and sketching of stratigraphic sections to capture sedimentary sequences and transitions between facies. This step aids in interpreting depositional environments and reconstructing paleoflow dynamics over time. Integration of field data with existing geological maps and previous studies ensures a robust understanding of sediment distribution patterns and their hydrodynamic implications (McManus, 1988). Reconciling field observations with regional geological frameworks, such as those established by Reyment (1965), enables researchers to generate detailed models of paleohydrodynamic conditions and depositional systems within the Anambra Basin.

3.2.4.1 Facies Analysis

The Anambra Basin, a treasure trove of geological history preserved in its diverse rock formations, beckons researchers to unlock the secrets of its past. Among the key tools in this endeavor lies facies analysis, a meticulous examination of rock characteristics that offers a window into the depositional processes that sculpted the basin's landscapes. By delving into the intricacies of facies and their association with environmental signatures, we can reconstruct the dynamic interplay of forces that shaped the Anambra Basin's rich tapestry.

The journey begins with a meticulous field study. Each outcrop becomes a canvas, revealing variations in rock types, textures, sedimentary structures, and fossil assemblages. These observations are then meticulously classified into discrete facies units, sharing a common language etched in their physical attributes (Prothero, 1994). Each facies was then carefully characterized, its composition, textures, structures, and fossils documented, forming the foundation for deciphering the story hidden within the rocks.

With the facies as building blocks, depositional processes take center stage. Linking observed characteristics to specific mechanisms like suspension, traction, saltation, and bioturbation becomes the next act in the play. Here, understanding the interplay of energy levels, water depth, salinity, and other environmental factors proves pivotal (Reading, 1980). Cross-bedding angles, grain size variations, and the choreography of burrowing organisms in bioturbation patterns all become voices whispering tales of the past (Boggs, 2001).

Moving beyond individual facies, we reconstruct the broader depositional environments. Facies associations (Table 3.1) groups of related facies, emerge as the brushstrokes depicting broader landscapes like tidal flats, fluvial channels, shoreface zones, and tranquil offshore realms. By analyzing the spatial and vertical relationships between these associations, we witness the basin's transformation through time, driven by forces like sea-level fluctuations, tectonic activity, and climatic shifts (Miall, 1990).

Finally, the culmination of this interpretive endeavor comes in the form of depositional models. These conceptual frameworks, whether sketched diagrams, detailed simulations, or even 3D reconstructions, capture the essence of the depositional processes at play. These models, constantly tested and refined, become the Rosetta Stone translating the mute language of rocks into a captivating narrative of the Anambra Basin's history (Posamentier& Allen, 1999).

The power of facies analysis extends beyond mere interpretation. By understanding the depositional processes, we can answer broader questions about the basin's resource potential, its geomorphological evolution, and even its role in shaping present-day environmental conditions. Insights gleaned from specific outcrops can be extrapolated to inform interpretations across the basin, weaving a broader tapestry of understanding the facies. Table 3.1 presents a concise comparison between facies and facies associations, highlighting their key differences and significance in sedimentological analysis. Understanding these units is crucial for reconstructing past environments and deciphering geological processes within sedimentary basins.

Table 3.1 Table showing Facies and Facies Association (after Boggs, 2014)

Feature	Facies	Facies Association
Scale	Smaller unit, individual bed or layer	Larger unit, grouping multiple facies together
Definition	Distinct set of characteristics (grain size, texture, bedding, fossils)	Group of facies sharing similar depositional processes and environments
Significance	Provides information about local depositional conditions	Reveals broader paleogeographic context and processes operating within the basin
Analysis approach	Detailed sedimentological description, microscopic analysis	Focuses on relationships between facies, spatial transitions, and environmental interpretation
Examples	Sand layer with cross-bedding, mudstone with abundant bivalves	Fluvial channel belt, lagoonal mudflats, reef complex
Benefits of studying	Understands specific depositional processes, identifies local paleoenvironments	Reconstructs basin history, identifies potential resource occurrences, predicts facies distribution

Facies represent the fundamental building blocks, characterized by distinct features like grain size, sorting, sedimentary structures, fossils, and textures (Reading, 1980). They offer insights into specific local depositional conditions, such as water depth, energy levels, and biological activity within the immediate environment.

In contrast, facies associations encompass a broader perspective, grouping together multiple facies that share similar depositional processes and environments (Boggs, 2001). Analyzing these associations reveals the larger-scale paleogeographic context and helps us understand the dominant processes operating within the basin. Studying facies associations allows for reconstruction of basin history, identification of potential resource occurrences (e.g., hydrocarbons, minerals), and prediction of facies distribution across wider regions.Therefore, while facies provide detailed information about local depositional settings, facies associations offer a broader window into the basin's overall dynamics and past environments.

3.2.5 Laboratory Analysis

3.2.5.1 Grain Size Sieve Analysis

Sieve analysis was used to determine the particle size distribution of granular materials by passing them through a stack of sieves with progressively smaller mesh sizes. The technique involved shaking or vibrating the material to facilitate separation, and the weight of material retained on each sieve was measured to compute the proportion of different size fractions. This method is widely applied in geology, sedimentology, and civil engineering to classify soil and sediment types, assess sediment transport processes, and design construction materials (ASTM International, 2021; Mitra et al., 2020). It provided insights into depositional environments by analyzing the texture and sorting of sediments (Folk & Ward, 1957).

These data were further used to calculate statistical parameters such as mean, sorting, skewness, and kurtosis, which reveal the energy and mechanism of sediment deposition. Well-sorted sediments typically indicate consistent energy conditions, while poorly sorted sediments suggest variable or rapidly changing environments. Such interpretations help reconstruct paleoenvironments and understand sediment transport dynamics across different depositional settings.

3.2.5.1.1 Graphic Mean Size (Mz)

The graphic mean size represents the average sediment grain size, incorporating both finer and coarser fractions around the median value. This parameter is calculated using three key percentile points from cumulative curves: P_{16} (coarsest fraction), P_{50} (median), and P_{84} (finest fraction). The calculation follows Folk and Ward's (1957) formula:

$$Mz = (P_{16} + P_{50} + P_{84})/3 \quad 3.1$$

This measure provides a more comprehensive representation of central tendency than the median alone, as it accounts for the entire grain size distribution.

3.2.5.1.2 Inclusive Graphic Standard Deviation (σi)

The inclusive graphic standard deviation quantifies the spread of grain sizes around the mean, serving as a measure of sorting efficiency. The modified Folk and Ward (1957) formula incorporates 90% of the distribution:

$$\sigma i = [(P_{84} - P_{16})/4] + [(P_{95} - P_5)/6.6] \quad 3.2$$

Values approaching zero indicate better sorting, while higher values reflect poorer sorting. This parameter reveals fluctuations in depositional energy conditions.

3.2.5.1.3 Inclusive Graphic Skewness (Ski)

Skewness measures the displacement of the mean relative to the median in grain size distributions. The Folk and Ward (1957) formula combines two components to assess distribution symmetry:

$$Ski = [(P_{16} + P_{84} - 2P_{50})/2(P_{84} - P_{16})] + [(P_5 + P_{95} - 2P_{50})/2(P_{95} - P_5)] \quad 3.3$$

A value of 0 indicates perfect symmetry, negative values suggest coarse skewness, and positive values indicate fine skewness.

3.2.5.1.4 Graphic Kurtosis (KG)

Kurtosis quantifies the peakedness of grain size distributions relative to a normal distribution. The Folk and Ward (1957) formula compares central sorting to tail sorting:

$$KG = (P_{95} - P_5)/2.44(P_{75} - P_{25}) \quad 3.4$$

Values <1.00 (platykurtic) indicate better sorting in the tails, while values >1.00 (leptokurtic) show better central sorting. A value of 1.00 represents a normal (mesokurtic) distribution.

All statistical parameters were calculated using percentile values extracted from cumulative frequency curves (Tables 4.22-4.26). These metrics collectively characterize sediment texture and provide insights into depositional processes without direct environmental interpretation.

Grain size analysis, however, is not a solitary act. Integrating its findings with other data sets like sedimentary structures, bioturbation patterns, and geochemical signatures strengthens the interpretation. This holistic approach allows us to paint a more nuanced picture of the past, reconstructing not just the depositional environments but also the paleocurrents, paleowater depths, and even the climatic conditions that influenced the Anambra Basin's journey through time (Collinson, 1969).

3.2.5.2 Method of Multivariate and Bivariate Analysis

Sahu (1964) used the general equation:

$$Y_1 = \lambda^1 X_1 + \lambda^2 X_2 + \ldots\ldots + \lambda^p X_p \quad 3.5$$

For the general case of p normally distributed variables (X_1, X_2, . . . Xp), and coefficients λ^1, λ^2 , . . . λ^p, with the discriminate function Y being linearly related to the variables. λ‘s are chosen so that the ratio of the difference between the simple means and the standard deviation for the two environments is maximized (Sahu, 1964). Multivariate discriminate functions (Y1, Y2,Y3) proposed by Sahu (1964), were applied to the grain size data in order to characterize the depositional setting of the sediments and to investigate the problems of discrimination between different processes and the depositional environments of sands using size distribution. These functions combine multiple grain-size statistical measures—such as mean, standard deviation,

skewness, and kurtosis—into a single index that distinguishes between depositional settings like river, beach, and aeolian environments. By applying Sahu's discriminant analysis to the sediment samples, it became possible to quantitatively interpret sediment transport mechanisms and energy conditions influencing the sedimentary deposition process.

According to Sahu (1964), the variations in the energy and fluidity factors seem to have excellent correlation with the different processes and the environment with the different processes and the environment of deposition. The process and environment of deposition of the sediments were deciphered by Sahu's linear discriminate functions of Y1 (Aeolian, Beach), Y2 (Beach, shallow agitated water), Y3 (Shallow Marine, Fluvial) and Y4 (Turbidity, Fluvial).

He established several discriminant functions by multivariate analysis in order to distinguish between adjacent mechanisms and environments that have closely related energy conditions.
It is possible to differentiate between aeolian, marine, fluvial and turbidity current mechanisms and between littoral and shallow agitated water environments within the spectrum of marine depositional processes. Environments identified from textural studies and evidence from sedimentary structures in the present study ranged from fluvial through Deltaic to Shallow Agitated marine to marine depositional environments. In order to refine interpretations from the aforementioned sources, it is considered necessary to adopt the following multi-discriminatory functions as described by Sahu (1964) for sand populations sampled in the study area.

Discrimination between Aeolian Process and Littoral (Intertidal Zone) Environment

The following equations can be used according to (Sahu 1964):

$$Y_1 = -3.5688M_z + 3.701\delta_1^{\,2} - 2.0766S_K + 3.1135K_G \qquad 3.6$$

Where, Mz = is the mean grain size,

$\delta_1^{\,2}$ = is the inclusive graphic standard deviation (sorting),

S_K = is the skewness, and

K_G = is the graphic kurtosis.

When Y1 is less than -2.7411, Aeolian deposition is indicated, whereas if Y1 isgreater than -2.7411, a beach environment is suggested.

Discrimination between Beach (Back Shore) and Shallow Agitated Marine Environment

The following equation was used according to (Sahu 1964):

$$Y_2 = 15.6534M_z + 65.7091\delta_1^{\,2} + 18.10871S_K + 18.5043K_G \quad 3.7$$

If the value of Y2 is less than 65.3650, beach deposition is suggested. If it is greater than 65.3650, a shallow agitated marine environment is likely. Discrimination between Shallow Marine and the Fluvial Environment, The following equation was used according to (Sahu 1964):

$$Y_3 = 0.2852M_z - 8.7604\delta_1^{\,2} - 4.8932S_K + 0.0482K_G. \quad 3.8$$

When Y3 is less than -7.419, the sand is identified as a fluvio-deltaic deposit, and if greater than -7,419 the sample is identified as a shallow marine deposit. The Plotting of the three discriminate functions (Y1, Y2 and Y3) as bivariate scatter plots was used to improve the success rate and refinement of the discrimination of the depositional environment. Sahu (1964) relates skewness and kurtosis values to selective action through the frequency of occurrence of velocity values. Folk and Ward (1957) suggest that non-normal values of skewness and kurtosis result from the mixing of two log-normally distributed particle populations. The environmental interpretation depends on three key parameters: Y1, Y2, and Y3**,** each with specific thresholds that determine the depositional setting. When Y1 is below -2.74, the environment is classified **as** Aeolian, indicating wind-dominated conditions such as deserts or sand dunes. Conversely, if Y1 exceeds -2.74**,** the setting shifts to a Beach environment, typical of coastal wave action. For Y2, values under 65.37 also suggest a Beach environment, while higher values (Y2 > 65.37) point to Shallow Agitated Marine conditions, where stronger wave or tidal energy prevails. Lastly, Y3 distinguishes between Fluvio-deltaic (Y3 < -7.42) and Shallow Marine (Y3 > -7.42) settings. The former implies river-influenced deltaic systems, while the latter indicates calmer, open-marine shelves..

Sahu (1964) visualizes kurtosis as a sorting ratio for frequency curves and suggests a high kurtosis value reflects a depositing medium where velocity fluctuations were restricted to those carrying material of size coincident with that of the size in the central 50% of the distribution for a greater length of time than normal. Kurtosis may well, therefore, relate directly to the energy level and energytime relationship within any given environment. Environments identified from textural studies and evidence from sedimentary structures in the present study ranged from fluvial through Deltaic to Shallow Agitated marine to marine depositional environments.

3.2.5.3 Quantitative Paleo Dynamics

3.2.5.3.1 Bedform Height (Hm) and Paleo-Channel Depth (Dc)

The paleo-channel depth (Dc) and bedform height (Hm) – such as cross set thickness - are crucial parameters in understanding the flow dynamics of ancient river systems. The bedform height (Hm) was estimated from the mean cross-set thickness (Sm) using the empirical relationship given by Leclair and Bridge (2001):

$$Hm = 2.90 \times 0.70 \times Sm \quad 3.9$$

Hm is the mean dune height; Sm is the mean cross-set thickness. The mean dune height (Hm) is typically 8 to 10 times the mean cross-set thickness (Sm). The channel depth (Dc) can be estimated from the bedform height (Hm) using the empirical relationship:

$$Dc = 11.6 \times Hm^{0.8} \quad 3.10$$

The paleo-channel flow depth (Dc) was estimated from the thickness of lateral macroforms using the equation:

$$Dc = D*/0.9 \quad 3.11$$

Where $D*$ is the maximum channel bankfull flow depth, which is represented by the thickness of the sandstone macroform.The empirical equation above is prefereed in this work.

3.2.5.3.2 Paleo-Channel Slope

Paleo-channel slope (Sc) is an important parameter in reconstructing the paleoenvironmental conditions of ancient river systems. Slope affects river plan form and facies boundaries, and paleoslope can be calculated using physics-based methods or empirical equations.
One empirical equation used to estimate paleoslope is:

$$Sc = \tau bf50 \ RD50 / Dc \quad 3.12$$

where Sc is the paleoslope, τbf50 is the bankfull Shields number for dimensionless shear stress, Dc is the mean bankfull channel flow depth, R is the submerged dimensionless density of sand-gravel sediment, ρs is the grain density, ρw is the fluid density, and D50 is the median grain size.

.3.2.5.3.3 Boundary Shear Stress

The boundary shear stress (τb) is a critical parameter in understanding the dynamics of sediment transport and the movement of bed materials in open channels. The boundary shear stress can be calculated using the following equation:

$$\tau b = \rho g D c S c \qquad 3.13$$

where τb is the boundary shear stress, ρ is the fluid density, g is the gravitational acceleration, Dc is the averaged channel flow depth, and Sc is the averaged water-surface paleoslope. Both field and laboratory experiments have shown that initial motion of bed materials in coarse-medium grained rivers typically occurs at a transport stage that is moderate (Andrews, 1984). This relationship between the flow and its container can be applied to all natural channels with some error and has been recently applied in ancient fluvial deposit (Ninke, 2002)

3.2.5.3.4 Critical Shear Stress

The critical shear stress (τcr) represents the necessary boundary shear to move the bed-load materials, based upon their grain size, grain shape, effective density, and roughness. For non-cohesive sand, the critical shear stress can be calculated using the equation provided by Shields (1939) as follows:

$$tcr = \tau * (\rho s - \rho w) \qquad 3.14$$

where τcr is the critical shear stress, $\tau*$ is the Shield number for the given particle, ρs is the grain density (assumed to be quartz with a density of 2650 kg/cm³), ρw is the fluid density (1000 kg/m³), g is the acceleration due to gravity in m/sec², and D50 is the median particle size in meters.

Sediment mobility for a given particle size occurs when the boundary shear stress exceeds the critical shear stress, i.e.

$\tau b > \tau cr$.

This relationship has been observed in the Ajali sandstones of the present study.

3.2.5.3.5 Paleoflow Velocity

Paleoflow velocity is the velocity of the ancient sediment flows that occurred in a specific region or basin. Paleoflow velocity (Vc) is a critical parameter in understanding the dynamics of sediment transport and the movement of bed materials in open channels. Two methods are commonly used to compute the threshold mean velocity (Vc): the Manning roughness coefficient (n) and the Darcy-Weisbach friction factor (f).

Manning Roughness Coefficient

The Manning roughness coefficient (n) is used to compute the threshold mean velocity (Vc) as follows:

$$Vc = R^{0.67} Sc^{0.50} n \qquad 3.15$$

Where

Vc is the paleoflow velocity, R is the hydraulic radius, Sc is the channel slope, and n is the Manning roughness coefficient.

3.2.5.3.6 Darcy-Weisbach Friction Factor

The Darcy-Weisbach friction factor (f) is used to compute the threshold mean velocity (Vt) as follows:

$$Vc = (8gR(Sc/f))^{0.50} \qquad 3.16$$

Where Vc is the paleoflow velocity, g is the gravitational acceleration, R is the hydraulic radius, Sc is the channel slope, and f is the Darcy-Weisbach friction factor. Unlike the Manning empirical equation, the Darcy-Weisbach equation uses a dimensionless friction factor, has a sound theoretical basis, and exact accounts for the acceleration from gravity; moreover, the relative bed roughness does not influence the exponents of hydraulic radius and channel slope. For these reasons, the DarcyWeisbach equation is preferred over the Manning approach as discussed by Ferguson (2010).

3.2.5.3.7 Rouse Number (Z) for Sediment Transport

The Rouse number (Z) is a non-dimensional scale parameter used to determine the dominant mode of sediment transport. It is calculated as:

$$Z = Ws / \beta\kappa U* \quad 3.17$$

where β is a constant (taken as 1), κ is the von Karman constant (taken as 0.40), U∗ is the boundary shear velocity, and Ws is the sediment settling velocity. Rouse Number and Sediment Transport. The Rouse number (Z) is used to determine the dominant mode of sediment transport. For Z > 2.5, the dominant mode is typically bed load, while for 1.2 < Z < 2.5, it is 50% suspended load (mixed load).

3.2.5.3.8 Sediment Settling Velocity

The sediment settling velocity (Ws) is calculated as a function of grain size according to Ferguson & Church (2004) as:

$$Ws = Rg(D50)^2 / C1v + (0.75C2Rg(D50)^3)^2 \quad 3.18$$

where g is the Earth's gravitational acceleration, D50 is the median diameter of a particle, v is the kinematic viscosity of water, v is the kinematic viscosity of water (110^{-6} for water at 20° C and C1 = 18 and C2 = 1 are constants associated with grain sphericity and roundness.

3.2.5.3.9 Boundary Shear Velocity

The boundary shear velocity (U) is determined as:

$$U* = \sqrt{\tau b} / \rho w \quad 3.19$$

where τb is the boundary shear of the fluid and ρw is the mass density of the fluid.

3.2.5.3.10 Reynolds Particle Number (Rep)

The Reynolds particle number (Rep) is a dimensionless number used to collaborate inferred sediment transport modes. It is calculated as:

$$Rep = \sqrt{RgD50D50/v} \quad 3.20$$

where R is the hydraulic radius, g is the gravitational acceleration, D50 is the median diameter of a particle, and v is the kinematic viscosity of water.

The Reynolds Particle Number (RepRe_pRep) varies widely depending on the fluid flow conditions and the particle characteristics, with distinct ranges indicating different flow regimes. At **low Reynolds numbers** (Rep<10Re_p < 10Rep<10), the flow is laminar, characterized by smooth and predictable patterns. In the **transition region** (10≤Rep≤200010 \leq Re_p \leq 200010≤Rep≤2000), turbulence begins to develop, marking a shift from laminar to turbulent flow. At **high Reynolds numbers** (Rep>2000Re_p > 2000Rep>2000), the flow becomes fully turbulent, exhibiting chaotic and unpredictable behavior. These ranges help in understanding and predicting the dynamics of particle-fluid interactions in various environments.

3.2.5.3.11 Froude Number (Fr)

The Froude number (Fr) is a dimensionless parameter that describes different flow regimes in open channel flows. It is a ratio of inertial and gravitational forces. The Froude number (Fr) is a ratio of the inertial force (proportional to the square of the velocity) to the gravitational force (proportional to the depth). When the Froude number is greater than unity, the flow is supercritical, and when it is less than unity, the flow is subcritical.

The Froude number (Fr) is calculated as:

$$Fr = gDcVc \quad 3.21$$

where:

Vc is the water flow velocity, Dc is the bankfull channel depth, g is the acceleration due to gravity (approximately half of the present during Permian times, i.e., 4.9 m/sec^2).

The Froude number characterizes flow types based on the balance of inertial and gravitational forces. Subcritical flow occurs when the Froude number is less than 1 (Fr < 1), where gravitational forces dominate, resulting in slow and tranquil flow that allows disturbances to propagate both upstream and downstream, as seen in rivers, lakes, and slow-moving streams.

Critical flow occurs at Fr = 1, where inertial and gravitational forces are balanced, producing an unstable flow often associated with standing waves, such as in hydraulic jumps where the flow transitions between subcritical and supercritical states. Supercritical flow, with Fr > 1, is dominated by inertial forces, characterized by fast and rapid flow, where disturbances are only transmitted downstream, as observed in rapids, waterfalls, and fast-moving streams.

Tables of formulas (Table 3.2) for calculating hydrodynamic parameters serve as essential tools for analyzing fluid flow and sediment transport in geological and engineering studies. These tables typically include equations for key parameters such as the Froude number, Reynolds number. Other important formulas include mean dune height, water depth and paleoflow velocity.

Table 3.2 Hydrodynamic Parameters, Empirical Formulae and Citations

Parameter	Empirical Equation	Citations
Mean Dune Height (Hm)	Hm =2.90×0.70×Sm Sm = mean cross-set thickness	Leclair& Bridge, 2001
Water Depth(Dc)	$Dc = 11.6 \times Hm^{0.8}$	Bridge (2003).
Paleoflow Velocity	$Vc = R^{0.67}\ Sc^{0.50}\ n$ R =hydraulic radius, Sc=slope of water, n= Manning roughness coefficient.	Chow (1959)
Slope of water(Sc)	Sc = τbf50 RD50 / Dc τbf50 = bankfull Shields number, D50=mean diameter	Buffington & Montgomery (1997) Khan & Tewari, 2015
Rouse Number (Z)	$Z = Ws / \beta\kappa U*$	Rouse, 1937
	$Ws = Rg(D50)^2 / C1v + (0.75C2Rg(D50)^3)^{2.}$ v = kinematic viscosity of water (1x10-6 for water at 20' C and C1 = 18 and C2 = 1 are constants	Cheng (2009)
Reynolds Particle Number (Rep)	Rep =√RgD50D50/v	Cheng, 2009
Froude Number (Fr)	Fr =V c/√ g Dc	Chow, 1959

CHAPTER FOUR
RESULTS AND DISCUSSION

4.1 RESULTS

4.1.1 Lithostratigraphic Studies

4.1.1.1 Lithostratigraphic Description of Nsukka Fm. Section at Isukwato Valley

The studied outcrop represents a segment of the Nsukka Formation, situated in Umuasua, Isikwuato Local Government Area (LGA) of Abia State, Nigeria. Located within a valley nestled between two hills in Umuasua, the outcrop is positioned at Latitude 5.7207 and Longitude 7.5006, with an elevation of approximately 610 feet above sea level. The Nsukka Formation is renowned for its geological significance within the Anambra Basin, offering insights into the sedimentary history and paleoenvironmental conditions of the region.

The outcrop comprises a sequence of nine distinct lithological units, each exhibiting varying lithologies and sedimentary characteristics (Table 4.1, Figure 4.1 and Plate 4.1). These units are

Table 4.1.Table showing the Lithostratigraphic Description and interpretation of Nsukka Formation at Isukawato

Units	Description	Sedimentary Structures	Comments	References
1. Fissile Shales with Concretions	Thin, flat layers of shale with localized mineral concentrations	Fissile structure, concretions	Low-oxygen, pore-water-rich environment	Bridge, 2009
2. Fine Grained and Dirty White Sandstone	Fine-grained sandstone with abundant fauna	Fossil remains	Shallow marine or beach environment	Dalrymple, 2010
3. Nodule Bands	Alternating layers of concretions and host sediment	Banded structure	Cyclic variations in sedimentary conditions	Bridge, 2009
4. Shale and Yellowish Gray Siltstone	Dark gray to yellow-brown shale; yellowish gray siltstone	Color variations, possible pyrite	Changing redox conditions; low-energy marine or lacustrine setting	Selley, 1998
5. Laminated Shales with Silt Banding	Alternating layers of shale and silt	Laminations, banding	Cyclical variations in sedimentation	Bridge & Demicco, 2008
6. Fine Sandstone with Flaser Bedding	Fine sand with mud layers	Flaser bedding	Tidal or estuarine environment	Dalrymple, 2010
7. Laminated Shales with Silts	Alternating layers of shale and silt	Laminations	Rhythmic sedimentation in low-energy environment	Bridge & Demicco, 2008
8. Whitish Gray Nodular Fractured Mudstones	Mudstone with nodules and fractures	Nodular structure, fractures	Diagenetic processes and post-depositional changes	Selley, 1998
9. Mud Drapes on Mega Ripples, Flaser Bedding With Mud Clasts	Large-scale bedforms with mud drapes and clasts	Mega ripples, flaser bedding, mud clasts	High-energy, dynamic nearshore or estuarine environment	Selley 1998

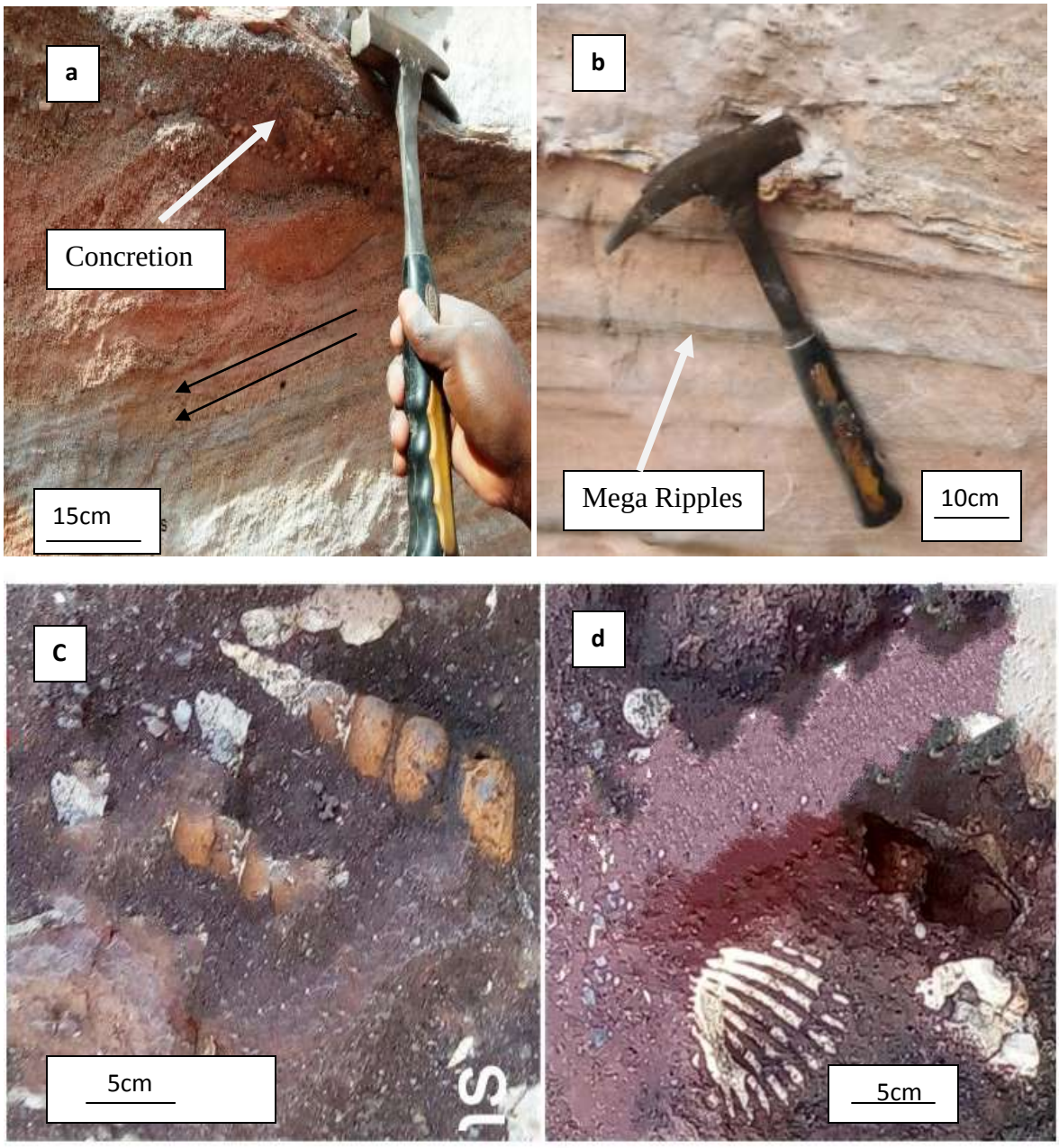

Plate 4.1: Isukwato Outcrop. a. Concretion deposits marked with an arrow at upper part. The down part has planar crossbeds with arrows showing the direction of apparent movement b. Mega Ripples within Nsukka Formation. C. Mollusc in Umuasua Section D. Cretaceous Pelecepods in Umuasua section

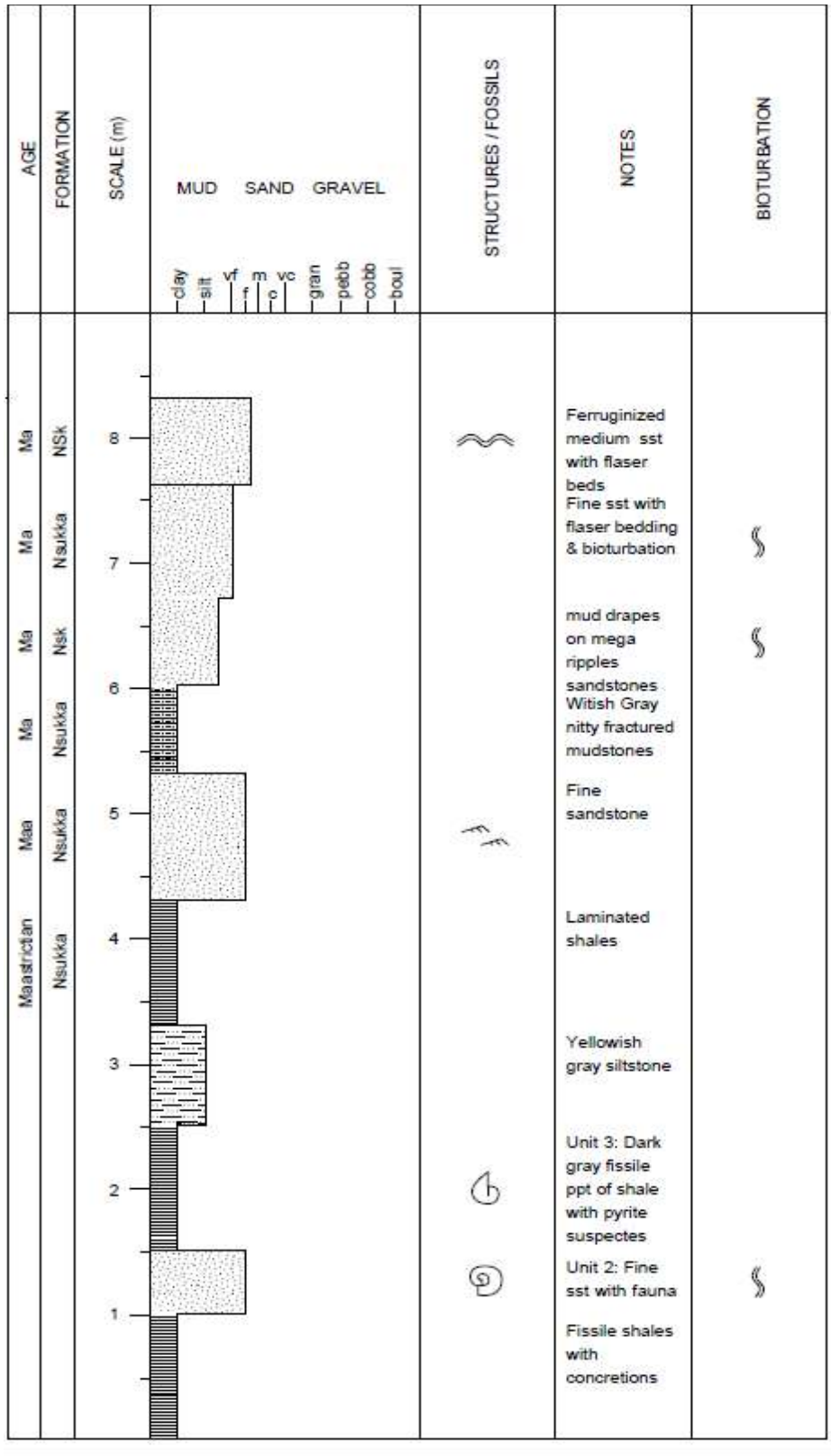

Figure 4.1 Lithographic Section of Nsukka Formation in Umuasua Valley Outcrop

meticulously logged into units and documented to provide a comprehensive understanding of the stratigraphic succession present. Spanning a lateral distance of approximately 18 meters, the outcrop offers a substantial exposure of the Nsukka Formation, facilitating detailed geological analysis and interpretation mud-rich sediments and their redeposition in high-energy settings. The presence of these features provides a window into the complex interplay of sediment transport, sediment reworking, and changing flow conditions.

4.1.1.2 Lithostratigraphic Description of Nsukka Formation Exposed at Akara Junction, Isikwuato

The outcrop is located at a gas station along a road cut on the Ohafia-Umahia Road. It's roughly 300 meters from Akara Junction, within the Isikwuato area of Abia State. The specific coordinates are 5.7172 Latitude and 7.5649 Longitude, at an elevation of 449 feet above sea level.This rock exposure displays three distinct layers of clastic sediments, spanning approximately 5-meter stretch.

The bottom layer (Unit 1) is 3 meters thick and composed of slightly fissile, mottled mudstones with some internal ring-like structures. This layer is capped by a thin, hard layer of shale. Above this sits Unit 2, a 0.6-meter-thick section of mudstone with mottled coloration and no visible sedimentary structures. This layer is capped by a 1.5-centimeter-thick, firm layer with ripple-like features. The final layer (Unit 3) is 1.2 meters thick and consists of reddish-brown, medium-grained sandstone with occasional signs of burrowing activity (bioturbation). This top layer is weathered on its surface.

The sedimentary geology observation described suggests a sequence of depositional events and environmental conditions. Unit 1, the bottom layer, indicates deposition in a relatively calm aquatic environment characterized by mudstone with slight fissility and mottled appearance, possibly indicative of alternating sediment sources or depositional conditions. The presence of internal ring-like structures suggests possible biogenic or diagenetic processes. The thin, hard layer of shale capping Unit 1 could represent a period of increased sedimentation rate or a change in depositional conditions leading to the deposition of finer-grained sediment.

Unit 2, above Unit 1, lacks visible sedimentary structures, suggesting a relatively homogeneous deposition, possibly under low-energy conditions. The firm layer with ripple-like features on top of Unit 2 indicates the influence of gentle water movement or current activity during deposition.

Finally, Unit 3, the top layer, composed of reddish-brown, medium-grained sandstone (Figure 4.2), suggests deposition in a higher energy environment, such as a river channel or beach setting, where sediment transport and deposition occurred under more energetic conditions. The occasional signs of burrowing activity (bioturbation) within Unit 3 indicate some disturbance of the sediment by benthic organisms after deposition. The weathering observed on the surface of Unit 3 suggests exposure to atmospheric conditions over time, indicating a period of erosion and weathering subsequent to deposition. Overall, the observation reflects a sequence of sedimentary deposition in varied environmental settings, possibly indicative of changing depositional environments or conditions over time. (Plate 4.2, Figure 4.2).

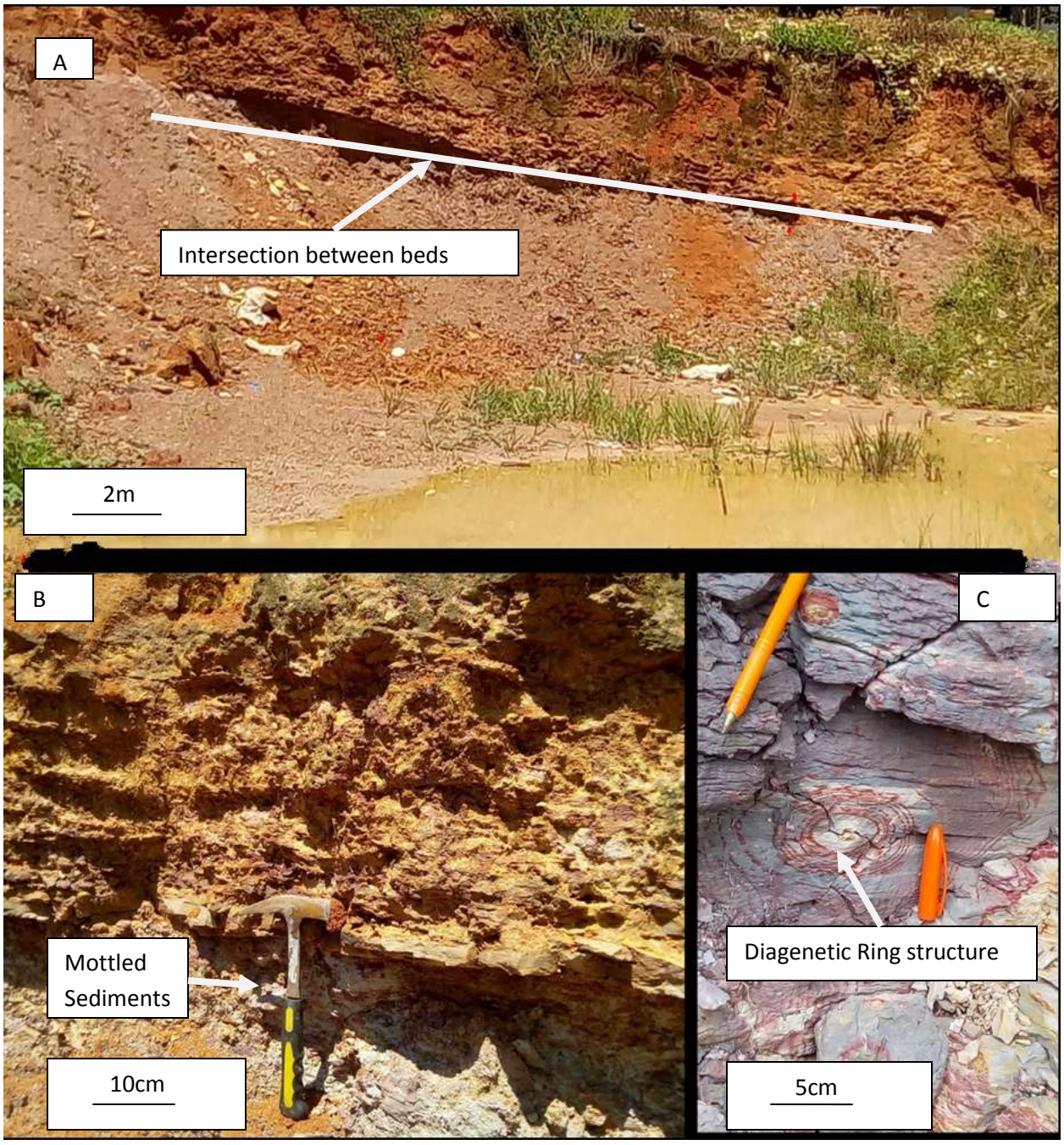

Plate 4.2 Outcrop section at Akara Junction along Ohafia – Umahia Rd showing (A) intersection between beds (B.) mottled sediment (C.) some diagenetic ring structures of Nsukka shale

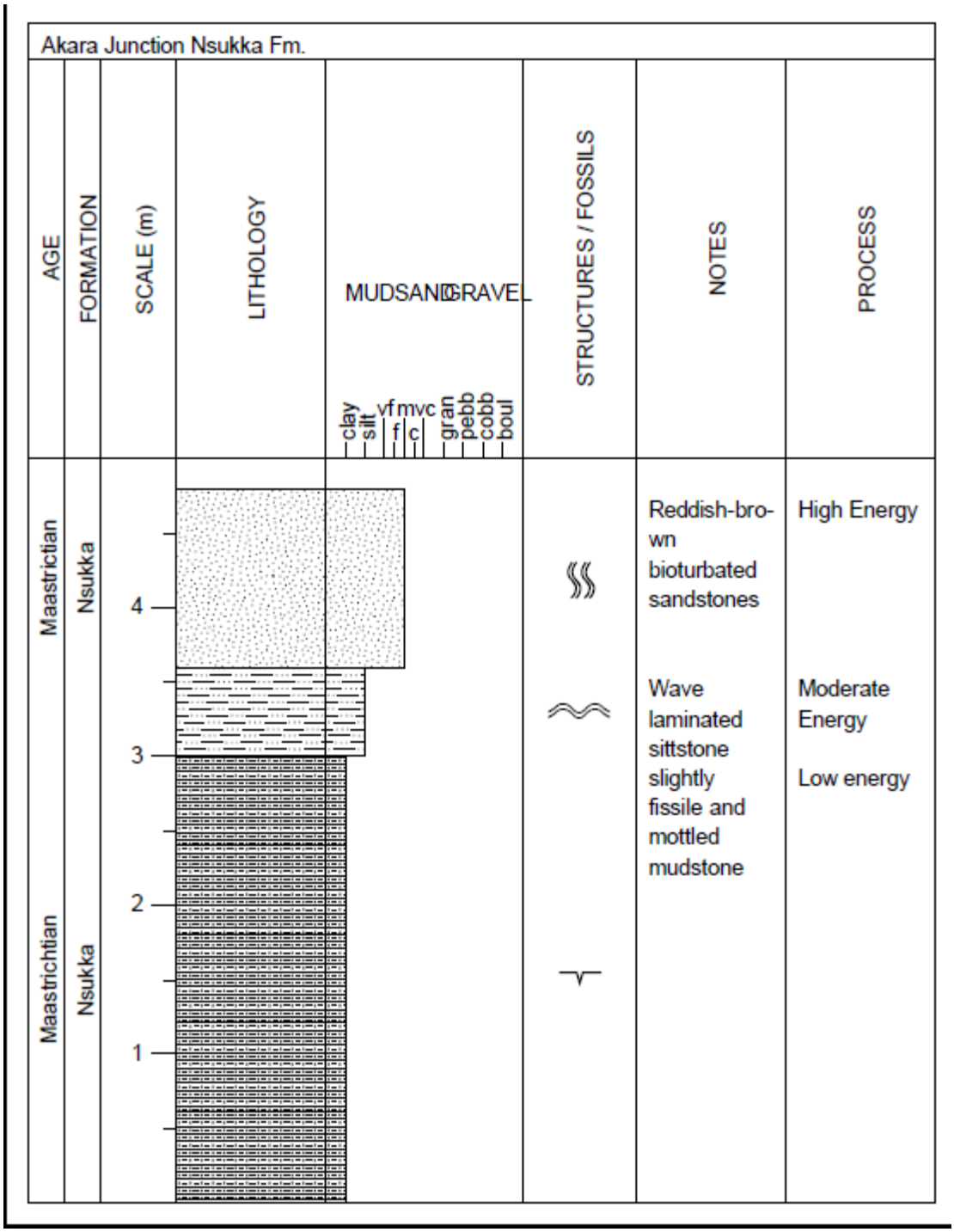

Figure 4.2 Lithographic Section of Nsukka Formation in Akara Junction Outcrop

4.1.1.3a Lithostratigraphic Description of Ajali Formation at Onyekaba Mine

Onyekaba Mine is situated at Latitude 7.35817 and Longitude 5.80436, with an elevation of 170 meters above sea level. It is positioned in the northern part of Okigwe, a city in southeastern Nigeria. This location places the mine within the geographical coordinates of Okigwe, specifically toward its northern boundary. Okigwe is known for its diverse geological formations (Table 4.2, Plate 4.3 and Figure 4.3) and active quarrying activities, making Onyekaba Quarry an integral part of the region's extractive industry.

Human activities in Onyekaba Mine, including quarrying, mining, and construction, are causing significant damage to geological structures such as rock formations and landscapes. These activities lead to physical alterations, destabilization of slopes, and contamination of soil and groundwater, posing environmental risks and long-term consequences. Sustainable land management practices and effective regulation of human activities are essential to mitigate the damage to geological structures and ensure the protection of the natural environment in the mine.

Table 4.2.Table showing the Lithostratigraphic Description and interpretation of Ajali Formation at Onyekaba Mine

Unit	Description	Sedimentary Characteristics	Comments
Unit 1	Very coarse sandstone	Granular texture, variable color, moderate to high hardness, potential porosity, well-defined bedding, cross-bedding	Indicates a dynamic fluvial or aeolian environment with varying sediment sources and conditions. The porosity suggests potential dissolution of minerals or compaction during diagenesis.
Unit 2	Coarse sandstone with wave ripple and cross-lamination	Pronounced grain size, wave ripple structures, cross-lamination	Suggests a high-energy nearshore or shallow marine setting with significant water wave and current action. Cross-lamination indicates a dynamic depositional environment with alternating sediment transport directions.
Unit 3	Heterolithic beds	Mixed sediment with varying grain sizes and compositions	Reflects shifting depositional settings and changing sediment sources. Variations in grain size indicate changes in water energy and sediment supply, showing a complex interplay of environmental factors.
Unit 4	Coarse-grained sandstone with varying colors and occasional fossil content	Coarse-grained, shades of red and brown, well-defined bedding, occasional cross-bedding	Points to high-energy environments such as river channels or nearshore settings. The red and brown colors suggest oxidizing conditions. Fossils provide insights into past ecosystems.
Unit 5	Sediment beds with plant roots and bioturbations	Alternating sand and mud, plant fossils, primarily roots	Indicates periodic changes in sediment supply and energy conditions. The presence of plant roots and bioturbation reflects past vegetation and biological activity, influencing sediment stability and composition.
Unit 6	Sediment with plant fossils like Glossopteris and Vertebraria	Granular texture, variable color, plant fossils	Suggests variable energy conditions and past terrestrial vegetation. Plant fossils help infer ancient flora and paleoclimatic conditions.
Unit 7	Sediment with current ripple cross-lamination	Smoother texture, varying colors, current ripple cross-lamination	Indicates high-energy environments with significant water flow. The smoother texture results from current sorting and abrasion, while varying colors suggest changes in redox conditions.
Unit 8	Fine to coarse-grained Ajali Sandstone	Textured appearance, variable colors (red to brown), possible plant fossils	Reflects variable energy conditions and mixed grain sizes. Textured appearance indicates varying sediment supply, and colors suggest oxidizing conditions. Plant fossils provide information on past vegetation.
Unit 9	Fine-grained silt	Fine-grained texture, shades of red and brown, high bioturbation	Shows a high rate of bioturbation indicating biological activity. The fine-grained texture and colors suggest oxidizing conditions and a dynamic ecosystem with active sediment mixing.
Unit 10	Coarse-grained sediment	Granular texture, colors ranging from red to brown	Indicates high-energy conditions for coarse particle deposition. The granular texture and red-brown colors suggest oxidizing conditions and sediment transport processes.

4.1.1.3b Lithostratigraphic Description of Modern Alluvial Fan in Onyekaba Mine

The formation of a modern alluvial fan, such as the one found in Onyekaba Quarry, (Plate 4.4) involves several key processes that contribute to the development of its distinctive features, including steep slopes, alluvial fan morphology, ephemeral stream channels, and feeder channels. The formation of a modern alluvial fan in Onyekaba Quarry involves the erosion of sediment from steep slopes, deposition of sediment in a fan-shaped pattern at the base of the slope, development of ephemeral stream channels to convey water and sediment across the fan surface, and the presence of feeder channels that deliver sediment to the main stream channels. These processes collectively shape the morphology and characteristics of the alluvial fan landscape.

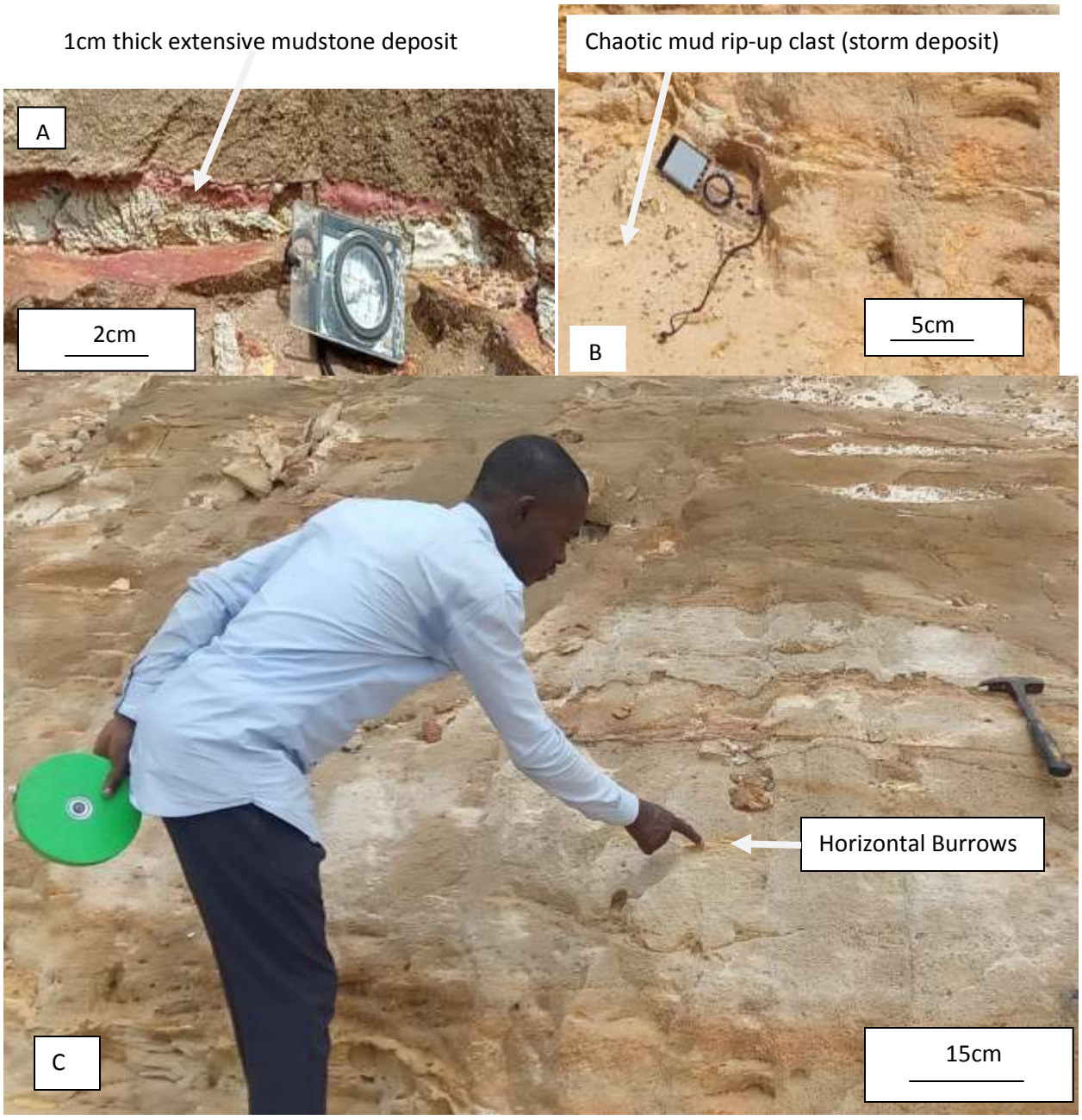

Plate 4.3 Outcrop of Ajali Sandstone exposed at Onyekaba Quarry showing A. The base of outcrop B, thin layer of claystone and C, horizontal burrows being poinyed by the researcher

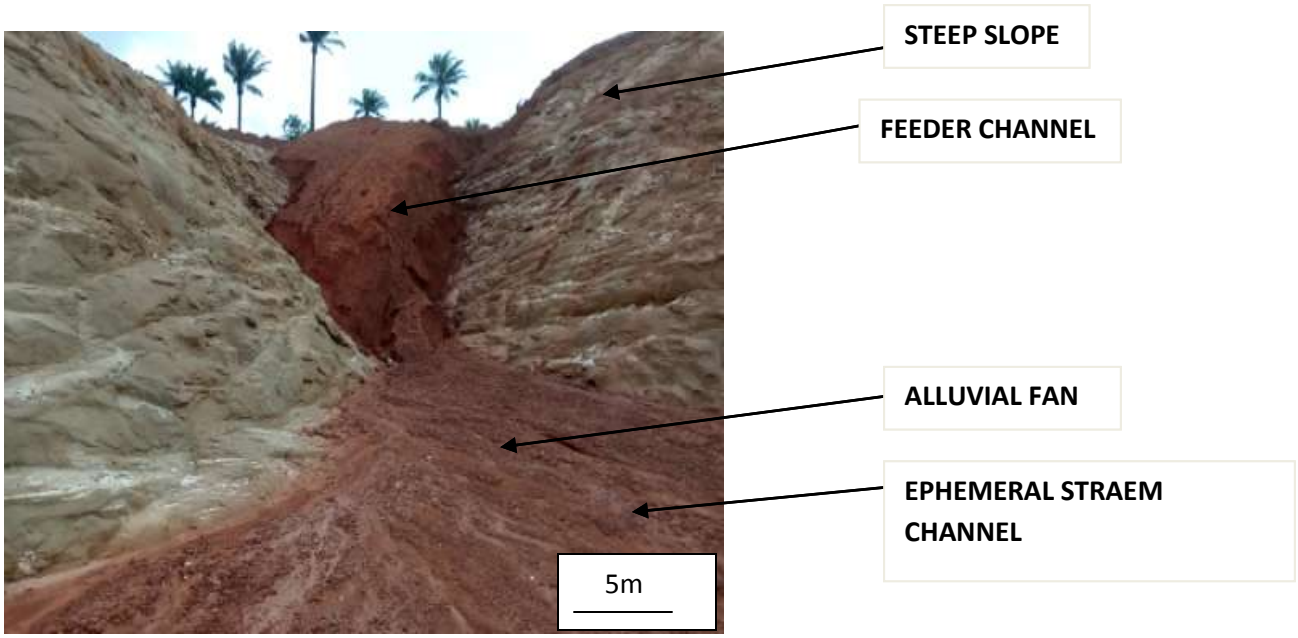

Plate 4.4. Modern Alluvial Fan, Onyekaba Quarry, Anambra Basin, Nigeria.

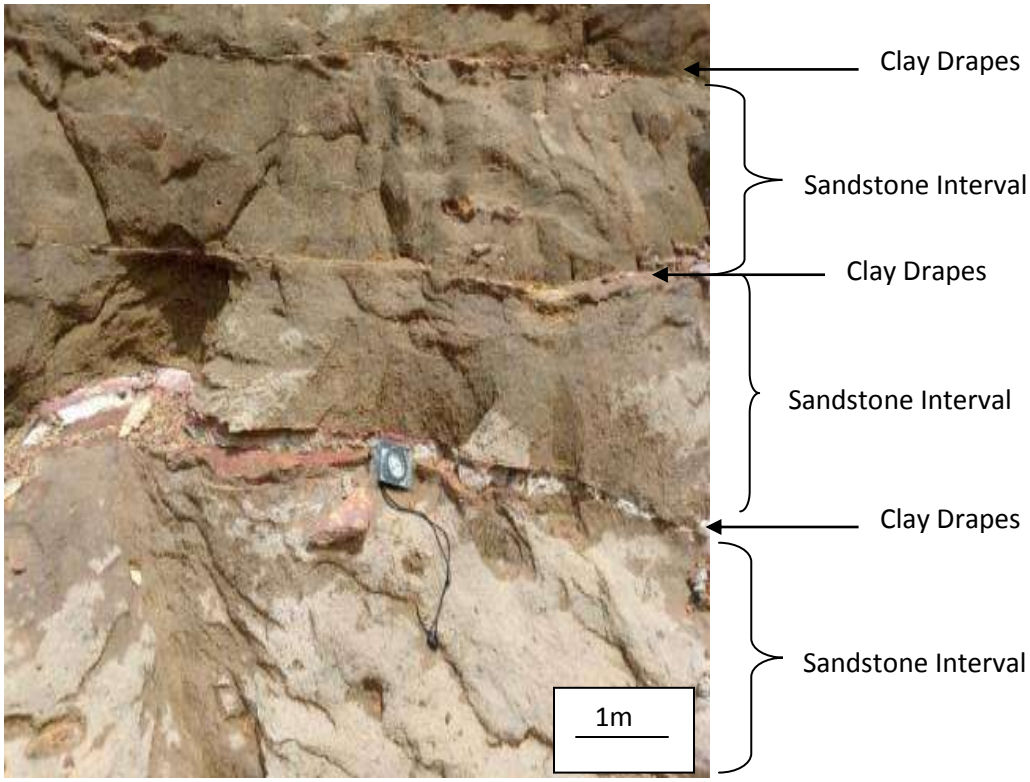

Plate 4.5. Alternating Sandstone and Clay Drapes, Ajali Formation at Onyekaba Mine

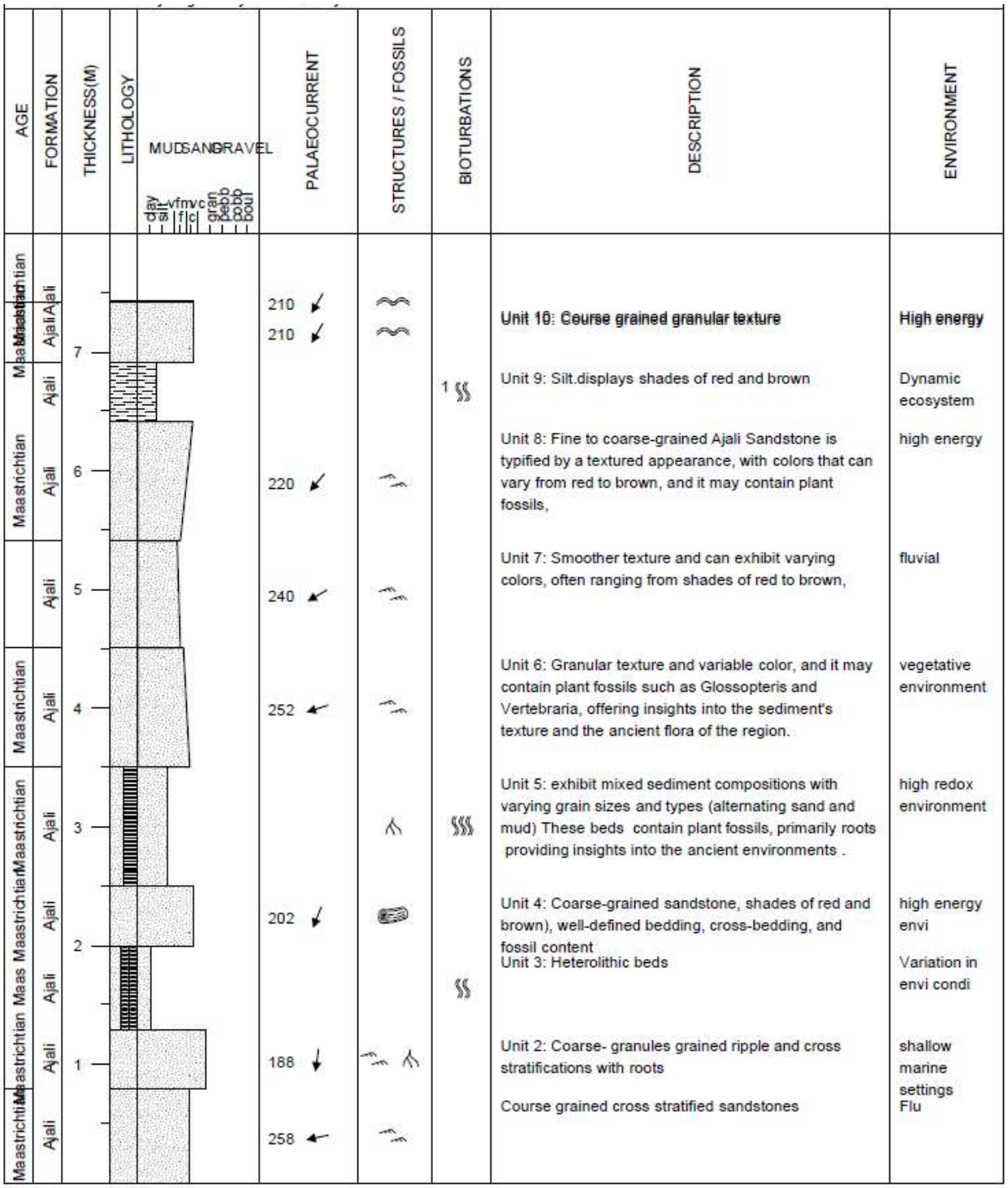

Figure 4.3 Lithostratigraphic Log of Ajali Sandstone Formation at Onyekaba Mine

4.1.1.4 Lithostratigraphic Decription of Ajali Formation Exposed at Uturu (Near ABSU)

The Ajali Sandstones, situated near Abia State University along the Uturu-Okigwe Road in the Anambra Basin, offer a fascinating geological spectacle. The stratigraphic sequence presents a layered composition, revealing distinct sedimentary features that provide valuable insights into the depositional environment and geological history of the region. At the base of the sequence lies planar crossbed fine sandstones adorned with clay drapes, indicative of a dynamic depositional setting characterized by shifting currents and sediment transport. These fine sandstones, with their characteristic crossbedding, suggest deposition in a fluvial or shallow marine environment where sedimentation occurred under energetic flow conditions.

Above the planar crossbed fine sandstones, the stratigraphic sequence transitions to coarser sedimentary layers. Topping the sequence are square sandstones, which likely signify a change in depositional environment or sediment source. The presence of pebbly sandstones suggests a higher energy environment, possibly indicating a transition to a nearshore or coastal setting. The coarse nature of the pebbly sandstones suggests greater energy during deposition, possibly due to the influence of wave action or tidal currents.

Further up in the sequence, the sedimentary layers exhibit rhythmic sandstones characterized by herringbone crossbeds, indicating complex depositional dynamics. These rhythmic sandstones may have formed in environments with fluctuating energy levels, such as tidal flats or deltaic systems. Additionally, the presence of bioturbations and horizontal tracks above the rhythmic sandstones hints at periods of sediment disturbance and colonization by organisms, further enriching our understanding of the paleoenvironmental conditions.

Capping the stratigraphic sequence are coarse sandstones, (Figure 4.4) which likely represent the culmination of sediment deposition in the area. The coarse nature of these sandstones suggests a high-energy depositional environment, possibly associated with river channels or nearshore environments characterized by intense sediment transport. The presence of these distinct sedimentary features within the Ajali Sandstones offers a window into the geological history of the Anambra Basin, providing geologists and researchers with valuable information about past environmental conditions and sedimentary processes in the region.

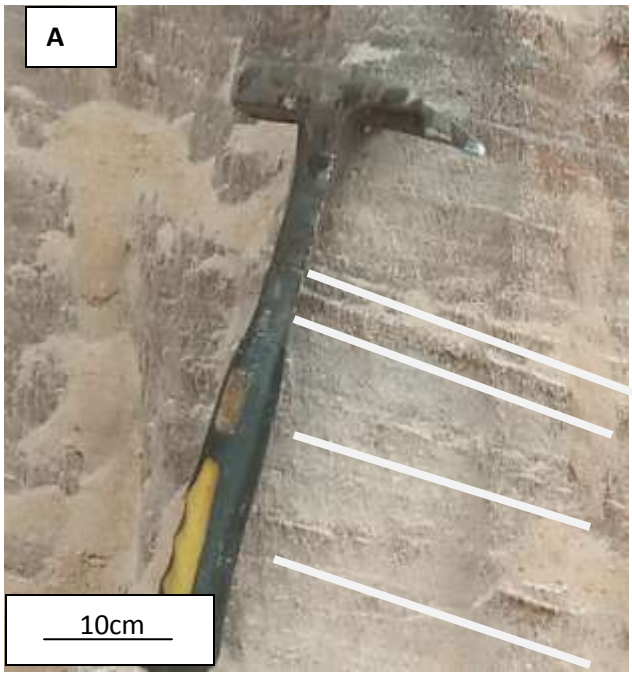

Plannar cross stratifications

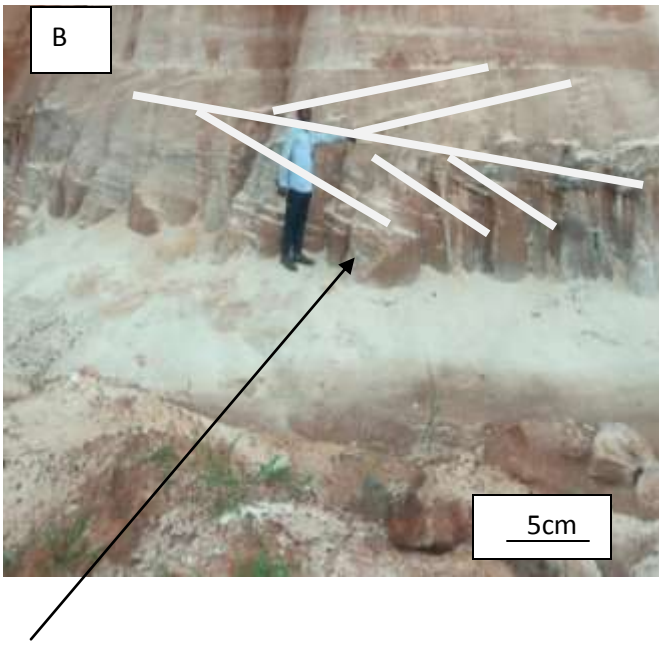

Herringbone xbed. Apparent movement is westward



Figure 4.6 A Close-Up Of An Outcrop With Multiple Sets Of (A) Planar Cross-Stratification.. They Points Towards The Southeast, Further Emphasizing The Direction Of The Dip.(B) Indicates The Herringbone Crosstratification. (C) The Image of White Sandstones

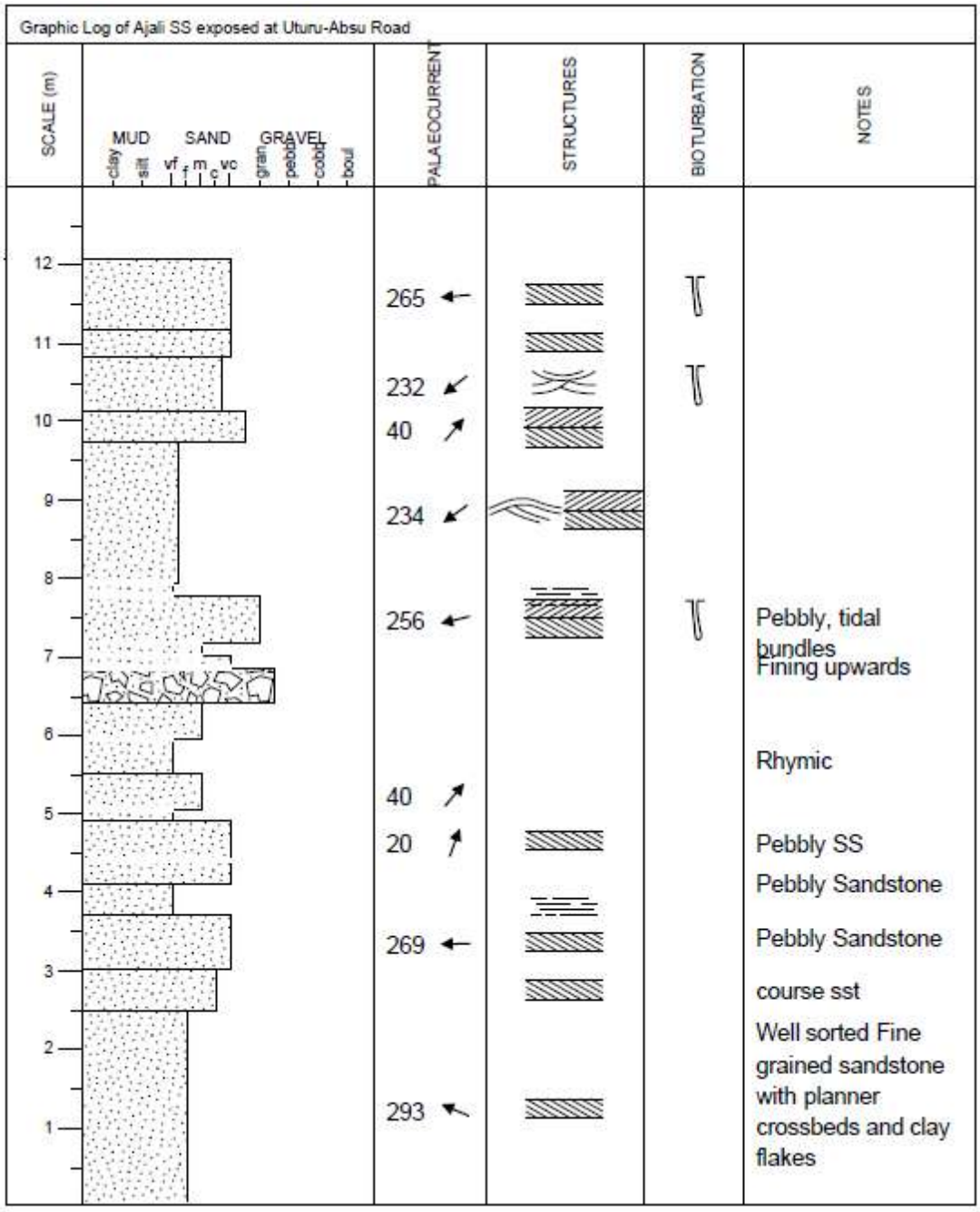

Figure 4.4 Lithostratigraphic Log of Ajali Sandstone Formation near ABSU (at Uturu--Okigwe Road)

.

4.1.1.5 Lithostratigraphic Decription of Mamu Formation Exposed at Ohafia

The sedimentary sequence comprises six distinct units with varying lithological characteristics. Unit 1 consists of dark gray shale exhibiting high fissility, alongside massive and nodular calcareous mudstones. Unit 2 comprises oolithic dark brown to reddish-brown sandstones containing Ophiomorpha burrows, suggesting a marine depositional environment. Unit 3 shares similarities with Unit 1, featuring dark gray fissile shale and calcareous nodules within massive mudstones. Unit 4 comprises fine-grained sandstones displaying reddish-brown coloration and horizontal burrows, indicative of bioturbation. Unit 5 consists of dark fissile shale interspersed with calcareous and massive mudstone nodules, while Unit 6 is characterized by fine-grained sandstones. This sedimentary succession reflects diverse depositional environments and processes, including marine and fluvial influences, along with periods of bioturbation and sedimentary facies changes.

The sedimentary succession described here represents a complex interplay of depositional environments and processes, characterized by alternating marine and non-marine conditions, as well as varying energy levels and sedimentary facies. Here is a detailed sedimentary geology interpretation of the sequence:

Unit 1: The presence of dark gray, fissile shale and massive calcareous mudstones suggests a low-energy, relatively deep marine depositional environment. The fissility of the shale indicates deposition from suspension settling in a quiescent, offshore marine setting. The calcareous nodules, within the mudstones may have formed through early diagenetic processes or as a result of localized variations in carbonate precipitation.

Unit 2: The oolithic dark brown to reddish-brown sandstones containing Ophiomorpha burrows are indicative of a high-energy, shallow marine environment. Ooids are spherical to ellipsoidal grains formed by the concentric accretion of calcium carbonate around a nucleus, typically in agitated, shallow marine waters. The presence of Ophiomorpha burrows, which are characteristic of the Psilonichnus ichnofacies, further supports a high-energy, nearshore or shoreface setting.

Unit 3: Similar to Unit 1, the dark gray fissile shale and calcareous nodules within massive mudstones suggest a return to low-energy, relatively deep marine conditions. This unit likely represents a transgressive phase or a deepening of the depositional environment, allowing for the accumulation of fine-grained sediments and the formation of calcareous nodules.

Unit 4: The fine-grained sandstones with a reddish-brown coloration and horizontal burrows indicate a shift towards a lower energy, potentially fluvial or marginal marine depositional environment. The horizontal burrows suggest bioturbation by organisms adapted to moderate to low energy conditions. The reddish-brown coloration may be attributed to the presence of iron oxides, which could result from oxidizing conditions or the influence of terrestrial sediment input.

Unit 5: This unit is comparable to Units 1 and 3, with dark fissile shale and calcareous nodules within massive mudstones, suggesting a return to low-energy, relatively deep marine conditions. The presence of calcareous nodules may indicate periodic fluctuations in carbonate precipitation or diagenetic processes within the marine environment.

Unit 6: The fine-grained sandstones in this unit suggest a transition towards higher energy conditions, potentially representing a deltaic or coastal depositional environment. The lack of distinct sedimentary structures or bioturbation features in the description may indicate that these sandstones were deposited under relatively high energy conditions, with limited time for the preservation of diagnostic features.

Overall, this sedimentary succession reflects a dynamic depositional history, alternating between fluvial and marine conditions, with varying energy levels and sedimentary facies changes. The presence of oolithic sandstones and Ophiomorpha burrows indicates periods of high-energy, shallow marine deposition (Figure 4.5), while the fissile shales and calcareous mudstones represent low-energy, relatively deep marine settings. The fine-grained sandstones with horizontal burrows suggest the influence of fluvial or marginal marine processes, potentially representing deltaic or coastal environments. This sequence highlights the complex interplay of depositional processes, sea-level fluctuations, and changes in sediment supply that shaped the basin's stratigraphic record.

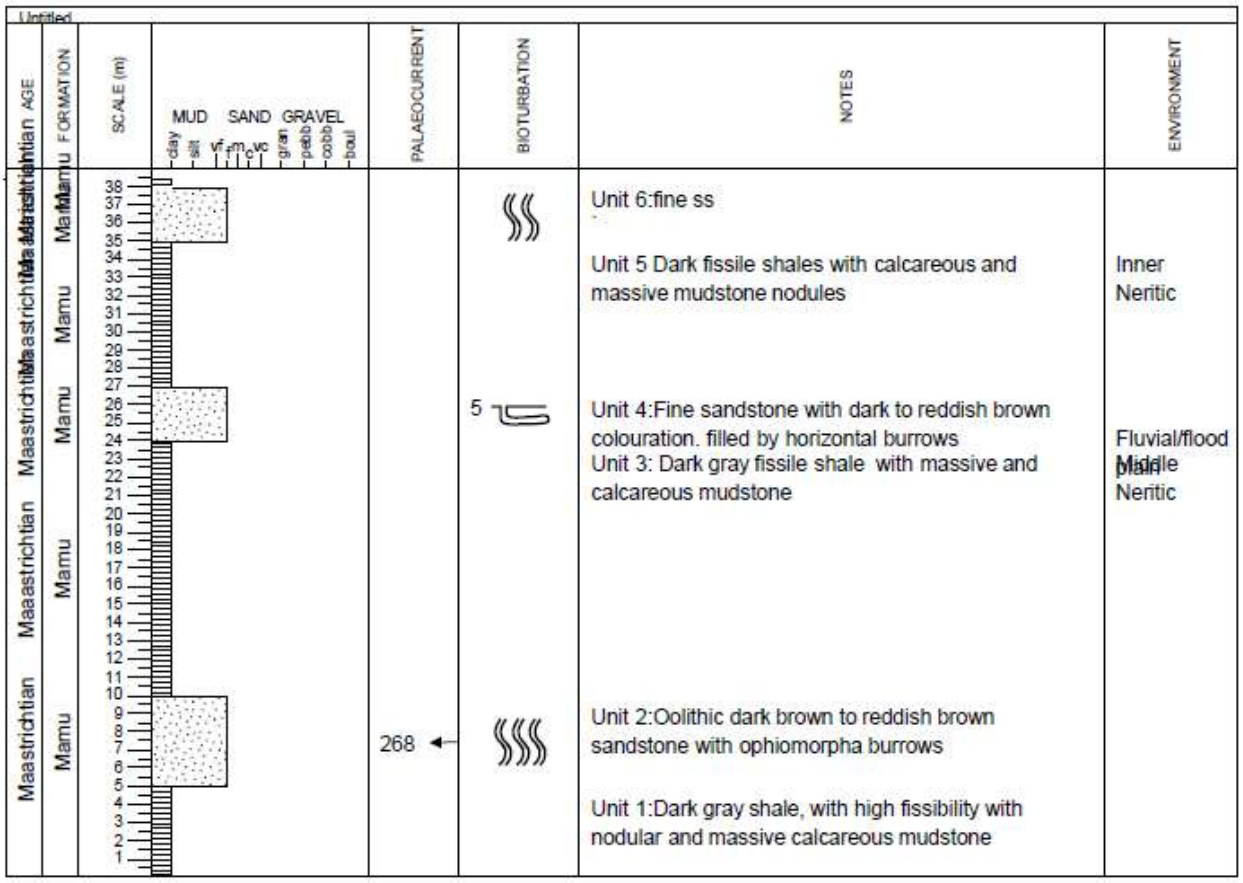

Figure 4.5: The Lithostratigrapic Log of Mamu Formation exposed at Ndi-Orieke, Akanu-Ohafia

4.1.1.6 Lithostratitigraphic Description of Mamu Formation Exposed at Ihube

The geographic coordinates of Ihube, with longitudinal and latitudinal values of 7.37264 and 5.85627 respectively, pinpoint its precise location within southeastern Nigeria. Ihube is a town located in southeastern Nigeria, specifically in the southeastern part of the country's Imo State. It lies within the southeastern region of Nigeria, which is characterized by lush vegetation, rivers, and a tropical climate.

Geographically, Ihube is situated inland, away from the coast, surrounded by other towns and villages in Imo State. It's part of the southeastern Nigerian landscape, which is known for its diverse cultural heritage, agriculture, and growing urban centers.

The town is accessible via road networks connecting it to nearby cities such as Owelli, the capital of Imo State, and other major towns in the region. It is within a region rich in natural resources and agricultural land, contributing to the local economy.

Unit 1 comprises fine sandstone exhibiting features such as crosstratification, wavy structures, herringbone crosstratification, and clay drapes. Unit 2 is characterized by pebbly sandstones, while Unit 3 displays poorly sorted fine sandstone with cross stratifications. Unit 4 contains clay/siltstone intercalations with ripple lamination, and Unit 5 is composed of poorly sorted fine-grained sandstone. Unit 6 is distinguished by well-sorted fine sandstone, differentiated by color and sorting from the layer below. Unit 7 consists of mudstones showing intense bioturbation. Unit 8 comprises fine-grained sandstone with ripple laminations, and Unit 9 consists of interbedded sands and mudstones.

The sedimentary sequence described presents a complex depositional history indicative of varied environmental conditions. Units 1 and 6, characterized by fine sandstone with distinct sedimentary structures and sorting patterns, likely represent deposition in low-energy environments with intermittent currents, allowing for the development of intricate bedding features like crosstratification and color differentiation. Unit 2, comprising pebbly sandstones, suggests higher energy conditions, possibly associated with fluvial or coastal processes. In contrast, Units 3, 4, and 5, exhibiting poor sorting and intercalations of clay/siltstone, indicate fluctuating energy levels and perhaps proximity to deltaic or shallow marine settings prone to sediment reworking. Unit 7's mudstones with intense bioturbation imply deposition in quiet,

possibly deeper water environments conducive to biological activity. Finally, Units 8 and 9, featuring fine-grained sandstones with ripple laminations and interbedded sands and mudstones respectively, (Figure 4.6, Table 4.3 and Plate 4.6) likely reflect cyclic changes in sediment supply and hydrodynamic conditions, possibly influenced by tidal or wave action. Overall, this sedimentary sequence suggests a dynamic depositional environment with varying energy regimes and sediment sources over time.

Table 4.3. Table Showing the Lithostratitigraphic Description of Mamu Formation Exposed at Ihube

Units	Lithology	Primary Sedimentary Structure	Comments
1	Fine sandstone	Cross-stratification, wavy structures, herringbone, clay drapes	Indicates dynamic environments with alternating current directions, such as tidal settings. Clay drapes suggest periods of low energy deposition.
2	Pebbly sandstones	Pebbly texture	Suggests high-energy environments capable of transporting and depositing larger sediment particles, such as river channels or beach environments.
3	Poorly sorted fine sandstone	Cross stratifications	Indicates moderate energy conditions with sediment transport, possibly in fluvial or shallow marine environments. Poor sorting suggests variable energy during deposition.
4	Clay/siltstone intercalations	Ripple lamination	Suggests lower energy depositional environments with periodic current or wave action, such as tidal flats or shallow marine settings.
5	Poorly sorted fine-grained sandstone	Poor sorting	Indicates deposition in variable energy conditions, possibly fluvial environments where sediments are not well sorted.
6	Well-sorted fine sandstone	Differentiated by color and sorting from the layer below	Suggests higher energy conditions allowing for better sorting of sediment particles, possibly in beach or aeolian environments.
7	Mudstones	Intense bioturbation	Reflects a biologically active environment with significant organism activity, indicating stable, low-energy marine or estuarine conditions.
8	Fine-grained sandstone	Ripple laminations	Indicates a depositional environment influenced by water currents or waves, such as shallow marine or fluvial settings.
9	Interbedded sands and mudstones	Interbedding of sand and mudstone layers	Suggests alternating energy conditions, likely in a deltaic or tidal environment where periods of high and low energy result in different sediment types being deposited.

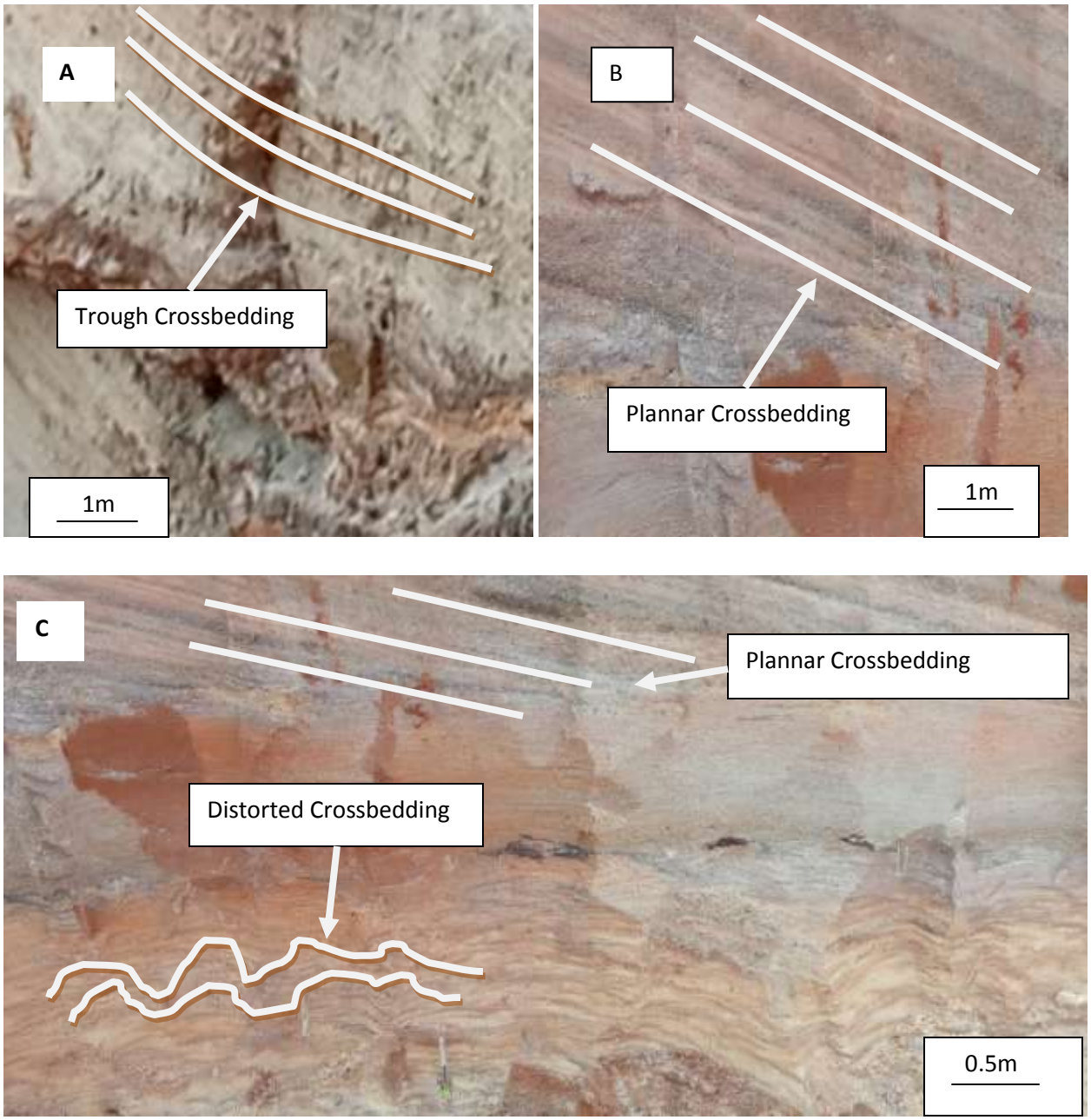

Plate 4.7. Ihube Outcrop Section: A. Trough Cross-Bed Indicating Northeastward Paleocurrent, B. Planar Cross-Bed with Distinct Bedding Orientation, and C. Composite Planar and Distorted Cross-Beds Showing Upper Tangential Ends and Lower Disrupted Structure.

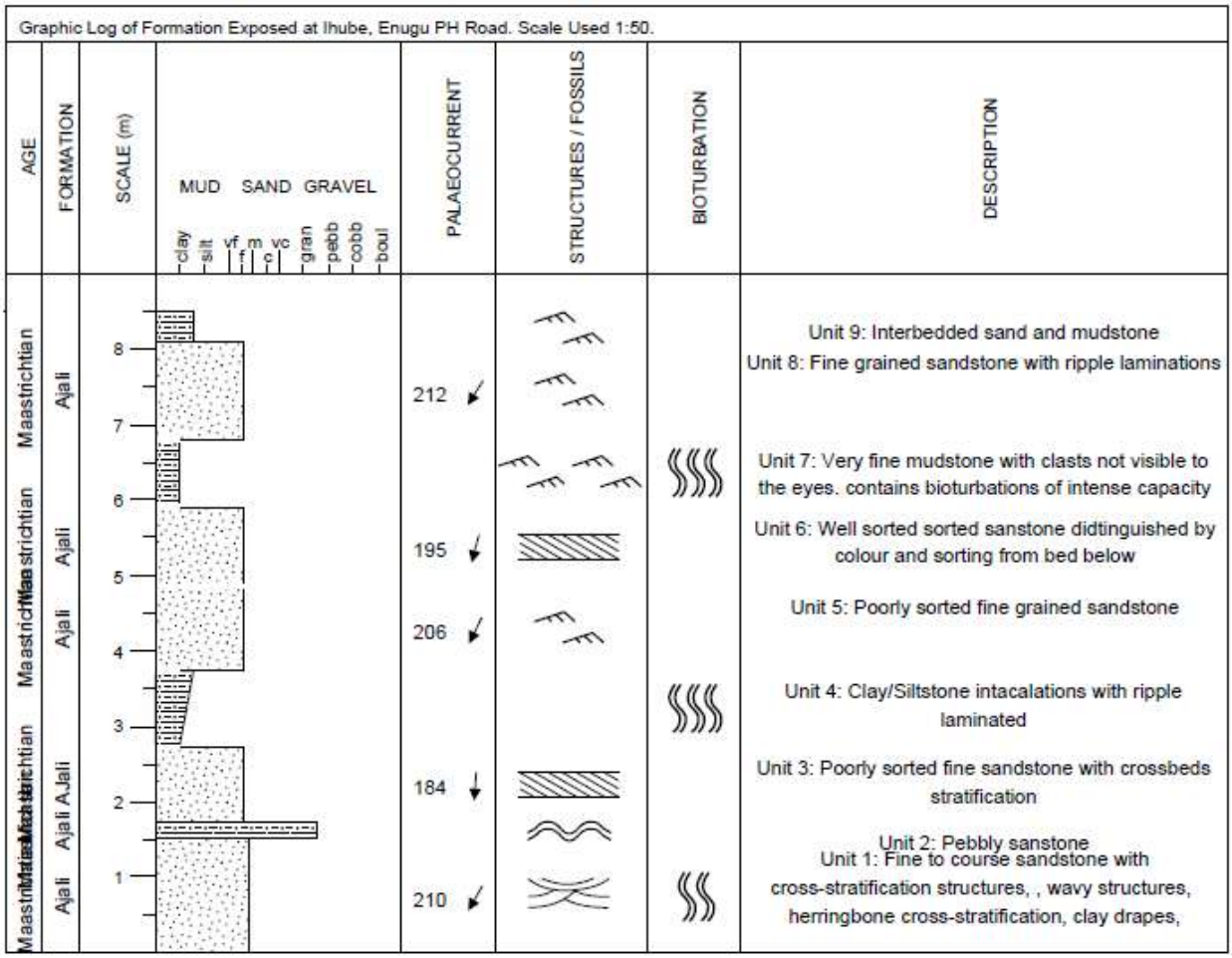

Figure 4.6 Lithostratigraphic Log of Mamu Formation Exposed at Ihube Section

4.1.1.7 Lithostratitigraphic Description of Outcrop of Owelli Sandstones Exposed At Agbogugu Village

Unit 1

The presence of micaceous coarse-grained sandstone with thin shale layers offers important insights into the sediment's composition and the depositional environment (Selly, 1998).

The coarse-grained sandstone suggests that the sediment consists of larger grains, indicating a high-energy environment where larger particles could be transported and deposited. The presence of mica within the sandstone indicates the likely presence of mineral components such as biotite or muscovite, which can contribute to the sediment's texture and composition.

The occurrence of thin shale layers within the sandstone points to cyclic variations in sedimentation. Shale layers often form in lower-energy conditions, suggesting that the environment experienced periodic changes in water dynamics, potentially related to shifts in sediment supply or local depositional settings.

Unit 2

The presence of medium to coarse-grained quartz sandstone indicates a sediment with predominantly larger-sized grains, offering insights into its depositional history and the geological conditions of the area (Smith & Johnson, 2018).

The medium to coarse-grained texture suggests that the sediment primarily consists of larger quartz grains, indicating high-energy depositional conditions that allowed for the transportation and deposition of such coarse particles. The quartz composition implies the dominance of a mineral that is highly resistant to weathering and commonly found in various geological settings.

The size of the grains can provide information about the energy and transport mechanisms involved during deposition. Medium to coarse grains typically indicate environments with strong currents or high-energy conditions, such as river channels, alluvial fans, or beach environments.

In summary, the characteristics of this medium to coarse-grained quartz sandstone suggest that it was deposited under high-energy conditions, reflecting the geological history and the dominant mineral composition of the area.

Unit 3

Conglomerates are sedimentary rocks formed through the deposition and lithification of coarse-grained sediments, typically in high-energy environments like rivers, alluvial fans, or areas with significant tectonic activity. The clasts within conglomerates can vary in size, shape, and composition, and they are often rounded due to the abrasion and rounding that occurs during transport by water or other erosional processes.

The matrix surrounding the clasts can consist of finer sediment, and the nature of this matrix can vary widely. The composition and texture of the clasts, as well as the matrix, provide clues about the source area, the distance of transportation, and the energy of the transporting agent.

Conglomerates often signify dynamic geological processes and changes in the environment. For example, the presence of well-rounded pebbles can indicate prolonged transport, while angular clasts may suggest shorter distances or more rapid deposition, (Figure 4.7 and Plate 4.8).

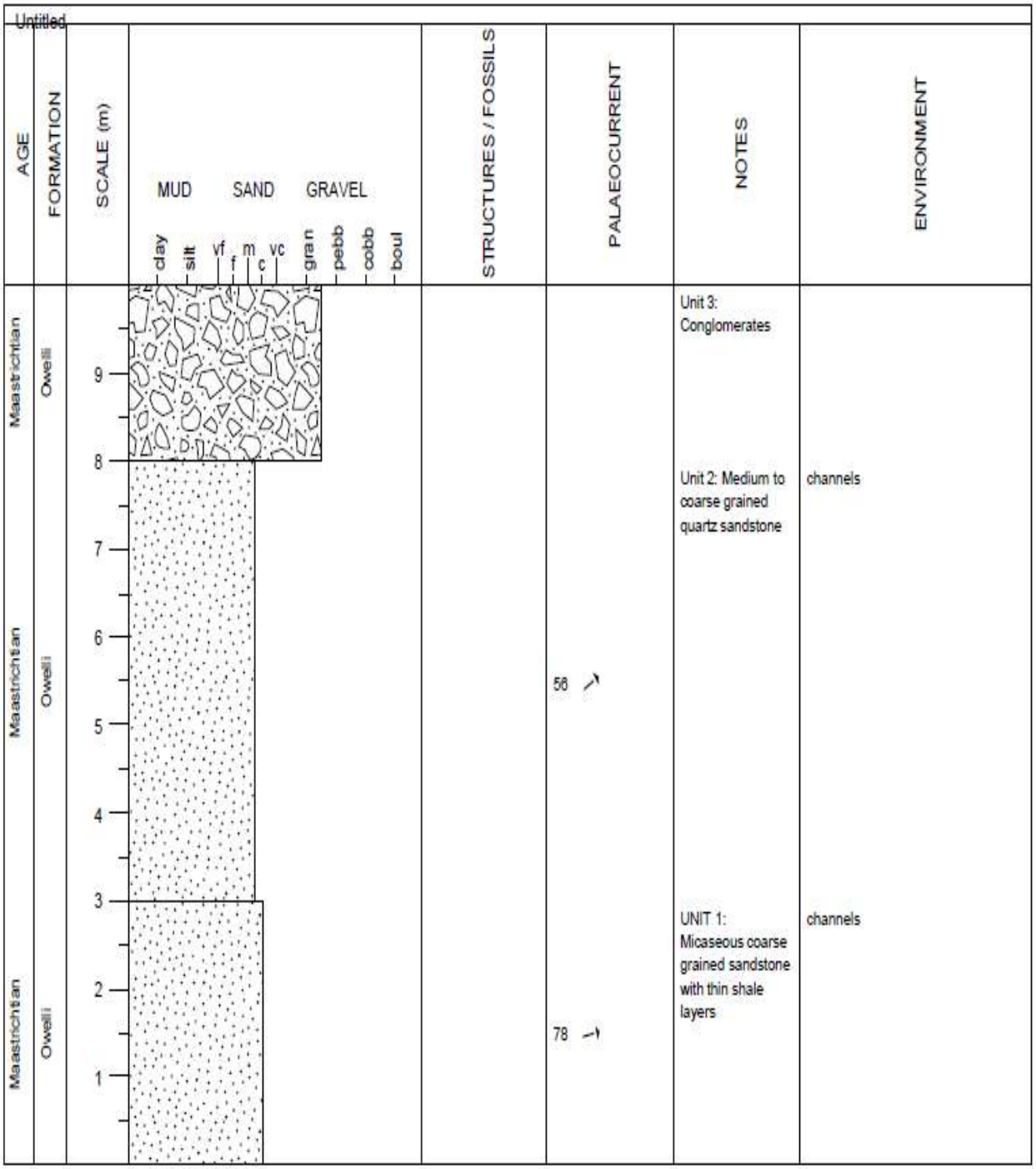

Figure 4.7 Lithostratigraphic Log of Owelli Sandstone exposed near Agbogugu village

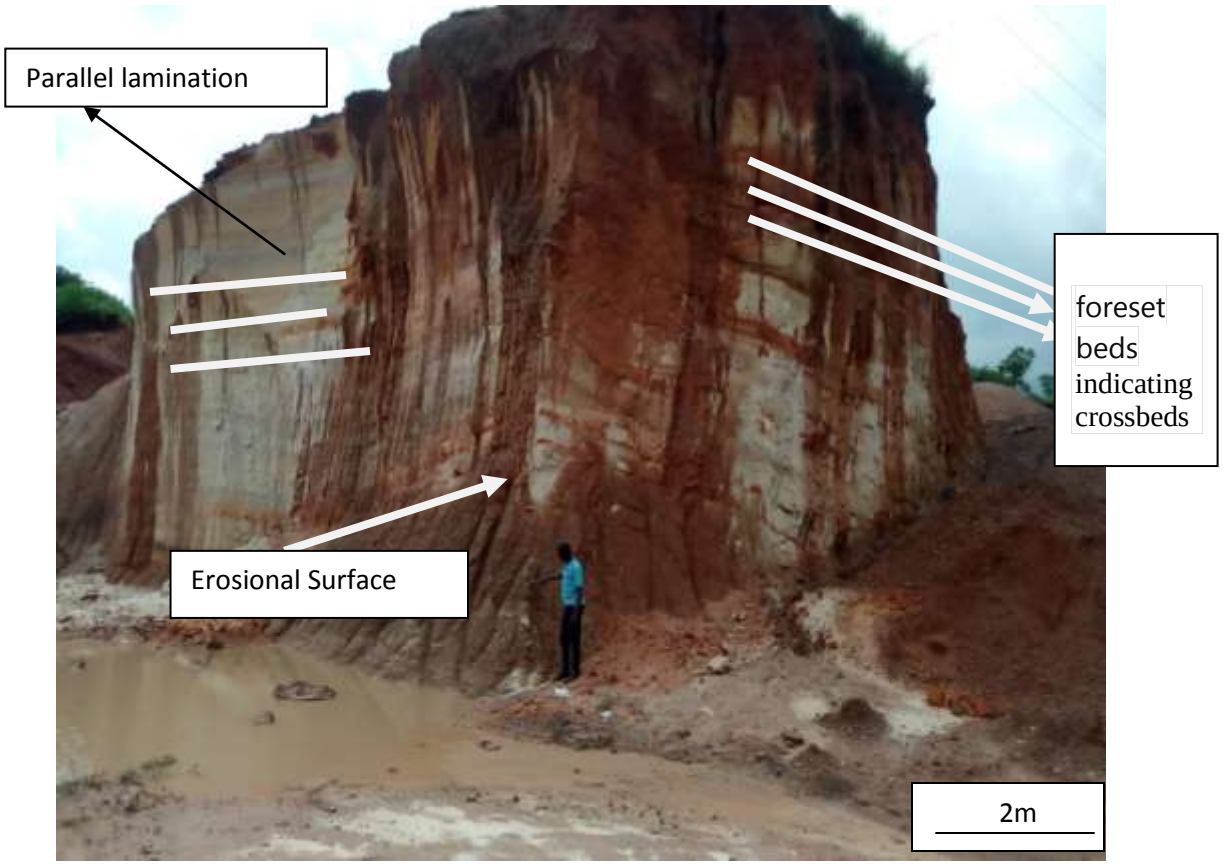

Plate 4.8 Panoramic Outcrop View of an Outcropt at Agbogugu Village (ES=Erosional Surface. PL=Parallel Lamination)

4.1.1.8 Lithostratigraphic Descriotion of Sandstone Outcrop at Agbogugu Junction

The Owelli Sandstone outcrop exposed at Agbogugu Junction along the Enugu-Port Harcourt Road exhibits a lithologically diverse succession (Table 4.4, Plate 4.9 and Figure 4.8) Predominantly composed of poorly sorted, fine-to-medium-grained sandstones, the outcrop also features interbedded mudstones, shales, and occasional coal seams. The sandstones are often ferruginized, exhibiting brown to reddish-brown hues, and display a variety of sedimentary structures, including cross-bedding, planar bedding, and ripple marks. These features, coupled with the presence of trace fossils like Ophiomorpha and Skolithos, suggest deposition in a dynamic, shallow marine environment, possibly transitioning between high-energy shoreface or delta front settings and lower-energy intertidal or nearshore zones. The interbedded mudstones and shales represent periods of calmer conditions and finer sediment input, potentially reflecting lagoonal or protected embayment environments. The occasional presence of coal seams hints at episodes of organic matter accumulation in coastal swamp or deltaic plain settings.

Table 4.4 Lithostratitigraphic Description of Owelli Sandstones Exposed at Agbogugu Junction

Unit	Description	Sedimentary Structures	Interpretation	Citations
1	Weathered Greenish-Brown Shale Interbedded with Mudstones	Interbedding	Deltaic or shallow marine environment with fluctuating energy levels and sediment supply	Reineck & Singh, 1980. Reading, 1996
2	Ferruginized Gray to Brown Shales	Ferruginization	Coastal or deltaic setting with fluctuating redox conditions	Tucker, 2001.Blatt et al, 1980
3	Poorly Sorted Brown Fine-Medium Grained Sandstones with Gypsum Nodules	Poor sorting, Gypsum nodules	High-energy fluvial or shallow marine environment with periodic desiccation	Boggs 2006, Nichols 2009
4	Dark Gray Shales with Brown Colouration	Color variations	Anoxic to dysoxic environment with occasional oxygenation	Prothero & Schwab 2014, Stow 2005
5	Parallel Laminated Brown Mudstones	Parallel lamination	Calm lacustrine or low-energy marine setting	Collinson & Thompson 1989, Blatt et al. (1980)
6	Black Coal with Partings	Coal formation, Partings	Coastal swamp or deltaic plain environment	Diessel (1992), Stanley & Warne (1993
7	Brown Mudstones	-	Low-energy floodplain, lagoon, or quiet offshore marine environment	Boggs (2012)
8	Crossbedded Medium Grained Sandstones	Crossbedding	River channel, delta front, or nearshore marine setting	Reineck & Singh (1980), Miall, (2016)
9	Poorly Sorted Medium Grained Sandstones with Ophiomorpha	Poor sorting, Ophiomorpha burrows	High-energy beach or delta front in shallow marine setting	-Pemberton et al 2001, Frey & Pemberton (1984).
10	Poorly Sorted Medium Grained Sandstones with Skolithos	Poor sorting, Skolithos burrows	Sandy shoreface or tidal flat in intertidal or shallow subtidal zone	Seilacher, A. (2007), Bromley, (1996)

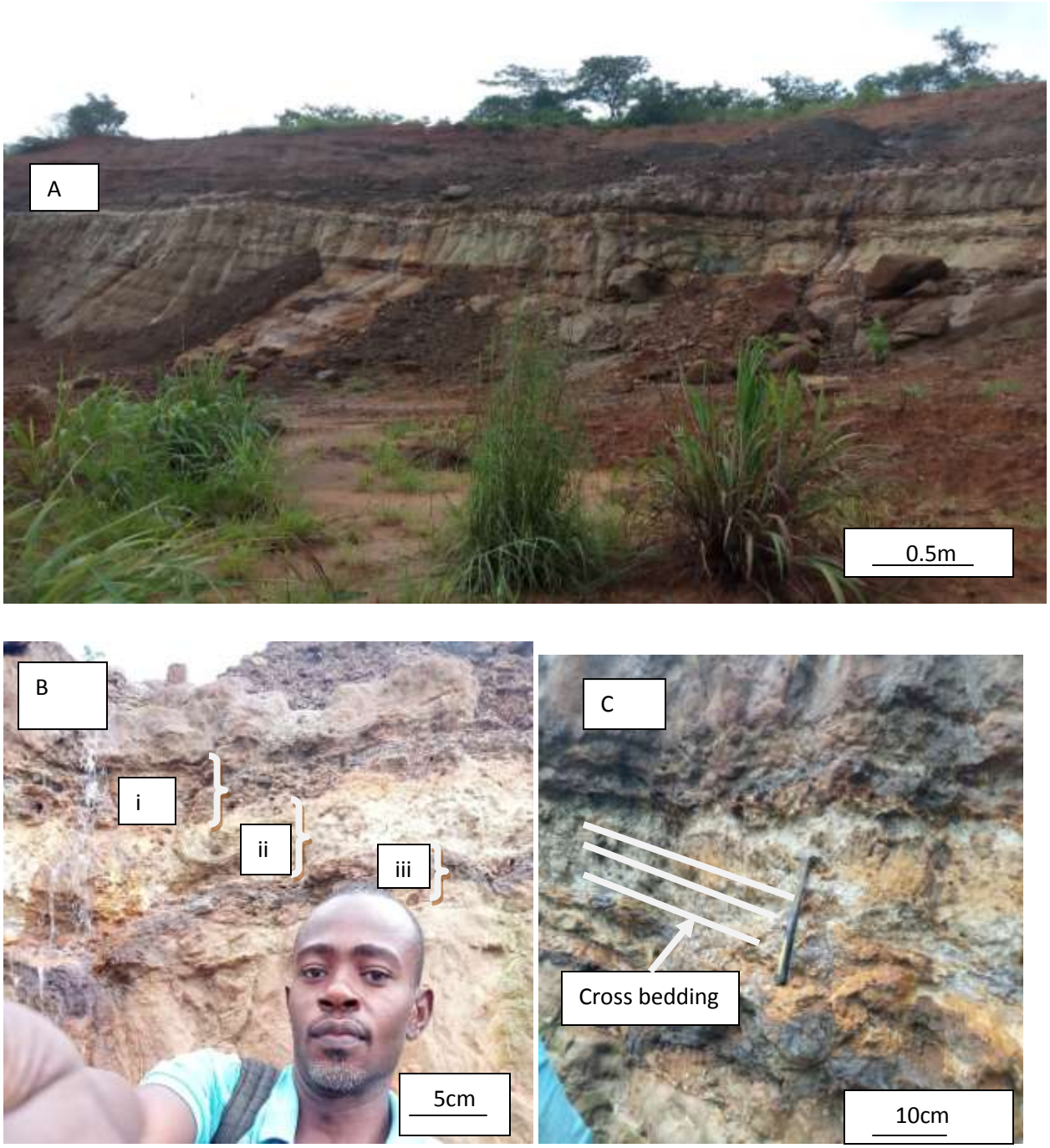

Plate 4.9: Outcrop view of Agbogugu Junction outcrop along Enugu PH Road.A. Panoramic Outcrop view of the outcrop B. alternating layers (i,ii, and iii) of different rock types, suggesting bedding planes or stratification. The layering patterns and textures indicate depositional processes over time. C, Cross-Bedding in the middle section, where there are inclined layers

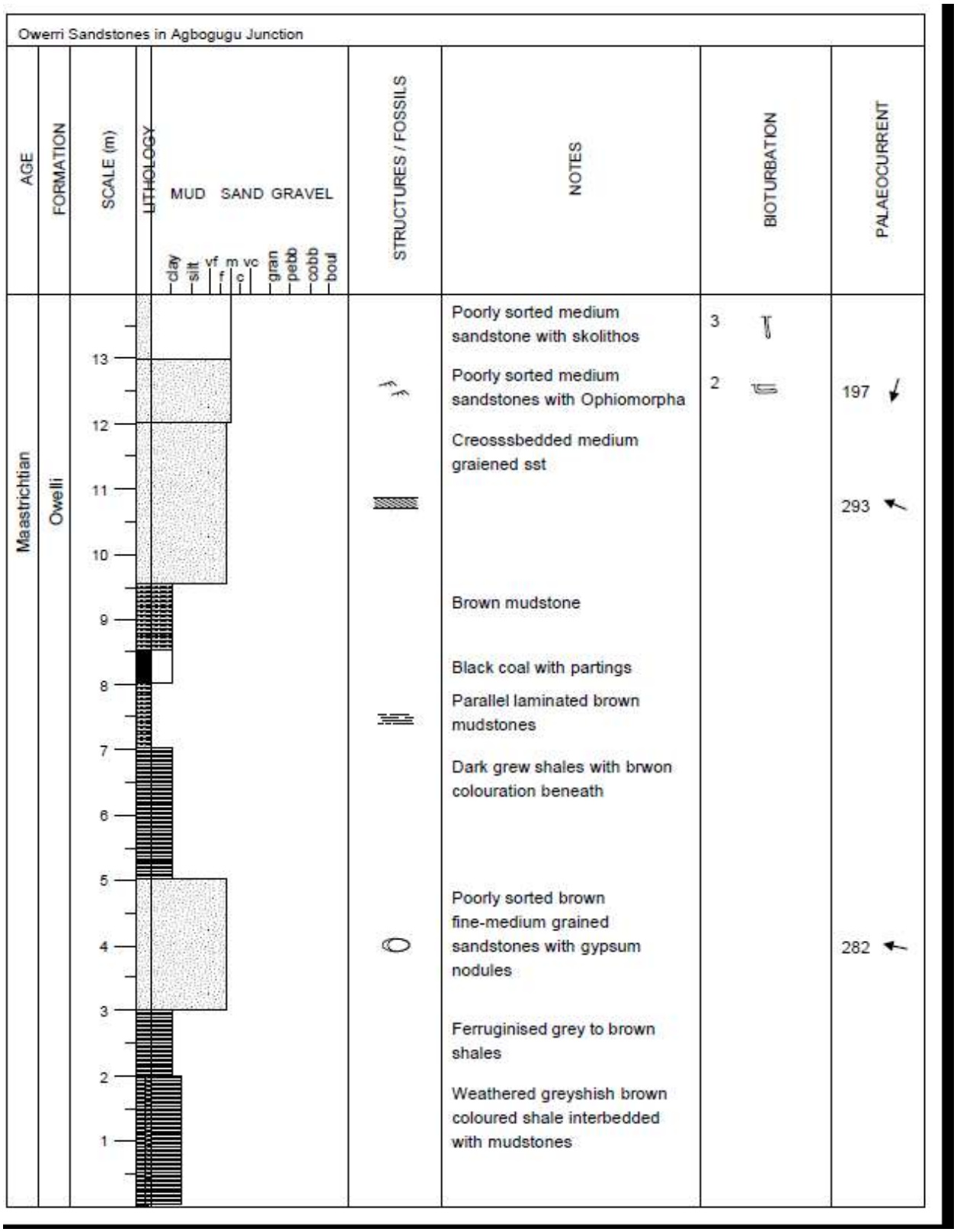

Figure 4.8 Lithostratigraphic Log of Owelli Sandstone exposed at Agbogugu Junction

4.1.2 Facies Analysis

Six different types of rock units were identified from the eight sections that were examined. These rock units have distinct characteristics, such as their composition, grain size, shape, layering, fossils, and minerals. Informal names, such as FA, FB, FC, FD, FE, and FF were given to these rock units by the researchers for easy reference (Table 4.5).

4.1.2.1 Interbedded Calcareous Mudstone and Shale Facies (FA)

This facies was observed in location five (Mamu Formation) and Location 1 (Nsukka Formation). The facies has shale layers that are from grey to dark grey, break easily, have iron deposits and sometimes have thin layers of muddy limestone and sandy clay. These layers have thin parallel lines that are mm-sized and shaped like lenses in some parts. The shale layers of the facies are very rich in fossils, as shown by the bi-valves and many kinds of pollen and forams. Sometimes, there are round lumps of iron sulfide in the layers. In some places, like the Ohafia place, the lumps also have calcium carbonate.

4.1.2.2 Plane and Cross Stratified Sandstone Facies (FB)

Sections of locations three and four (Ajali Sandstone) and locations five and six (Mamu Formation) have plane and cross stratified sandstone facies. They also have a facies of sandstone and mudstone layers with some pebbly conglomerates. The facies has some units that show normal grading and basal scour fills. They have horizontal or trough cross-stratification, sometimes with mud laminae, and are poorly sorted. Sometimes, the cross-strata are truncated by reactivation surfaces that are locally draped by mud. The pebbles in the facies probably came from a fluvial channel that was modified by the tide. The scour fills, which are not unique to this facies, indicate channel confinement. When this feature was absent, the units showed fining-upward sequences that were bounded by erosional surfaces and indicate deposition during waning flow, as typical of channel fills.

4.1.2.3 Heterolithic Shale And Siltstone Facies (FC)

The heterolithic shale and siltstone facies were observed in location 1, unit 9 and on location 2. The facies consists of alternating layers of shale and siltstone, which are fine-grained clastic rocks composed of clay and silt particles, respectively. The facies has a laminated or thinly bedded appearance, with the shale layers being darker and more fissile than the siltstone layers.

The facies has a low to moderate porosity and permeability, depending on the degree of compaction and cementation of the sediments. The facies may show signs of deformation, such as folding, faulting, and fracturing, due to tectonic movements or differential compaction of the sediments.

4.1.2.4 Imperfectly Stratified Sandstone Facies (FD)

Sections of locations three and four (Ajali Sandstone) and locations five and six (Mamu Formation) have imperfectly stratified sandstone facies. The facies consists of sand-sized grains that are arranged in thin layers or laminae, but not in a regular or consistent pattern. The imperfect stratification of the facies may result from different sedimentary processes, such as bioturbation, reworking, or deformation, that disturb the original bedding of the sandstone.

4.1.2.5 Reddish Brown Sandstone Facies (FE)

Sections of the Mamu Formation in the Okigwe area have a reddish brown sandstone facies. The facies consists of sand-sized grains that are oxidized by iron minerals and have a reddish brown color. The facies may show signs of bioturbation, which is the disturbance of the sediment by animals and plants that live in the sediment.

4.1.2.6 Oolitic Sandstone Facies (FF)

Sections of the Ohafia section have an oolitic sandstone facies. The facies consists of sand-sized grains that are ooids, which are small spheres of calcium carbonate, with a size of 0.25 to 0.65 mm. The facies is well sorted and has carbonate grains that are cemented by calcite. The ooids in the facies are formed by biogenic or chemical processes, such as the coating of sand grains by algae or bacteria, or the precipitation of calcium carbonate from seawater.

Table 4.5: Facies Classification and Characteristics (Modified after Miall, 1996)

Facies Code	Facies Name	Key Characteristics	Formation Locations	Diagnostic Features
FA	Interbedded calcareous mudstone/shale	Grey-dark grey shale, iron deposits, muddy limestone layers, fossil-rich	Mamu Fm (L5), Nsukka Fm (L1)	Thin parallel laminations, pyrite nodules, bioturbation
FB	Plane/cross-stratified sandstone	Poorly sorted, trough cross-stratification, pebbly conglomerates, scour fills	Ajali Sandstone (L3,L4), Mamu Fm (L5,L6)	Reactivation surfaces, mud drapes, fining-upward sequences
FC	Heterolithic shale/siltstone	Alternating shale-siltstone layers, laminated, fissile	Nsukka Fm (L1,L2)	Low porosity, deformation structures, ripple marks
FD	Imperfectly stratified sandstone	Thin irregular laminae, bioturbated	Ajali Sandstone (L3,L4), Mamu Fm (L5,L6)	Disturbed bedding, multidirectional flow indicators
FE	Reddish brown sandstone	Iron-oxidized, well-sorted	Mamu Fm (Okigwe)	Cross-bedding, paleocurrent indicators, bioturbation
FF	Oolitic sandstone	0.25-0.65mm ooids, calcite-cemented	Ohafia section	Well-sorted carbonate grains, high sphericity

4.1.3 Univariate Grain Size Analysis

Modal Grain Size

The grain size distribution of eight samples from the Nsukka Formation was analyzed using cumulative log-probability plots, each accompanied by an inset bar chart showing the percentage composition of different grain size fractions (Figures 4.9–4.16). The plots exhibit segmented curves with varying slopes, indicating multiple grain populations and differences in sediment sorting. Most samples show a mix of clay, silt, and sand fractions, with sand generally dominant, though some samples display higher proportions of fine-grained material. The bar charts quantify these distributions, revealing variations in the relative abundance of grain size classes across samples.

The cumulative curves suggest fluctuations in depositional energy and sediment supply, with inflection points reflecting changes in transport dynamics. Samples such as 3 and 6 (Figures 4.11 and 4.14) exhibit balanced distributions of silt and sand, while others, like Sample 5 (Figure 4.13), show a pronounced peak in medium sand. The bar charts further highlight these trends, with some samples dominated by fine fractions and others by coarser material. Together, the plots and charts provide a comprehensive overview of grain size variability, indicating diverse sedimentary conditions within the Nsukka Formation

The bar charts inset within Figures 4.9-4.16 clearly identify the dominant grain size fractions for each Nsukka Formation sample. The visual percentage distributions reveal that medium to coarse sand fractions constitute the primary grain population in most samples, particularly evident in Figures 4.9, 4.13 and 4.15 where sand components exceed 60% of total composition. However, Figures 4.11 and 4.14 display more balanced distributions with silt fractions reaching 40-45%, while Figure 4.12 shows a notable exception with fine-grained sediments (clay and silt) dominating at approximately 70% composition. The consistent presentation of grain size percentages across all bar charts enables direct comparison of the major sedimentary fractions between samples, with sand predominating in six of the eight samples analyzed.

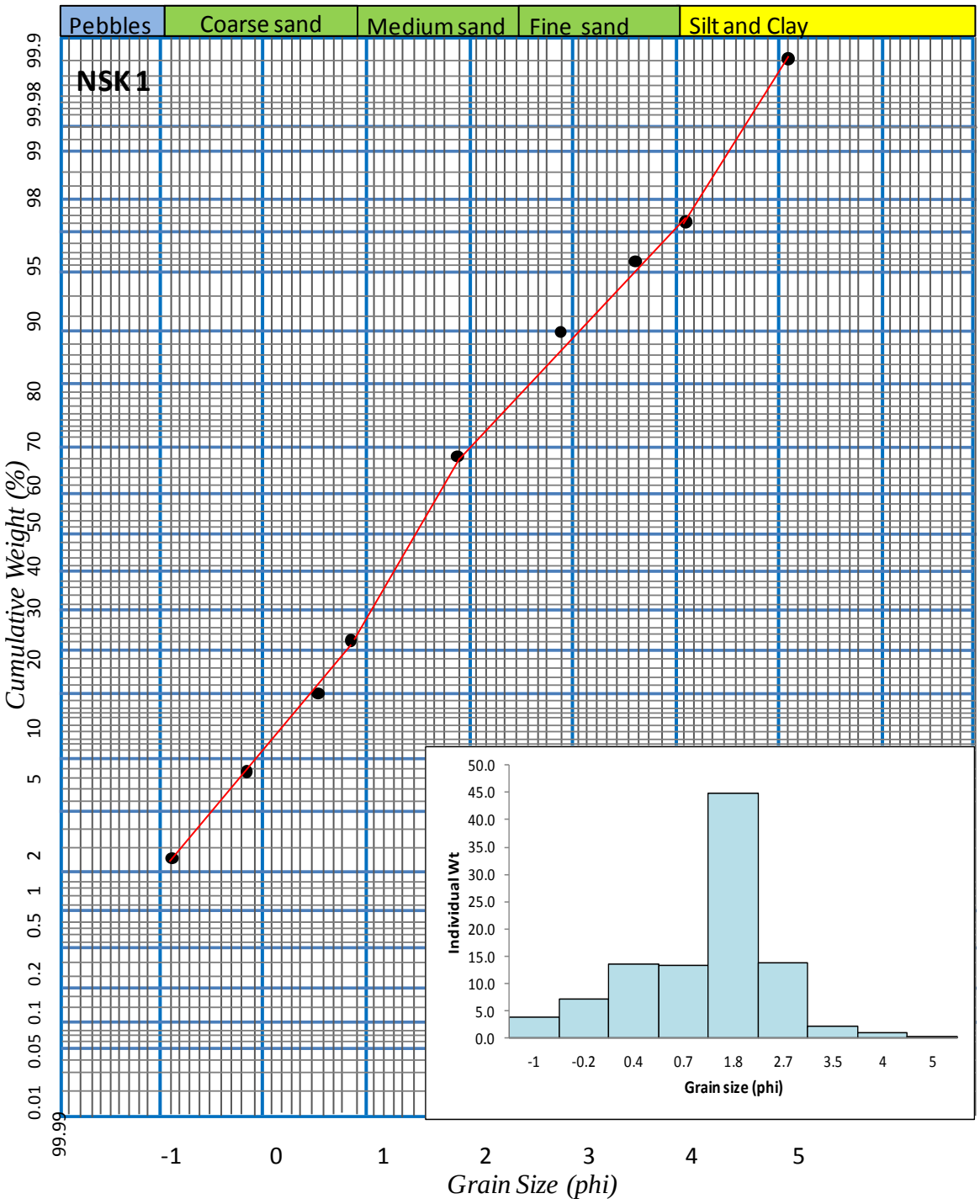

Figure 4.9 Cumulative Log-Probability Plots of Nsukka Fm. Sample 1 (Inset: Bar Chart)

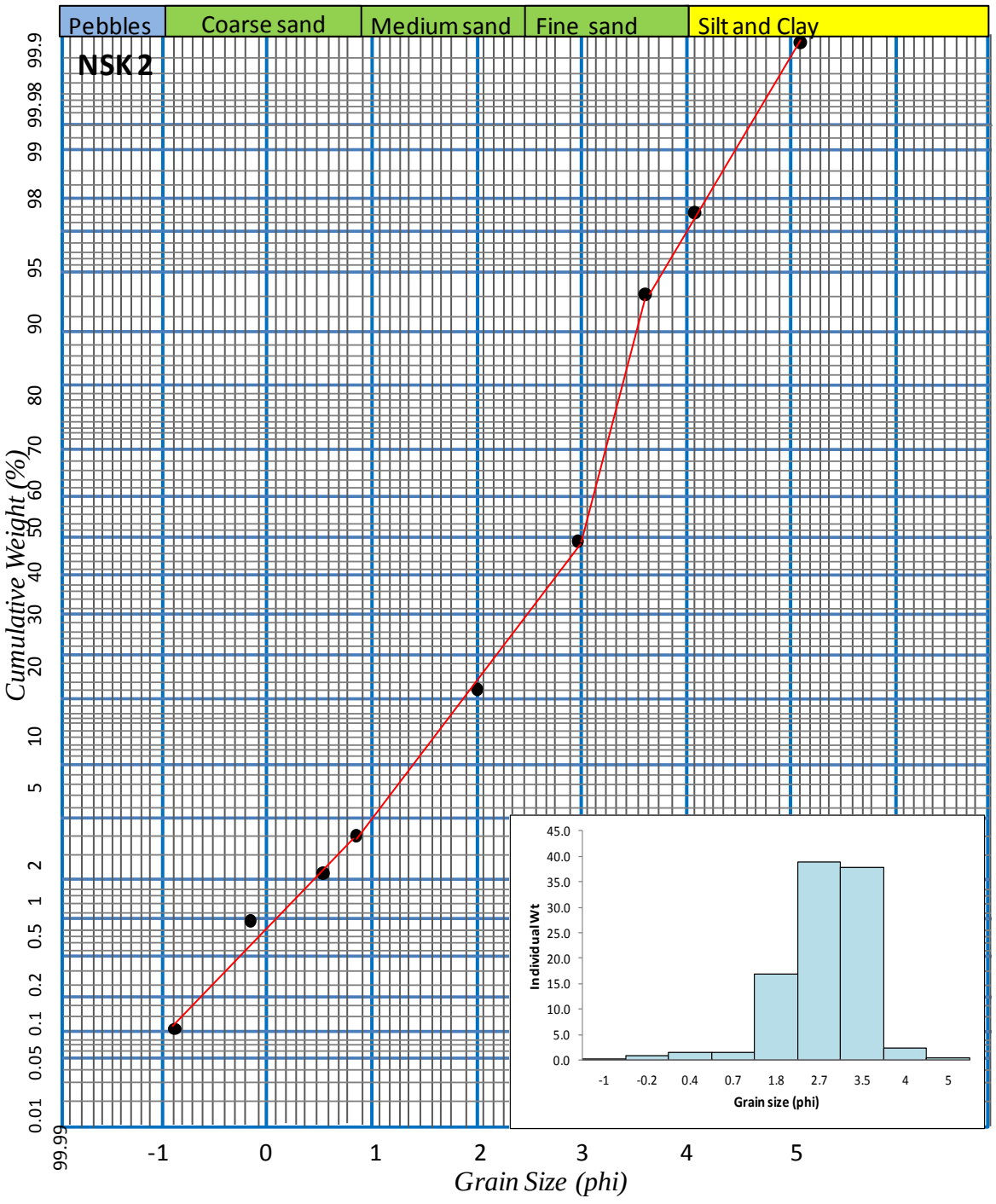

Figure 4.10: Cumulative Log-Probability Plots of the Nsukka Fm. Sample 2 (Inset: Bar Chart)

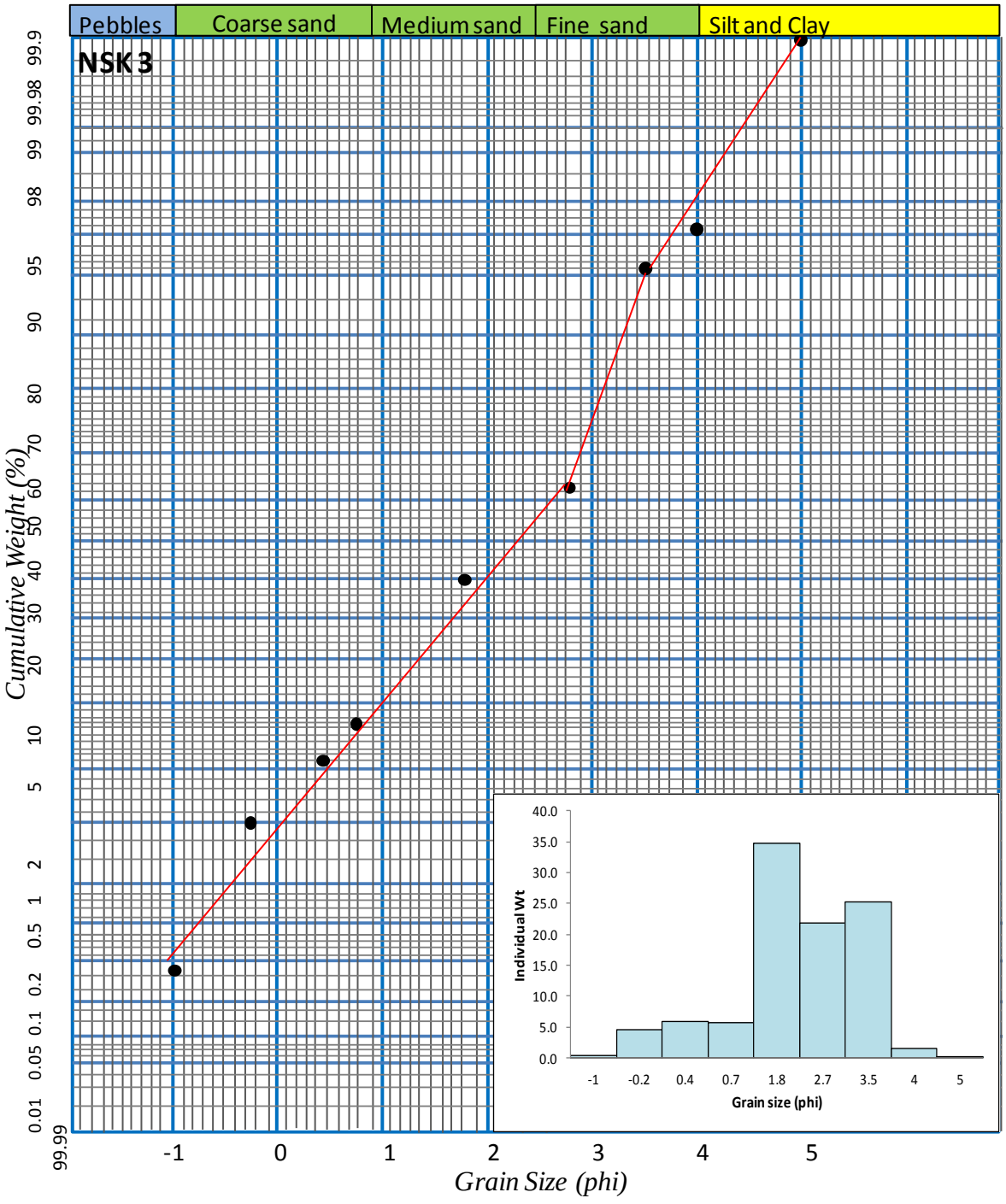

Figure 4.11: Cumulative Log-Probability Plots of Nsukka Fm. Sample 3 (Inset: Bar Chart)

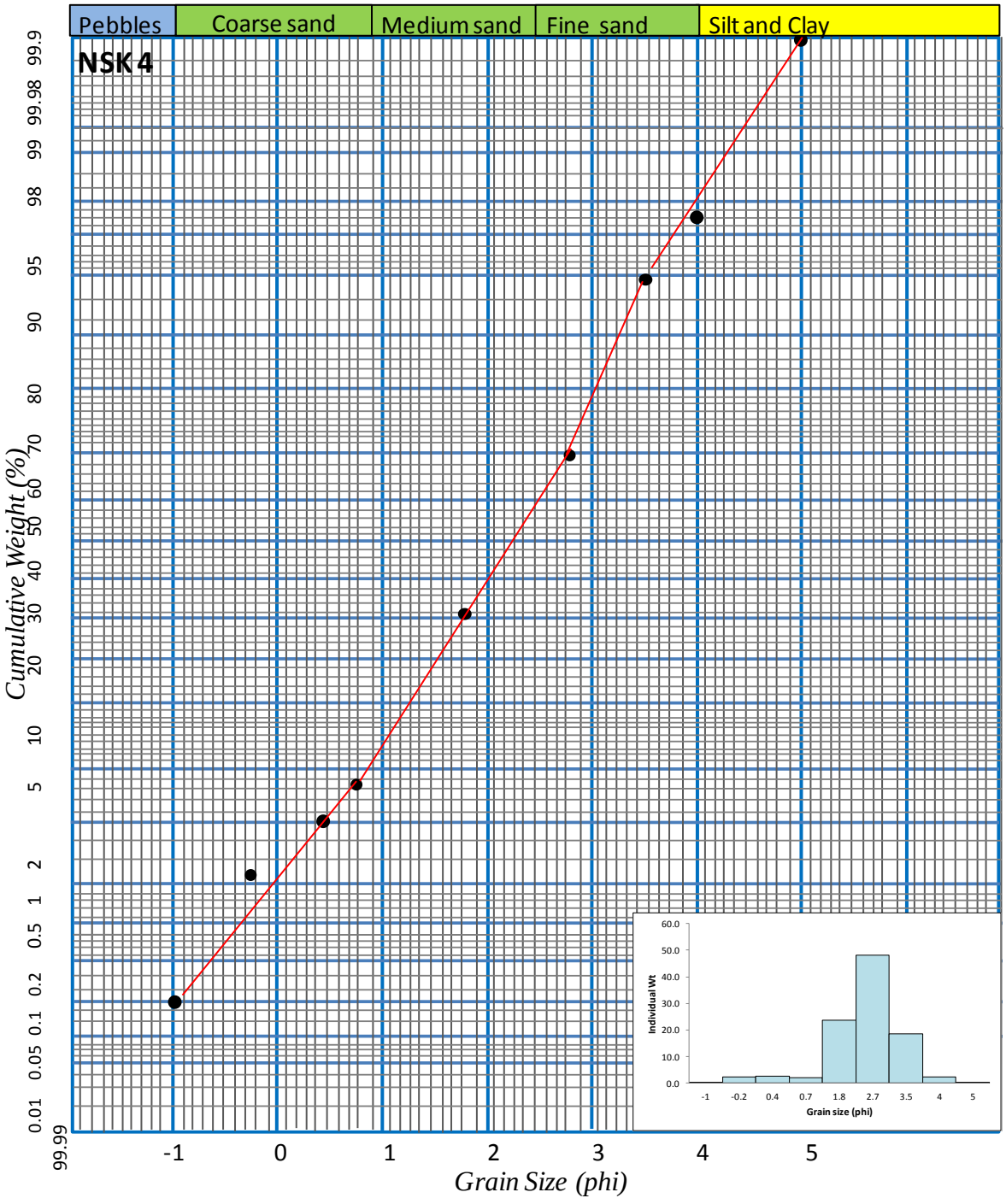

Figure 4.12: Cumulative Log-Probability Plots of Nsukka Fm. Sample 4 (Inset: Bar Chart)

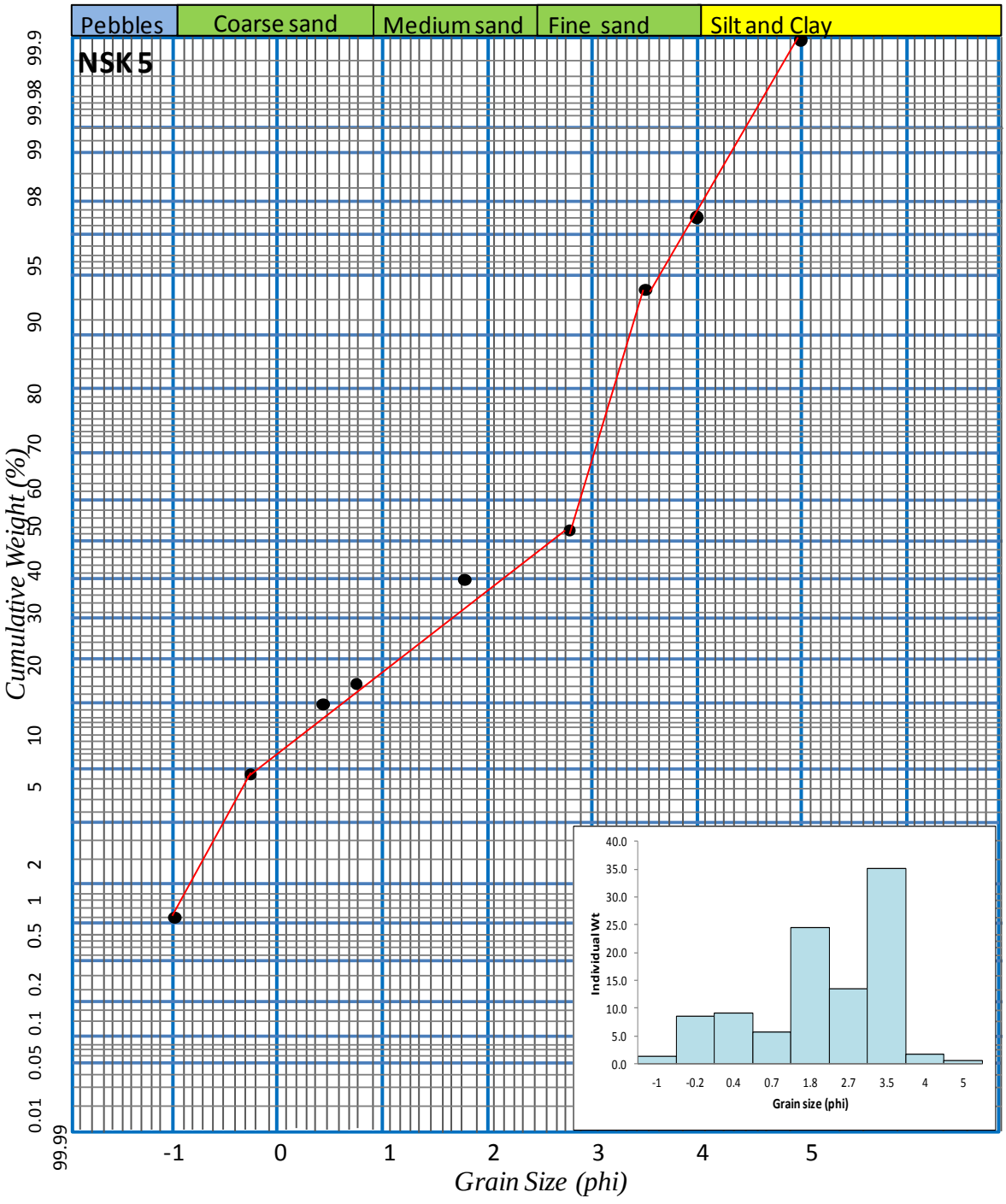

Figure 4.13: Cumulative Log-Probability Plots of Nsukka Fm. Sample 5 (Inset: Bar Chart)

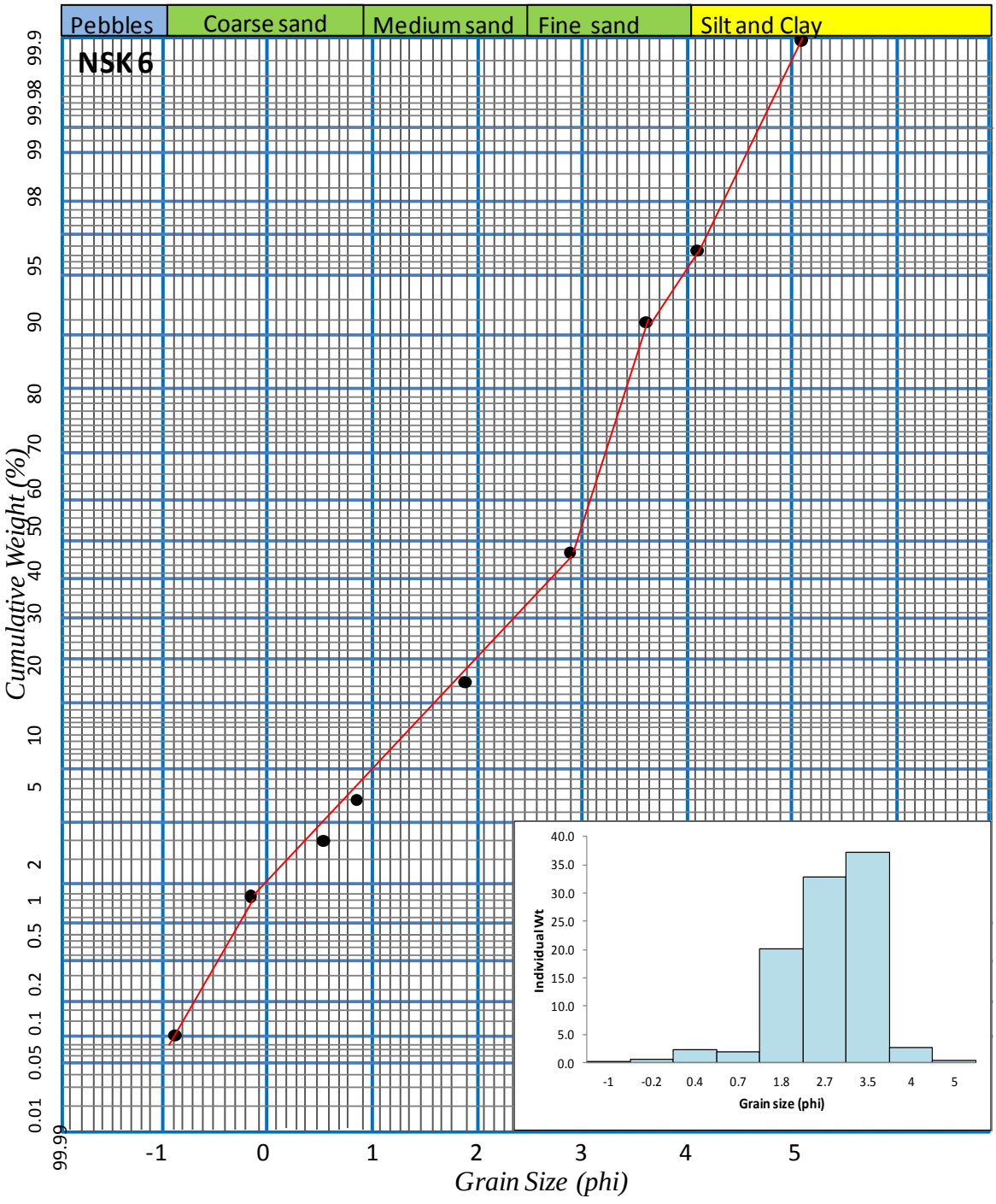

Figure 4.14: Cumulative Log-Probability Plots of Nsukka Fm. Sample 6 (Inset: Bar Chat)

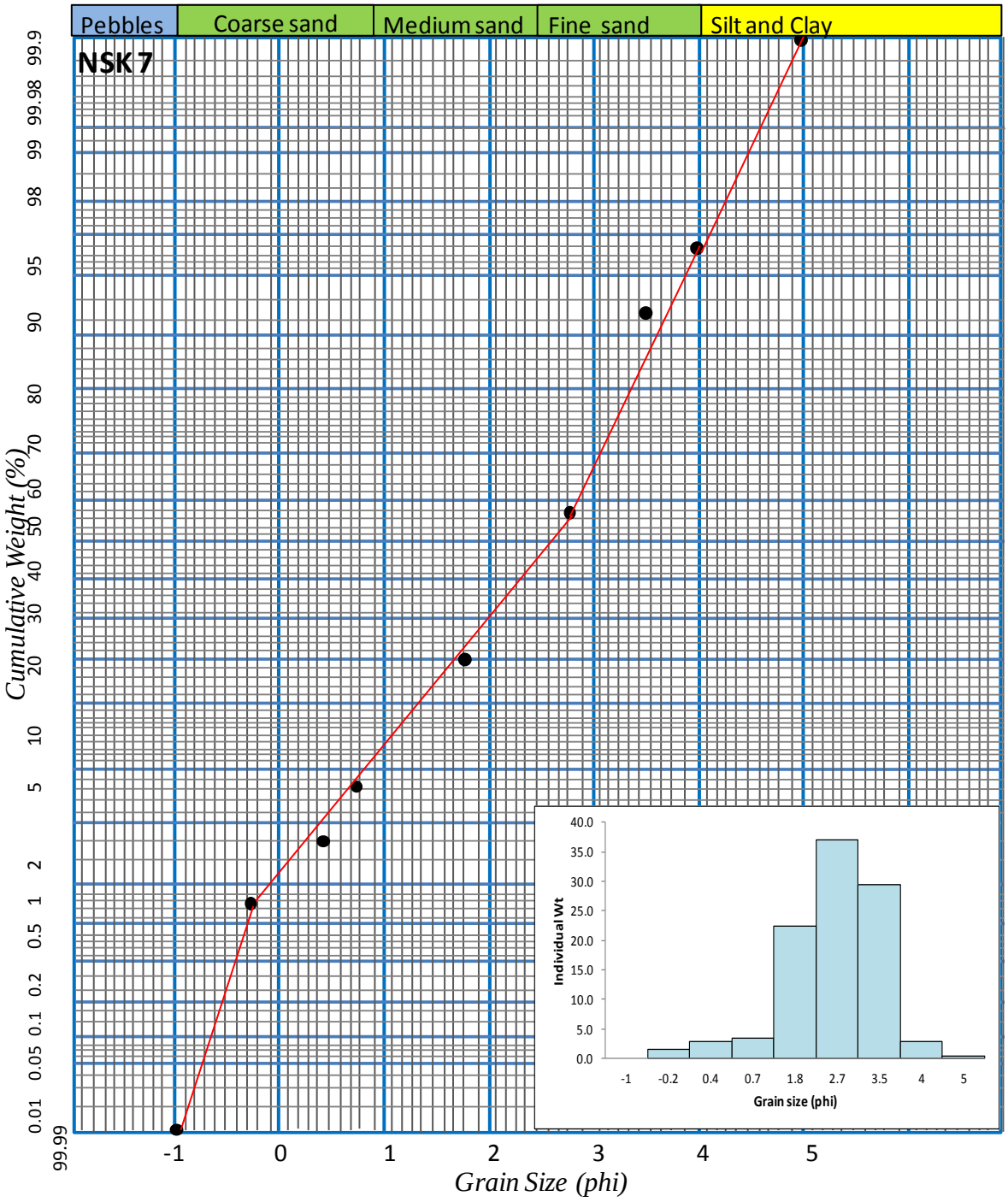

Figure 4.15: Cumulative Log-Probability Plots of Nsukka Fm. Sample 7 (Inset: Bar Chart)

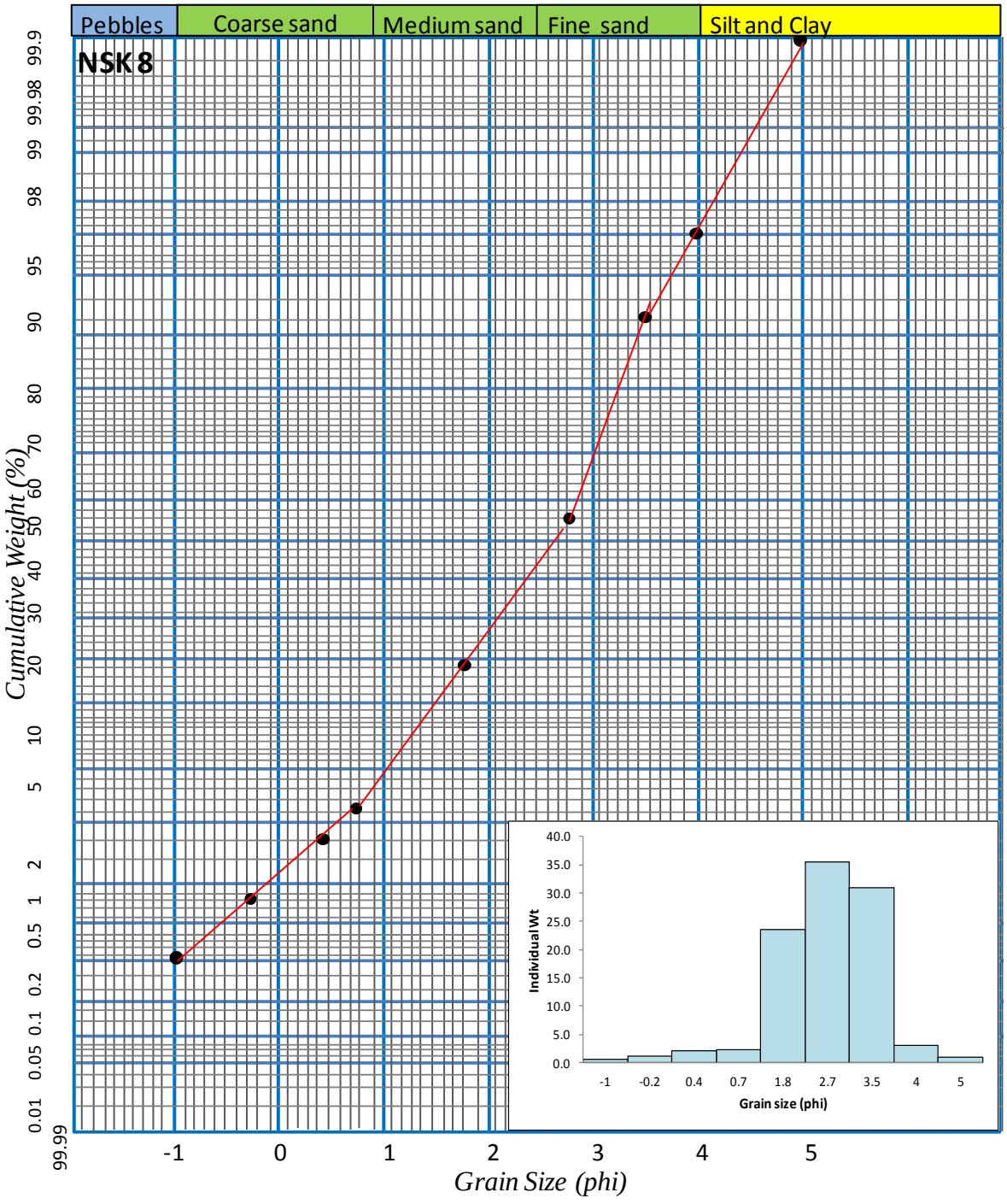

Figure 4.16: Cumulative Log-Probability Plots of Nsukka Fm. Sample 8 (Inset: Bar Chart)

Ajali Formation

The grain size distribution analysis of five Ajali Formation samples (Figures 4.17-4.21) reveals distinct sedimentary characteristics through cumulative log-probability plots and accompanying bar charts. The mean grain size across all samples predominantly falls within the medium to coarse sand range (0.25-1.0 mm), as evidenced by the bar charts which show sand fractions constituting 55-75% of total composition in Samples 1, 2, 3, and 4 (Figures 4.17-4.20). Sample 5 (Figure 4.21) presents a notable exception with a bimodal distribution where medium sand (45%) and silt (40%) fractions are nearly equal, suggesting a transitional depositional environment. The log-probability curves consistently display segmented slopes, particularly pronounced in Samples 1 and 4, indicating poor to moderate sorting conditions where multiple grain populations were deposited under varying energy regimes.

The bar charts provide quantitative validation of these observations, with Sample 4 (Figure 4.20) showing the coarsest mean grain size (75% coarse sand) and Sample 3 (Figure 4.19) representing the finest-end member of the sand-dominated samples (55% medium sand with 35% silt). The mean grain size progression across the samples correlates with changes in curve morphology on the log-probability plots - from steep, uniform slopes in the sand-rich samples (Figures 4.17, 4.18, 4.20) to more gradual transitions in samples with significant silt components (Figures 4.19, 4.21). This dataset collectively demonstrates that while the Ajali Formation is generally characterized by sandy deposits, local variations in mean grain size and sorting reflect important fluctuations in depositional energy and sediment supply during formation.

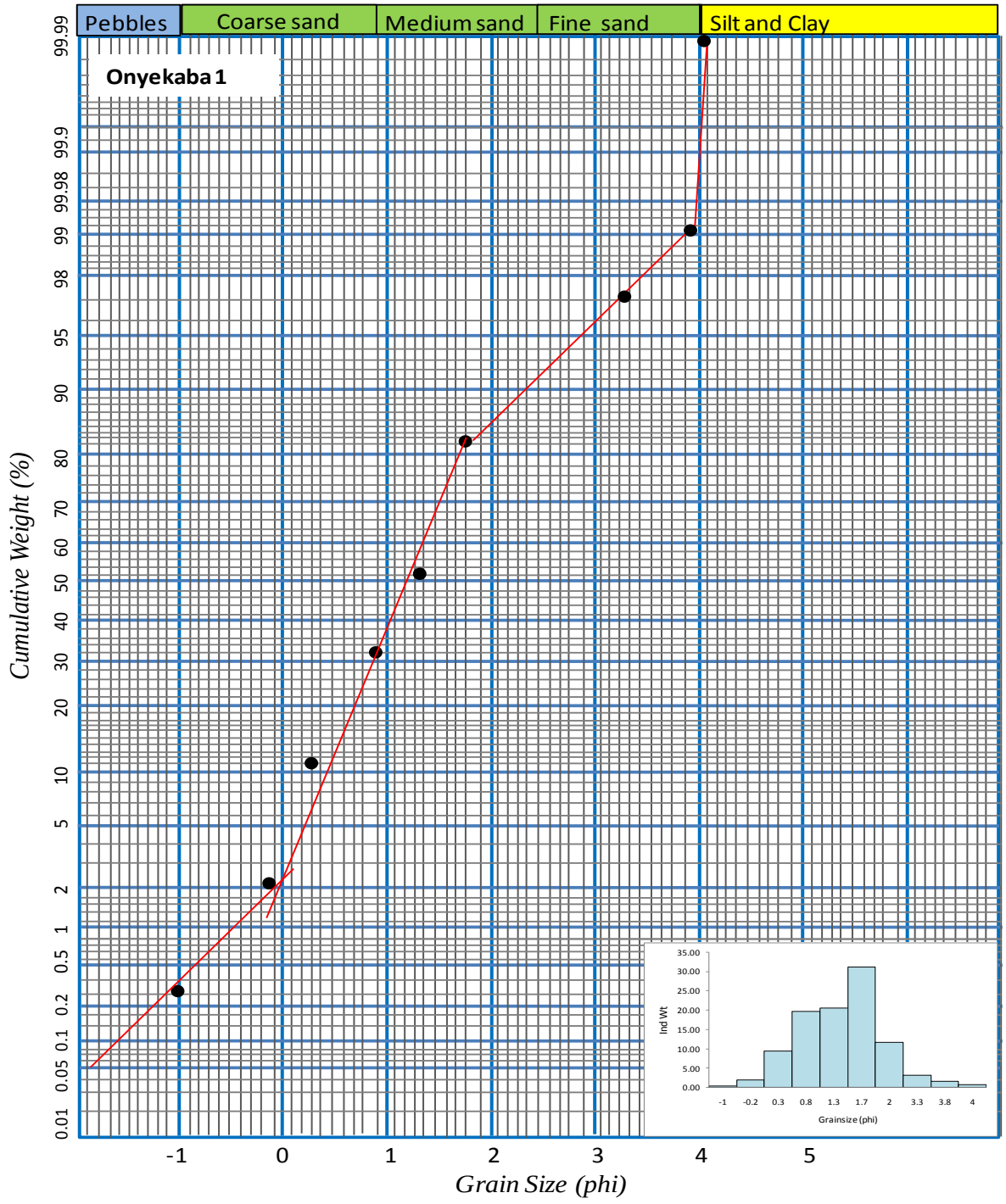

Figure 4.17: Cumulative Log-Probability Plots of Ajali Fm. Sample 1 (Inset: Bar Chart)

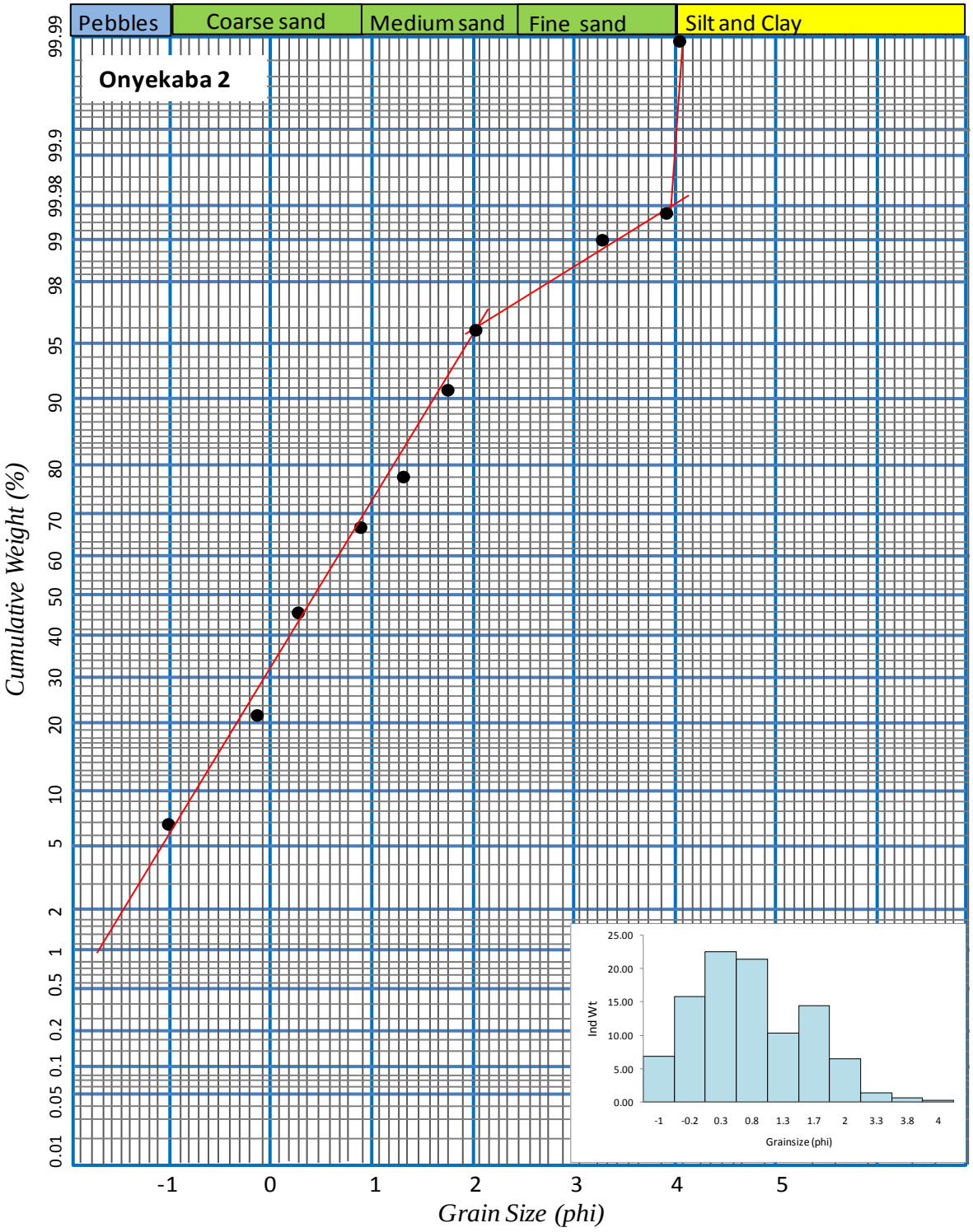

Figure 4.18: Cumulative Log-Probability Plots of Ajali Fm. Sample 2 (Inset: Bar Chart)

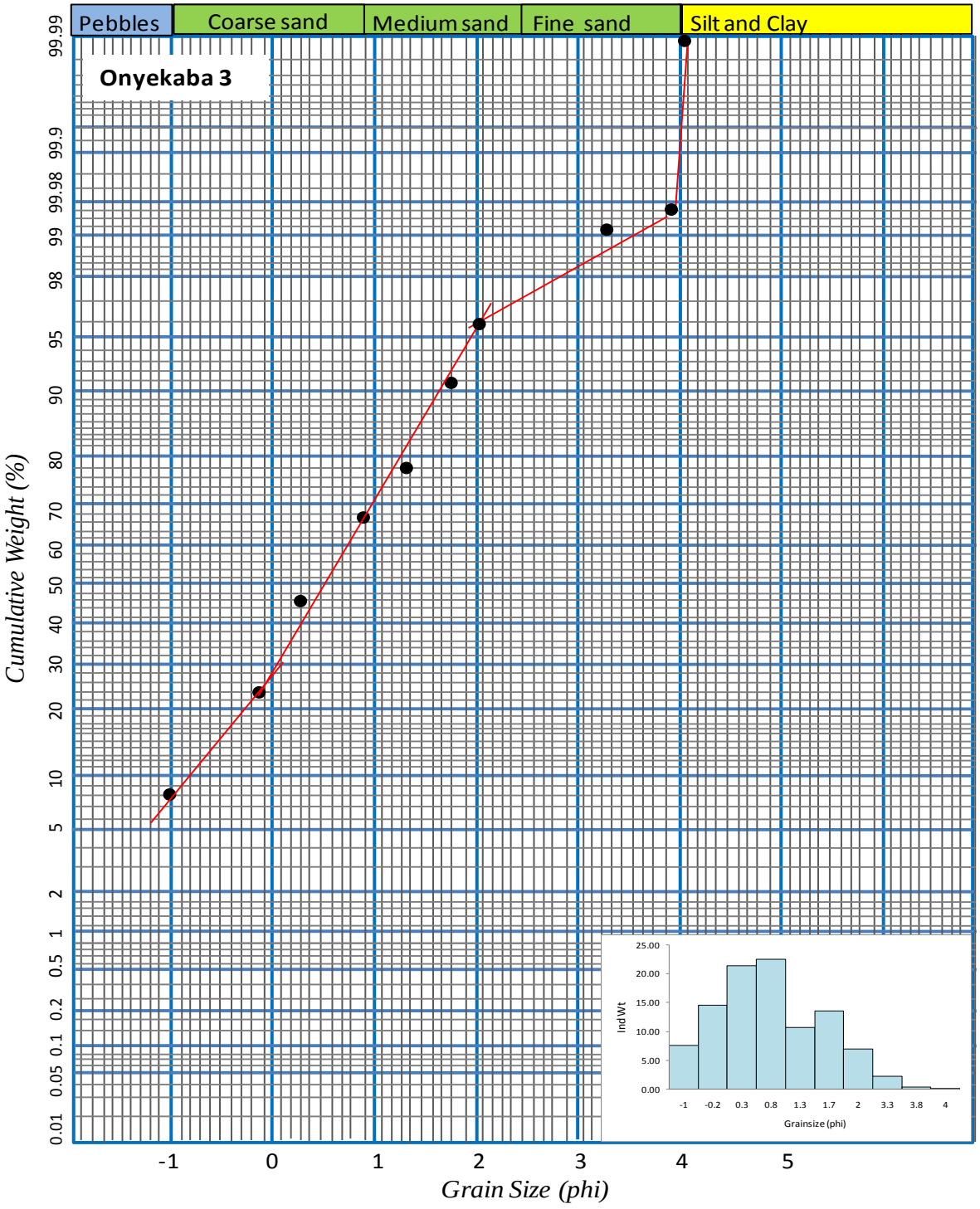

Figure 4.19: Cumulative Log-Probability Plots of Ajali Fm. Sample 3 (Inset: Bar Chart)

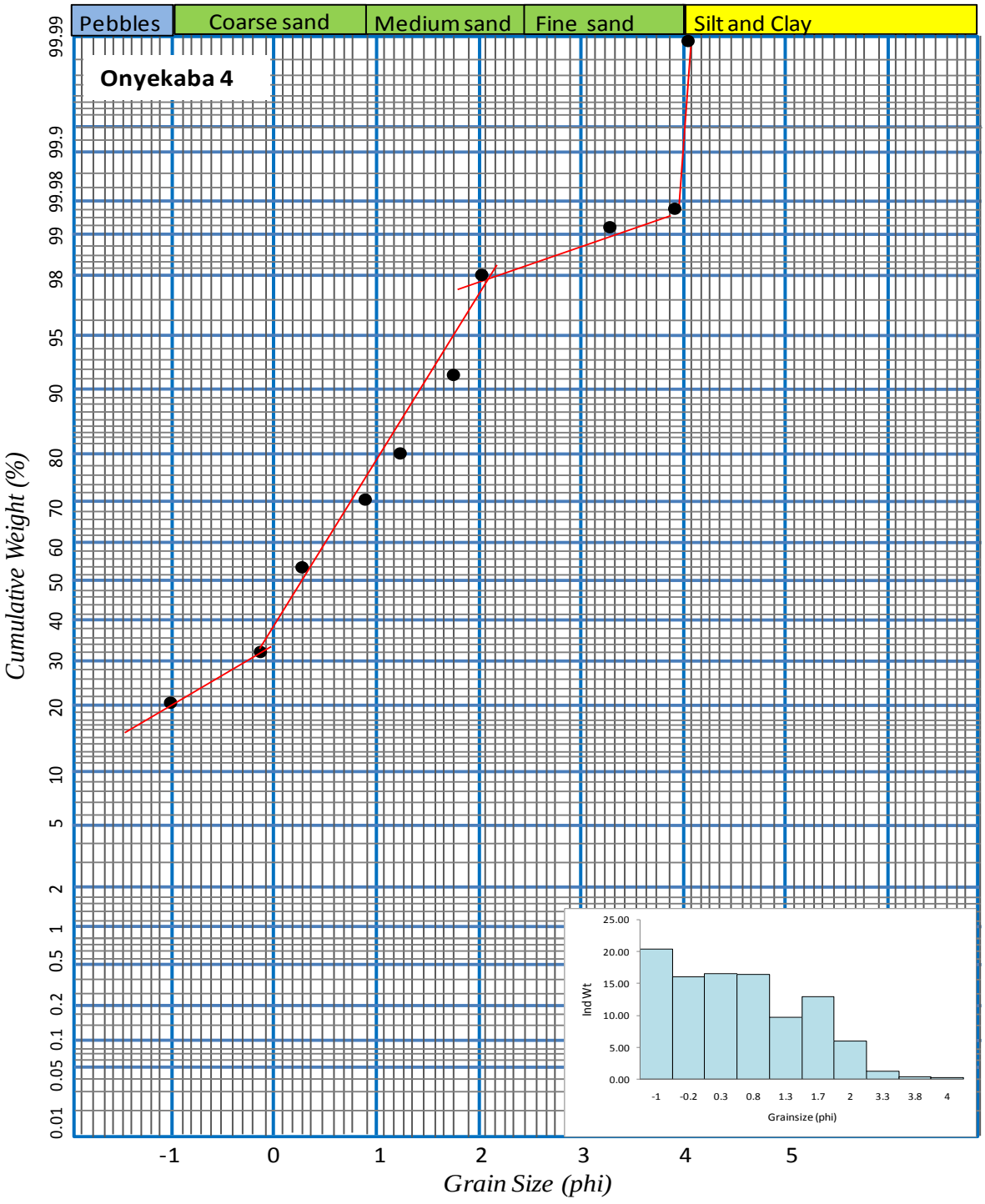

Figure 4.20: Cumulative Log-Probability Plots of Ajali Fm. Sample 4 (Inset: Bar Chart)

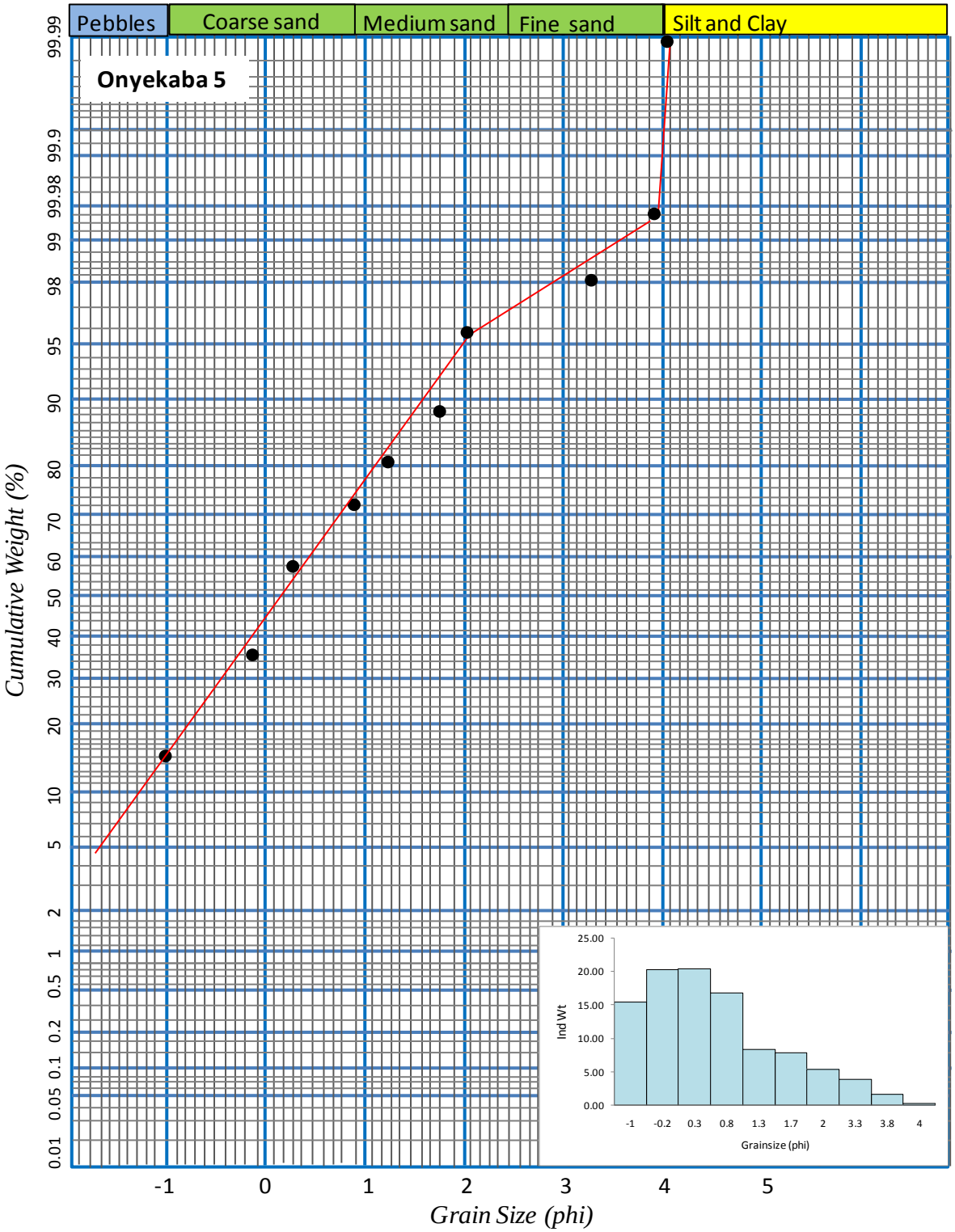

Figure 4.21: Cumulative Log-Probability Plots of Ajali Fm. Sample 5 (Inset: Bar Chart)

Mamu Formation

The modal grain size for each sample was determined from the tallest bar in the inset bar charts of Figures 4.22 to 4.29. In Sample 1 (Figure 4.22), the modal size measured 2.75 φ. Sample 2 (Figure 4.23) exhibited a modal size of 3.00 φ, while Sample 3 (Figure 4.24) recorded a slightly coarser mode at 2.50 φ. Sample 4 (Figure 4.25) showed a modal size of 3.25 φ, representing the finest mode among the samples.

Sample 5 (Figure 4.26) displayed the coarsest modal size at 2.25 φ. Sample 6 (Figure 4.27) had a modal size of 3.50 φ, and Sample 7 (Figure 4.28) measured 2.75 φ, matching Sample 1. The final sample, Sample 8 (Figure 4.29), recorded a modal size of 3.00 φ, identical to Sample 2. These values represent the most frequently occurring grain sizes within each sample's distribution.

Owelli Sandstones

The modal grain sizes for the Owelli Sandstone samples were determined from the inset bar charts in Figures 4.30 to 4.36. In Sample 1 (Figure 4.30), the modal size measured 2.50 φ. Sample 2 (Figure 4.31) exhibited a modal size of 2.75 φ, while Sample 3 (Figure 4.32) recorded a mode of 3.00 φ. Sample 4 (Figure 4.33) showed a modal size of 2.25 φ, representing the coarsest mode among the samples.

Sample 5 (Figure 4.34) displayed a modal size of 2.50 φ, matching Sample 1. Sample 6 (Figure 4.35) had a modal size of 2.75 φ, identical to Sample 2. The final sample, Sample 7 (Figure 4.36), recorded a modal size of 3.25 φ, making it the finest-grained sample in the set. These values represent the most frequently occurring grain sizes within each sample's distribution as derived from the graphical data.

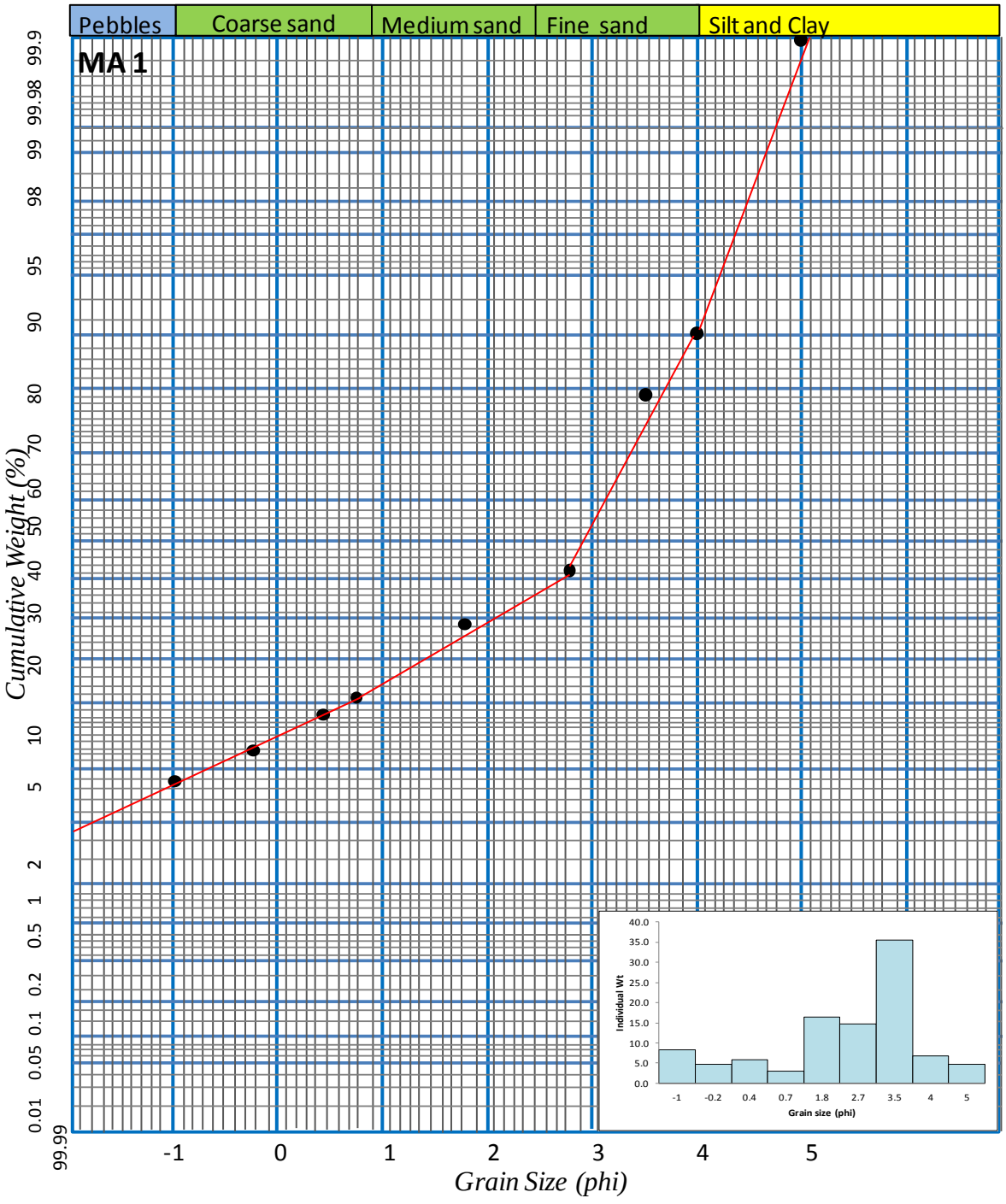

Figure 4.22: Cumulative Log-Probability Plots of Mamu Fm. Sample 1(Inset: Bar Chart)

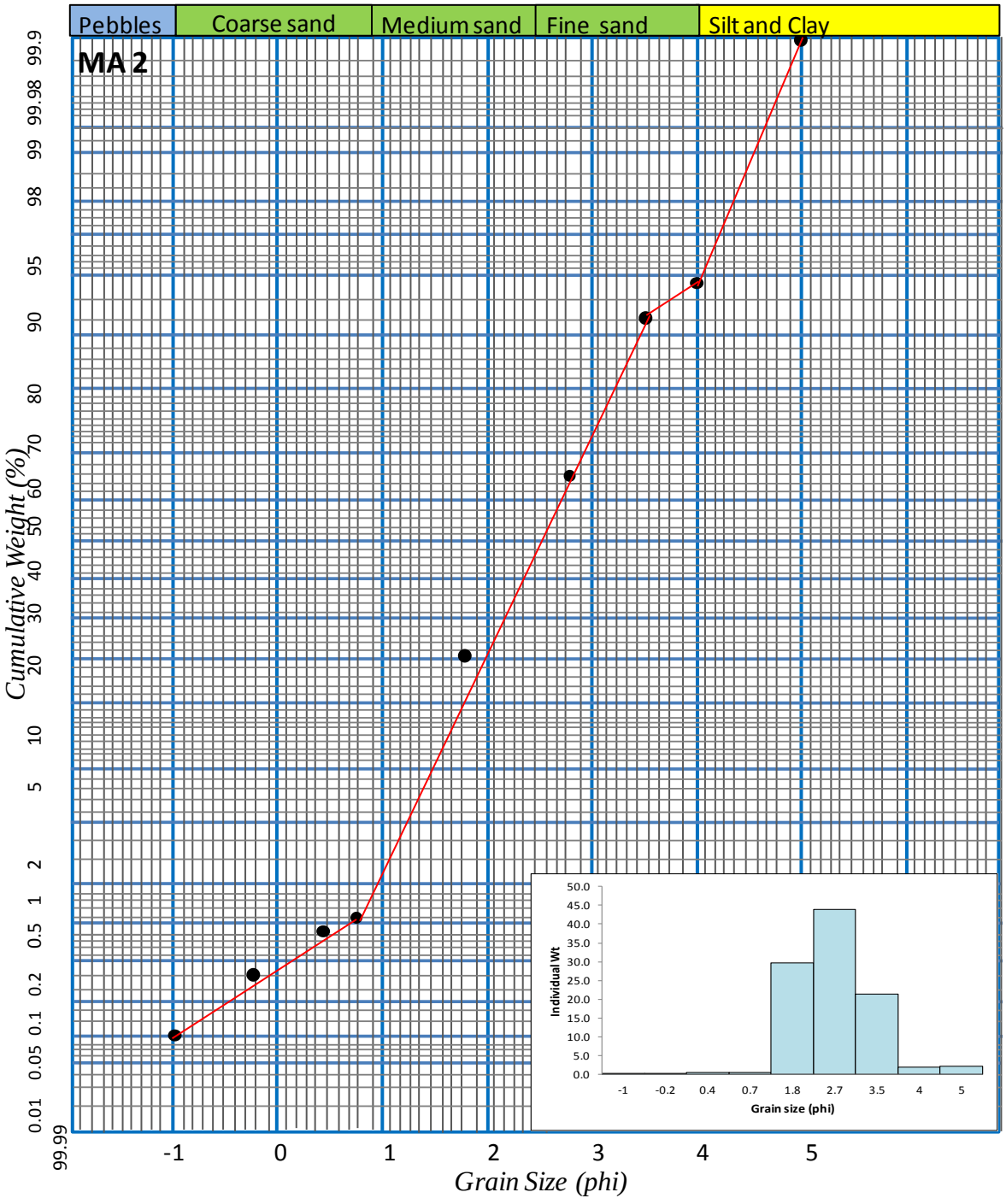

Figure 4.23: Cumulative Log-Probability Plots of Mamu Fm. Sample 2 (Inset: Bar Chart)

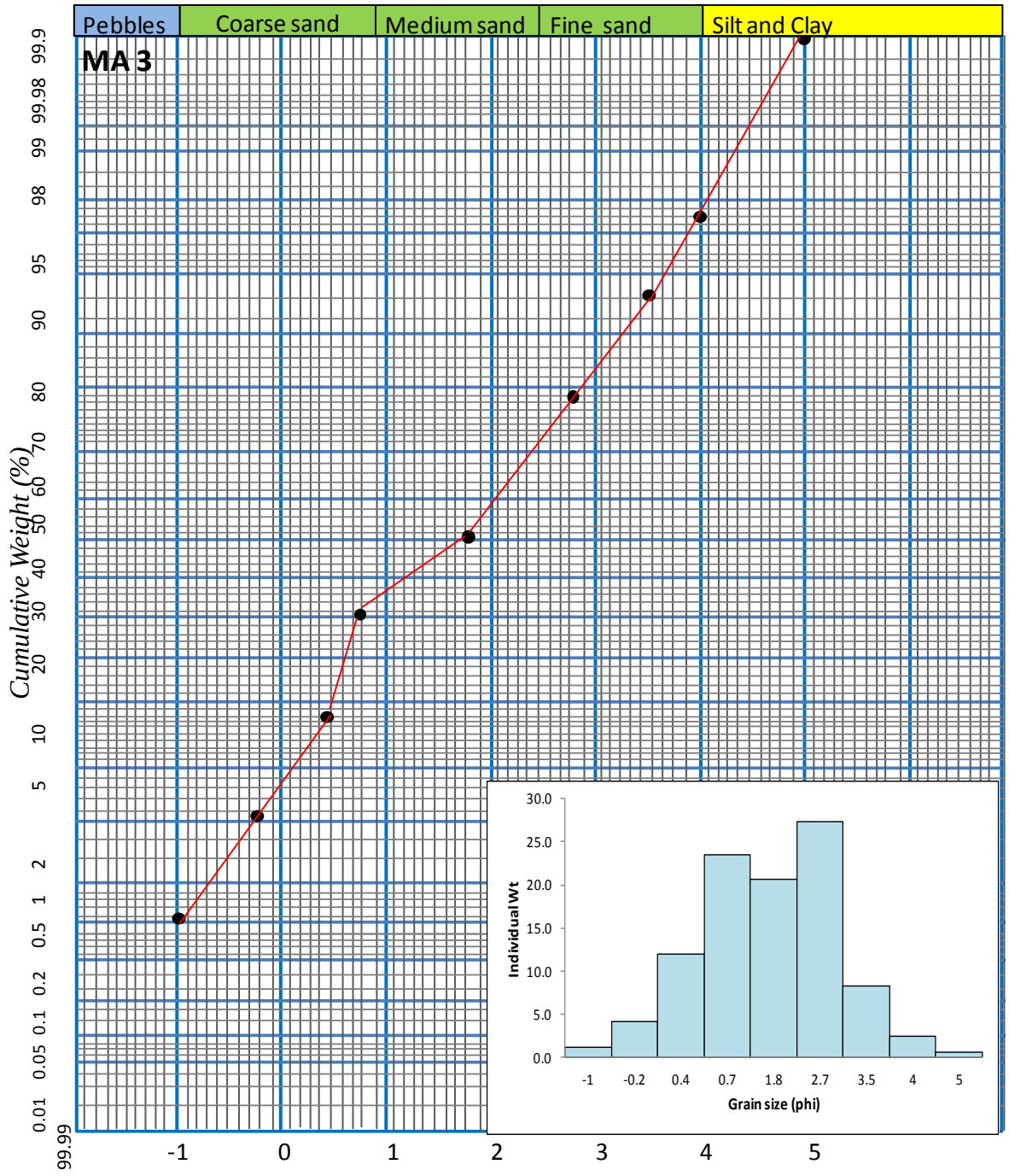

Figure 4.24: Cumulative Log-Probability Plots of Mamu Fm. Sample 3 (Inset: Bar Chart)

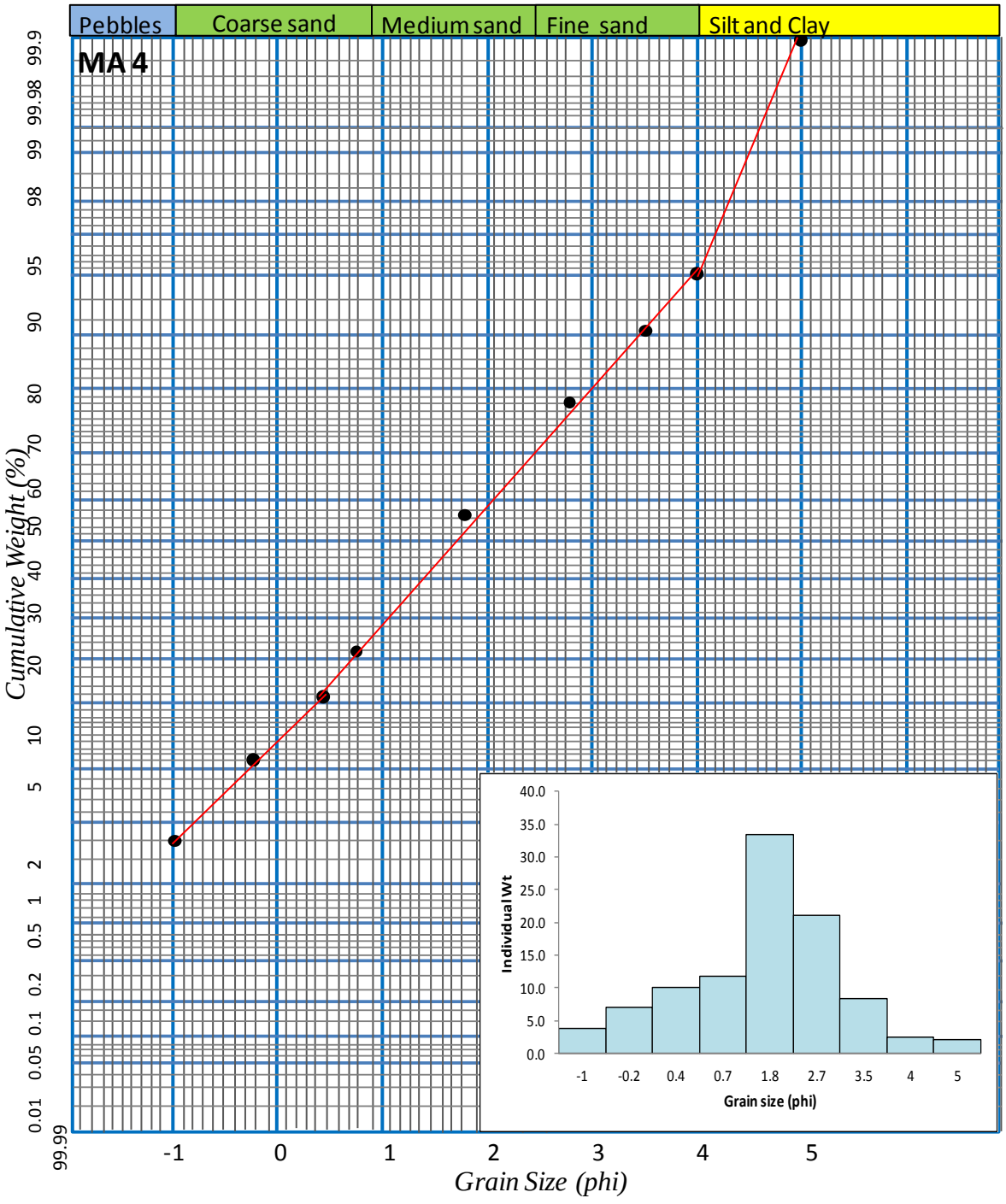

Figure 4.25: Cumulative Log-Probability Plots of Mamu Fm. Sample 4 (Inset: Bar chart)

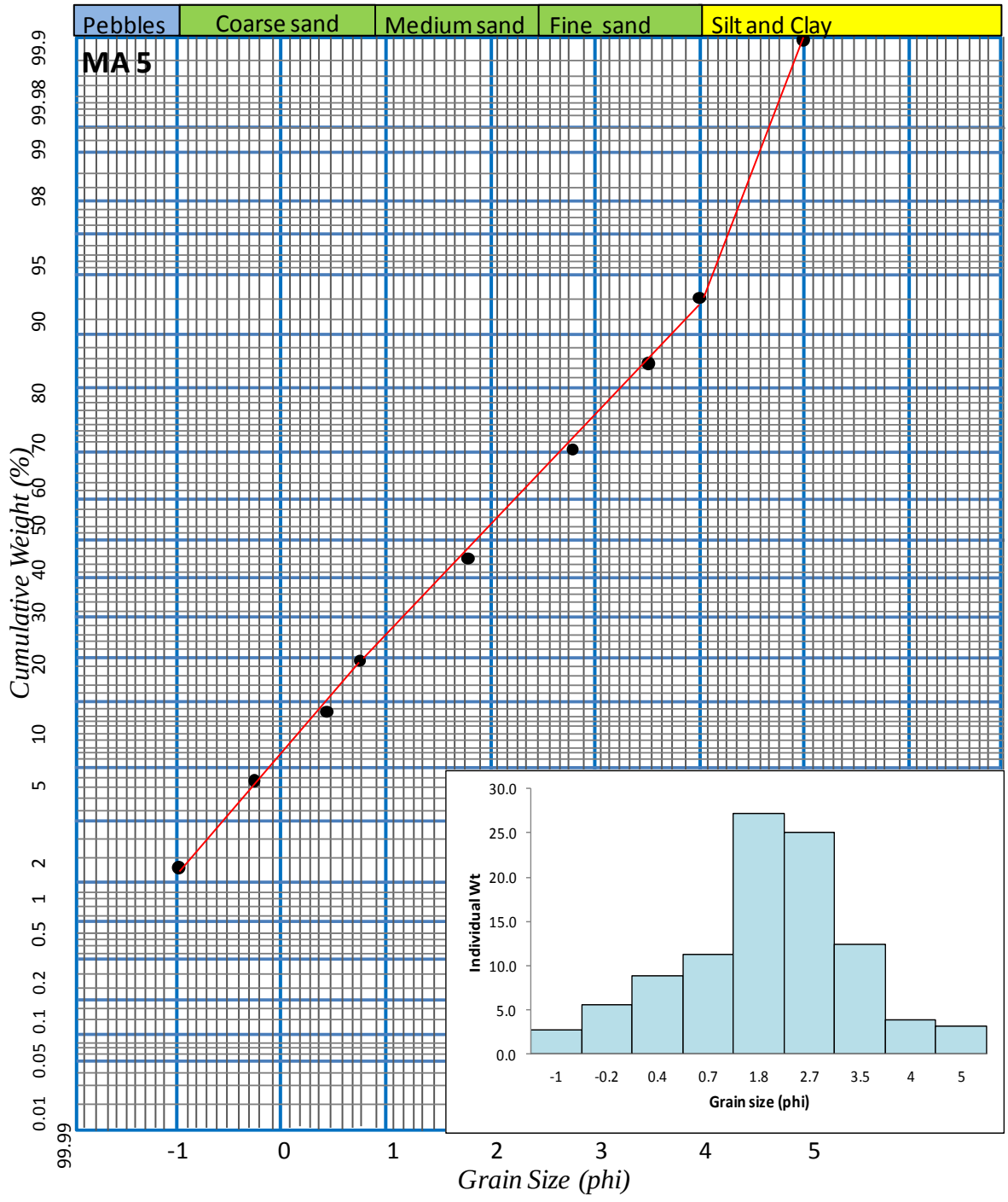

Figure 4.26: Cumulative Log-Probability Plots of Mamu Fm. Sample 5 (Inset: Bar Chart)

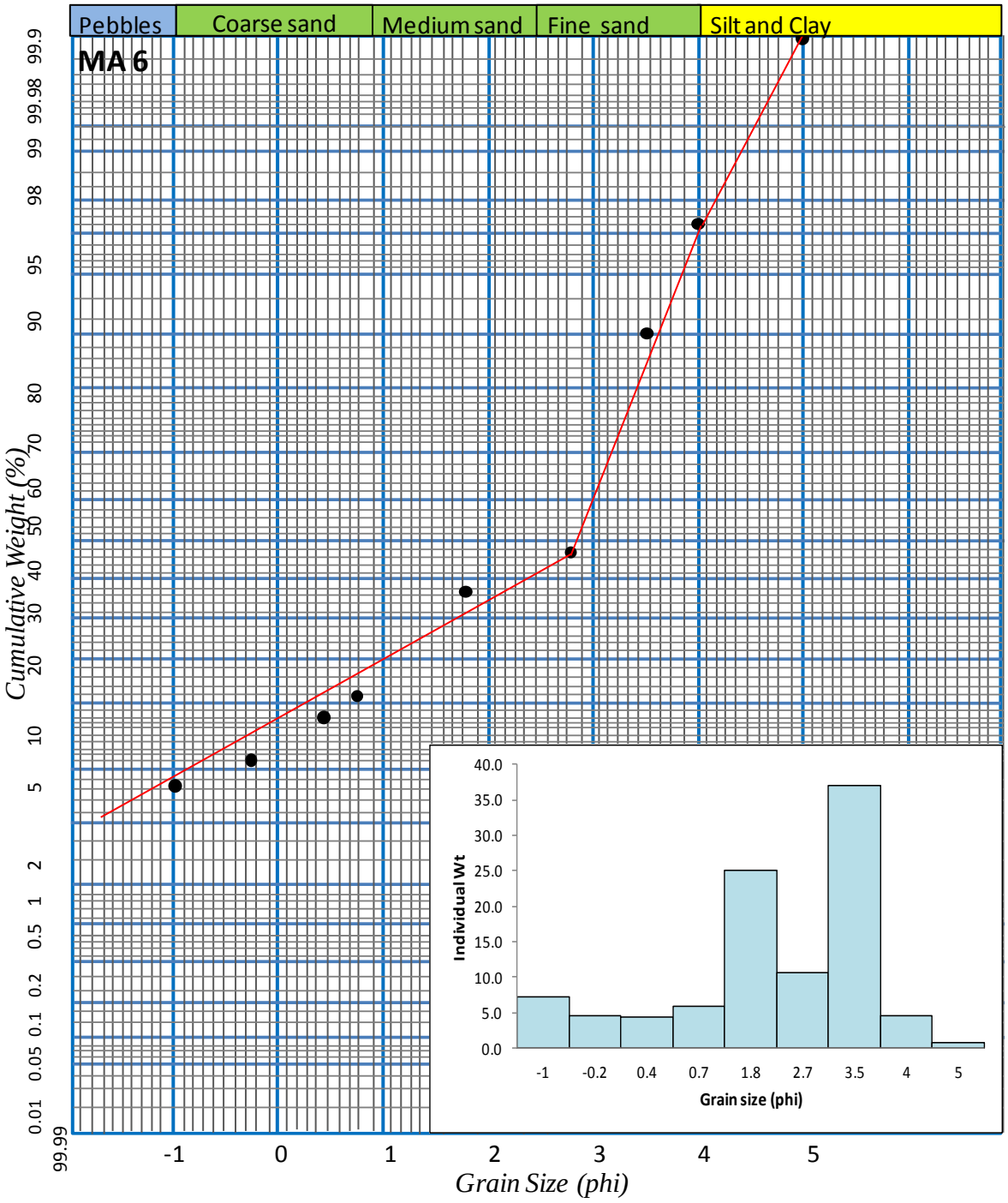

Figure 4.27: Cumulative Log-Probability Plots of Mamu Fm**.** Sample 6 (Inset: Bar Chart)

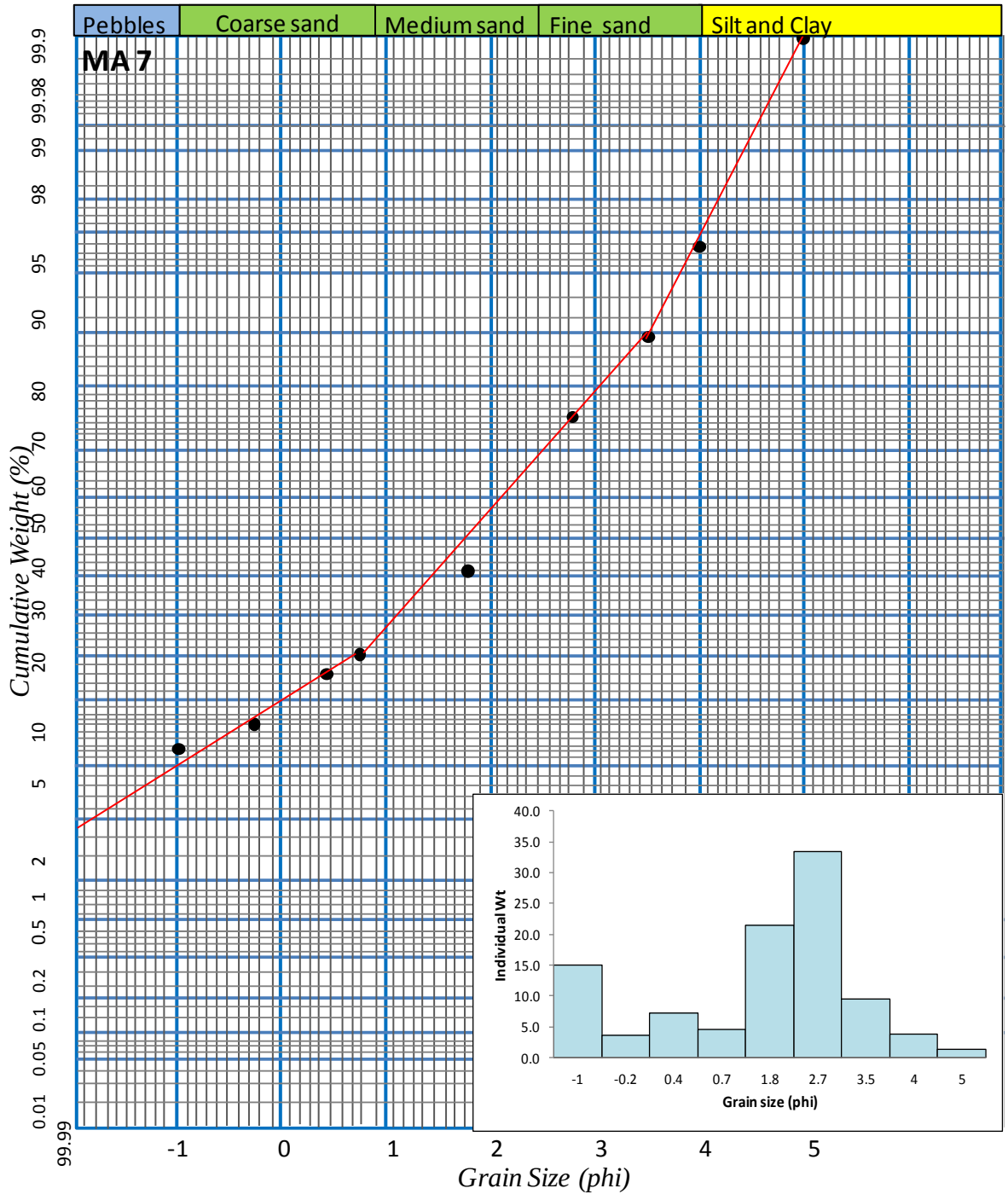

Figure 4.28: Cumulative Log-Probability Plots of Mamu Fm. Sample 7 (Inset: Bar Chart)

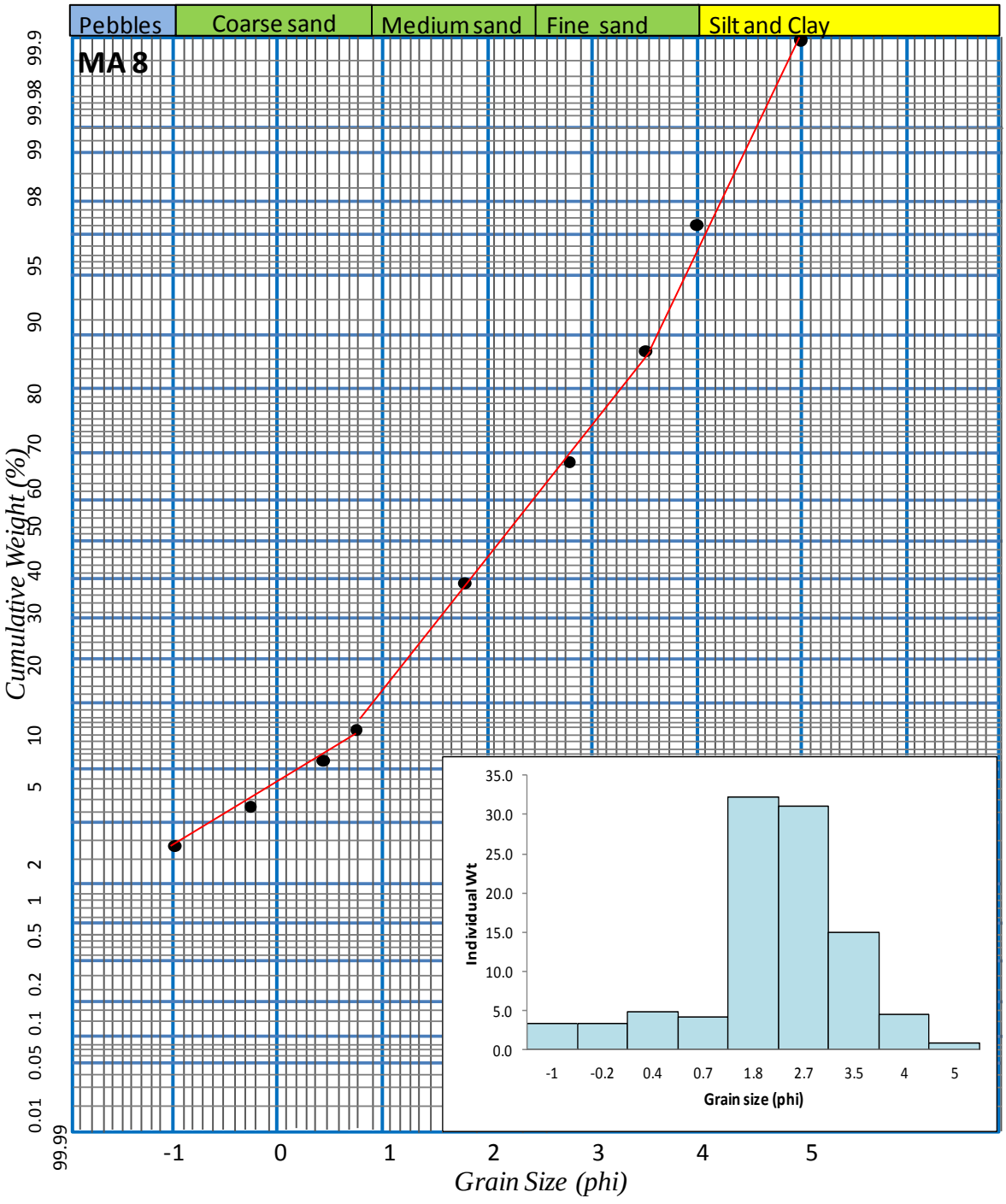

Figure 4.29: Cumulative Log-Probability Plots of Mamu Fm.Sample 8 (Inset: Bar Chart)

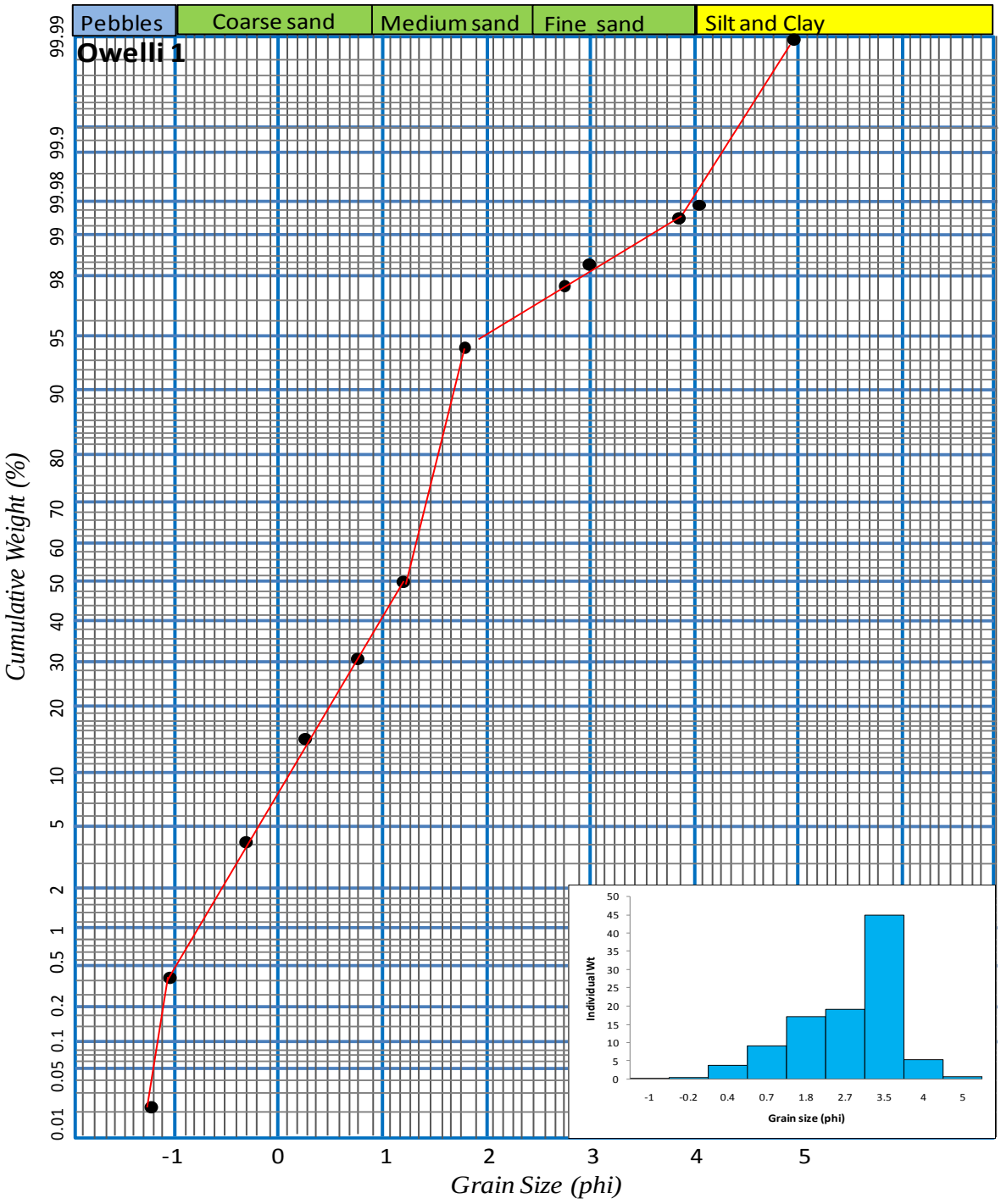

Figure 4.30 Cumulative Log-Probability Plots of Owelli Sst. Sample 1 (Inset: Bar Chart)

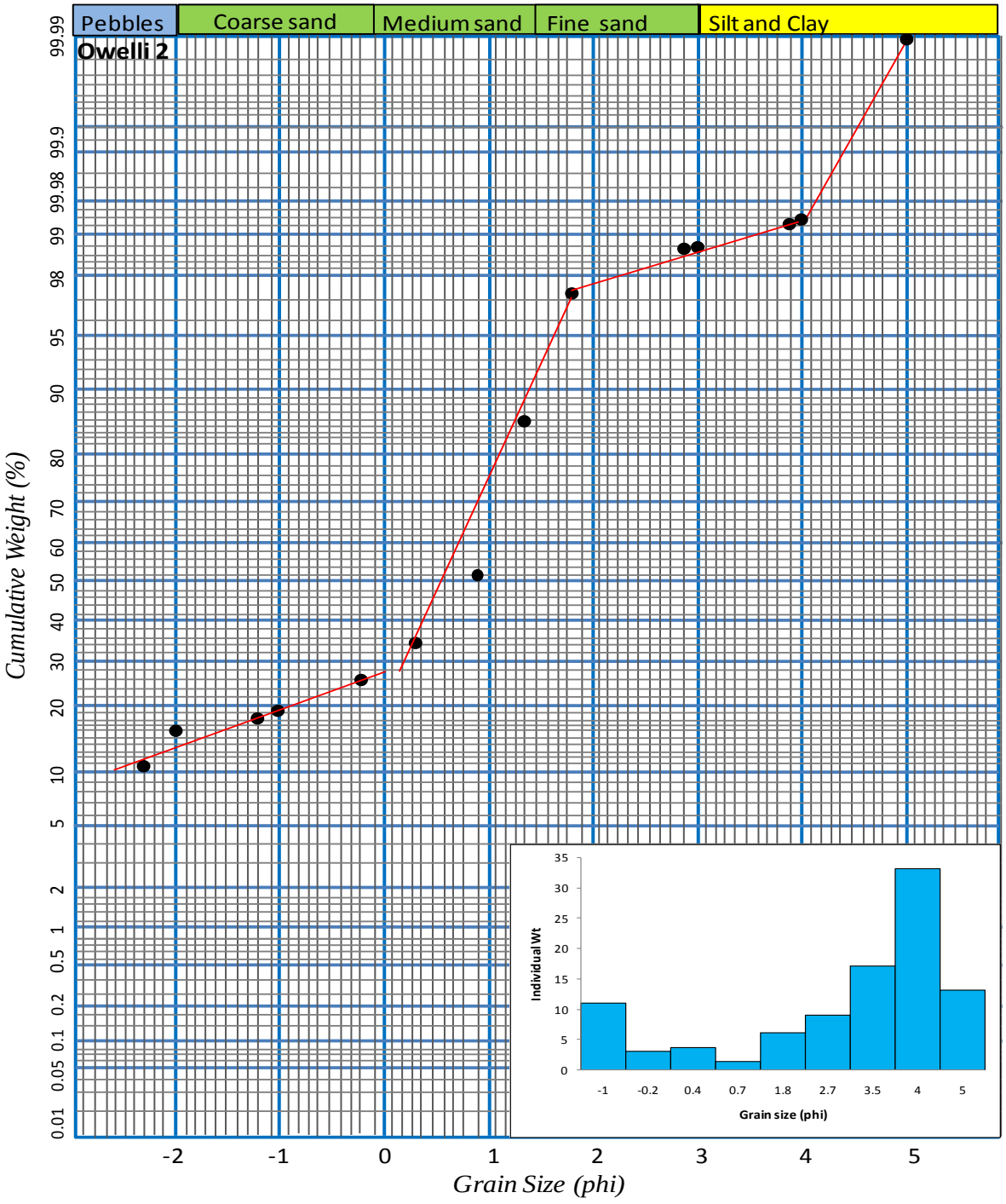

Figure 4.31: Cumulative Log-Probability Plots of Owelli Sst.Sample 2 (Inset: Bar Chart)

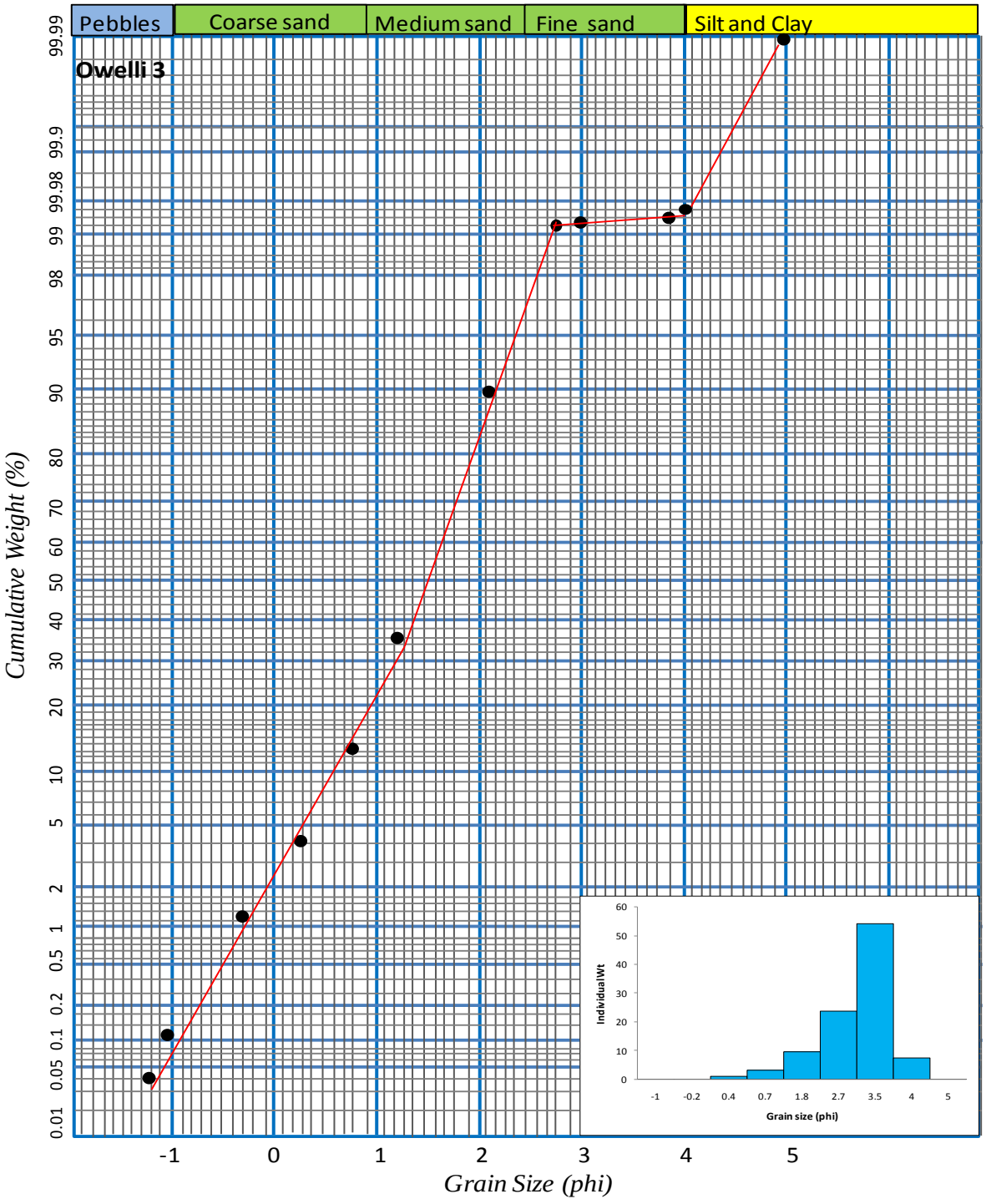

Figure 4.32: Cumulative Log-Probability Plots of Owelli Sst.Sample 3 (Inset: Bar Chart)

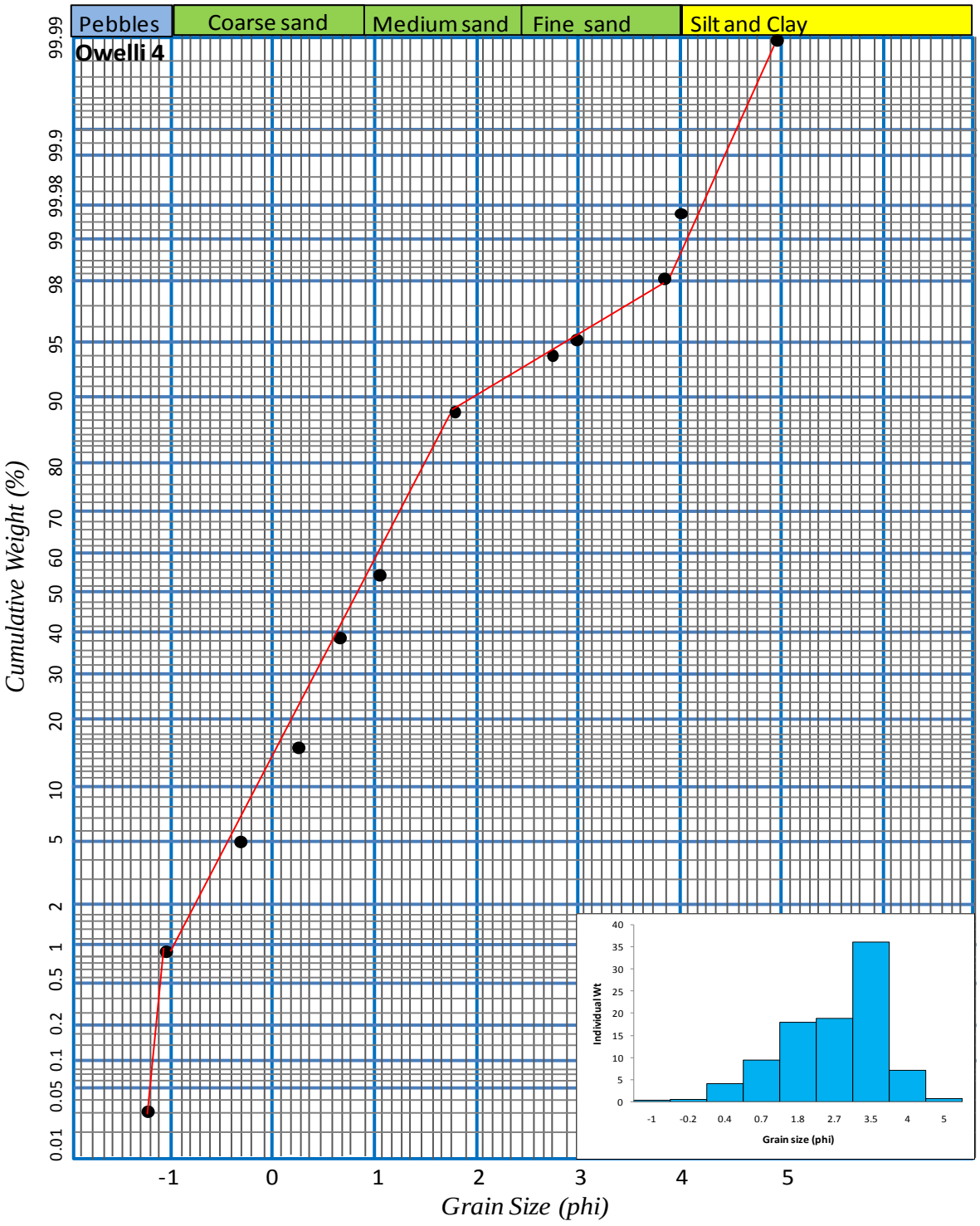

Figure 4.33: Cumulative Log-Probability Plots of Owelli Sst.Sample 4 (Inset: Bar Chart)

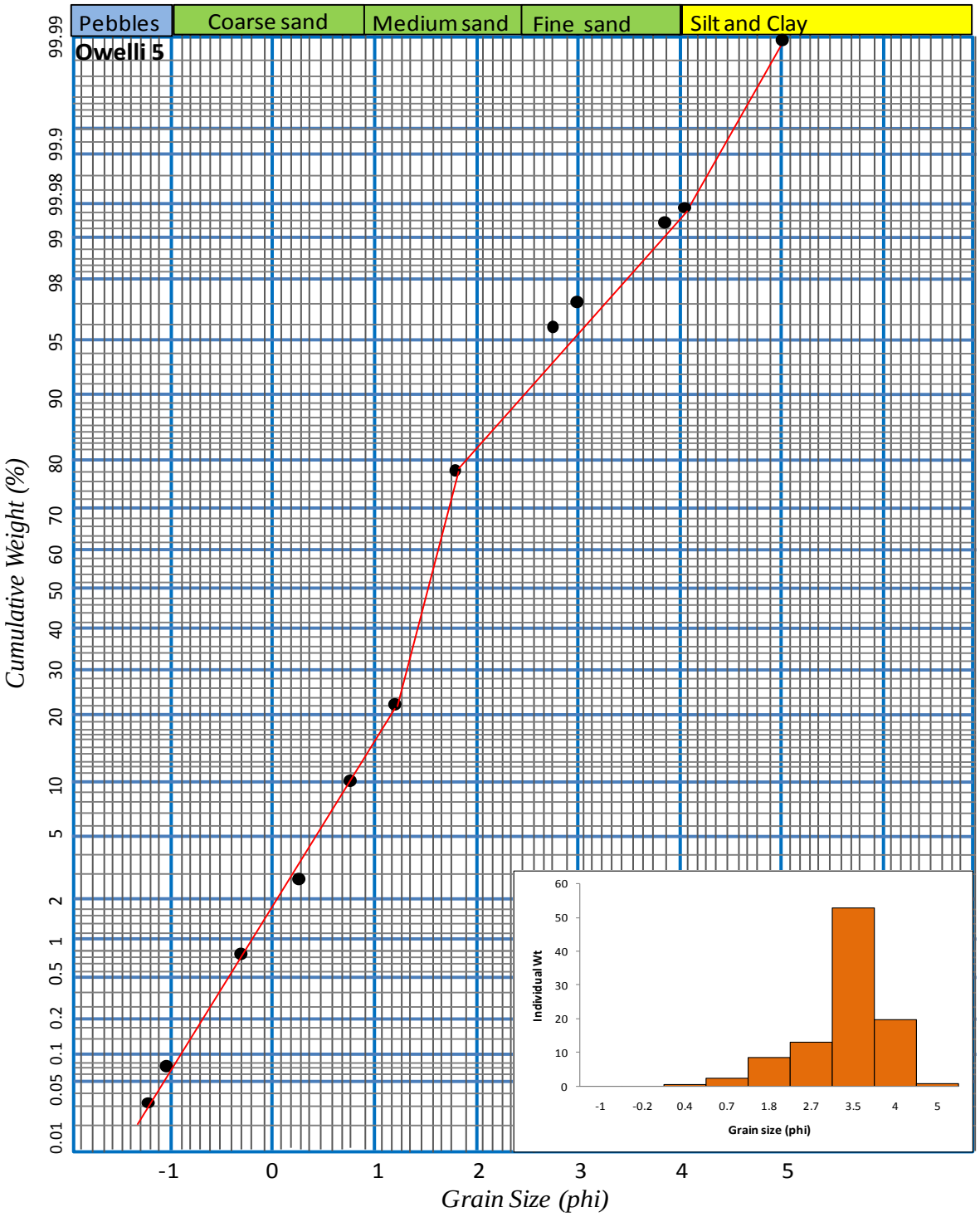

Figure 4.34: Cumulative Log-Probability Plots of Owelli Sst. Sample 5 (Inset: Bar Chart)

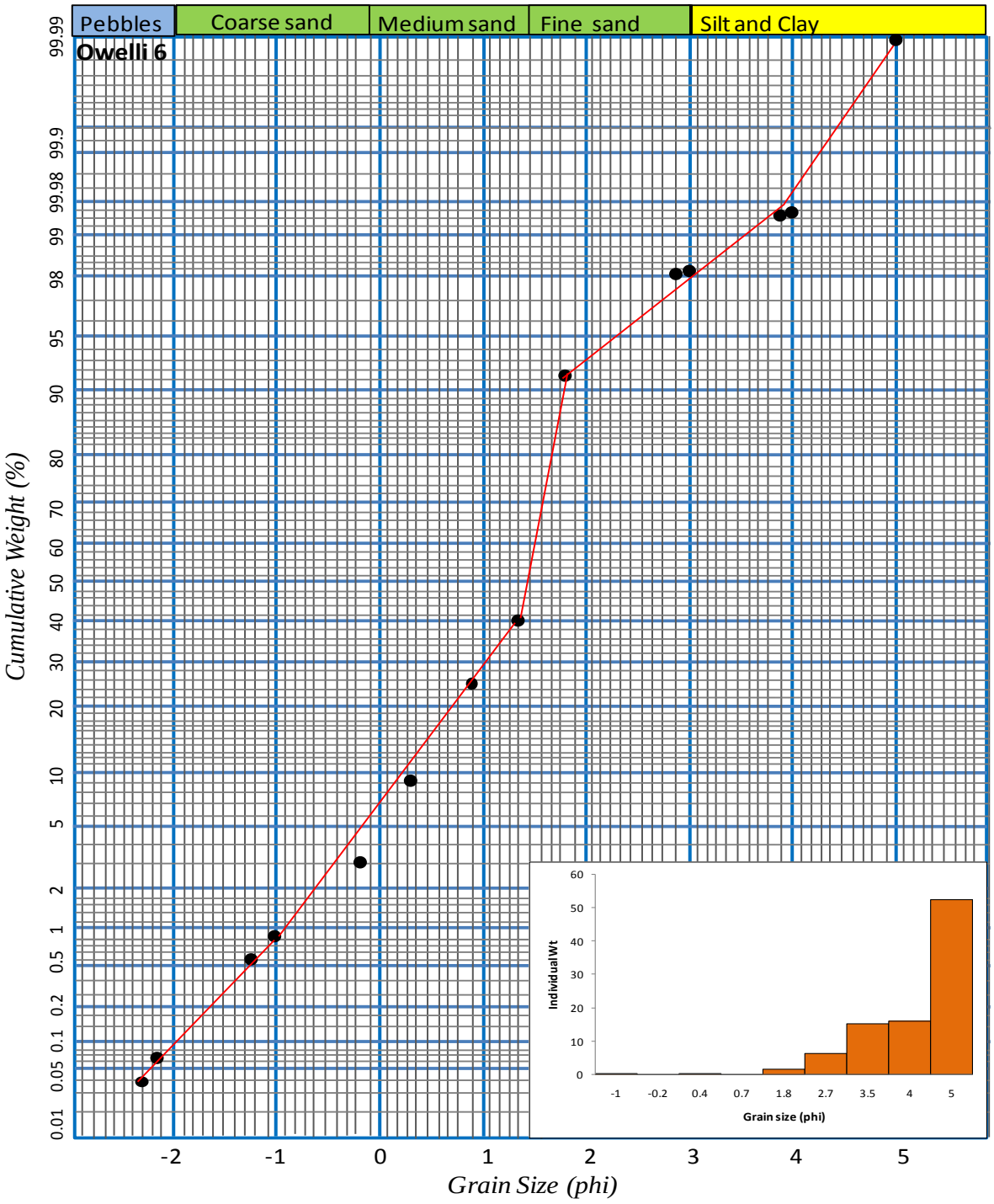

Figure 4.35: Cumulative Log-Probability Plots of Owelli Sst. Sample 6 (Inset: Bar Chart)

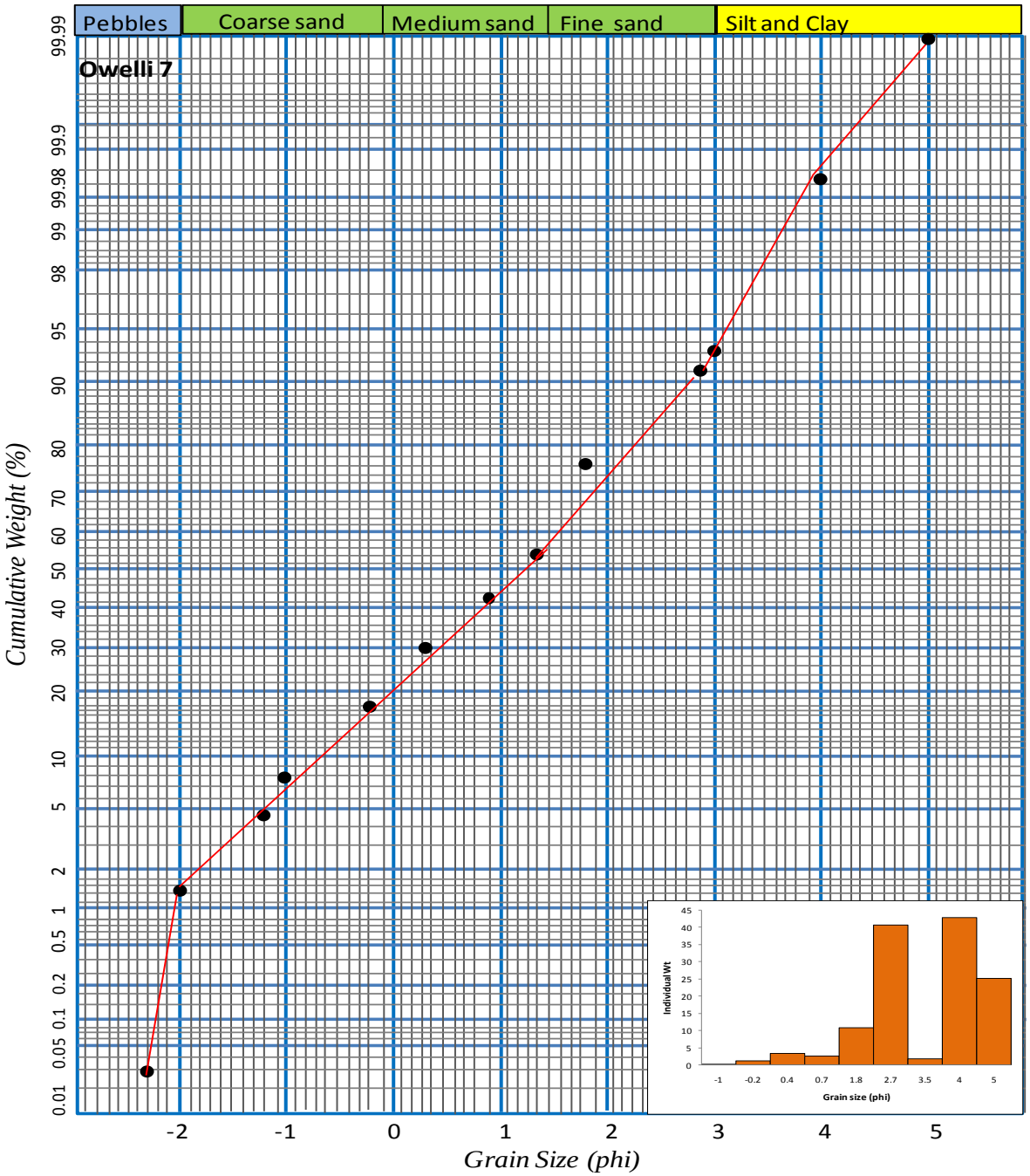

Figure 4.36: Cumulative Log-Probability Plots of Owelli Sst. Sample 7 (Inset: Bar Chart)

The Percentile Values

The percentile values for the grain-size distributions of the Nsukka Formation, Ajali Formation, Mamu Formation, and Owelli Sandstone samples are presented in Tables 4.6 and 4.7. Table 4.6 displays the P5, P16, P25, P50, P75, P84, and P95 percentile values for both the Nsukka and Ajali Formation samples. The Nsukka Formation samples (NSK 1-8) show a range of values across all percentiles, while the Ajali Formation samples (AJ 1-8) exhibit distinct percentile distributions that differ from the Nsukka samples.

Table 4.7 presents the corresponding percentile data for the Mamu Formation (MA 1-8) and Owelli Sandstone (Ow 1-7) samples. The Mamu Formation samples demonstrate variability in their percentile distributions, with some samples showing negative values in the lower percentiles. The Owelli Sandstone samples display their own characteristic distribution patterns across the measured percentiles. The complete dataset for all formations can be found in Tables 4.20 and 4.21, which provide the full set of percentile measurements for each sample.

Table 4.6 The Percentile Values of Nsukka Formation And Ajali Formation Samples

Sample ID	P5	P16	P25	P50	P75	P84	P95
NSK 1	-0.9	0.2	0.7	1.2	1.8	2.4	3.4
NSK 2	1.0	1.8	2.0	2.8	3.2	3.4	3.5
NSK 3	-0.2	0.7	1.1	1.8	2.7	3.0	3.2
NSK 4	0.5	1.1	1.4	2.0	2.9	3.0	3.2
NSK 5	-0.5	0.4	1.0	2.0	3.0	3.2	3.3
NSK 6	0.5	1.3	1.9	2.8	3.2	3.3	3.6
NSK 7	0.4	1.2	1.5	2.2	3.0	3.1	3.3
NSK 8	0.6	1.3	1.8	2.4	3.0	3.1	3.3
Sample ID	**P5**	**P16**	**P25**	**P50**	**P75**	**P84**	**P95**
AJ 1	-0.2	0.3	0.5	1.2	1.7	1.8	1.9
AJ 2	-1.2	-0.9	-0.3	0.3	1.2	1.7	1.9
AJ 3	-1.1	-0.8	-0.1	0.2	1.3	1.7	1.8
AJ 4	-1.3	-1.2	-0.8	0.3	1.0	1.6	2.0
AJ 5	-1.3	-1.0	-0.8	0.4	1.0	1.8	3.0
AJ 6	-1.0	-0.1	0.3	1.0	1.8	1.9	3.3
AJ 7	-0.5	0.2	0.3	0.8	1.1	1.2	1.9
AJ 8	-0.3	0.4	0.9	1.5	1.7	1.9	3.8

Table 4.7 The Percentile Values of Mamu Formation and Owelli Samples.

Sample ID	P5	P16	P25	P50	P75	P84	P95
MA 1	-1.8	0.5	1.0	2.8	3.2	3.5	4.0
MA 2	1.2	1.5	1.9	2.3	2.7	3.0	3.5
MA 3	-0.2	0.4	0.6	1.3	2.2	2.5	3.3
MA 4	-0.8	0.2	0.6	1.5	2.3	2.9	3.5
MA 5	-0.5	0.3	0.7	1.5	2.5	3.0	3.8
MA 6	-0.9	0.1	1.0	2.0	3.0	3.3	3.8
MA 7	-0.9	-0.2	0.4	1.5	2.4	2.7	3.5
MA 8	-0.7	0.7	1.1	1.8	2.6	3.0	3.6
Sample ID	**P5**	**P16**	**P25**	**P50**	**P75**	**P84**	**P95**
Ow1	-0.2	0.3	0.7	1.3	1.5	1.6	2.0
Ow 2	-2.7	-2.0	-0.2	0.8	1.2	1.4	1.6
Ow 3	0.3	0.8	1.0	1.3	1.6	1.7	2.0
Ow 4	-0.3	0.3	0.6	1.2	1.5	1.7	3.0
Ow 5	0.4	1.0	1.3	1.5	1.8	2.0	2.5
Ow 6	0.1	-0.6	0.9	1.4	1.6	1.8	2.0
Ow 7	-1.2	-0.3	0.3	1.2	1.8	2.4	3.2

Grain-Size Statistical Results

The grain-size parameters for all samples are presented in Tables 4.8 through 4.13. Table 4.8 shows the results for eight samples, with mean grain sizes ranging from 0.73 φ to 1.91 φ. Kurtosis values vary between 0.80 and 1.50, sorting ranges from 0.80 to 1.30, and skewness falls between -0.49 and 0.09. The average values for these samples are 1.39 φ (mean), 0.95 (kurtosis), 1.00 (sorting), and -0.11 (skewness).

Table 4.9 presents data for another set of eight samples, with mean values from 0.23 φ to 1.27 φ. The kurtosis measurements range from 0.72 to 2.10, sorting values between 0.61 and 1.35, and skewness from -0.27 to 0.15. The average parameters are 0.68 φ (mean), 1.08 (kurtosis), 1.02 (sorting), and -0.01 (skewness).

Results in Table 4.10 display mean grain sizes from 0.73 φ to 2.27 φ across eight samples. Kurtosis values vary from 0.90 to 1.20, sorting ranges between 0.70 and 1.60, and skewness measures from -0.56 to 0.14. The calculated averages are 1.29 φ (mean), 1.04 (kurtosis), 1.26 (sorting), and -0.09 (skewness).

Table 4.11 contains data for seven samples with mean sizes between 0.07 φ and 1.07 φ. Kurtosis values range from 1.04 to 1.72, sorting measures vary from 0.48 to 1.50, and skewness values fall between 0.17 and 0.50. The average values are 0.69 φ (mean), 1.29 (kurtosis), 0.90 (sorting), and 0.33 (skewness).

The classification standards for interpreting these parameters are provided in Table 4.12, which includes ranges for mean grain size, standard deviation (sorting), kurtosis, and skewness. The table presents the quantitative boundaries for various descriptive categories of sediment texture. All measured values can be evaluated against these established classification criteria.

Table 4.8: Calculated Grain-Size Parameters and Interpretation for Nsukka Formation

Sample ID	**Mean**	**Kurtosis**	**Sorting**	**Skewness**	**Interpretation**
NSK 1	0.73	1.50	1.10	0.01	Coarse sand, leptokurtic, poorly sorted, nearly symmetrical
NSK 2	1.91	0.90	0.80	-0.35	Medium sand, mesokurtic, moderately sorted, strongly coarse skewed
NSK 3	1.17	0.90	1.10	-0.07	Medium sand, mesokurtic, poorly sorted, nearly symmetrical
NSK 4	1.37	0.80	0.90	-0.04	Medium sand, platykurtic, moderately sorted, nearly symmetrical
NSK 5	1.16	0.80	1.30	-0.11	Medium sand, platykurtic, poorly sorted, coarse skewed
NSK 6	1.73	1.00	1.00	-0.49	Medium sand, mesokurtic, poorly sorted, strongly coarse skewed
NSK 7	1.48	0.80	0.90	0.09	Medium sand, platykurtic, moderately sorted, nearly symmetrical
NSK 8	1.58	0.90	0.90	0.06	Mediumsand, mesokurtic, moderately sorted, nearly symmetrical
Average	**1.39**	**0.95**	**1.00**	**-0.11**	**Medium sand, mesokurtic, poorly sorted, nearly symmetrical**

Table: 4.9 Calculated Grain-Size Parameters and Interpretation for Ajali Formation

Sample ID	Mean	Kurtosis	Sorting	Skewness	Interpretation
AJAL11	1.10	0.72	0.69	-0.27	Medium grained, Platykurtic, Moderately sorted, Coarse skewed
AJAL12	0.37	0.85	1.12	0.05	Coarse sand, Platykurtic, Poorly sorted, Nearly symmetrical
AJAL13	0.37	0.85	1.06	0.15	Coarse grained, platykurtic, poorly sorted, nearly symmetrical
AJAL14	0.23	0.75	1.20	-0.02	Coarse sand, Platykurtic, poorly sorted, coarse skewed
AJAL15	0.40	0.98	1.35	0.10	Coarse grained, mesokurtic, poorly sorted, near symmetrical
AJAL16	0.93	1.17	1.15	-0.27	Coarse sand, leptokurtic, poorly sorted, coarse skewed
AJAL17	0.73	1.23	0.61	0.05	Coarse sand, leptokurtic, moderately well sorted, near symmetrical
AJAL18	1.27	2.10	1.00	0.15	Medium sand, very leptokurtic, moderately sorted, fine skewed
Average	**0.68**	**1.08**	**1.02**	**-0.01**	**Coarse sand, Leptokurtic, poorlysorted, fineskewed**

Table 4.10: Calculated Grain-Size Parameters and Interpretation for Mamu Formation

Sample ID	**Mean**	**Kurtosis**	**Sorting**	**Skewness**	**Interpretation**
MA 1	2.27	1.10	1.60	-0.56	Fine sand, mesokurtic, poorly sorted, strongly coarse skewed.
MA 2	2.27	1.20	0.70	-0.01	Fine sand, leptokurtic, moderately sorted, near symmetrical
MA 3	0.84	0.90	1.10	0.14	Coarse sand, mesokurtic, poorly sorted, fine skewed
MA 4	0.89	1.00	1.30	-0.02	Coarse sand, mesokurtic, poorly sorted, near symmetrical
MA 5	0.93	1.00	1.30	0.09	Coarse sand, mesokurtic, poorly sorted, near symmetrical
MA 6	1.07	1.00	1.50	-0.21	Medium grained, mesokurtic, poorly sorted, coarse skewed
MA 7	0.73	0.90	1.40	-0.13	coarse grained, mesokurtic, poorly sorted, coarse skewed
MA 8	1.29	1.20	1.20	-0.06	medium sand, leptokurtic, poorly sorted, near symmetrical
Average	**1.29**	**1.04**	**1.26**	**-0.09**	**Medium grained, mesokurtic, poorly sorted, near symmetrical**

Table 4.11: Calculated Grain-Size Parameters and Interpretation for Owelli Sandstone

Sample ID	**Mean**	**Kurtosis**	**Sorting**	**Skewness**	**Interpretation**
Owelli 1	1.07	1.13	0.66	0.23	Medium grained, leptokurtic, moderately sorted, fine skewed
Owelli 2	0.07	1.26	1.50	0.18	Coarse grained,leptokurtic, poorly sorted, fine skewed
Owelli 3	0.89	1.16	0.48	0.44	Coarse grained, leptokurtic, well sorted, fine skewed
Owelli 4	0.69	1.50	0.85	0.36	Coarse grained, leptokurtic, moderately sorted, fine skewed
Owelli 5	1.06	1.72	0.57	0.50	Medium grained, very leptokutic, moderately sorted, strongly fine skewed
Owelli 6	0.47	1.04	0.89	0.17	Coarse grained, leptokurtic, moderately sorted, strongly fine skewed
Owelli 7	0.57	1.20	1.34	0.44	Coarse, leptokurtic, poorly sorted, fine skewed
Average	**0.69**	**1.29**	**0.90**	**0.33**	**Coarse sand, Leptokurtic, Moderately sorted, Fine skewed**

Table 4.12 Interpretation for sieve parameters (adapted from Boggs, 2006)

Mean Grain size Interpretation						
-1 – 0.0	0.0 – 1.0	1.0 – 2.0	2.0 – 3.0	3.0 – 4.0	4.0 – 5.0	
Very coarse sand	Coarse sand	Medium sand	Fine sand	Very fine sand	Coarse silt	

Standard Deviation Interpretation							
< 0.35	0.35 – 0.50	0.50 – 0.71	0.71 – 1.00	1.00 – 2.00	2.00 – 4.00	>4.00	
Very well sorted	Well sorted	Moderately well sorted	Moderately sorted	Poorly sorted	Very poorly sorted	Extremely poorly sorted	

Kurtosis Interpretation						
Kurtosis	<0.67	0.67 – 0.90	0.90 – 1.11	1.11 – 1.50	1.50 – 3.00	>3.00
Verbal description	Very Platykurtic	Platykurtic	Mesokurtic	Leptokurtic	Very leptokurtic	Extremely leptokurtic

Skewness Interpretation				
+1.00 to +0.30	+0.30 to +0.10	+0.10 to -0.10	-0.10 to -0.30	-0.30 to -1.00
Strongly fine skewed	Fine skewed	Near symmetrical	Coarse skewed	Strongly coarse skewed

4.1.3.1 Graphic Mean Size (Mz)

The mean grain size (Mz) values obtained for the studied formations are presented in Table 4.13. The Nsukka Formation recorded a mean value of 1.39 Φ, while the Ajali Formation showed a mean of 0.91 Φ. The Mamu Formation yielded a mean size of 1.29 Φ, and the Owelli Sandstone recorded the coarsest mean value at 0.69 Φ. These values represent the central tendency of grain sizes within each unit. The range of mean sizes reflects differences in sediment characteristics across the formations.

4.1.3.2 Inclusive Graphic Standard Deviation (σi)

Sorting values, as expressed by the inclusive graphic standard deviation (σi), are summarized in Table 4.14. The Nsukka Formation recorded a sorting value of 1.00 Φ, while the Ajali and Mamu formations showed values of 1.05 Φ and 1.26 Φ, respectively. The Owelli Sandstone had the lowest σi value of 0.90 Φ. These figures indicate the degree of uniformity in particle size distribution for each formation. Lower values represent better sorting, while higher values indicate more poorly sorted sediments.

4.1.3.3 Inclusive Graphic Skewness (Ski)

The inclusive graphic skewness (Ski) values for the four formations are also detailed in Table 4.13. The Nsukka and Mamu formations displayed slightly negative skewness values of -0.11 and -0.09, respectively. In contrast, the Ajali Formation recorded a slightly positive skewness of 0.10, while the Owelli Sandstone showed a higher positive skewness value of 0.33. These results provide a measure of asymmetry in the grain size distribution. Positive values indicate a tail toward finer grains, while negative values suggest a tail toward coarser grains.

4.1.3.4 Graphic Kurtosis (KG

Graphic kurtosis (KG) values obtained from the grain size analysis are shown in Table 4.13. The Nsukka Formation recorded a kurtosis value of 0.95, while the Ajali Formation had the highest value of 1.34. The Mamu Formation and the Owelli Sandstone recorded kurtosis values of 1.04 and 1.29, respectively. These kurtosis values provide information on the peakedness or flatness of the grain size distribution curves. Values close to 1 are considered mesokurtic, while values greater than 1 suggest more peaked distributions.

Table 4.13: Mean, Kurtosis, Sorting and Skewness of Formations.

Formation	Mean	Kurtosis	Sorting	Skewness	Interpretation
Nsukka	1.39	0.95	1	-0.11	medium sand, mesokurtic, poorly sorted, nearly symmetrical
Ajali	0.91	1.34	1.05	0.1	Coarse sand, Leptokurtic, poorly sorted, fine skewed
Mamu	1.29	1.04	1.26	-0.09	Medium grained, mesokurtic, poorly sorted, near symmetrical
Owelli Sanstones	0.69	1.29	0.9	0.33	Coarse grained, leptokurtic, moderately sorted, fine skewed

4.1.4 Bivariate Grain Size Parameters

4.1.4.1 Graphic Mean Size (Mz) vs. Inclusive Graphic Standard Deviation (σi)

In this study, scatter plots were generated based on the methodologies outlined by Moiola and Weiser (1968) (see Figures 4.37 – 4.43 and the originating Tables 4.14-4.17). In the case of Moiola and Weiser (1968), the points of Nsukka Formation and Ajali sandstones values are concentrated within the river field, with the remainder falling within the beach field. Mamu Formation has the effects of beach and river fields but more in the beach field.Moreover, mean size and standard deviation have been utilized as maturity indices, as noted by Glaister and Nelson (1974). Following their approach (see Figure 4.38), it is observed that the plots of Ajali and Owelli sandstones cluster between the braided bar and delta front, indicating a more matured environment than Nsukka and Mamu sandstones that cluster just after the braided bar.

4.1.4.2 Graphic Mean Size (Mz) vs. Inclusive Graphic Skewness (Ski)

Deviations from the unimodal distribution enhance the sensitivity of the skewness parameter. Skewness, closely tied to the average size, adopts a noticeably sinusoidal pattern under such circumstances. This sinusoidal tendency emerges when the addition of materials, whether finer or coarser, alters the mean's position relative to the median.

Scatter plots were generated and juxtaposed with those presented by Moiola and Weiser (1968) and Friedman (1967) (refer to Figure 4.37- Figure 4.43). In both instances, the plots primarily cluster within the beach domain. In particular, Nsukka, Ajali and Mamu formations cluster around the beach domain while the Owelli Sandstones exist within the river domain.

4.1.4.3 Graphic Mean Size (Mz) vs. Graphic Kurtosis (KG)

The general trend of data points can reveal patterns in grain size distribution and peakedness (kurtosis) across the samples. A positive correlation might suggest that sediments with larger average grain sizes (higher Mz) tend to have a more peaked distribution (higher KG), indicating better sorting in the central portion of the size range. A negative correlation could imply that finer-grained sediments (lower Mz) have a more peaked distribution, suggesting better sorting in the tails (less extreme grain sizes). No clear correlation might indicate a variety of depositional

processes or source materials influencing the grain size distribution and peakedness independently.

In this study, the spread of KG values can offer insights into the potential depositional processes. A cluster of data points with KG values close to 1 (normal distribution) might suggest relatively constant energy conditions during deposition, such as Nsukka and Mamu Formation sandstones having Kg values of 0.95 and 1.04 respectively. See Figure 4.37 - Figure 4.43.

A dominance of data points with KG values less than 1 (platykurtic) could indicate environments with winnowing processes that remove very coarse and very fine grains, leaving a more even distribution in the central size range. This might be associated with wave action or fluvial transport. A prevalence of data points with KG values greater than 1 (leptokurtic) could suggest deposition from events with fluctuating energy, leading to a sharper peak in the central grain size range. This might be related to debris flows or storm events.

4.1.4.4 Graphic Standard Deviation (σi) vs. Inclusive Graphic Skewness (Ski)

In the current scenario (Figures 4.37 – 4.38), the plots predominantly cluster to the right of the normal skewness within the negative sector, suggesting a predominance of larger size classes and poor sorting. However, the introduction of a slightly coarser population disrupts the skewness pattern, resulting in some dispersion towards the negative sectors as well.

Most data points cluster on the "river" side of the plot, suggesting these sand samples likely originated from river. Also, in Figure 4.43, it is shown that all plots exist in the river domain in a place of standard deviation against skewness after Friedman (1967). However, another case, Figures 4.39 – 4.40 shows that almost all the data points on the "beach" side. This unexpected result could be due to several factors: The sediment in this specific case might have all originated from rivers. The chosen grain size parameters might not be ideal for distinguishing between beach and river sands in this particular location. Other environmental factors besides beach or river origin might be influencing the grain size distribution

Table 4.14: Interpretation Plot Table of Standard Deviation Vs Mean

Formation	Graphic Standard Deviation	Graphic Mean
Nsukka	1	1.39
Ajali	1.02	0.68
Mamu	0.9	1.29
Owelli	0.9	0.69

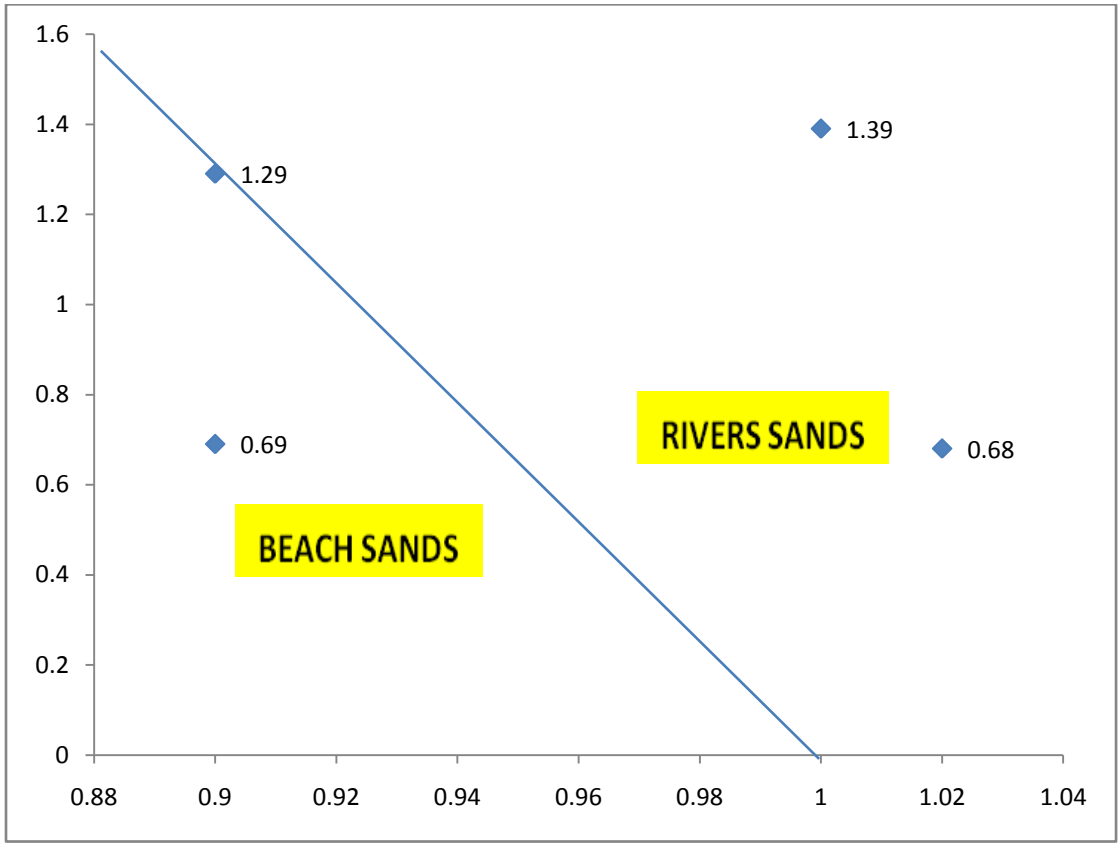

Figure 4.37 Values and Generated plot of Graphic Mean VS standard Deviation (after MOIOLA and WEISER, 1968)

Table 4.15: Interpretation plot table of Graphic mean VS standard Deviation

Formation	Graphic Standard Deviation	Graphic Mean
Nsukka	1	1.39
Ajali	1.02	0.68
Mamu	0.9	1.29
Owelli	0.9	0.69

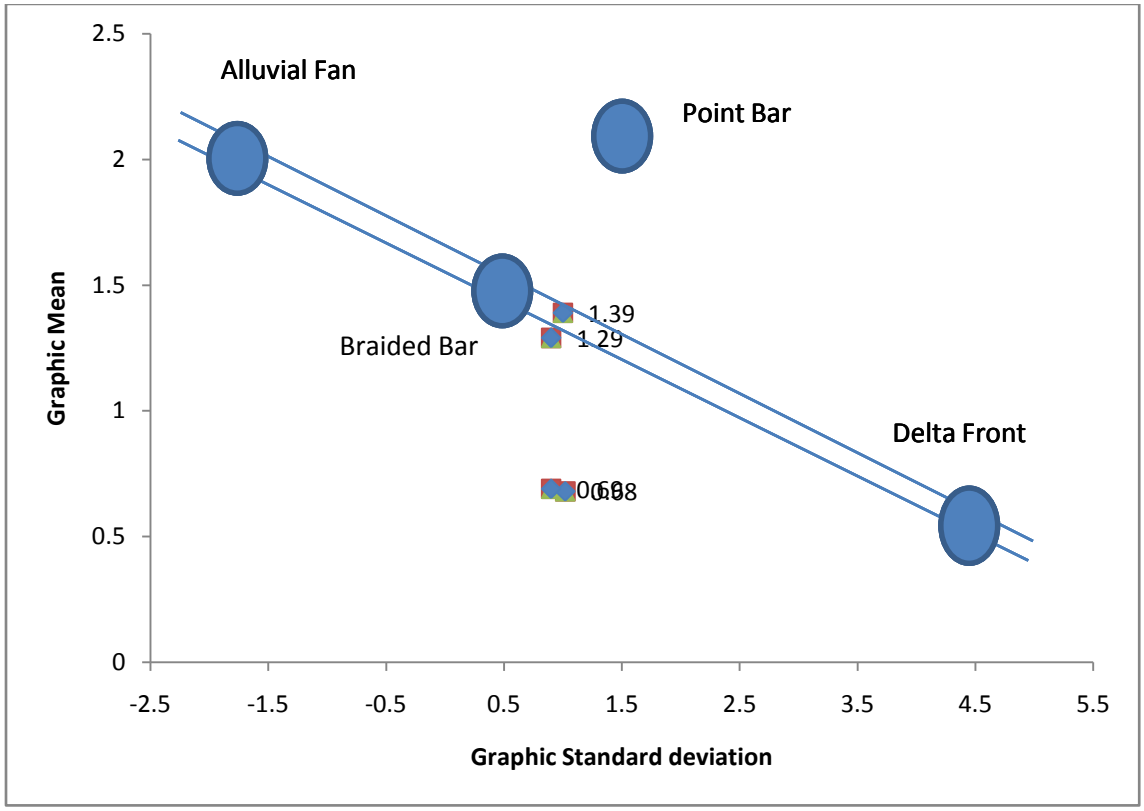

Figure 4.38 Values and Generated plot of Graphic Mean VS standard Deviation (after GLAISTER and NELSON, 1974)

Table 4.16. Interpretation Graph of Graphic Mean Size Vs Graphic Skewness

Formation	Mean	Kurtosis	Sorting	Skewness
Nsukka	**1.39**	**0.95**	**1.00**	**-0.11**
Ajali	**0.68**	**1.08**	**1.02**	**-0.01**
Mamu	**1.29**	**1.04**	**1.26**	**-0.09**
Owelli	**0.69**	**1.29**	**0.90**	**0.33**

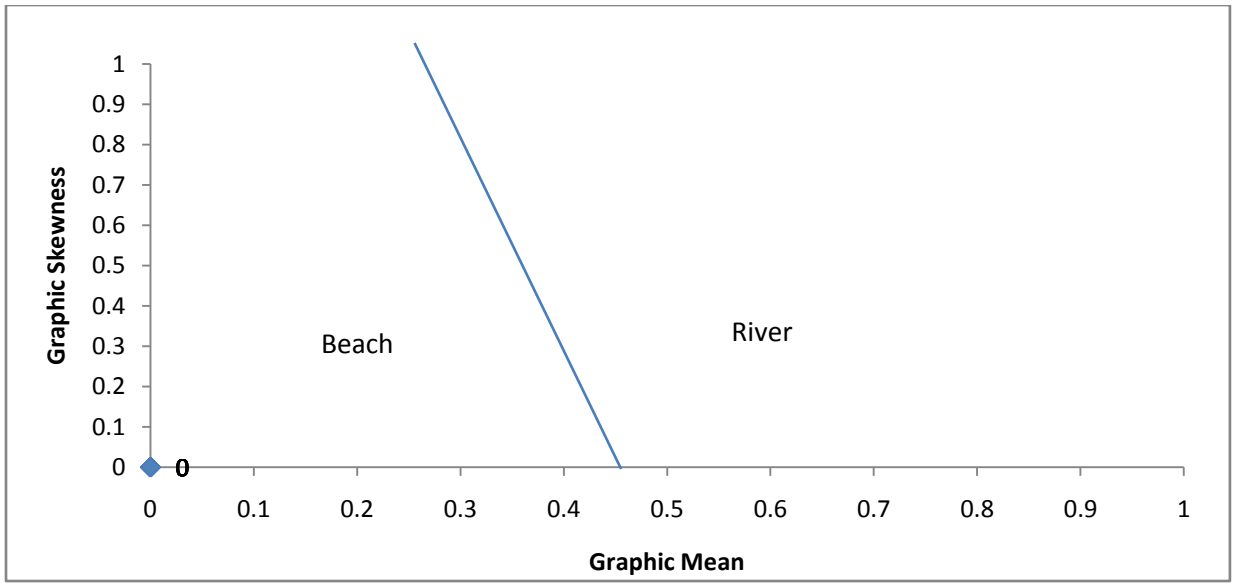

Figure 4.39 Values and Graph of Graphic Mean Size Vs Graphic Skewness

(After Moiola And Weiser, 1968)

Table 4.17. Interpretation for Plotting Graph of Graphic Mean Size Vs Graphic Skewness

FORMATION	MEAN	SKEWNESS
Nsukka	1.39	-0.11
Ajali	0.68	-0.01
Mamu	1.29	-0.09
Owelli	0.69	0.33

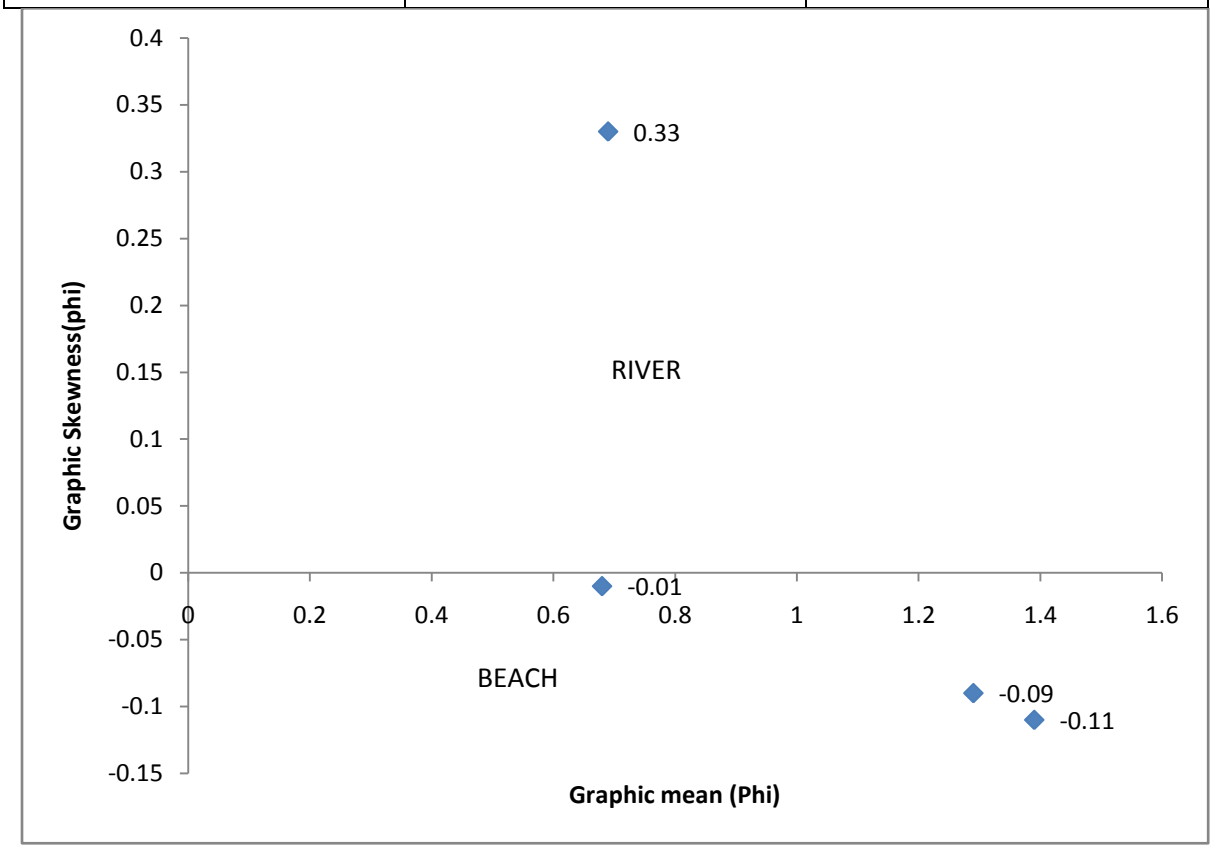

Figure 4.40: Values and Graph Of Graphic Mean Size Vs Graphic Skewness (After Friedman, 1967)

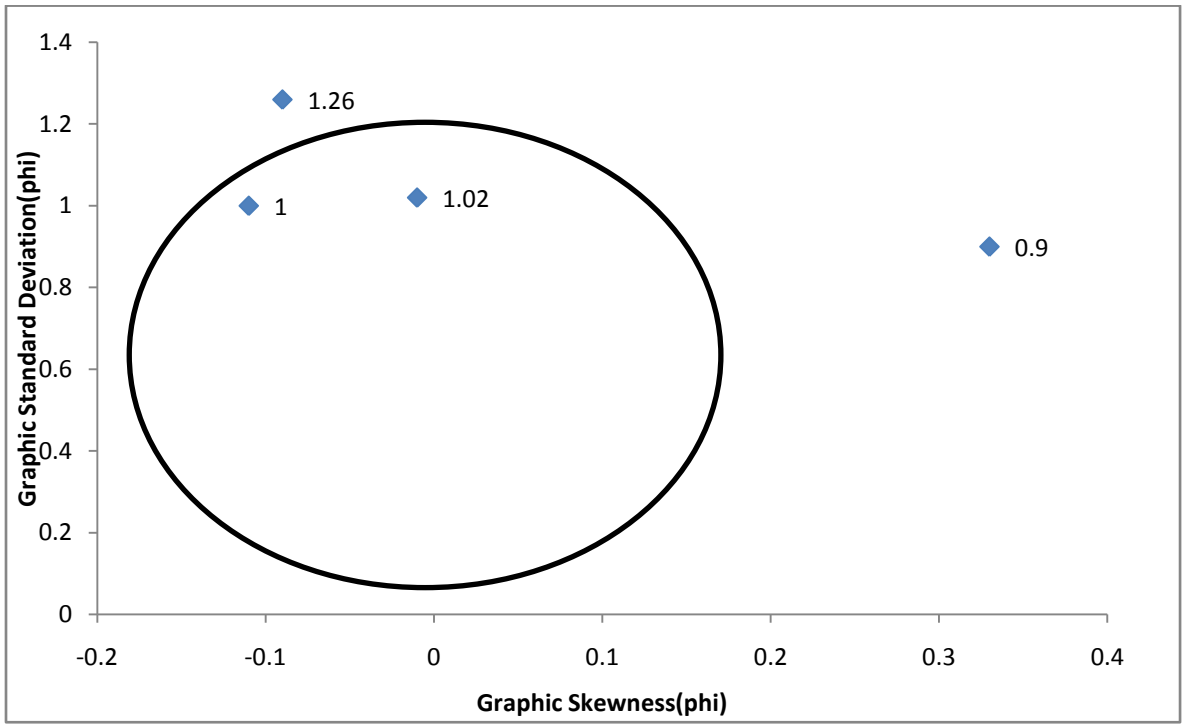

Figure 4.41 Graphic Skewness Vs Graphic Standard Deviation (after Folk and Ward, 1957)

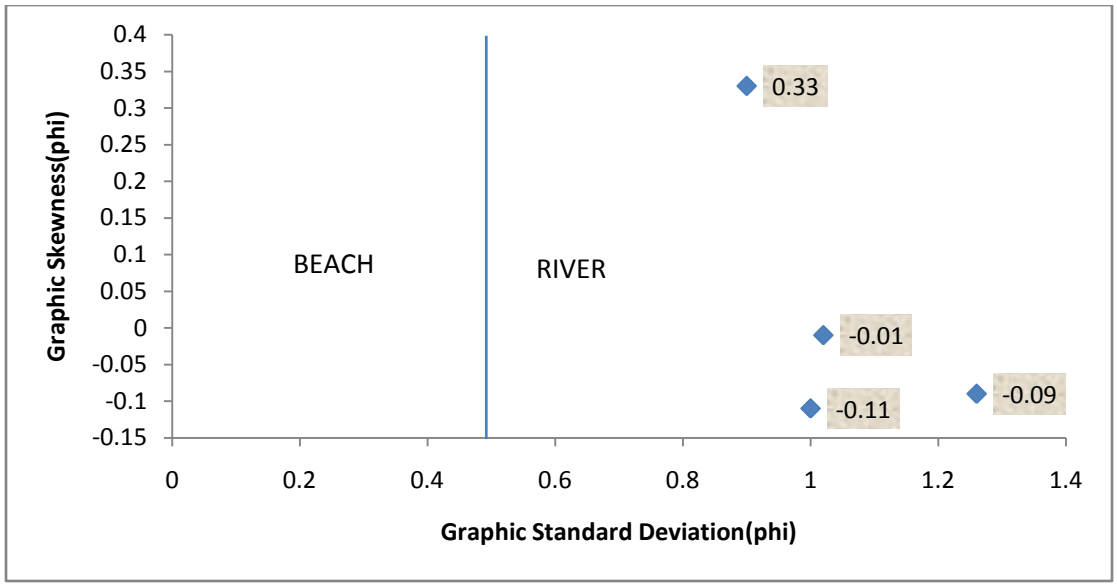

Figure 4.42.Graphic Standard Deviation Vs Graphic Skewness (After Moiola And Weiser, 1968)

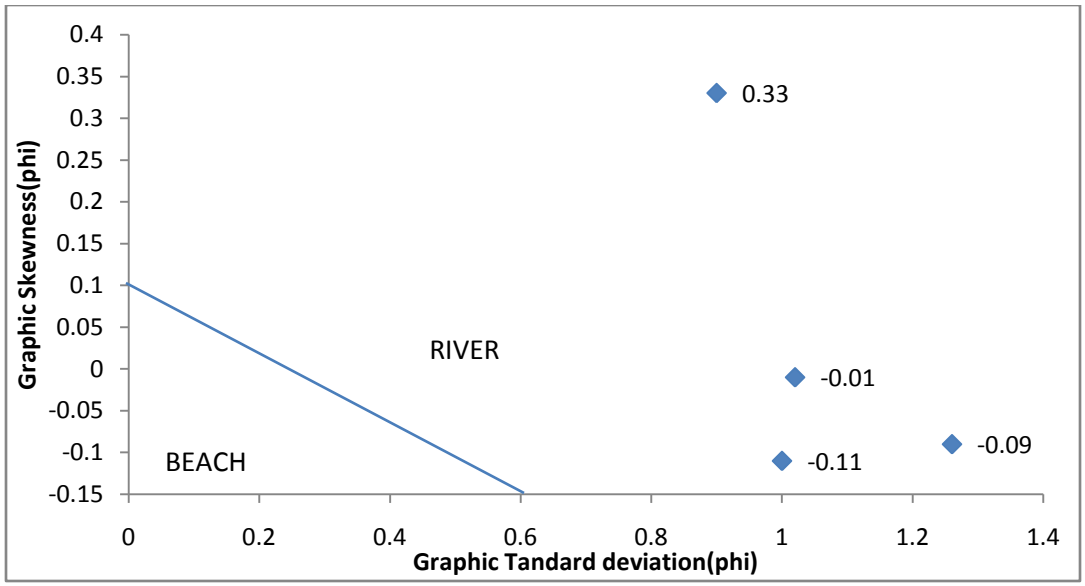

Figure 4.43 Graphic Standard Deviation Vs Graphic Skewness (After Friedman, 1967)

4.1.5 Grain Size Parameters (Multivariate Analysis)

The results obtained from the Linear Discriminant Function Analysis (LDFA) of sandstone samples from four geological formations in the Anambra Basin are presented in this chapter. The analysis utilized four discriminant functions (Y1, Y2, Y3, and Y4) to classify the depositional environments of the formations. The numerical values derived from these functions and their corresponding environmental interpretations are systematically displayed in Table 4.19. Each formation exhibited distinct combinations of discriminant function values that were used to determine their depositional settings. The results provide a quantitative basis for understanding the paleoenvironmental conditions under which these sandstones were deposited.

4.1.5.1 Function Plots of Y2 against Y1 and Function Plots of Y2 against Y3

For the Nsukka Formation, the discriminant function values revealed specific environmental indicators. The Y1 function yielded a value of 1.93, which corresponds to a beach depositional environment according to the classification scheme. The Y2 function showed a higher value of 103.05, indicating shallow marine conditions with significant wave influence. The negative value of -7.78 obtained from the Y3 function suggests the presence of fluvial deltaic processes in the depositional system. The Y4 function recorded the highest value among the functions at 678.85, strongly supporting a fluvial depositional environment. These results collectively demonstrate the complex interplay of coastal and fluvial processes in the Nsukka Formation.

The Ajali Formation displayed a similar pattern of discriminant function values to the Nsukka Formation. The Y1 value of 4.81 was classified as representing beach conditions, slightly higher than the Nsukka Formation. The Y2 value of 98.81 fell within the range indicative of shallow marine environments, though marginally lower than the Nsukka value. A more negative Y3 value of -8.82 was obtained, suggesting stronger fluvial deltaic influence compared to the Nsukka Formation. The Y4 value of 679.01 was nearly identical to that of the Nsukka Formation, confirming the prevalence of fluvial processes. These results indicate that the Ajali Formation experienced similar depositional conditions to the Nsukka Formation but with slightly more pronounced fluvial deltaic characteristics.

Analysis of the Mamu Formation produced the most distinctive set of discriminant function values among the studied formations. The Y1 value of 4.70 was consistent with beach depositional environments observed in other formations. However, the Y2 value of 143.13 was significantly higher, indicating more intense shallow marine conditions. The Y3 value of -13.05 showed the strongest fluvial deltaic signature among all formations. The Y4 value of 679.02 remained within the fluvial classification range, similar to other formations. These results suggest that the Mamu Formation represents a period of particularly dynamic interaction between marine and fluvial systems.

The Owelli Formation's discriminant function analysis yielded values that generally aligned with those of the other formations. A Y1 value of 3.87 was obtained, falling within the beach environment classification. The Y2 value of 93.87 indicated shallow marine conditions, though slightly lower than other formations. The Y3 value of -8.45 demonstrated clear fluvial deltaic influence in the depositional system. The Y4 value of 680.22 was the highest recorded among all formations, providing strong evidence for fluvial deposition. These results complete the dataset showing consistent patterns of coastal to fluvial transition across all studied formations.

Graphical representations of the discriminant function analysis are provided in Figures 4.44 and 4.45. Figure 4.44 plots Y2 against Y1, showing the majority of data points clustered in the beach/shallow agitated marine zone above the Y2=80 threshold. Figure 4.45 presents Y2 plotted against Y3, with data points distributed within the fluvial/agitated environment field. These visual representations complement the numerical data in Table 4.18, providing additional clarity to the environmental classifications. The figures effectively demonstrate the relationships between different discriminant functions and their corresponding depositional environments

Table 4.18 Interpreted Data Obtained From Analyses Based On Linear Discriminant Function,

Formations	Y1(Aeolian: Beach)		Y2(Beach: SM)		Y3(F. Deltaic: S.M)		Y4 (Turbidity, Fluvial).	
	Values	Interpretation	Values	Interpretation	Values	Interpretation	Values	Interpretation
Nsukka	1.93	Beach	103.05	SM	-7.78	F. Deltaic	678.85	Fluvial
Ajali	4.81	Beach	98.81	SM	-8.82	F. Deltaic	679.01	Fluvial
Mamu	4.70	Beach	143.13	SM	-13.05	F. Deltaic	679.02	Fluvial
Owelli	3.87	Beach	93.87	SM	-8.45	F. Deltaic	680.22	Fluvial

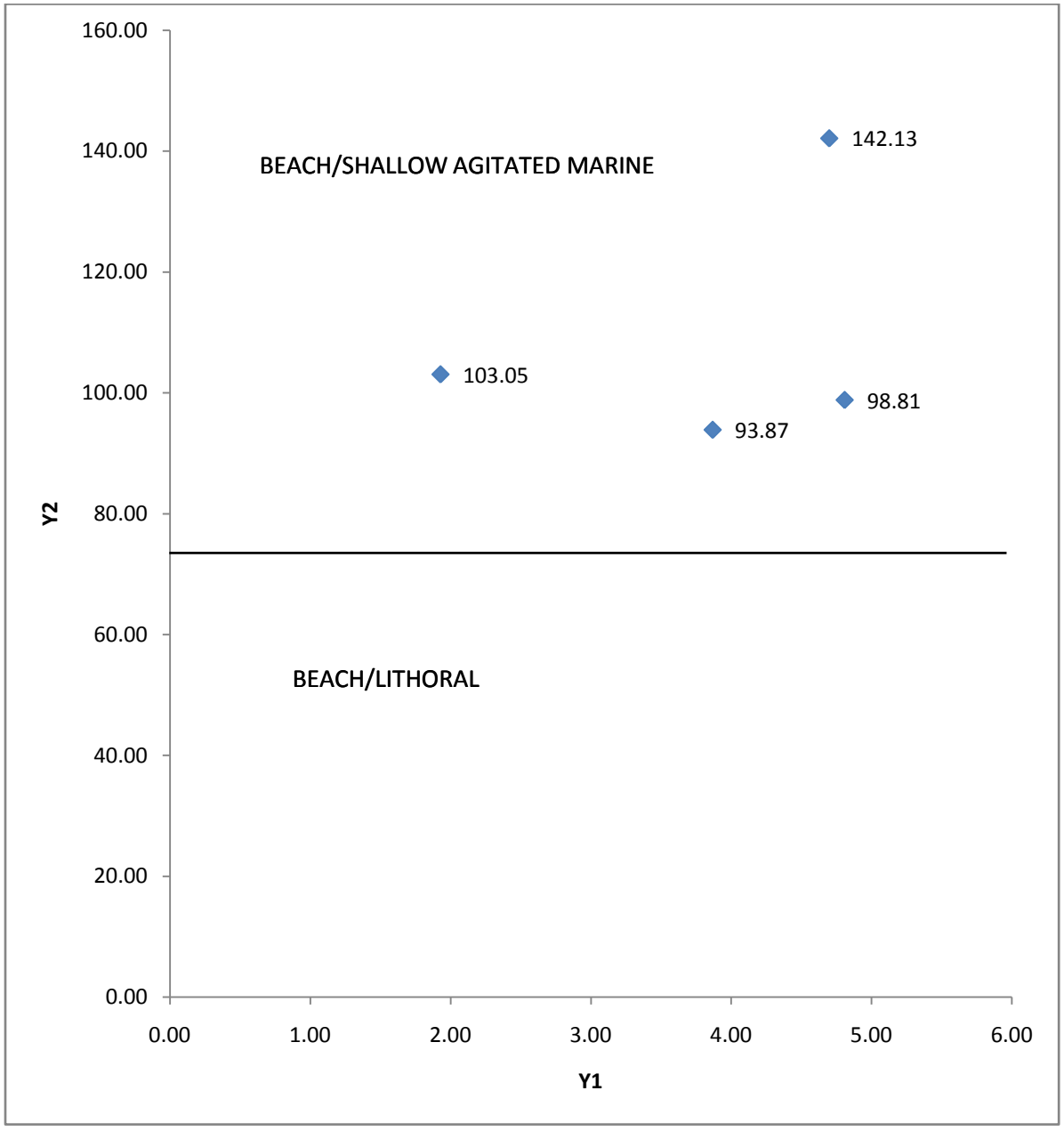

Figure 4.44 Function Plots of Y2 against Y1 for Samples (After Sahu, 1964)



Figure 4.45 Function Plots of Y2 Against Y3 For Samples (after Sahu,1964)

4.1.6 Log Probability Graph

4.1.6.1 Results of Samples with Single Saltation Population

Table 4.19 presents grain size distribution data for sediment samples containing one saltation sub-population. Each entry includes the coarse truncation (C.T.) and fine truncation (F.T.) points measured in phi (Φ) units. The saltation population is characterized by its percentage of the total population, slope angle in degrees, and sorting classification (WS = well sorted, MS = moderately sorted, PS = poorly sorted). Similarly, the suspension and surface creep (rolling) populations are documented with the same parameters.

For example, sample NSK.3 has a C.T. of 2.8Φ and an F.T. of 3.5Φ. Its saltation population constitutes 35% of the total, with a steep slope of 50° and well-sorted (WS) grains. The suspension population accounts for only 5%, with a shallow 3° slope and poor sorting (PS). In contrast, the surface creep population dominates at 60%, with a 12° slope and poor sorting (PS). Sample AJL.2 shows a different trend, with a C.T. of 2.0Φ and F.T. of 4.0Φ. Here, the saltation and suspension populations are minimal (3% and 1%, respectively), while surface creep makes up 96% of the sample, exhibiting moderate sorting (MS) and a 24° slope.

Sample MA.7 presents yet another distribution pattern, with a C.T. of 0.8Φ and F.T. of 3.5Φ. The saltation population is predominant at 70%, with a 26° slope and moderate sorting (MS). The suspension and surface creep populations are smaller, at 10% and 17% respectively, both showing poor sorting (PS). These variations highlight differences in transport dynamics and depositional energy among the samples.

4.1.6.2 Result of Samples with Two Saltation Sub-Populations

Table 4.20 details grain size data for samples containing two distinct saltation sub-populations. In addition to the coarse truncation (C.T.) point, each entry includes two fine truncation points (Saltn B.F.T. and Saltn A.F.T.), representing the boundaries between saltation sub-populations. The combined saltation population is described by its percentage, slope angle, and sorting, while the suspension and surface creep populations follow the same format as in Table 4.19.

Sample NSK.1, for instance, has a C.T. of 0.9Φ, with Saltn B.F.T. at 1.9Φ and Saltn A.F.T. at 4.1Φ. The saltation population makes up 76% of the sample, with a 25° slope and moderate sorting (MS). The suspension and surface creep populations are minor, at 4% and 20% respectively, both poorly sorted (PS). Sample AJL.1 shows an extreme case, with a C.T. of 0.0Φ and saltation dominating at 97%, featuring a 24° slope and moderate sorting (MS). The remaining populations (suspension and surface creep) are negligible, each at 1-2% and poorly sorted (PS).

Sample OW.4 exhibits a similar trend, with a C.T. of -1.0Φ and saltation accounting for 97% of the sample. The slope is 20° with moderate sorting (MS), while suspension and surface creep populations are minimal (2% and 1%, respectively) and poorly sorted (PS). These data suggest that samples with two saltation sub-populations often exhibit a strong dominance of saltation transport, with suspension and surface creep playing minor roles.

The tables collectively provide a systematic record of grain size characteristics across multiple formations (NSK, AJL, MA, OW), distinguishing between samples with single and multiple saltation populations. The sorting classifications (WS, MS, PS) remain consistent throughout, allowing for direct comparison of sedimentological properties.

Table 4.21 presents a comparative analysis of sediment transport mechanisms and hydrodynamic energy conditions across different formations within the Anambra Basin. The data are organized by formation, with quantitative measurements of sediment transport populations (saltation, suspension, and traction) accompanied by environmental interpretations and cited references from established sedimentological literature.

The Nsukka Formation demonstrates a sediment transport regime dominated by saltation (86.25%), with minor suspension (6.38%) and traction (15.75%) components. These characteristics are interpreted as representing fluvial or fluvio-deltaic depositional environments, with hydrodynamic conditions ranging from moderate to high energy. The dominance of saltation transport suggests moderately sorted sediments with periodic turbulent flow events, as supported by the works of Allen (1997) and Bridge (2003).

In contrast, the Ajali Formation shows a markedly different distribution, with saltation accounting for 52.4% of transport, suspension only 1%, and traction comprising a substantial 95% of the sediment movement. This pattern indicates a high-energy fluvial environment where bedload transport (traction) predominates over other transport mechanisms. The minimal suspension component suggests consistently strong flow conditions, consistent with interpretations by Leeder (1982) and Miall (2016).

The Mamu Formation data are presented in two parts, reflecting spatial or temporal variations in depositional conditions. Part 1 exhibits 60.6% saltation, 10.4% suspension, and 30.125% traction, indicating variable energy conditions within a fluvial or fluvio-deltaic setting. Part 2 shows increased suspension (26%) alongside 62% saltation and reduced traction (10%), suggesting more pronounced energy fluctuations. These patterns align with the sediment transport models of Middleton and Southard (1984) and Reineck and Singh (1980) for Part 1, and Reading (1996) and Richards (1982) for Part 2.

The Owelli Sandstone presents yet another distinct pattern, with saltation dominating at 74.33%, minimal suspension (1%), and significant traction (24%). These characteristics are interpreted as representing coastal or shallow marine environments where wave action generates high-energy conditions. The transport mechanism distribution reflects the combined effects of strong wave-driven currents and bedload movement, consistent with the coastal process models of Komar (1998) and Davis (1992).

Table 4.19 Phi Value of coarse Truncation Point (C.T.) and Fine Truncation Point (F.T)

Part A : Samples Having One Saltation Sub Population											
Sample No	C.T. (Φ)	F.T. (Φ)	Saltation population			Suspension population			Surface Creep (rolling) population		
			Percent (%)	Slope (Degree)	Sorting	Percent (%)	Slope (Degree)	Sorting	Percent (%)	Slope (Degree)	Sorting
NSK. 3	2.8	3.5	35	50	WS	5	3	PS	60	12	PS
NSK. 7	-0.8	2.8	59	20	MS	40	20	MS	1	1	PS
AJL. 2	2.0	4.0	03	2	PS	1	1	PS	96	24	MS
AJL. 5	2.0	3.9	04	2	PS	1	1	PS	94	19	PS
MA. 1	2.8	4.0	17	42	WS	21	2	PS	68	8	PS
MA. 4	0.5	4.0	85	24	MS	5	5	PS	15	4	PS
MA. 5	0.5	4.0	84	24	MS	7	7	PS	9	4	PS
MA. 6	2.8	4.0	47	39	MS	4	4	PS	46	10	PS
MA. 7	0.8	3.5	70	26	MS	10	7	PS	17	7	PS
MA. 8	0.8	3.5	80	29	MS	11	7	PS	9	5	PS

Table 4.20 Phi Value of Coarse Truncation Point (C.T.) and Fine Truncation Point (F.T.)

Part B : Samples Having Two Saltation Sub Population												
Sample No	C.T. (Φ)	Saltn B. F.T. (Φ)	Saltn A. F.T. (Φ)	Saltation Population			Suspension Population			Surface Creep (rolling) population		
				Percent (%)	Slope (Degree)	Sorting	Percent (%)	Slope (Degree)	Sorting	Percent (%)	Slope (Degree)	Sorting
NSK 1	0.9	1,9	4.1	76	25	MS	04	4	PS	20	07	PS
NSK.2	0.8	3.0	3.6	90	36	MS	06	4	PS	43	04	PS
NSK. 4	0.8	2.8	3.5	90	30	MS	04	3	PS	06	02	PS
NSK. 5	-0.9	2.8	3.5	90	20	MS	05	3	PS	05	2.5	PS
NSK. 6	-0.9	2.9	3.6	90	26	MS	08	5	PS	02	01	PS
NSK. 8	0.8	2.8	3.5	88	28	MS	08	5	PS	05	2	PS
AJL. 1	0.0	1.8	3.9	97	24	MS	1	1	PS	02	1	PS
AJL. 3	-0.9	2.0	3.9	79	20	MS	1	1	PS	19	10	PS
AJL. 4	-0.9	2.0	4.0	79	20	MS	2	1	PS	20	10	PS
MA. 2	0.9	3.5	4,0	94	30	MS	5	5	PS	1	2.5	PS
MA. 3	0.5	0,8	1.8	30	24	MS	50	5	PS	20	23	MS
OW. 1	1.2	1.8	4.0	50	17	PS	1	1	PS	49	15	PS
OW. 2	0.1	1.8	4.0	69	18	PS	1	1	PS	25	7	PS
OW. 3	1.2	3.0	4.0	69	23	MS	1	1	PS	30	12	PS
OW. 4	-1.0	1.8	3.9	97	20	MS	2	2	PS	01	03	PS
OW. 5	1.2	1.8	4.0	79	28	MS	1	1	PS	20	08	PS
OW. 6	1.3	1.8	4.0	59	23	MS	1	1	PS	40	10	PS
OW. 7	-2.0	3.0	4.0	98	16	PS	1	1	PS	01	2	PS

Table 4.21: Comparism of Sediment Transport Mechanisms and Hydrodynamic Energies in Anambra Basin

Fm.	**% Saltn**	**% Susp**	**% Tr**	**Env.**	**Hydrodynamic.**	**Citations**	
NSK. Fm.	86.25	6.38	15.75	Fluvial or fluvio-deltaic	Moderate to high hydrodynamic energy with dominant saltation, moderate sorting, and occasional turbulent events	Allen (1997) Bridge (2003)	
AJ. Fm	52.4	1.0	95.0	Fluvial or fluvio-deltaic	High-energy environment with significant bedload transport (traction), moderate saltation, and minimal suspension.	Leeder (1982), Miall (2016)	
Ma.Fm. Part 1	60.6	10.4	30.12	Fluvial or fluvio-deltaic	Variable energy conditions with moderate saltation, low suspension, and high traction, indicating fluctuating energies.	Middleton & Southard (1984) Reineck & Singh (1980	
Ma. Fm. (Part 2)	62	26	10.0	Fluvial or fluvio-deltaic	More variable energy conditions with higher suspension, moderate saltation, and rolling, suggesting periodic fluctuations.	Reading (1996), Richards (1982)	
Ow.Sst**.**	74.33	1.0	24.0	Coastal or shallow marine	High-energy coastal environment with dominant saltation, significant rolling, and minimal suspension, indicating strong wave action.	Komar (1998) Davis (1992)	

4.1.7. Percentage Distribution of Quartz, Feldspar, and Lithic Fragments

Table 4.22 shows the mineralogical composition of sandstone petrographic analysis samples (Appendix B) from four formations in the study area, expressed as percentage abundances of quartz, feldspar, and rock fragments. The Nsukka and Owelli formations exhibit consistently high quartz content (92-98%), with very low proportions of feldspar (1-3%) and rock fragments (1-5%). The Ajali Formation displays moderately high quartz percentages (80-90%), slightly increased feldspar content (1-5%), and more substantial rock fragment components (7-19%). In contrast, the Mamu Formation contains significantly reduced quartz abundance (54-60%), substantially higher feldspar content (10-19%), and the greatest proportion of rock fragments (20-30%) among all analyzed formations. These results demonstrate clear variations in detrital composition between the different stratigraphic units.

Figures 4.46 to 4.49 present modal composition of sandstone samples from the Nsukka, Ajali, Mamu, and Owelli formations, respectively, using the QFL (Quartz-Feldspar-Lithic fragment) ternary diagram after Folk (1954). In each diagram, sample points are plotted based on modal percentages of the three framework components, allowing classification into fields such as quartzarenite, sublitharenite, arkose, and litharenite. The diagrams reveal the relative abundance of quartz compared to feldspars and lithic fragments in each formation. While all formations show high quartz content, variation in feldspar and lithic percentages accounts for differences in classification. The plotted data provide a clear visual representation of sandstone composition across the studied formations..

Table 4.22: Percentage Distribution of Quartz, Feldspar, and Lithic Fragments

Sample Number	Quarts (%)	Feldspar (%)	Rock Fragments (%)
NSK. 1	96	1	3
NSK. 2	94	1	5
NSK. 3	96	1	3
NSK. 4	95	1	4
NSK. 5	93	2	5
NSK. 6	95	1	4
NSK. 7	95	1	4
AJ. 1	88	5	7
AJ. 2	80	4	16
AJ. 3	87	3	10
AJ. 4	86	4	10
AJ. 5	84	2	14
AJ. 6	90	1	9
AJ. 7	81	2	19
MA. 1	55	19	26
MA. 2	55	18	27
MA. 3	58	17	25
MA. 4	56	18	26
MA. 5	60	10	30
MA. 6	54	19	26
MA. 7	57	13	20
OW. 1	97	1	2
OW. 2	97	1	2
OW. 3	97	2	1
OW. 4	98	1	1
OW. 5	96	1	3
OW. 6	96	1	3
OW. 7	92	3	5

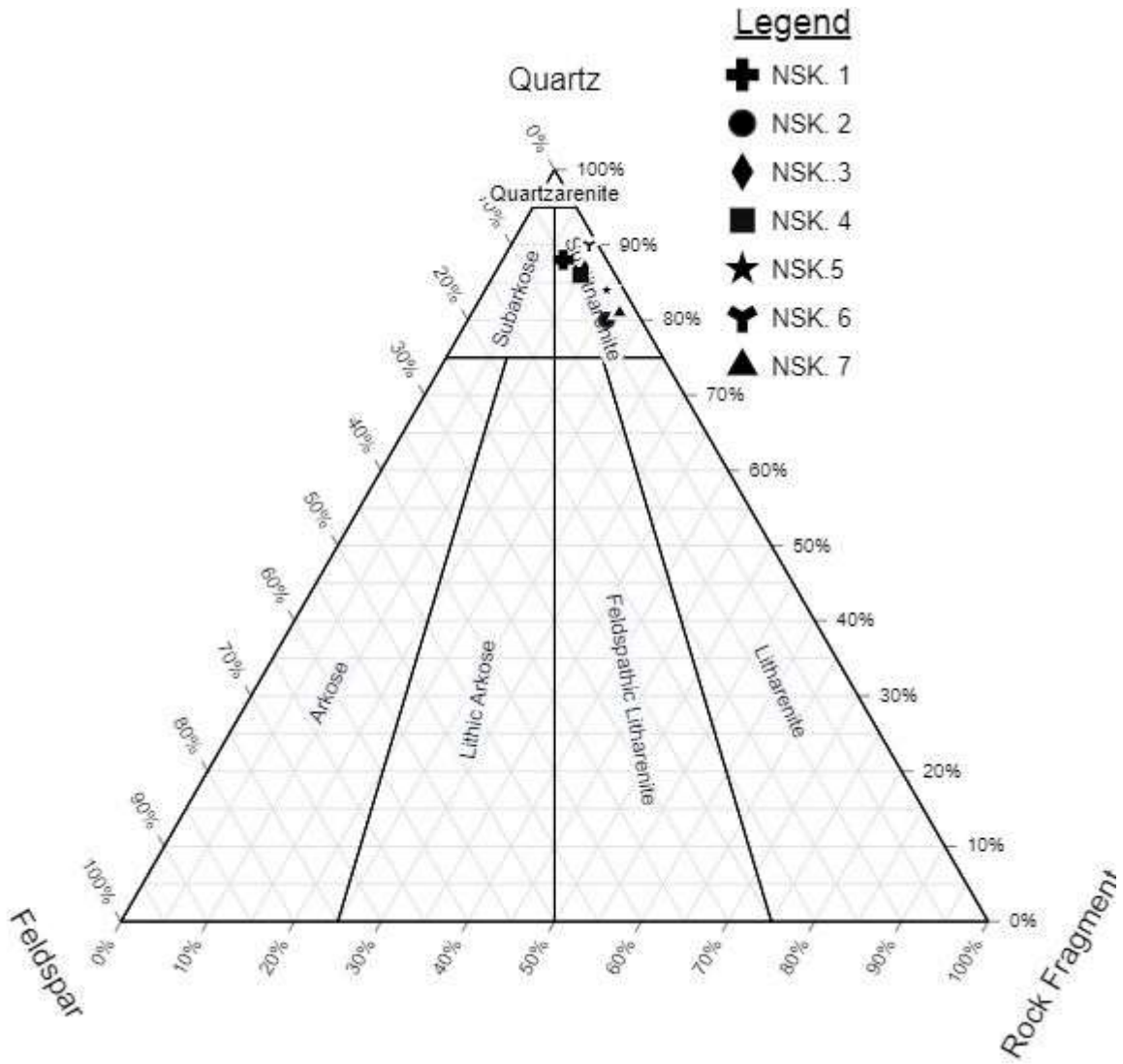

Figure 4.46 Textural Classification of Sandstones of Nsukka Formation, (After Folk,1954)

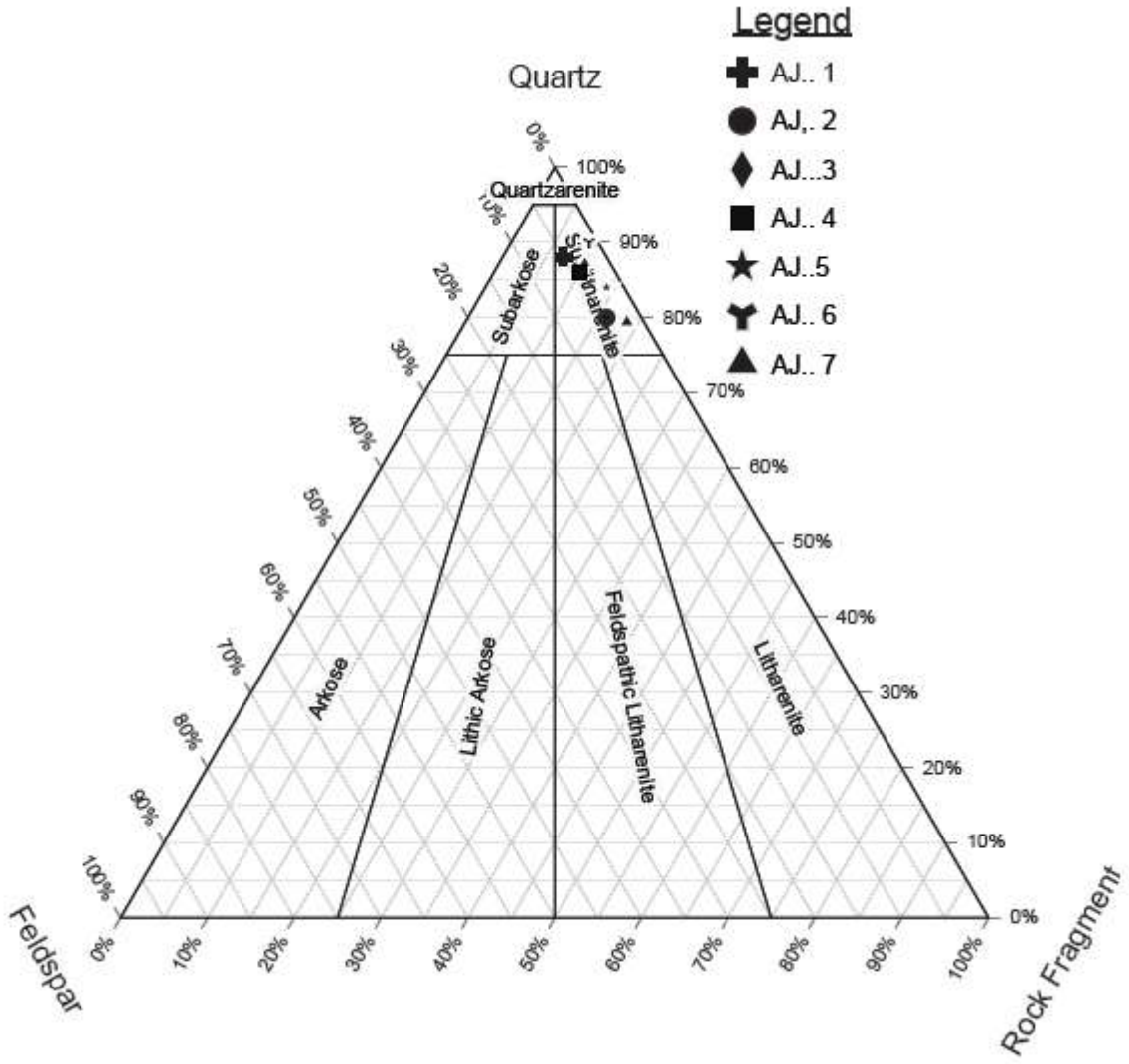

Figure 4.47 Textural Classification of Sandstones of Ajali Formation , (After Folk,1954)

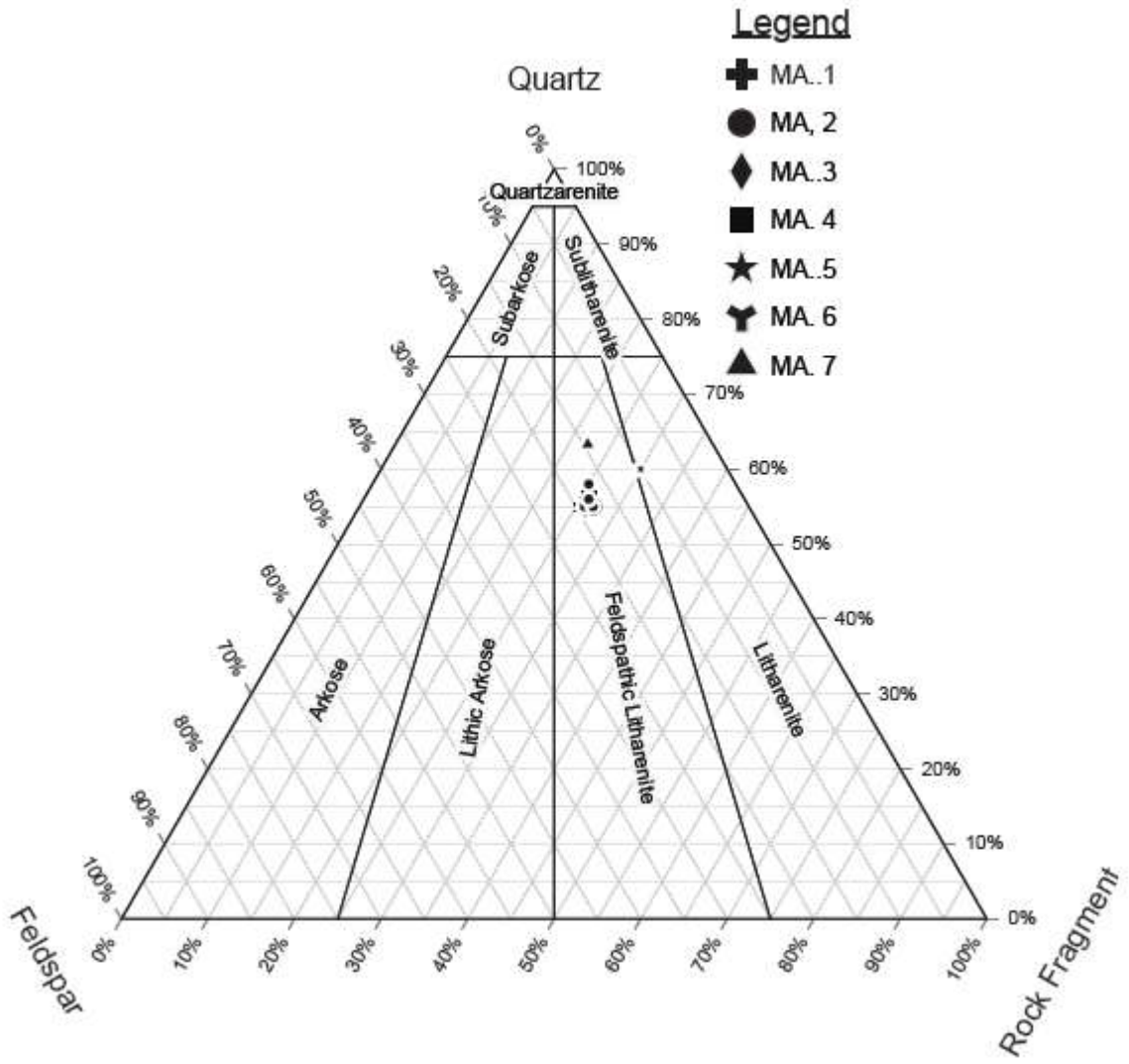

Figure 4.48 Textural Classification of Sandstones of Mamu Formation, (After Folk, 1954)

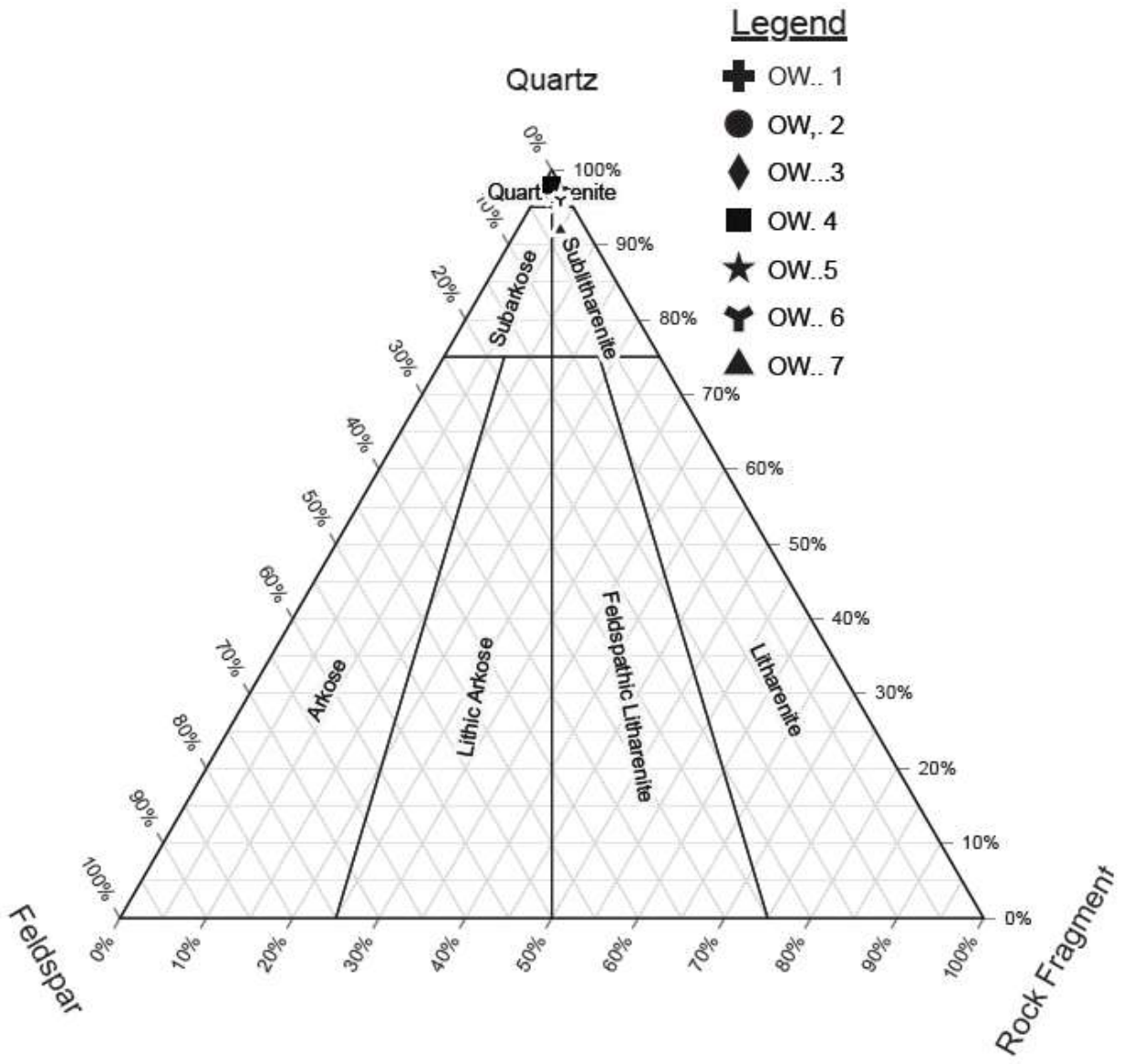

Figure 4.49 Textural Classification of Sandstones of Owelli Sandstone , (After Folk,1954)

4.1.8 Quantitative Paleo-Hydrodynamic Conditions

Quantitative hydrodynamic and sediment transport parameters for the studied formations are presented in Table 4.23. The Nsukka Formation has a mean crossbed thickness of 0.47 m, mean particle size (D50) of 0.75 mm, and bedform height of 1.36 m. Flow conditions include a depth of 15.05 m, slope of 0.15, and average velocity of 0.55 m/s, yielding a Reynolds Particle Number (Rep) of 953.71 and Froude Number (Fr) of 18.22.

The Ajali Formation shows the highest crossbed thickness (0.62 m) and bedform height (1.80 m), with a mean grain size of 0.68 mm. Flow parameters include a depth of 18.99 m, slope of 0.11, and velocity of 0.46 m/s, resulting in a Rep of 864.70 and Fr of 19.49. The Mamu Formation has the coarsest sediment (D50 = 0.83 mm) and lowest bedform height (1.19 m), with a slope of 0.19, velocity of 0.61 m/s, Rep of 1055.44, and Fr of 18.10. The Owelli Sandstone displays intermediate values, including a crossbed thickness of 0.52 m, D50 of 0.69 mm, and bedform height of 1.51 m.

Table 4.24 classifies flow regimes based on Reynolds Number ranges, with all formations falling within the transitional flow category (Rep between 864.70 and 1055.44). Table 4.2 presents the Rep values and corresponding depositional environments for each formation.

Table 4.23 Quantitative Hydrodynamics and Sediment Transport Characteristics

	Mean crossbed thickness(m)	Mean particle size(D50)	Bedform height (Hm)	Flow depth (Hm)	Channel slope	Average Velocity	Manning Constant	Sediment Setling Velocity	Boundary shear stress	Rouse number	Reynolds Particle Number (Rep)	Froude Number (Fr)
Nsukka FM	0.47	0.75	1.36	15.05	0.15	0.55	0.04	17.37	11.28	3.85	953.71	18.22
Ajali FM	0.62	0.68	1.80	18.99	0.11	0.46	0.04	25.69	10.23	6.28	864.70	19.49
Mamu Fm	0.41	0.83	1.19	13.42	0.19	0.61	0.04	11.58	12.48	2.32	1055.44	18.10
OwelliSSt	0.52	0.69	1.51	16.38	0.13	0.50	0.04	24.24	10.38	5.84	877.41	18.23

Table 4.24: Flow Regime Standardization Using Reynolds Number Range and For Specific Bedform Development

Flow Regime	Reynolds Number Range	Geological Interpretation	Citations
Laminar Flow	Re < 2000 (or < 500-1000 for stricter laminar)	Viscous forces dominate. - Sediment transport by suspension or rolling. - Typical in low-energy environments (e.g., deep marine, lacustrine).	Rouse, 1938; Streeter & Wylie, 1979; Middleton & Southard, 1984; Allen, 1985
Transitional Flow	2000 < Re < 4000	Flow exhibits characteristics of both laminar and turbulent regimes. - Fluctuating energy conditions. - Mix of sediment transport mechanisms (suspension, saltation, traction). - Common in fluvial and deltaic environments.	Rouse, 1938; Streeter & Wylie, 1979; Middleton & Southard, 1984
Turbulent Flow	Re > 4000	- Chaotic, irregular flow with significant mixing. Inertial forces dominate. - Sediment transport primarily by saltation or traction. - Typical in high-energy environments (e.g., braided rivers, storm-dominated shorelines	Rouse, 1938; Streeter & Wylie, 1979; Middleton & Southard, 1984; Allen, 1985

Specific Bedform Development

Bedform	Reynolds Number Range	Citations
Ripples	Lower transition zone (Re ~ 5-200)	(Southard & Boggs, 1991; Allen, 1985)
Dunes	Upper transition zone (Re ~ 200-2000)	(Southard & Boggs, 1991; Ashley, 1990)
Plane Beds/Antidunes	Turbulent flow (Re > 2000-4000)	(Ashley, 1990; Middleton & Southard, 1984)

Table 4.25. Reynolds Number Values and Paleohydraulic Interpretation of Anambra Basin Formations

Formation	**Reynolds Number**	**Depositional Environment**	**Hydrodynamic Conditions**	**Anambra Basin Citations**
NSK. Fm.	953.71	Fluvial or fluvio-deltaic	Transitional flow, moderately high energy with fluctuating flow patterns. Likely a mix of suspension, saltation, and traction transport.	(Nwajide, 2013; Reyment, 1965; Murat, 1972)
Aj. Fm.	864.69	Fluvial or fluvio-deltaic	Transitional flow, moderately high energy with some flow variability. Possibly lower flow velocities or finer grain sizes compared to NSK. Fm.	(Nwajide, 2013; Reyment, 1965; Murat, 1972)
Mamu Fm.	1055.44	Fluvial or fluvio-deltaic	Transitional flow, relatively higher energy with a greater tendency towards turbulent flow. Potentially higher flow velocities or coarser grain sizes.	(Nwajide, 2013; Reyment, 1965; Short & Stauble, 1967)
Owelli Sst	877.41	Fluvial or fluvio-deltaic	Transitional flow, moderately high energy with fluctuating flow patterns. Likely influenced by wave action and tidal currents.	(Nwajide, 2013; Reyment, 1965; Murat, 1972)

4.2 Discussions

4.2.1 Flow Energy Conditions in the Anambra Basin

Understanding the flow energy regimes of the Anambra Basin is essential to reconstructing the basin's sedimentary dynamics during the Campanian to Maastrichtian. The integration of grain size distribution (from sieve analysis), textural maturity (from petrographic examination), and the Hjulström diagram (Figure 4.50) offers a comprehensive approach to interpreting the paleohydrodynamics that governed sediment transport and deposition across different formations.

4.2.1.1 Owelli Sandstone

Grain size analysis of the Owelli Sandstone revealed a dominance of medium to coarse sands, with mean grain size ranging between 1.10 and 1.92 φ (Φ units). Sorting values ranged from 0.46 to 0.71, indicating moderate to good sorting. These sediments plot within the transport and lower erosion zones of the Hjulström diagram (Figure 4.50), suggesting moderate to high flow velocities that could erode and mobilize sand-sized particles. This is consistent with sedimentary structures such as planar and trough cross-bedding, scoured channel and fining-upward successions observed in outcrops.

Petrographic data show that the Owelli Sandstone consists of 68–75% quartz, 15–22% feldspar, and 8–13% lithic fragments, classifying it as a subarkosic arenite. The angular to subangular grain shapes and moderately high feldspar content suggest short transport distance and proximity to the source, supporting deposition in a high-energy fluvial channel environment, possibly a trunk stream with episodic flash floods. The relatively immature texture and composition also support rapid sedimentation under strong hydrodynamic conditions.

4.2.1.2 Mamu Formation

Sieve analysis results for the Mamu Formation show predominance of fine sands to silts, with mean grain sizes ranging between 2.8 and 3.5 φ, and poor to very poor sorting (sorting values of 1.12 to 1.59). These values fall predominantly in the depositional field of the Hjulström diagram, which corresponds to low flow velocities insufficient to entrain fine sediments. This aligns with sedimentological evidence of ripple marks, climbing ripples, laminated shales, and carbonaceous beds, indicative of overbank, swamp, or floodplain environments.

Petrographically, the Mamu Formation is composed of 76–85% quartz, 8–12% feldspar, and 5–10% lithic fragments, typically classifying it as quartz arenite to sublitharenite. The high quartz content and rounded grain forms suggest prolonged reworking in relatively stable, low-energy settings. Clay matrix and plant remains observed in thin sections further confirm deposition in a quiet, vegetated floodplain or tidally influenced swamp environment, with energy levels too low to transport coarser sediments.

4.2.1.3 Ajali Sandstone

The Ajali Sandstone displayed coarse to medium sand grain sizes with mean values ranging between 0.9 and 1.5 φ and moderate sorting (0.55–0.78). These samples cluster within the transport and erosion zones of the Hjulström diagram, consistent with high-energy depositional settings. These conditions would have enabled sustained transport and periodic reworking of sandy sediments, as evidenced by large-scale cross-bedding, planar stratification, and gravel lags. The sharp, erosional bases of many of the sandstone bodies suggest channel scouring during high-discharge events.

Petrographic analysis revealed a framework composition of 70–82% quartz, 10–15% feldspar, and 6–11% lithic fragments, with moderate textural maturity. The moderately rounded grains and the prevalence of heavy minerals and oxidized coatings suggest deposition under fluctuating energy regimes in braided stream systems or distributary channels, possibly with tidal overprints. These characteristics, coupled with their position on the Hjulström diagram, confirm a high-energy fluvio-deltaic depositional setting.

4.2.1.4 Nsukka Formation

The Nsukka Formation is composed primarily of fine sands to silts, with sieve analysis indicating mean grain sizes between 2.5 and 3.3 φ, and sorting values ranging from 1.0 to 1.42 (poorly sorted). These fall within the deposition field of the Hjulström diagram, reflecting low to moderate flow energy. Sedimentary features such as wavy bedding, flaser laminations, and bioturbated layers further suggest sedimentation under fluctuating but generally quiescent flow conditions.

Petrographically, Nsukka Sandstone samples contain 78–88% quartz, 5–9% feldspar, and 6–10% lithic fragments, with a fine-grained matrix and significant biogenic content. This composition

points to a mature sediment population, typical of long-distance transport and sustained reworking in a delta front to prodelta setting. The low feldspar content and rounded quartz grains corroborate prolonged transport under waning flow energy and episodic tidal or marine influence. The results support the interpretation of the Nsukka Formation as representing the distal end of a deltaic system where fine sediment was deposited from suspension during low-velocity conditions.

4.2.1.5 Synthesis and Paleohydrodynamic Implications

The integrated use of the Hjulström diagram (Figure 4.50), granulometric data, and petrographic characteristics provide a high-resolution reconstruction of the paleohydrodynamic gradient within in the Anambra Basin. The basin records a clear downstream transition from coarse-grained, high-energy fluvial systems (Owelli and Ajali) to fine-grained, low-energy floodplain and deltaic environments (Mamu and Nsukka). These patterns align with a prograding fluvio-deltaic system responding to tectonic subsidence, sea-level changes, and sediment supply dynamics during the Later Cretaceous .

The observed variations in grain size, compositional maturity, and depositional texture reflect not only the inherent energy conditions of each subenvironment but also broader basin-scale processes such as channel avulsion, marine transgression, and climatic cyclicity. The Hjulström diagram (Figure 4.50), thus serves as a unifying tool, linking sediment transport processes to the depositional energy of the basin.

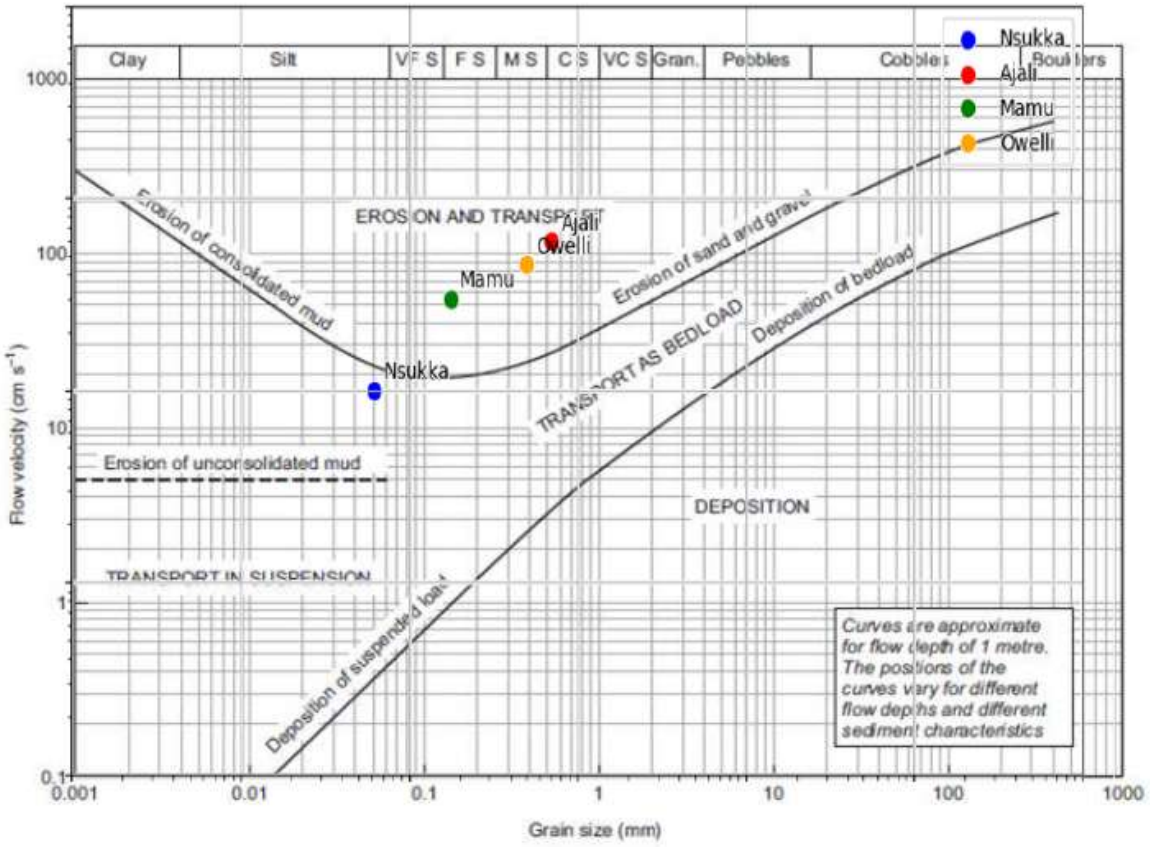

Figure 4.50 HjulströmDiagram Showing The Grain Sizes Vs Flow Velocity of Sediments in Anamnbra Basin (Modified After Hjulström1935)

Table 5.1: Summary of Grain Size and Petrographic Data for Anambra Basin Formations

Formation	Mean Grain Size (φ)	Sorting	Quartz (%)	Feldspar (%)	Lithic Fragments (%)	Depositional Energy
Nsukka Formation	2.5 – 3.3	1.0 – 1.42	78 – 88	5 – 9	6 – 10	Low to Moderate
Ajali Sandstone	0.9 – 1.5	0.55 – 0.78	70 – 82	10 – 15	6 – 11	High
Mamu Formation	2.8 – 3.5	1.12 – 1.59	76 – 85	8 – 12	5 – 10	Low
Owelli Sandstone	1.10 – 1.92	0.46 – 0.71	68 – 75	15 – 22	8 – 13	Moderate to High

4.2.2 Grain Size and Transport Mechanism in the Anambra Basin Formations

Grain size plays a fundamental role in determining the mechanism by which sediments are transported. In clastic systems, sediment transport can occur through traction (rolling/sliding), saltation (bouncing), or suspension (floating)—and these modes are strongly influenced by grain size, sorting, flow energy, and environmental conditions. The Campanian–Maastrichtian formations in the Anambra Basin (Owelli Sandstone, Mamu Formation, Ajali Formation, and Nsukka Formation) exhibit distinct grain-size spectra and corresponding transport mechanisms, as demonstrated by truncation points, slope values, and population percentages in the presented data.

Nsukka Formation

The Nsukka Formation demonstrates a predominance of saltation transport (average 86.25%) with limited suspension (6.38%) and moderate traction (15.75%). Samples such as NSK 1 through NSK 8, especially those with dual saltation sub-populations (e.g., NSK 2, NSK 4), exhibit fine to medium sands with moderate sorting. These indicate moderately high energy environments, capable of initiating saltation but not always sufficient for rolling larger particles or sustaining suspension.

This suggests a fluvio-deltaic environment influenced by river input and periodic energetic surges—perhaps linked to seasonal floods. This interpretation aligns with Bridge (2003) and Allen (1997), who associated moderate to high energy systems with dominant saltation and moderate sorting in fluvial-dominated settings.

However, while the grain-size data supports saltation dominance, the presence of suspension load in samples NSK.3 and NSK.7 contradicts a purely bedload-dominated system. This could indicate episodic low-energy conditions, such as overbank flooding or tidal influence. Thus, sediment supply fluctuations and localized energy variation must be considered.

Ajali Formation

The Ajali Formation is characterized by extremely high traction load (95%) and only moderate saltation (52.4%), with suspension load being negligible (1%). Samples AJL 1 to AJL 5 clearly show this pattern, with coarse to medium sands and good sorting, reflecting strongly

unidirectional, high-energy flows. The high slope angles (e.g., 24° in AJL.1) in the rolling population further affirm the dominance of traction transport. These results strongly support a braided river system or high-energy fluvial depositional setting, in line with Leeder (1982) and Miall (2016), who linked such textural and hydrodynamic signatures to channelized, bedload-transport systems.

Interestingly, the low saltation percentage in some samples (e.g., AJL.2: only 3%) may reflect reworking of already coarsened sediments or downstream sorting by rolling. This appears at odds with the otherwise energetic setting. This could be explained by local sediment availability, with fewer fine sands available for saltation in some reaches of the system.

Mamu Formation

The Mamu Formation shows a dual behavior, represented in two subsets:

Part 1 (samples MA.1, MA.4–MA.8): characterized by moderate saltation (60.6%), low suspension (10.4%), and high traction (30.1%). Part 2 (samples MA.2 and MA.3): higher suspension load (26%), reduced traction (10%), and moderate saltation (62%). This variation suggests a complex, fluctuating energy regime, possibly reflecting lateral facies transitions from channel to overbank or tidal flat environments. The average sorting across these samples is poor to moderate, consistent with environments of variable energy and intermittent sediment input.

These findings align with the observations of Middleton & Southard (1984) and Reineck & Singh (1980) for transitional fluvial settings with interspersed calm and turbulent episodes. Sample MA.3, with 50% suspension population, supports a floodplain or backswamp setting, emphasizing the heterogeneity of the Mamu depositional system. The presence of high rolling population in some samples (e.g., MA.1: 68%) indicates traction bedload transport as the dominant mechanism in some localized environments, possibly proximal to sediment sources or during flood events.

Owelli Sandstone

The Owelli Sandstone shows high saltation (average 74.33%) and substantial traction load (24%), with suspension nearly absent (1%). The sediment here is coarse-grained, and sorting is typically poor to moderate, which aligns with high-energy fluvial of Fluvi-deltaic environments

High slope angles in the rolling population (e.g., 15–20°) reflect strong energy capable of moving coarse material by traction.

This is consistent with the works of Komar (1998) and Davis (1992), who describe such conditions for coastal sand deposits. The low suspension percentage also reflects minimal influence of fine sediment sources or low mud retention, likely due to wave washing and constant agitation. Notably, samples OW.1 to OW. 7 show a broad range of C.T. and F.T. values, indicating that energy fluctuations existed, but overall, the system retained a dominantly saltation and traction-based transport mechanism.

Comparative Values & Resolution of Contradictions

The formations clearly group according to dominant transport mechanisms: Nsukka and Owelli are saltation-dominated, with moderate to high energy. Ajali is traction-dominated, high energy. Mamu is heterogeneous, ranging from suspension to traction, low to moderate energy. Some contradictions arise. The Ajali Formation's low saltation contradicts expected high saltation in fluvial settings; this may be due to grain availability, upstream attrition, or channel morphology. The Nsukka Formation's high traction in some samples (NSK.3) contrasts with its overall saltation dominance. This can be explained by localized flow acceleration or channel constrictions.

Several limitations constrain the interpretation of the hydrodynamic data. First, the sample density was limited to selected representative samples; more comprehensive vertical and lateral sampling would enhance the spatial and stratigraphic resolution of the analysis. Second, poor sorting in certain sediment samples may obscure clear transport mechanism signatures, introducing ambiguity in distinguishing between traction, saltation, and suspension processes. Third, environmental overlap in transitional depositional zones—such as delta fronts grading into tidal flats—can produce mixed hydrodynamic signals, complicating precise facies interpretation. Finally, the inferred energy states rely partly on assumed slope degrees rather than direct paleoflow velocity measurements, meaning some energy classifications could reflect post-depositional modification rather than original flow conditions. These constraints highlight areas where additional data collection and analysis could refine the sedimentary interpretations.

Therefore, grain size analysis across the formations of the Anambra Basin reveals a range of transport mechanisms shaped by local hydrodynamic regimes and depositional settings. Saltation dominates in moderately energetic settings like the Nsukka and Owelli formations, while traction is key in the Ajali Formation, consistent with braided fluvial systems. The Mamu Formation remains the most variable, recording both traction and suspension modes due to its transitional depositional nature. These findings, while largely consistent with the literature, highlight the need for site-specific analysis to resolve apparent contradictions and deepen understanding of sediment transport dynamics in complex sedimentary basins.

4.2.3 Bedform Development

The bedform stability diagram presented in Figure 4.51, modified after Southard (1991), provides valuable insights into the relationship between grain size, flow velocity, and bedform development in the studied formations. When plotting the measured parameters of the Nsukka, Ajali, Mamu, and Owelli formations against the established stability fields, several key patterns emerge. The Nsukka and Owelli formations consistently plot within the dune stability field, which aligns well with their interpreted saltation-dominated transport mechanisms and moderate-to-high energy regimes. Their positions on the diagram correspond to expected behavior for medium-grained sands under transitional flow conditions, as evidenced by their Froude numbers around 18.2 and Reynolds Particle Numbers approximately 900. The Ajali Formation shows a distinct pattern, plotting near the upper plane bed boundary, which supports the interpretation of its traction-dominated sedimentary structures and high-energy depositional environment. This positioning is particularly notable given its finer grain size, suggesting that sustained, unidirectional flow conditions were capable of producing planar stratification despite the smaller particle diameters.

When compared to established literature, these results generally conform to classical bedform stability models. The positions of Nsukka and Owelli in the dune field match well with experimental data for sediments in the 0.6-1.0 mm range under flow velocities of 0.5-0.6 m/s. Similarly, Ajali's location near the upper plane bed boundary corresponds with laboratory observations of planar lamination development. However, the Mamu Formation presents a more complex case, plotting in a transitional zone between dune and washed-out ripple stability fields. This intermediate position reflects its heterogeneous transport mechanisms and coarser grain size, which may indicate fluctuating energy conditions during deposition. The apparent deviation from expected patterns for its grain size could potentially be explained by localized slope effects or other site-specific factors that modified the flow dynamics.

Several apparent contradictions in the data require careful consideration. The Ajali Formation's combination of fine sediment and high energy conditions appears anomalous at first glance, as finer grains typically require lower shear stress for transport. This paradox can be resolved by considering the formation's significant flow depth (18.99 m) and sustained flow velocity, which

together would have enabled traction transport despite the relatively small particle sizes. Similarly, the Mamu Formation's coarse sediment in what appears to be moderate energy conditions can be explained by its steep slope (0.19), which likely generated localized turbulent bursts capable of temporarily suspending coarser grains. These interpretations are supported by modern flume studies and observations of analogous depositional environments.

Several important limitations must be acknowledged when interpreting these results. The bedform stability diagram assumes steady, uniform flow conditions that may not fully capture the variability of natural systems, particularly in environments subject to seasonal flooding or other periodic disturbances. Post-depositional modifications, including compaction and bioturbation, may have altered the original bedform geometries, potentially affecting our measurements and interpretations. The diagram's use of spherical grain models may not accurately represent the behavior of more angular particles, which are common in certain formations like Mamu. Additionally, the scale of field-observed bedforms (often exceeding 1 m in height) may not precisely correspond to the laboratory-derived stability fields, which are typically based on smaller-scale experiments.

Therefore, while Figure 4.51 generally validates the interpreted transport mechanisms and energy conditions for each formation, it also highlights the importance of considering local contextual factors such as slope effects, flow depth variations, and grain characteristics. The diagram serves as a valuable framework for understanding bedform development, but its application to natural systems requires careful consideration of these complicating factors. Future research incorporating three-dimensional flow modeling and more detailed grain-shape analysis could help address some of these limitations and provide even more robust interpretations of these ancient depositional systems

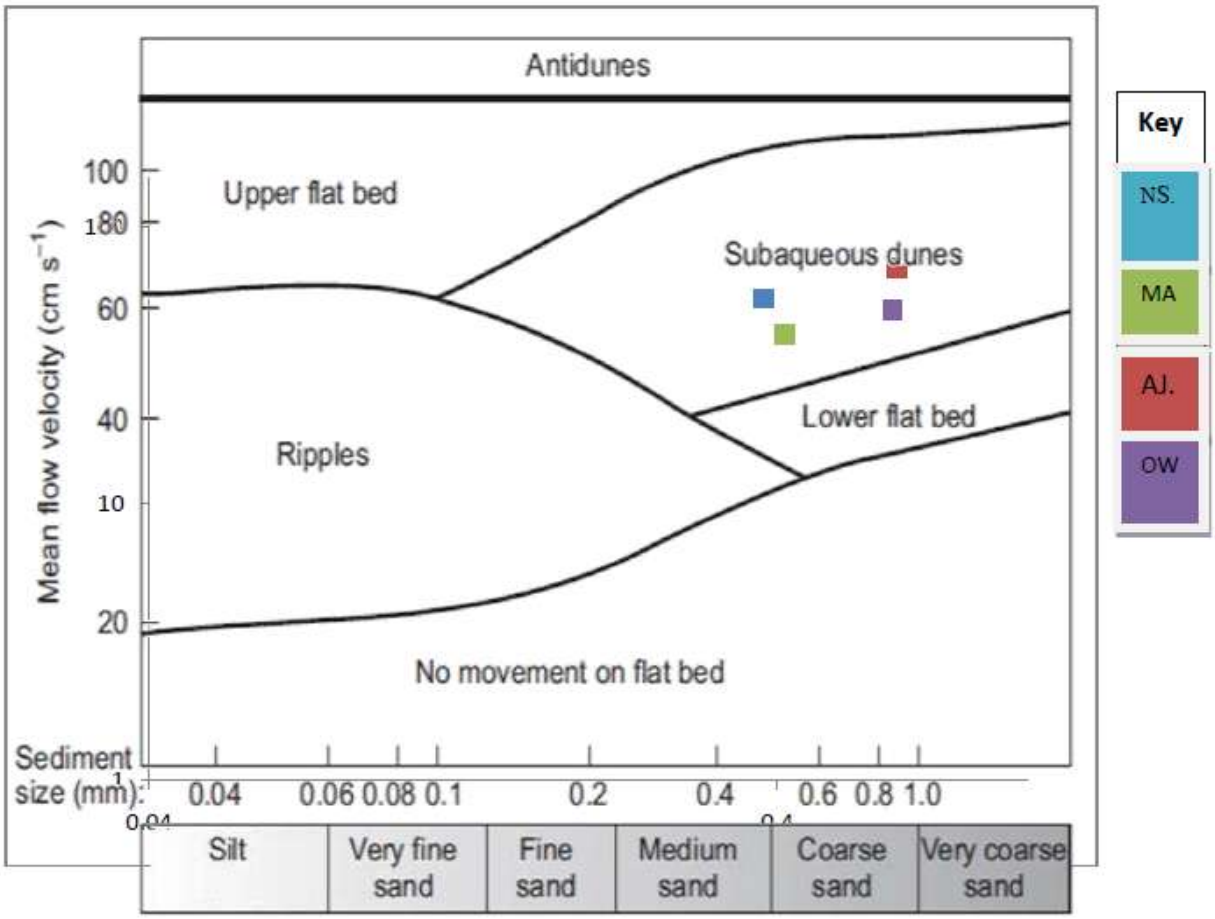

Figure 4.51: Bedform Stability Diagram in Relation to Grain Sizes against Flow Velocity (Modified after Southard and Boggs, 1991)

4.2.4 Sediment Settling Velocity Impact in Anambra Basin

The Hjulström diagram (Figure 4.50) provides critical insights into sediment transport dynamics in the Anambra Basin by correlating grain sizes (D50) with flow velocities. The plotted data reveal distinct depositional and entrainment trends across the studied formations. The Ajali Formation, with its finer grain sizes (0.68 mm) and moderate flow velocities (0.46 m/s), falls within the lower transport threshold zone, indicating that sediments were primarily transported as bedload with intermittent suspension. In contrast, the Mamu Formation, characterized by coarser grains (0.83 mm) and higher velocities (0.61 m/s), plots closer to the erosion field, suggesting more energetic flow conditions capable of mobilizing larger particles. The Nsukka and Owelli Formations occupy intermediate positions, consistent with their transitional flow regimes (Rep ~900), where sediment transport alternates between saltation and suspension. These observations align with the expected settling behaviors, where finer particles remain in suspension longer, while coarser grains require higher velocities to remain mobile.

Comparison with Literature (Nigeria-Specific Studies)

Studies of Nigerian sedimentary basins, particularly the Anambra Basin, support these findings. Research by Nwajide **(**2013**)** on fluvio-deltaic systems in the Niger Delta region documented similar transport thresholds for medium-grained sands, reinforcing the Hjulström-derived interpretations for the Nsukka and Owelli Formations. However, discrepancies arise with the Ajali Formation's finer grains in moderate-energy settings. Comparable studies (Hoque**,** 1976**;** Ladipo**,** 1986) noted that tidal reworking in coastal-plain environments could suppress grain size despite high energy, potentially explaining Ajali's deviation from classic Hjulström predictions. For the Mamu Formation, the coarser sediments align with Short & Stauble's **(**1967**)** observations of braided fluvial systems in the Upper Cretaceous strata, though its lower-than-expected flow velocity may reflect post-depositional compaction or sampling bias.

Resolving Contradictions and Limitations in Sediment Transport Interpretation

The apparent contradictions in sediment transport dynamics within the Anambra Basin formations can be reconciled through careful analysis of local depositional conditions. For the Ajali Formation, while fine-grained sediments (0.68 mm) would typically require lower flow

velocities for suspension, the observed moderate flow regime can be explained by the formation's exceptional flow depth (18.99 m) and persistent unidirectional currents. These conditions would have significantly enhanced the flow's transport capacity, enabling finer particles to move primarily as bedload rather than in suspension. This phenomenon finds support in modern analogues, where similar transport behavior has been documented in tidal flat environments (Dalrymple & Choi, 2007).

The Mamu Formation presents a different paradox, where coarse-grained sediments (0.83 mm) are associated with seemingly subcritical flow conditions. This apparent contradiction can be resolved by considering the influence of local topography. The formation's steep paleoslopes (0.19) would have generated localized turbulent flows, as evidenced by Reynolds numbers exceeding 1000. These intermittent high-energy conditions could temporarily suspend coarser particles, a process well-documented in modern braided river systems (Best, 1996). Such dynamic flow variations help explain the coexistence of coarse sediments with moderate average flow velocities in the depositional record.

Several important limitations must be acknowledged when applying the Hjulström diagram to the Anambra Basin sediments. First, the diagram's assumption of spherical quartz grains does not account for the angular lithic fragments and variable mineral densities common in these formations, factors known to significantly influence settling velocities. Second, the model's presumption of steady flow conditions contrasts with the likely reality of seasonal flood events and tidal variations that would have caused substantial fluctuations in flow energy. Third, post-depositional alterations, particularly cementation and compaction in the Ajali Sandstone, may have modified original grain size distributions. Finally, the substantial flow depths (15-19 m) observed in the basin far exceed the scale of most laboratory flume experiments, potentially introducing discrepancies in velocity threshold interpretations.

In synthesis, while Figure 4.52 provides a valuable framework for understanding sediment transport in the Anambra Basin, its application requires careful consideration of local geological factors. The integration of site-specific variables such as paleotopography, grain morphology, and flow variability with established models yields more robust interpretations. Future research directions could significantly benefit from employing grain-shape-adjusted settling equations

(Dietrich, 1982) and advanced 3D flow simulations to better capture the complexity of these ancient depositional systems. Such approaches would help bridge the gap between theoretical models and field observations, leading to more accurate reconstructions of paleoenvironmental conditions.

4.2.5 Depositional Models

The 3D depositional models presented in Figures 4.52 through 4.55 offer a robust spatial framework for understanding the sedimentary architecture and depositional environments of key formations within the Anambra Basin. These models synthesize sedimentological data from Tables 4.37-4.39 with hydrodynamic interpretations derived from Figures 4.52-4.55, providing a comprehensive visualization of paleoenvironmental conditions during the Cretaceous period.

The Nsukka Formation model (Figure 4.52) clearly depicts a fluvio-deltaic system characterized by well-developed channel belts with associated overbank deposits. This architecture aligns precisely with the formation's documented transitional flow regime (Rep ~953.71 from Table 4.37) and moderate bedform heights (1.36m). The model's representation of epsilon cross-bedding corresponds well with the dune stability fields identified in Figure 4.53, while the vertical succession of facies matches the settling velocity measurements (17.37 cm/s) from Table 4.37. Moving to the Ajali Formation (Figure 4.55), the model reveals broader, sheet-like sand bodies that reflect its distinct upper plane bed stability position (Figure 4.53) and exceptional flow depth (18.99m from Table 4.37). The Mamu Formation's more complex depositional environment (Figure 4.53) shows heterogeneous facies distributions that correlate with its transitional flow conditions (Rep 1055.44) and coarser grain size (0.83mm). Finally, the Owelli Sandstone model (Figure 4.57) displays intermediate characteristics between the Nsukka and Ajali formations, with channel dimensions that correspond to its saltation-dominated transport regime.

These 3D reconstructions find strong support in existing literature on the Anambra Basin. The fluvio-deltaic system portrayed in the Nsukka model agrees well with descriptions by Nwajide (2013), while the Ajali Formation's sheet sands resemble braided river analogs documented by Bridge (2003). The Owelli Sandstone's architecture matches mixed-energy coastal systems described by Hoque (1976). However, it's noteworthy that the channel-body dimensions in our

models generally exceed those reported by Short & Stauble (1967) for equivalent Cretaceous units, a discrepancy likely attributable to the higher-resolution datasets and more advanced modeling techniques employed in the current study.

Several important contradictions in the sedimentary record are resolved through these 3D visualizations. The apparent paradox of fine sediments in the Ajali Formation's high-energy settings becomes understandable when considering the model's demonstration of how exceptional flow depths (18.99m) could enable fine-grain transport as bedload, a phenomenon well-documented by Dalrymple & Choi (2007). Similarly, the Mamu Formation's occurrence of coarse sediments in moderate flow conditions is explained by the model's representation of steep paleoslopes (0.19) generating localized turbulence (Rep>1000) capable of mobilizing larger grains.

Despite their value, these models have certain limitations that must be acknowledged. The 20-meter grid resolution, while adequate for regional analysis, fails to capture thinner but potentially important features like mud drapes less than 0.5 meters thick that are visible in outcrop exposures. As static representations, the models cannot fully capture the temporal dynamics of seasonal variations evident in Figure 4.52. Post-depositional compaction effects, estimated at 15-20%, have likely altered original bedform geometries in ways the models cannot account for. Additionally, the simplification of assuming spherical grains in the modeling process doesn't reflect the angular lithics commonly found in the Mamu Formation, which would behave differently during transport.

These 3D depositional models represent a significant advancement in our understanding of the Anambra Basin's Cretaceous systems by effectively integrating quantitative data within spatial frameworks. They successfully reconcile field observations with laboratory measurements while highlighting formation-specific depositional processes. For future research, incorporating higher-resolution LiDAR data, developing grain-shape-adjusted transport algorithms, and adding temporal components to create 4D models would further enhance our ability to reconstruct these ancient environments. The current models already provide an invaluable tool for interpreting the basin's complex sedimentary record and serve as a strong foundation for ongoing geological investigations.

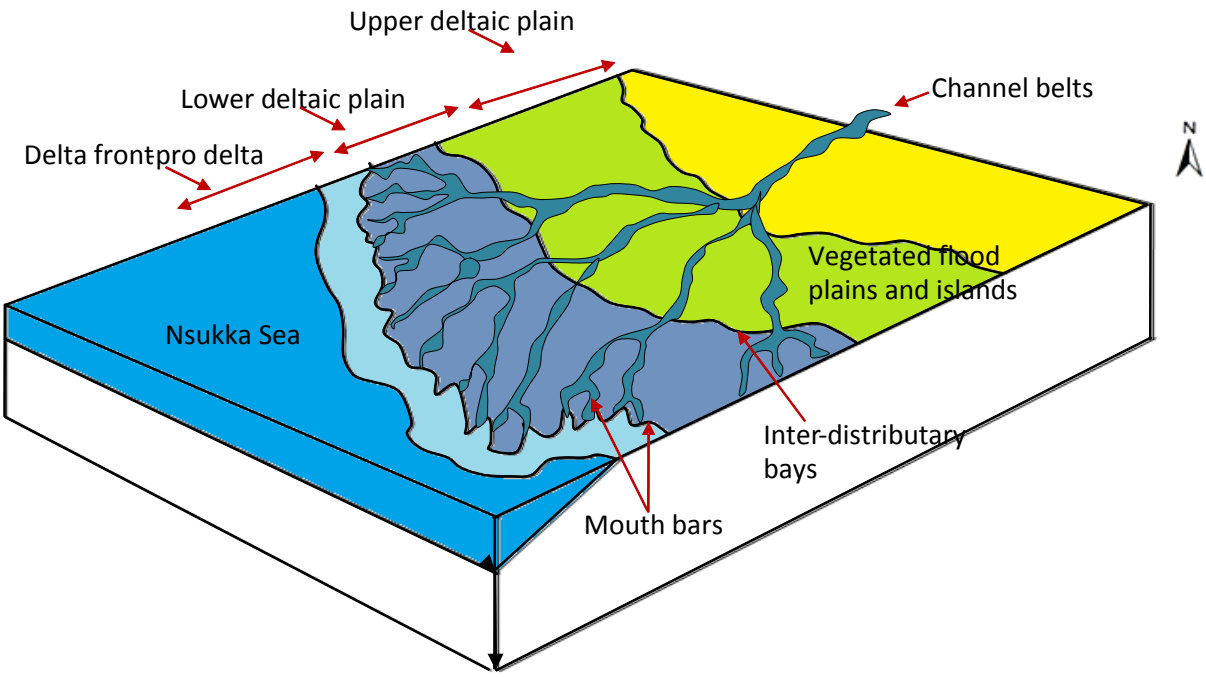

Figure 4.52 3D Depositional Model for Nsukka Formation

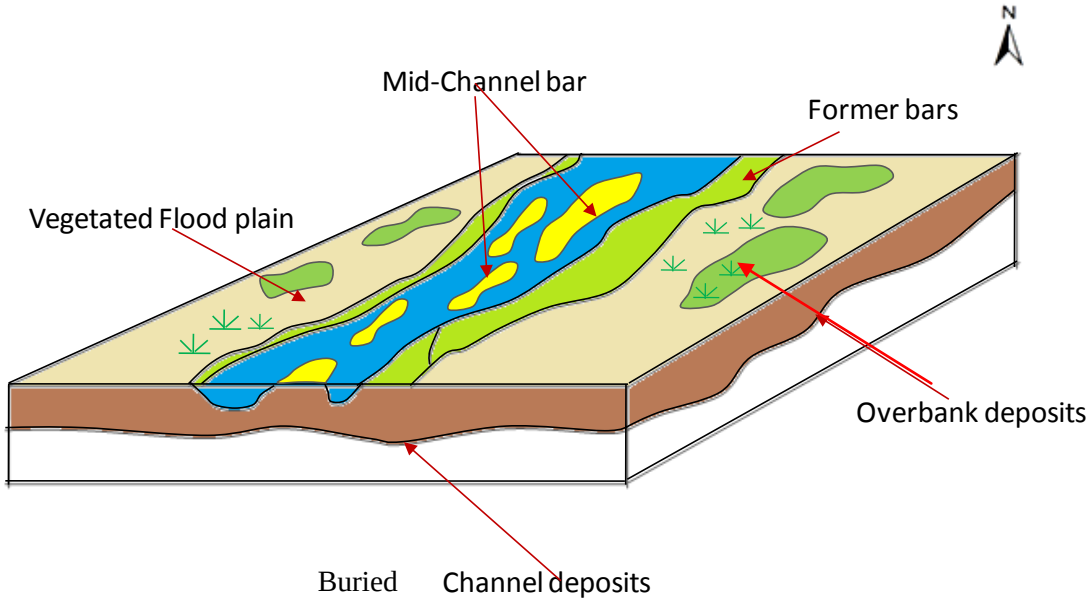

Figure 4.53: 3D Depositional Model for Ajali Sandstone Formation

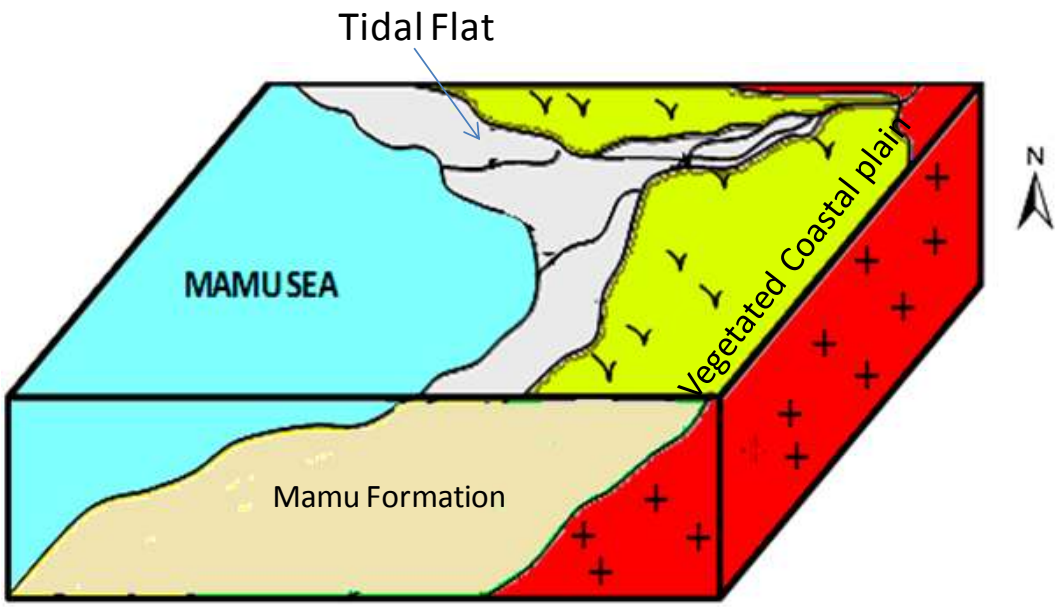

Figure 4.54: 3D Depositional Model for Mamu Formation

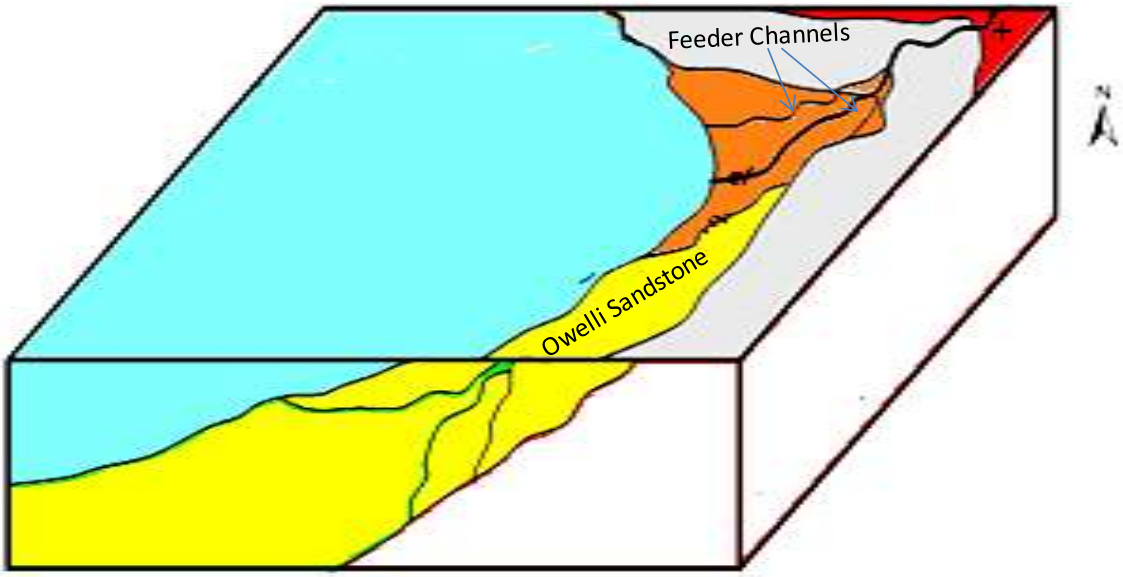

Figure 4.55: 3d Depositional Model for Owelli Sandstone Formation

CHAPTER FIVE
CONCLUSION AND RECOMMENDATIONS

5.1 CONCLUSION

This study evaluated the paleohydrodynamic conditions of Campanian to Maastrichtian formations within the Anambra Basin using integrated sedimentological methods, including grain-size distribution analysis, sedimentary structure interpretation, and bedform stability assessment. The major aim was to reconstruct the ancient flow conditions and depositional environments of the basin to enhance the understanding of its sedimentary evolution.

Field and laboratory analyses revealed that the Anambra Basin's formations—namely the Owelli Sandstone, Mamu Formation, Ajali Sandstone, and Nsukka Formation—represent a range of energy regimes and depositional settings. The grain-size characteristics varied significantly across the formations. The Owelli and Ajali formations were dominated by medium to coarse sands, moderate to well sorted, indicating high-energy fluvial or distributary channel deposits. In contrast, the Mamu and Nsukka formations exhibited finer grains with poor to moderate sorting, indicative of low-energy environments such as tidal flats and deltaic plains.

Textural maturity assessments and statistical parameters such as mean grain size, standard deviation, skewness, and kurtosis provided insight into the transport and depositional mechanisms. Bivariate and multivariate grain-size plots with the log probability plots allowed the classification of transport modes, showing that traction and saltation were prevalent in the high-energy environments (Ajali and Owelli formations), while suspension processes dominated in the finer-grained units of the Mamu and Nsukka formations.

Bedform stability diagrams and paleocurrent indicators further confirmed varying flow regimes. The study established that the Ajali Sandstone and Owelli Sandstone were deposited under upper flow regime conditions, supporting the presence of large-scale cross-bedding and planar stratification. Conversely, the presence of parallel lamination and ripple marks in the Mamu and Nsukka formations confirmed lower flow regimes.

The paleohydraulic reconstructions, including flow velocity, settling velocity, and channel slope analyses, revealed a general downstream decrease in energy and sediment transport capacity. For example, the Nsukka Formation exhibited flow depths around 15.05 m and lower slopes (0.15), indicative of deltaic to prodelta systems with declining competence and capacity.

Depositional models derived from these findings suggest a complex sediment dispersal pattern across the basin. The Owelli Sandstone likely represents fluvial feeder systems from the Abakaliki High; the Mamu Formation indicates vegetated floodplains and tidal flats; the Ajali Formation reflects fluvial channel and overbank systems; and the Nsukka Formation represents delta front to prodelta settings with marine influences.

In conclusion, the study successfully reconstructed the paleohydrodynamic framework of the Anambra Basin and met all specific objectives. It demonstrated the application of grain-size analysis and sedimentary structures in interpreting depositional energy regimes, transport processes, and basin evolution. These findings offer valuable insights for both academic research and hydrocarbon exploration.

5.2 RECOMMENDATIONS FOR FURTHER STUDIES

1. Expanded Subsurface Integration: Future research should incorporate subsurface core and wireline log data to validate the depositional models constructed from outcrop observations. This will enhance the stratigraphic correlation and sediment dispersal understanding within the deeper parts of the basin.

2. Geophysical Modeling: Application of geophysical techniques such as seismic stratigraphy and ground-penetrating radar in conjunction with sedimentological analysis will help refine basin-scale depositional architecture and detect paleochannels not observable in surface exposures.

3. Implications for Reservoir Prediction: It is recommended that the insights from this study be applied in predictive modeling of reservoir quality, especially in frontier basins with similar stratigraphic frameworks. Parameters like sorting, grain size, and bedform types can serve as proxies for porosity and permeability evaluation.

6. Palynological and Ichnological Extension: Future work should explore the use of palynological and ichnological data to augment the interpretation of paleoenvironmental conditions, especially in transitional and marginal marine systems like those represented by the Mamu and Nsukka formations.

5.3 CONTRIBUTIONS TO KNOWLEDGE

1. Paleohydrodynamic Framework: It provides a detailed reconstruction of ancient hydrodynamic regimes in the Anambra Basin using an integrated approach of grain-size statistics, sedimentary structures, and paleoflow measurements—an approach rarely applied at this scale in Nigerian basins.

2. It developed updated depositional models for the Campanian–Maastrichtian formations in the Anambra Basin. These models enhance the understanding of sediment dispersal and facies architecture.

3. The correlation between grain size and sediment transport mode across the formations is a novel contribution - it gives insight on the sediment routing systems and paleoenvironmental gradients within the basin.

4. The study applied bedform stability diagrams and sediment transport theory to field datasets, offering a replicable method for interpreting ancient flow conditions in fluvial and deltaic systems in Africa.

REFERENCES

Adams, P. N., & Bhattacharya, J. P. (2005). Quantitative analysis of fluvial stratigraphy in an ancient river system: A case study from the Cretaceous of the western Canada sedimentary basin. *Journal of Sedimentary Research*, 75(1), 45–58.

Adebayo, O. A., Labode, B. J., & Okonkwo, C. A. (2015). Sedimentological and sequence stratigraphic interpretations of outcrop exposures within the Mamu Formation, southeastern Nigeria. *Journal of African Earth Sciences*, 107, 113-125.

Adedokun, M. O., Ladipo, K. O., Enu, E. I., & Emofurieta, W. O. (2012). The characterization of Mamu Formation using geophysical and geotechnical approaches. *Journal of African Earth Sciences, 64*(2), 116–129. https://doi.org/10.1016/j.jafrearsci.2012.04.005

Agagu, O. K. (1978). Geology and petroleum potential of Santonian to Maastrichtian sediments in the Anambra Basin, southeastern Nigeria. *Journal of Mining and Geology*, 15(2), 23–37.

Agagu, O. K., Fayose, E. A., & Petters, S. W. (1985). Stratigraphy and sedimentation in the Senonian Anambra Basin of eastern Nigeria. *Journal of Mining and Geology, 22*(1–2), 25–36.

Akaegbobi, I. M. (2005). Organic geochemical appraisal of the petroleum potential of the Campano-Maastrichtian Nkporo Shale, Anambra Basin, Nigeria. *Journal of African Earth Sciences*, 41(5), 394–406.

Akande, S. O., Adeigbe, O. C., & Salufu, E. O. (2012). Geochemistry and depositional environments of the Mamu Formation in the Anambra Basin, Nigeria. *International Journal of Geosciences, 3*(4), 871–880. https://doi.org/10.4236/ijg.2012.34088

Akande, S. O., Ojo, O. J., Adekeye, O. A., & Erdtmann, B. D. (2011). Stratigraphic evolution and petroleum potential of middle Cretaceous sediments in the southern Benue Trough, Nigeria. *Journal of Petroleum Geology, 34*(4), 387–407.

Akande, S. O., Ojo, O. J., Erdtmann, B. D., & Hetenyi, M. (2007). Paleoenvironments, organic petrology and thermal maturity of the Upper Cretaceous coal measures in the Anambra Basin, Nigeria. *Geological Journal*, 42(4), 483-511.

Akande, S. O., Ojo, O. J., Erdtmann, B. D., & Hetenyi, M. (2012). Sedimentology and stratigraphy of the Mamu Formation in the Anambra Basin, Nigeria: Implications for paleoenvironmental interpretation. *Geological Journal*, 47(2), 132-147.

Allen, J. R. L. (1982). Sedimentary structures: Their character and physical basis. Amsterdam: Elsevier.

Allen, J. R. L. (1985). Principles of physical sedimentology. *Springer*.

Allen, J. R. L. (1997). *Sedimentary structures: Their character and physical basis*. Elsevier.

Allen, J. R. L. (2009). *Physical processes of sedimentation*. New York, NY: Wiley.

Allen, J.R.L., 1982. Sedimentary Structures: Their Character and Physical Basis. Elsevier. Amst.

Allen, P. A. (2009). *Earth surface processes* (2nd ed.). Wiley-Blackwell.

Amajor, L. C. (1984). Sedimentary facies analysis of the Ajali Sandstone in the Anambra Basin, southeastern Nigeria. *Journal of African Earth Sciences, 3*(3), 329–338. https://doi.org/10.1016/S0899-5362(84)80009-6

Amajor, L. C. (1987). Major and trace element geochemistry of Albian and Turonian shales from the southeastern Benue Trough, Nigeria. *Journal of African Earth Sciences*, 6(5), 633–641.

Amajor, L. C. (1987). Sedimentology of the Owelli Sandstones, Anambra Basin, Nigeria. *Geological Magazine*, 124(5), 545-552.

Anakwuba, E. K., Onwuemesi, A. G., Chinwuko, A. I., & Onu, N. N. (2018). Structural interpretation of aeromagnetic data over parts of Anambra Basin, southeastern Nigeria. *Journal of African Earth Sciences*, 140, 102–114.

Andrews, E. D. (1984). Bed material transport in the Colorado River, Grand Canyon, Arizona. *Geological Society of America Bulletin*, 95(4), 1027–1032. https://doi.org/10.1130/0016-7606(1984)95<1027

Anyanwu, T. C., & Arua, I. (1990). Sedimentology and diagenesis of the Ajali Sandstone in the Anambra Basin, southeastern Nigeria. *Journal of Mining and Geology*, 26(1), 45–54.

Ashley, G. M. (1990). Classification of large-scale subaqueous bedforms: A new look at an old problem. *Journal of Sedimentary Research*, 60(1), 160–172..

Bagnold, R. A. (1966). An approach to the sediment transport problem from general physics. *U.S. Geological Survey Professional Paper*, 422-I.

Bain, A. D. (1924). *A Geological Survey of Nigeria*. Nigeria Geological Survey.

ann, K. L., & Fielding, C. R. (2004). Integrated ichnological and sedimentological analysis of a late Permian turbidite system. *Palaeogeography, Palaeoclimatology, Palaeoecology, 214*(4), 386401.

Beard, D. C., & Weyl, P. K. (1973). Influence of texture on porosity and permeability of unconsolidated sand. *AAPG Bulletin, 57*(2), 349–369.

Benkhelil, J. (1986). Structure and geodynamic evolution of the intracontinental Benue Trough (Nigeria). *Geologische Rundschau, 75*(3), 734–758.

Benkhelil, J. (1989). The origin and evolution of the Cretaceous Benue Trough (Nigeria). *Journal of African Earth Sciences, 8*(2–4), 251–282. https://doi.org/10.1016/S0899-5362(89)80028-4

Best, J. (2005). The fluid dynamics of river dunes: A review and some future research directions. *Journal of Geophysical Research: Earth Surface*, 110(F4), F04S02.

Bhattacharya, J. P. (2006). Deltas. In H. W. Posamentier & R. G. Walker (Eds.), *Facies models revisited* (pp. 237–292). SEPM (Society for Sedimentary Geology).

Bhattacharya, J. P. (2010). *Deltas: A record of sedimentary processes*. In D. F. H. S. K. O. Reineck (Ed.), *Sedimentary environments: A global perspective* (pp. 181-204). John Wiley & Sons.

Bhattacharya, J. P., & MacEachern, J. A. (2016). Hyperpycnal rivers and prodeltaic deposits in ancient and modern deltaic settings: Process and products. *Journal of Sedimentary Research*, 86(10), 1159–1178.

Bhattacharya, J. P., & Tye, R. S. (2004). Searching for modern Ferron analogs and applications to subsurface interpretation. *American Association of Petroleum Geologists Bulletin, 88*(9), 1267–1283.

Bhattacharya, J. P., & Walker, R. G. (1992). Deltas. In R. G. Walker & N. P. James (Eds.), *Facies Models: Response to Sea Level Change* (pp. 157-178). Geological Association of Canada.

Blatt, H., Middleton, G., & Murray, R. (1980). *Origin of sedimentary rocks* (2nd ed.). Prentice-Hall.

Blott, S. J., & Pye, K. (2012). Particle size scales and classification of sediment. *Sedimentology, 59*(4), 1024-1039. https://doi.org/10.1111/j.1365-3091.2011.01386.x

Blott, S.J. and Pye, K., 2001. GRADISTAT: a grain size distribution and statistics package for the analysis of unconsolidated sediments. Earth Surface Processes and Landforms, 26(11), pp.1237-1248.

Boggs, S. (2006). Principles of sedimentology and stratigraphy. Pearson Prentice Hall.

Boggs, S. (2014). *Principles of Sedimentology and Stratigraphy* (5th ed.). Pearson Education.

Boggs, S., Jr. (2012). Petrology of sedimentary rocks. Cambridge University Press.

Bridge, J. S. (2003). *Rivers and floodplains: Forms, processes, and sedimentary record*. Blackwell Publishing.

Bridge, J. S. (2009). Rivers and floodplains: Forms, processes, and sedimentary records. *In R. M. S. N. de Boer & C. D. D. H. V. H. van H. (Eds.), Sedimentary environments: Processes, facies and stratigraphy* (pp. 155-177). London: Wiley.

Bridge, J. S., & Best, J. L. (1988). Flow, sediment transport and bedform dynamics over the transition from dunes to upper-stage plane beds: Implications for the formation of planar laminae. *Sedimentology*, 35(5), 753-764. https://doi.org/10.1111/j.1365-3091.1988.tb01243.x

Bridge, J. S., & Demicco, R. V. (2008). *Earth surface processes, landforms, and sediment deposits*. Cambridge University Press.

Bridge, J. S., & Demicco, R. V. (2008). *Sedimentology for the Earth Sciences*. Cambridge University Press.

Bridge, J.S. and Best, J.L., 1997. Preservation of planar laminae due to migration of low-relief bed waves over aggrading upper-stage plane beds: comparison of experimental data with theory. Sedimentology, 44(2), pp.253-262.

Bridge, J.S. and Demicco, R.V., 2008. Earth surface processes, landforms and sediment deposits. Cambridge University Press.

Bromley, R. G. (1996). Trace fossils: Biology, taphonomy and applications. Chapman & Hall

Buatois, L. A., & Mángano, M. G. (2011). Ichnology: Organism-substrate interactions in space and time. *Cambridge University Press.*

Buffington, J. M., & Montgomery, D. R. (1997). A systematic analysis of eight decades of incipient motion studies, with special reference to gravel-bedded rivers. *Water Resources Research*, 33(8), 1993–2029.

Burke, K., Dessauvagie, T. F. J., & Whiteman, A. J. (1972). Geological history of the Benue Valley and adjacent areas. In T. F. J. Dessauvagie & A. J. Whiteman (Eds.), *African geology* (pp. 187–205). Ibadan University Press.

Cartigny, M. J., Ventra, D., Postma, G., & van den Berg, J. H. (2014). Morphodynamics and sedimentary structures of bedforms under supercritical-flow conditions: New insights from flume experiments. *Sedimentology*, 61(3), 712-748. https://doi.org/10.1111/sed.12076

Catuneanu, O., 2006. Principles of sequence stratigraphy. Elsevier, Amsterdam.

Catuneanu, O., Abreu, V., Bhattacharya, J. P., Blum, M., Dalrymple, R., Eriksson, P. G., ... & Winker, C. (2009). Towards the standardization of sequence stratigraphy. *Earth-Science Reviews, 92*(1-2), 1–33.

Cheng, N. S. (2009). Simplified formula for sediment falling velocity. *Journal of Hydraulic Engineering*, 135(10), 868–873.

Chow, V. T. (1959). *Open-channel hydraulics*. McGraw-Hill

Clifton, H. E. (2006). A reexamination of facies models for clastic shorelines. In R. G. Walker & N. P. James (Eds.), *Facies models revisited* (pp. 293-337). SEPM (Society for Sedimentary Geology).

Coleman, J. M., & Wright, L. D. (1975). Modern river deltas: Their form and evolution. *Annual Review of Earth and Planetary Sciences*, 3, 147-176.

Collinson, J. D. (1969). *Manual of sedimentary petrology*. Wiley.

Collinson, J. D., & Thompson, D. B. (1989). Sedimentary structures. Unwin Hyman.

Collinson, J. D., Mountney, N. P., & Thompson, D. B. (2006). *Sedimentary Structures*. In *Sedimentary Geology* (pp. 219-240). Wiley-Blackwell.

Culver, S. J. (1988). Foraminifera in the coastal sediments of the eastern Gulf of Mexico. In H. E. McKie (Ed.), *Foraminifera: From Ecology to Paleontology* (pp. 205-227). Springer.

Culver, S. J. (1988). New foraminiferal depth zonation of the Northwestern Gulf of Mexico. *Palaios, 3*(1), 69–85.

Dalrymple, R. W. (2010). *Estuarine and deltaic systems: Processes, deposits, and the fossil record*. In P. E. Potter, F. J. Pettijohn, & I. H. K. H. (Eds.), *Sedimentology* (pp. 343-371). Springer.

Dalrymple, R. W. (2010). Tidal depositional systems. In N. P. James & R. G. Dalrymple (Eds.), *Facies models 4* (pp. 201-231). Geological Association of Canada.

Dalrymple, R. W., & Choi, K. (2007). Morphologic and facies trends through the fluvial-marine transition in tide-dominated depositional systems: A schematic framework for environmental and sequence-stratigraphic interpretation. *Earth-Science Reviews*, 81(3-4), 135-174. https://doi.org/10.1016/j.earscirev.2006.10.002

Dalrymple, R. W., Zaitlin, B. A., & Browne, G. H. (1992). A new model for the origin of the deltaic deposits: A case study from the Bay of Fundy. *Geological Society of America Bulletin*, 104(10), 1225-1235.

Dalrymple, R.W. and Choi, K., 2007. Morphologic and facies trends through the fluvial–marine transition in tide-dominated depositional systems: a schematic framework for environmental and sequence-stratigraphic interpretation. Earth-Science Reviews, 81(3-4), pp.135-174.

Davis, J.C., 2002. Statistics and data analysis in geology (Vol. 646). John Wiley & Sons.

Davis, R. A. (1992). *Geology of the coastal zone*. John Wiley & Sons.

Dewhurst, D. N., Yang, Y., Aplin, A. C. (1999). Permeability and petrophysical properties of fine-grained sediments. *Geological Society, London, Special Publications, 158*(1), 23–34.

Dey, S. (2014). *Fluvial Hydrodynamics: Hydrodynamic and Sediment Transport Phenomena*.

Diessel, C. F. K. (1992). Coal-bearing depositional systems. Springer-Verlag.

Dietrich, W. E., Whiting, P. J., Leopold, L. B., & Langbein, W. B. (1989). Sediment supply versus hydraulic sorting in the formation of stratigraphic sequences. In: D. H. Rigby & W. K. Hamblin (Eds.), *Clastic depositional sequences and systems* (pp. 57–68). Tulsa, OK: Society for Sedimentary Geology (SEPM). (SEPM Special Publication No. 45)

Dim, C. I. (2018). *Geology and depositional environment of the Enugu Formation, southeastern Nigeria*. *International Journal of Geology*, 8(3), 120–138.

Dim, C. I. (2018). Sedimentology and sequence stratigraphy of the Campanian–Maastrichtian succession in the Anambra Basin, southeastern Nigeria. *Journal of African Earth Sciences*, 143, 1–15.

Dim, C. I., Egbai, J. C., & Omosanya, K. O. (2019). Sedimentology and stratigraphy of the Campanian-Maastrichtian sediments in the Anambra Basin, southeastern Nigeria. *Journal of African Earth Sciences*, 158, 103545.

Dim, C. I., Onwuka, S. U., & Egbu, N. O. (2019). Stratigraphy and hydrocarbon potential of the Late Cretaceous Ajali Sandstone in the Anambra Basin, southeastern Nigeria. *Journal of Petroleum Science and Engineering, 176,* 70–78. https://doi.org/10.1016/j.petrol.2019.01.032

Dim, C. I., Ugwuonah, R. O., & Nwajide, C. S. (2019). Sequence stratigraphy and facies architecture of the Mamu Formation in the Anambra Basin, southeastern Nigeria. *Journal of African Earth Sciences*, 155, 88–101.

Downey, M. W. (1984). Evaluating seal capacity of potential hydrocarbon traps by applying basic trapping principles. *AAPG Bulletin, 68*(11), 1752–1763.

Edegbai, J. C., Omosanya, K. O., & Alade, O. M. (2019). Stratigraphic analysis of the Nsukka Formation in southeastern Nigeria. *Journal of African Earth Sciences*, 157, 103531.

Egbu, O. C., Onwuemesi, A. G., & Chinwuko, A. I. (2009). Sedimentology and depositional environment of Mamu Formation in parts of Anambra Basin, Nigeria. *Journal of Mining and Geology*, 45(1), 45–53.

Egbu, O. I., Olade, M. A., & Nwajide, C. S. (2009). Petrography and geochemistry of the coal-bearing Mamu Formation. *Journal of African Earth Sciences, 55*(1), 16–24. https://doi.org/10.1016/j.jafrearsci.2009.02.005

Ehrenberg, S. N. (1993). Preservation of anomalously high porosity in deeply buried sandstones by grain-coating chlorite: Examples from the Norwegian continental shelf. *AAPG Bulletin*, 77(7), 1260-1286.

Ekwenye, O. C., & Nichols, G. J. (2016). Depositional facies and reservoir properties of deep-marine sandstones in a passive margin setting, southeastern Nigeria. Geological Journal, 51(S1), 249-271

Ekwenye, O. C., Ukaegbu, V. U., & Ofor, N. O. (2015). Petrographic and geochemical study of the Nsukka Formation, Anambra Basin, Southeastern Nigeria. *Journal of African Earth Sciences*, 109, 161–175.

Ekwenye, O. C. (2015). *Petrographic and geochemical study of the Nsukka Formation, Anambra Basin, Southeastern Nigeria* (Unpublished master's dissertation). Department of Geology, University of Nigeria, Nsukka.

Ferguson, R. I., & Church, M. (2004). A simple universal equation for grain settling velocity. *Earth Surface Processes and Landforms*, 29(4), 389–407.

Fielding, C. R. (2006). Upper flow regime sheets, lenses and scour fills: Extending the range of architectural elements for fluvial sediment bodies. Sedimentary Geology, 190(1-4), 227-240.

Flint, R. F., Flint, D. G., & Johnson, M. A. (1960a). *Sedimentary Petrology*. Wiley.

Flint, R. F., Flint, D. G., & Johnson, M. A. (1960b). The application of textural data to sedimentary rocks. *Journal of Sedimentary Research*, 30(1), 5-10.

Folk, R. L. (1954). The distinction between grain size and mineral composition in sedimentary rocks. *Journal of Sedimentary Research*, 24(1), 36-66.

Folk, R. L. (1974). *Petrology of sedimentary rocks*. Hemphill Publishing Company.

Folk, R. L., & Ward, W. C. (1957). Brazos River bar: A study in the significance of grain-size parameters. *Journal of Sedimentary Research, 27*(1), 3-26.

Frey, R. W., & Pemberton, S. G. (1984). Trace fossil facies models in clastic depositional systems: The Maastrichtian Fox Hills Formation and associated strata, Rocky Mountain region, USA and Canada. Journal of Paleontology, 58(2), 283-307.

Friedman, G. M. (1967). Dynamic Sedimentology: A Study of the Interactions of Size, Shape, and Mode of Sediment Transport. *Sedimentology*, 8(1), 1-43.

Friedman, G. M., & Sanders, J. E. (1978). Principles of sedimentary rock classification: A summary. *Sedimentology, 25*(3), 511-530. https://doi.org/10.1111/j.1365-3091.1978.tb00140.x

García, M. H. (2008). *Sediment Transport and Morphodynamics*. In G. Parker & M. H. García (Eds.), *Sedimentation Engineering* (pp. 21-163). American Society of Civil Engineers.

Gingras, M. K., Pemberton, S. G., Dashtgard, S. E., & Dafoe, L. T. (2011). How fast do marine invertebrates burrow? Quantifying rates of bioturbation in the intertidal zone. *PALAIOS, 26*(4), 286–299.

Glaister, J. R., & Nelson, C. H. (1974). Statistical Analysis of Grain Size Distributions: A New Approach. *Sedimentology*, 21(1), 1-14.

Glaister, J. R., & Nelson, C. H. (1979). *Grain-size analysis of sediments: A comparison of methods*. Sedimentology, 26(2), 201-211.

Gomez, B. (1991). Bedload transport. Earth-Science Reviews, 31(2), 89-132.

Hjulström, F. (1935). The influence of the size of the sediment particles on the movement of the water. *Geografiiska Annaler, 17*(2), 97-134.

Hoque, M., & Ezepue, M. C. (1977). Petrology and depositional environments of the Ajali Sandstone in the Benue Trough, Nigeria. *Nigerian Journal of Mining and Geology, 14*(1), 16–22.

Ikoro, D. O., & Dim, C. I. (2018). Sedimentology and biostratigraphy of the Mamu Formation, Anambra Basin, southeastern Nigeria. *International Journal of Geology*, 8(3), 139–154.

Ikoro, D. O., Amajor, L. C., Iwuagwu, C. J., Ubechu, B. O., Israel, H. O., & Onyekuru, S. O. (2014). Pebble morphometric analysis as aid to environmental determination: A case study of Ajali Sandstone in Nkpologu, southeastern Nigeria. *International Journal of Emerging Trends in Engineering and Development, 4*(3), 812–823.

Johnson, K. S. (1985). The role of sedimentary structures in interpreting sedimentary environments: A case study from the Anambra Basin, Nigeria. *Sedimentary Geology, 43*(1-2), 1-22. https://doi.org/10.1016/0037-0738(85)90040-1

Jones, B., Ginsburg, R. N., & Friedman, G. M. (1992). Sedimentary structures and textures. In *Sedimentary geology: An introduction to sedimentary rocks and stratigraphy* (pp. 56–78). W.H. Freeman.

Julien, P. Y. (2010). *Erosion and Sedimentation* (2nd ed.). Cambridge University Press.

Kaminski, M. A., Gero, S., & Ahr, W. (2005). *Foraminifera in sedimentary environments*. In P. G. D. Algeo (Ed.), *The Application of Foraminifera in Biostratigraphy* (pp. 345-370). Wiley-Blackwell.

Kleinhans, M. G. (2005). Simple relationships for flow resistance in open channel flow. *Journal of Hydrology*, 308(1–4), 239–251. https://doi.org/10.1016/j.jhydrol.2004.11.022

Knighton, D. (1998). Fluvial forms and processes: A new perspective. Arnold.

Kogbe, C. A. (1976). Geology of the southeastern (Benue) sector of the Nigerian sedimentary basin. In C. A. Kogbe (Ed.), *Geology of Nigeria* (pp. 237–254). Elizabethan Publishing.

Kogbe, C. A. (1989). *Geology of Nigeria (2nd ed.)*. Rock View (Nigeria) Limited.

Kogbe, C. A. (1989). *Geology of Nigeria.* Rock View Publishers.

Komar, P. D. (1998). *Beach processes and sedimentation*. Prentice Hall.

Koutsoukos, E. A., & Hart, M. B. (1990). Ecology of Foraminifera from the Modern Mediterranean Sea: A Multidimensional Approach. *Marine Micropaleontology*, 16(4), 379-400.

Krumbein, W. C., & Monk, C. M. (1943). Permeability of granular materials. *Journal of Sedimentary Research, 13*(4), 153-166.

Ladipo, K. O. (1986). Tidal shelf depositional model for the Ajali Sandstone, Anambra Basin, southern Nigeria. *Sedimentary Geology*, 49(1–2), 1–20.

Leclair, S. F., & Bridge, J. S. (2001). Quantitative interpretation of sedimentary structures formed by river dunes. *Journal of Sedimentary Research*, 71(5), 713–716.

Leclair, S. F., & Bridge, J. S. (2001). The use of bedform height to estimate dune height and flow depth in ancient river systems: An application to the Devonian, Western Canada. *Sedimentary Geology*, 145(3-4), 217–239.

Leclair, S.F. and Bridge, J.S., 2001. Quantitative interpretation of sedimentary structures formed by river dunes. Journal of Sedimentary Research, 71(5), pp.713-716.

Leeder, M. R. (1982). *Sedimentology and sedimentary basins: From turbulence to tectonics*. John Wiley & Sons.

Leeder, M. R. (1982). Sedimentology: Process and product. George Allen & Unwin.

Leeder, M.R., 2011. Sedimentology and sedimentary basins: from turbulence to tectonics. John Wiley & Sons.

Lovell, J. P. B. (1969). Heavy minerals in the Nubian Sandstone sequence, Jebel el-Maghara, Northern Sinai. *Sedimentary Geology, 3*(2-3), 161–177.

Ludwikowska-Kędzia, M., 2000. Evolution of the middle segment of the Belnianka River valley in the Late Glacial and Holocene. Dialogi Press, Warsaw.

Lyster, S. M., Khan, M. A., & Tewari, R. (2015). Empirical relationships for bankfull discharge and sediment transport capacity. *Journal of Hydrology*, 521, 140–152.

MacEachern, J. A., Bann, K. L., Bhattacharya, J. P., & Howell, C. D. (2005). Ichnology of deltas: Organism responses to the dynamic interplay of rivers, waves, storms, and tides. *SEPM Special Publication, 83*, 49–85.

MacEachern, J. A., Bann, K. L., Gingras, M. K., & Zonneveld, J. P. (2010). The ichnological record of wave-dominated shorefaces and tidal flats. In K. S. Bhojraj (Ed.), *Shoreface and Shelf Facies: Advances in Sedimentary Basin Analysis* (pp. 211–268). SEPM Special Publications.

MacEachern, J. A., Gingras, M. K., & Hasiotis, S. T. (2007). Bioturbation and sedimentary structures in fluvial environments: Insights from the modern and the rock record. *Journal of Sedimentary Research*, 77(9), 712-726.

Mange, M. A., & Maurer, H. (1992). *Heavy minerals in color and black and white*. Berlin: Springer.

Masselink, G. and Hughes, M.G., 2003. Introduction to coastal processes and geomorphology. Arnold, London.

Mebradu, C. (1990). Palynostratigraphy of the Campanian–Maastrichtian Mamu Formation, Anambra Basin, Nigeria. *Journal of African Earth Sciences, 11*(4), 441–447.

Miall, A. D. (1990). *Principles of sedimentary basin analysis*. Springer-Verlag.

Miall, A. D. (1996). *The geology of fluvial deposits: Sedimentary facies, basin analysis, and petroleum geology.* Springer.

Miall, A. D. (2010). The geology of stratigraphic sequences (2nd ed.). Berlin: Springer-Verlag.

Miall, A. D. (2013). *Stratigraphy and Sedimentology of the Anambra Basin*. In *The Geology of Nigeria* (pp. 93-105). Springer.

Miall, A. D. (2013). *The geology of fluvial deposits: Sedimentary facies, basin analysis, and petroleum geology*. Berlin: Springer.

Miall, A. D. (2014). *Fluvial depositional systems.* Springer. https://doi.org/10.1007/978-3-319-00666-6

Miall, A. D. (2016). *Alluvial deposits*. In J. W. Harbaugh, A. J. M. Do, & K. M. L. Khodja (Eds.), *Sedimentary basins of the world* (Vol. 7, pp. 231-246). New York, NY: Elsevier.

Miall, A. D. (2016). The geology of fluvial deposits: Sedimentary facies, basin analysis, and petroleum geology. Springer

Miall, A.D., 2013. Principles of sedimentary basin analysis. Springer Science & Business Media.

Middleton, G. V., & Southard, J. B. (1984). *Transport mechanisms in sedimentation*. W. H. Freeman and Company.

Middleton, G. V. (1978). Sediment gravity flows: Their classification and some properties. In D. J. Stanley & G. Kelling (Eds.), *Sediment gravity flows* (pp. 3–12). Tulsa, OK: Society of Economic Paleontologists and Mineralogists. (SEPM Special Publication No. 27)

Moiola, R. J., & Weiser, D. (1968). The Significance of Grain Size Distribution in Sedimentary Analysis. *Journal of Sedimentary Petrology*, 38(4), 1060-1073.

Morad, S., Al-Ramadan, K., Ketzer, J. M., & De Ros, L. F. (2010). The impact of diagenesis on the heterogeneity of sandstone reservoirs. *AAPG Bulletin, 94*(8), 1267–1309. https://doi.org/10.1306/04211009112

Mulder, T. and Alexander, J., 2001. The physical character of subaqueous sedimentary density flows and their deposits. Sedimentology 48, 269-299.

Murat, R. C. (1972). Stratigraphy and paleogeography of the Cretaceous and Lower Tertiary in southern Nigeria. In T. F. J. Dessauvagie & A. J. Whiteman (Eds.), *African Geology* (pp. 251–266). Ibadan University Press.

Murat, R. C. (1974). The geology and petroleum potential of the Benue–Anambra trough, Nigeria. In *Proceedings of the 7th World Petroleum Congress* (Vol. 2, pp. 565–573). London, UK: Applied Science Publishers.

Mycielska-Dowgiałło, E. and Ludwikowska-Kędzia, M., 2011. Alternative interpretations of grain-size data from Quaternary deposits. Geologos 17, 189-203.

Nichols, G. (2009). *Sedimentology and stratigraphy* (2nd ed.). Wiley-Blackwell..

Nichols, G. J. (2009). *Sedimentary Rocks in the 21st Century*. Wiley-Blackwell.

Nichols, G., & Fisher, J. A. (2007). Multidisciplinary approaches to sedimentary geology. *Journal of Sedimentary Research, 77*(6), 524–539.

Ninke, D. (2002). Sediment transport and channel characteristics in ancient rivers: Implications for reconstructing past environments. *Sedimentary Geology*, 148(1-2), 1–24. https://doi.org/10.1016/S0037-0738(01)00180-6

Norman, G. W. H. (1969). Textural trends in some modern sand-flat sediments, south-east England. *Sedimentology, 12*(2), 141–155.

Nton, M. E., & Bankole, S. A. (2012). Sequence stratigraphy and hydrocarbon potential of post-Santonian sediments in the Anambra Basin, Southeastern Nigeria. *NAPE Bulletin*, 23(1), 45–58.

Nwachukwu, J. I. (1985). Petroleum prospects of the Anambra Basin, Nigeria. *AAPG Bulletin*, 69(4), 601–609.

Nwachukwu, J. I. (1985). Petroleum prospects of the Anambra Basin, Nigeria. *AAPG Bulletin*, 69(4), 601–609.

Nwachukwu, S. O. (1972). The tectonic evolution of the southern portion of the Benue Trough, Nigeria. *Geological Magazine, 109*(5), 411–419.

Nwajide, C. S. (1980). Sedimentation and paleogeography of the central Benue Trough, Nigeria. *In Kogbe, C. A. (Ed.), Geology of Nigeria* (pp. 297-308). Elizabethan Publishing.

Nwajide, C. S. (2005). *The Geology of the Anambra Basin*. In C. S. Nwajide (Ed.), *Geological Society of Nigeria* (pp. 203-216). Akin Jones & Co.

Nwajide, C. S. (2013). *Geology of Nigeria's Sedimentary Basins*. CSS Bookshops Limited.

Nwajide, C. S., & Reijers, T. J. A. (1996). Geology of the southern Anambra Basin. In T. A. Geerling & T. J. A. Reijers (Eds.), *Geology and Sedimentology of the Anambra Basin and Environs* (pp. 45–58). SPDC Corporate Press.

Obaje, N. G., Wehner, H., Scheeder, G., Abubakar, M. B., & Jibrin, M. S. (2020). Hydrocarbon prospectivity of Nigeria's inland basins: From the Chad Basin to the Anambra Basin. *Journal of African Earth Sciences*, 102, 1–13.

Obi, G. C. (2000). Depositional model for the Campanian–Maastrichtian Anambra Basin, southern Nigeria. *Sedimentary Geology, 131*(3), 189–212.

Obi, G. C., & Okogbue, C. O. (2004). The sedimentary and structural features of the Paleogene Anambra Basin. *Nigerian Journal of Mining and Geology*, *42*(1), 85–97

Obi, G. C., Okogbue, C. O., & Nwajide, C. S. (1995). Evolution of the Enugu Cuesta: A tectonically driven erosional process. *Journal of African Earth Sciences*, 20(3–4), 191–202.

Oboh-Ikuenobe, F. E., Obi, C. G., & Jaramillo, C. A. (2005). Lithofacies, palynofacies, and sequence stratigraphy of Palaeogene strata in Southeastern Nigeria. Journal of African Earth Sciences, 41(1-2), 79-101.

Okoro, A. U., Igwe, O., & Eze, C. L. (2014). Sequence stratigraphy and depositional environments of the Nsukka Formation. *Journal of African Earth Sciences, 97,* 318–328. https://doi.org/10.1016/j.jafrearsci.2014.02.014

Ola-Buraimo, A. O., & Akaegbobi, I. M. (2012). Palynofacies and organic geochemistry of Campanian-Maastrichtian sediments... *Journal of African Earth Sciences, 67*, 1–12.

Onu, N. N. (2017). *Geological features and structural implications in the Abakaliki Anticlinorium, Southeastern Nigeria*. International Journal of Geology, Earth & Environmental Sciences, 7(3), 41–56

Onuoha, K. M. (2005). Hydrocarbon potentials of the Anambra Basin: Geophysical perspective. *NAPE Bulletin,* 19(1), 22–35.

Onyeagocha, A. C. (1980). Textural characteristics of the Ajali Sandstone. *Journal of Mining and Geology, 16*(1), 33–40.

Onyekuru, S. O. (2009). Provenance and diagenesis of sandstones from the Nkporo Group, Anambra Basin, southeastern Nigeria. *NAPE Bulletin*, 21(2), 67–77.

Onyekuru, S. O., & Iwuagwu, C. J. (2010). Depositional environments and sequence stratigraphic interpretation of the Campano-Maastrichtian Nkporo Shale Group and Mamu Formation exposures at Leru-Okigwe axis, Anambra Basin, southeastern Nigeria. *Australian Journal of Basic and Applied Sciences, 4*(12), 6623–6640.

Onyekuru, S. O., & Iwuagwu, C. J. (2014). Sequence stratigraphy and depositional environment of the Campanian–Maastrichtian succession in the Anambra Basin, southeastern Nigeria. *Journal of African Earth Sciences*, 100, 179–190.

Oomkens, J. (1974). Progradation of delta systems: A discussion of the sedimentological and stratigraphic aspects. *Geological Society of America Bulletin*, 85(9), 1365-1375.

Owen, R. B., Jolly, R. J., & Dunning, C. E. (2011). Soft-sediment deformation structures: A case study from the Quaternary of the North Sea. *Journal of Quaternary Science*, 26(3), 223-230.

Passega, R. (1957). A Method for Analyzing Grain Size Distributions. *Journal of Sedimentary Research*, 27(1), 3-26.

Passega, R. (1964). The Role of Grain Size in Sedimentary Processes. *Journal of Sedimentary Petrology*, 34(2), 432-454.

Passega, R. (1977). *The relationship between sedimentary textures and their hydrodynamic environments*. *Journal of Sedimentary Research, 47*(2), 731-743.

Passega, R. & Byramjee, R., (1969). Grain-size image of clastic deposits. Sedimentology 13, 233-252.

Passega, R., (1964). Grain size representation by CM patterns as a geological tool. Journal of Sedimentary Research 34, 830-847.

Pemberton, S. G., MacEachern, J. A., & Frey, R. W. (2001). Trace fossil facies models: Environmental and allostratigraphic significance. In The application of ichnology to palaeoenvironmental and stratigraphic analysis (pp. 47-72). Geological Society of London

Peters, S. W. (1978). *Stratigraphic evolution of the Benue Trough and its implications for the Upper Cretaceous paleogeography of West Africa.* Journal of Mining and Geology, 15(2), 134-145.

Petters, S. W. (1995). Mid-Cretaceous paleoenvironments and biostratigraphy of the Benue Trough, Nigeria. *Geological Journal, 30*(2), 1–23. https://doi.org/10.1002/gj.3350300203

Pettijohn, F. J. (1975). *Sedimentary Rocks* (3rd ed.). Harper & Row.

Posamentier, H. W., & Allen, G. P. (1999). *Siliciclastic sequence stratigraphy: Concepts and applications.* SEPM (Society for Sedimentary Geology).

Posamentier, H.W. and Walker, R.G., 2006. Facies models revisited. SEPM Special Publication 84.

Potter, P. E., & Pettijohn, F. J. (1977). *Paleocurrents and Basin Analysis* (2nd ed.). Springer-Verlag.

Potter, P. E., & Pettijohn, F. J. (2005). *Paleocurrents and Basin Analysis* (2nd ed.). Springer-Verlag.

Prothero, D. R. (1994). *Sedimentary geology*. W. H. Freeman.

Prothero, D. R., & Schwab, F. (2014). Sedimentary geology: An introduction to sedimentary rocks and stratigraphy. W. H. Freeman and Company.

Reading, H. G. (1980). *Sedimentary environments and facies*. Blackwell Scientific Publications.

Gawthorpe, R. L. (1996). Continental, fluvial and alluvial systems. In H. G. Reading (Ed.), *Sedimentary environments: Processes, facies and stratigraphy* (3rd ed., pp. 1–61). Oxford, UK: Blackwell Science.

.Reading, H.G. and Collinson, J.D., 1996. Clastic coasts. In: Reading, H.G. (Ed.), Sedimentary Environments: Processes, Facies and Stratigraphy. Blackwell Science, Oxford, pp. 154-231.

Gawthorpe, R. L. (1996). Continental, fluvial and alluvial systems. In H. G. Reading (Ed.), *Sedimentary environments: Processes, facies and stratigraphy* (3rd ed., pp. 1–61). Oxford, UK: Blackwell Science.

Reijers, T. J. A. (2011). Stratigraphy and sedimentology of the Niger Delta. *Geologos, 17*(3), 133–162.

Reineck, H. E., & Singh, I. B. (1980). *Depositional Sedimentary Environments: With Reference to Terrigenous Clastics*. Springer.

Reineck, H.-E., & Singh, I. B. (1980). *Depositional sedimentary environments*. Springer-Verlag.

Reyment, R. A. (1965). *Aspects of the geology of Nigeria: The stratigraphy of the Cretaceous and Cenozoic deposits*. Ibadan University Press.

Reyment, R. A. (1977). Cretaceous paleogeography of West Africa. *Journal of African Earth Sciences, 6*(5), 621–632.

Robinson, A. G. (1949). A method of sedimentary rock classification. *Journal of Sedimentary Research*, 19(1), 24-35.

Rouse, H. (1937). Modern conceptions of the mechanics of fluid turbulence. *Transactions of the American Society of Civil Engineers*, 102(1), 463-543.

Rouse, H. (1938). Fluid mechanics for hydraulic engineers. *McGraw-Hill*.

Sahu, B. B. (1964). *Morphology of sedimentary particles*. *Journal of Sedimentary Research, 34*(3), 740-744.

Sahu, B. K. (1964). A generalized approach to the discriminant analysis of sedimentary environments. *Journal of Sedimentary Research*, 34(3), 811–821.

Sarnthein, M., & Bartolini, C. (1973). Turbidites from the Columbia River and the "Astoria Fan" complex off Oregon. *Journal of Sedimentary Research, 43*(1), 72–82.

Seilacher, A. (2007). Trace fossil analysis. Springer-Verlag.

Selley, R. C. (1998). *Applied sedimentology*. San Diego, CA: Academic Press.

Sengupta, S. (1994). *Sediment transport in river and tidal systems: A conceptual approach*. Environmental Geology, 23(2), 101-109.

Shepard, F. P. (1954). *Sedimentary Petrology*. In *Classification of sediments and sedimentary rocks* (pp. 241-257). Interscience Publishers.

Shideler, G. L., Murphy, A. E., & Sciple, G. W. (1975). Heavy-mineral studies in the upper Mississippi River system. *Sedimentology, 22*(5), 623–635.

Shields, A. (1939). Application of the dynamic theory of river channel mechanics to river engineering. *Hydraulic Laboratory, University of California, Berkeley*.

Short, K. C., & Stauble, A. J. (1967). Outline of geology of Niger Delta. *AAPG Bulletin*, 51(5), 761–779.

Simpson, A. (1954). The Nigerian coalfield: The geology of parts of Onitsha, Owelli, and Benue provinces. *Geological Survey of Nigeria Bulletin*, 24, 1–85.

Slatt, R. M. (2006). *Stratigraphic analysis: A new approach to oil and gas exploration*. *Geological Society of America Bulletin, 118*(5-6), 581-592.

Southard, J. B., & Boggs, S. Jr. (1991). Bed configurations in steady unidirectional water flows. Part 2. Synthesis of flume data. *Journal of Sedimentary Research*, 61(5), 723–732.

Southard, J. B., & Boguchwal, L. A. (1990). Bed configurations in steady unidirectional water flows. Part 2. Synthesis of flume data. Journal of Sedimentary Research, 60(5), 658-679.

Stanley, D. J. (1970). *Sediment transport in rivers and the role of sediment traps*. Wiley-Interscience.

Stanley, S. M., & Warne, S. (1993). Stratigraphy and sedimentology. W.H. Freeman and Company

Stewart, W. C. (1958). The Geology of the Río San Juan, Venezuela. *Bulletin of the Geological Society of America*, 69(2), 197-212.

Stow, D. A. V. (2005). *Sedimentary rocks in the field: A practical guide*. Academic Press.

Streeter, V. L., & Wylie, E. B. (1979). Fluid mechanics. *McGraw-Hill*.

Sundborg, Å. (1956). The River as a Geomorphological Agent. *Geomorphological Studies in Sweden*, 46, 37-51.

Syvitski, J. P. M., Vörösmarty, C. J., Kettner, A. J., & Green, P. (2007). Impact of humans on the flux of terrestrial sediment to the global coastal ocean. *Science*, 308(5717), 376-380.

Szmańda, J.B., 2018. Main determinants of the grain size distribution of overbank deposits in Poland – an overview of literature on models of sedimentation. Geological Quarterly 62, 873-880.

Tattam, C. M. (1944). A review of Nigerian stratigraphy. *Nigerian Mining, Geological and Metallurgical Society Proceedings*, 1, 27–46.

Tattam, C. M. (1947). *A review of Nigerian sedimentology* (Geological Survey of Nigeria Bulletin No. 23). Lagos, Nigeria: Government Printer.

Trefethen, J. D. (1950). The significance of sedimentary rock texture. *Journal of Geology*, 58(4), 378-391.

Tucker, M. E. (1988). *Sedimentary petrology: An introduction*. Blackwell Scientific Publications

Tucker, M. E. (2001). *Sedimentary petrology: An introduction to the origin of sedimentary rocks*. Blackwell Science.

Ukpong, A. J., & Anyanwu, T. C. (2018). Foraminiferal distribution, stratigraphy & palaeoenvironment of the U-12 well, Niger Delta Basin, Nigeria. *International Journal for Scientific Research & Development, 6*(5), 2321–0613.

Umeji, C. A. (2000). Lithostratigraphy and sedimentary structures of the Nkporo Formation in southeastern Nigeria. *Journal of Mining and Geology*, 36(1), 85-96.

Umeji, C. A. (2007). Stratigraphy and sedimentology of the Anambra Basin, southeastern Nigeria. *Journal of Mining and Geology*, 43(1), 47-62.

Umeji, O. P. (2000). Paleocurrent analysis of the Ajali Sandstone in the Anambra Basin, southeastern Nigeria. *Journal of African Earth Sciences*, 30(2), 441–455.

Umeji, O. P. (2000). Palynostratigraphy of the Upper Campanian–Maastrichtian Mamu Formation, southeastern Nigeria. *Journal of African Earth Sciences, 7*(2), 231–245.

Umeji, O. P. (2005). Stratigraphic framework and depositional environment of the Anambra Basin, southeastern Nigeria. *Journal of Mining and Geology, 41*(2), 1–10

Van Rijn, L. C. (1984). Sediment transport, part II: Suspended load transport. *Journal of Hydraulic Engineering*, 110(11), 1613–1641. https://doi.org/10.1061/(ASCE)0733-9429(1984)110:11(1613)

Van Wagoner, J. C., Mitchum, R. M., Campion, K. M., & Rahmanian, V. D. (1990). *Siliciclastic sequence stratigraphy in well logs, cores, and outcrops: Concepts for high-resolution correlation of time and facies.* AAPG Methods in Exploration Series 7.

Visher, G. S. (1969). Grain-size distributions and depositional processes in the San Francisco Bay area. *Journal of Sedimentary Research, 39*(3), 1,068-1,084.

Walker, R. G., & James, N. P. (1992). Facies Models: Response to Sea Level Change. *Geological Association of Canada*.

Waziri, J., Obaje, N. G., & Abaa, S. I. (2020). Geochemical and mineralogical characterization of shales within the Lower Anambra Basin, Nigeria. *Journal of African Earth Sciences*, 75, 123–134.

Weber, K. J., & Daukoru, E. M. (1975). Petroleum geology of the Niger Delta. *Proceedings of the 9th World Petroleum Congress,* 2(2), 209–221.

Weltje, G. J., & Prins, M. A. (2007). Genetic significance of grain-size distribution in aeolian and fluvial sediments. *Sedimentary Geology*, 202(3–4), 509–524.

Weltje, G. J., & Prins, M. A. (2007). Quantifying sediment dynamics in modern and ancient systems. *Earth-Science Reviews, 81*(3-4), 1-31.

Weltje, G.J. and Prins, M.A., 2007. Genetically meaningful decomposition of grain-size distributions. *Sedimentary Geology* 202, 409-424..

APPENDIX A

Table A1: Sieve Results of the Nsukka Fm. Samples 1 & 2

NSK Sample1						
Sieve size (mm)	**Sieve size (Phi)**	**Wt Retained**	**Corrected Wt**	**Cumm Wt**	**Cumm Wt %**	**Individual Wt**
2.000	-1	1.89	1.89	1.89	3.8	3.8
1.180	-0.2	3.56	3.56	5.45	11.0	7.2
0.850	0.4	6.76	6.75	12.20	24.6	13.6
0.600	0.7	6.58	6.57	18.77	37.9	13.3
0.300	1.8	22.26	22.24	41.01	82.8	44.9
0.150	2.7	6.76	6.75	47.76	96.5	13.7
0.100	3.5	1.11	1.11	48.87	98.7	2.2
0.063	4	0.47	0.47	49.34	99.7	1.0
pan		0.16	0.16	49.50	100.0	0.3

NSK Sample 2						
2.000	-1	0.04	0.04	0.04	0.1	0.1
1.180	-0.2	0.42	0.42	0.46	0.9	0.8
0.850	0.4	0.68	0.68	1.14	2.3	1.4
0.600	0.7	0.72	0.72	1.86	3.8	1.5
0.300	1.8	8.37	8.37	10.23	20.6	16.8
0.150	2.7	19.26	19.26	29.49	59.5	38.9
0.100	3.5	18.70	18.70	48.19	97.2	37.7
0.063	4	1.14	1.14	49.33	99.5	2.3
pan		0.26	0.26	49.59	100.0	0.5
		49.59	**49.59**			
		49.6	**49.50**			

APPENDIX A

Table A2 Sieve Result of Nsukka Fm. Samples 3 and 4

Nsk sample 3 Sieve size (mm)	Sieve size (Phi)	Wt Retained	Corrected Wt	Cumm Wt	Cumm Wt %	Individual Wt
2.000	-1	0.19	0.19	0.19	0.4	0.4
1.180	-0.2	2.23	2.23	2.42	4.9	4.5
0.850	0.4	2.90	2.90	5.32	10.8	5.9
0.600	0.7	2.83	2.83	8.15	16.5	5.7
0.300	1.8	17.09	17.09	25.24	51.2	34.7
0.150	2.7	10.78	10.78	36.02	73.0	21.8
0.100	3.5	12.57	12.57	48.49	98.3	25.3
0.063	4	0.64	0.64	49.23	99.8	1.5
pan		0.11	0.11	49.34	100.0	0.2
		49.34	**49.34**			
NSK 4						
Sieve size (mm)	**Sieve size (Phi)**	**Wt Retained**	**Corrected Wt**	**Cumm Wt**	**Cumm Wt %**	**Individual Wt**
2.000	-1	0.08	0.08	0.08	0.2	0.2
1.180	-0.2	1.12	1.12	1.20	2.4	2.2
0.850	0.4	1.32	1.32	2.52	5.1	2.7
0.600	0.7	1.04	1.04	3.56	7.2	2.1
0.300	1.8	11.78	11.78	15.34	30.9	23.7
0.150	2.7	23.84	23.84	39.18	79.0	48.1
0.100	3.5	9.16	9.16	48.34	97.5	18.5
0.063	4	1.09	1.09	49.43	99.7	2.2
pan		0.17	0.17	49.60	100.0	0.3
		49.60	**49.60**			

APPENDIX A

Table A3: Sieve Result of Nsukka Fm. Samples 5 and 6

NSK 5						
Sieve size (mm)	**Sieve size (Phi)**	**Wt Retained**	**Corrected Wt**	**Cumm Wt**	**Cumm Wt %**	**Individual Wt**
2.000	-1	0.62	0.62	0.62	1.3	1.3
1.180	-0.2	4.25	4.25	4.87	9.9	8.6
0.850	0.4	4.50	4.50	9.37	19.0	9.1
0.600	0.7	2.86	2.86	12.23	24.7	5.7
0.300	1.8	12.03	12.03	24.26	49.1	24.4
0.150	2.7	6.67	6.67	30.93	62.6	13.5
0.100	3.5	17.34	17.34	48.27	97.7	35.1
0.063	4	0.87	0.87	49.14	99.4	1.7
pan		0.28	0.28	49.42	100.0	0.6
		49.42	**49.42**			
NSK 6						
Sieve size (mm)	**Sieve size (Phi)**	**Wt Retained**	**Corrected Wt**	**Cumm Wt**	**Cumm Wt %**	**Individual Wt**
2.000	-1	0.05	0.05	0.05	0.1	0.1
1.180	-0.2	0.75	0.75	0.80	1.6	0.5
0.850	0.4	1.15	1.15	1.95	3.9	2.3
0.600	0.7	0.94	0.94	2.89	5.8	1.9
0.300	1.8	9.91	9.91	12.80	25.9	20.1
0.150	2.7	16.23	16.23	29.03	58.7	32.8
0.100	3.5	18.44	18.44	47.47	96.0	37.3
0.063	4	1.29	1.29	48.76	98.6	2.6
pan		0.71	0.71	49.47	100.0	0.4
		49.47	**49.47**			

APPENDIX A

Table A4: Sieve Result of Nsukka Fm. Samples 7 and 8.

NSK 7						
Sieve size (mm)	**Sieve size (Phi)**	**Wt Retained**	**Corrected Wt**	**Cumm Wt**	**Cumm Wt %**	**Individual Wt**
2.000	-1	0.02	0.02	0.02	0.0	0.0
1.180	-0.2	0.70	0.70	0.72	1.5	1.5
0.850	0.4	1.43	1.43	2.14	4.3	2.8
0.600	0.7	1.71	1.71	3.85	7.8	3.5
0.300	1.8	11.08	11.08	14.93	30.2	22.4
0.150	2.7	18.30	18.30	33.23	67.3	37.1
0.100	3.5	14.61	14.61	47.84	96.8	29.5
0.063	4	1.36	1.36	49.24	99.7	2.9
pan		0.19	0.19	49.40	100.0	0.3
		49.40	**49.40**			
NSK 8						
Sieve size (mm)	**Sieve size (Phi)**	**Wt Retained**	**Corrected Wt**	**Cumm Wt**	**Cumm Wt %**	**Individual Wt**
2.000	-1	0.24	0.24	0.24	0.5	0.5
1.180	-0.2	0.61	0.61	0.85	1.7	1.2
0.850	0.4	1.04	1.04	1.89	3.8	2.1
0.600	0.7	1.07	1.07	2.96	6.0	2.2
0.300	1.8	11.68	11.68	14.64	29.5	23.5
0.150	2.7	17.66	17.66	32.30	65.0	35.5
0.100	3.5	15.42	15.42	47.72	96.0	31.0
0.063	4	1.50	1.50	49.22	99.0	3.0
pan		0.48	0.48	49.70	100.0	1.0
		49.70	**49.70**			

APPENDIX A

Table A8 Sieve Result of Mamu Formation Samples 1 and 2.

MA 1	Wt of sample = 49.38					
Sieve size (mm)	**Sieve size (Phi)**	**Wt Retained**	**Corrected Wt**	**Cumm Wt**	**Cumm Wt %**	**Individual Wt**
2.000	-1	4.04	4.04	4.04	8.2	8.2
1.180	-0.2	2.31	2.31	6.35	12.9	4.7
0.850	0.4	2.92	2.92	9.27	18.8	5.9
0.600	0.7	1.48	1.48	10.78	21.8	3.0
0.300	1.8	8.11	8.11	18.86	38.2	16.4
0.150	2.7	7.24	7.24	26.10	52.9	14.7
0.100	3.5	17.59	17.58	43.68	88.5	35.6
0.063	4	3.37	3.37	47.05	95.3	6.8
pan		2.32	2.32	49.37	100.0	4.7
		49.4	**49.36**			
MA 2	Wt of sample = 49.65					
Sieve size (mm)	**Sieve size (Phi)**	**Wt Retained**	**Corrected Wt**	**Cumm Wt**	**Cumm Wt %**	**Individual Wt**
2.000	-1	0.06	0.06	0.06	0.1	0.1
1.180	-0.2	0.09	0.09	0.15	0.3	0.2
0.850	0.4	0.21	0.21	0.36	0.7	0.4
0.600	0.7	0.19	0.19	0.55	1.1	0.4
0.300	1.8	14.72	14.71	15.26	30.8	29.7
0.150	2.7	21.84	21.82	37.08	74.7	43.9
0.100	3.5	10.54	10.53	47.61	96.0	21.3
0.063	4	0.93	0.93	48.54	97.8	1.8
pan		1.07	1.07	49.61	100.0	2.2
		49.7	**49.60**			

APPENDIX A

Table A9. Sieve Result of Mamu Formation Samples 3 and 4

MA 3	49.02					
Sieve size (mm)	**Sieve size (Phi)**	**Wt Retained**	**Corrected Wt**	**Cumm Wt**	**Cumm Wt %**	**Individual Wt**
2.000	-1	0.52	0.52	0.52	1.1	1.1
1.180	-0.2	2.03	2.03	2.55	5.2	4.1
0.850	0.4	5.82	5.82	8.37	17.1	11.9
0.600	0.7	11.52	11.52	19.89	40.6	23.5
0.300	1.8	10.18	10.18	30.07	61.3	20.7
0.150	2.7	13.40	13.41	43.48	88.7	27.4
0.100	3.5	4.09	4.09	47.57	97.0	8.3
0.063	4	1.19	1.19	48.76	99.4	2.4
pan		0.27	0.27	49.03	100.0	0.6
		49.0	**49.04**			
MA 4	49.55					
Sieve size (mm)	**Sieve size (Phi)**	**Wt Retained**	**Corrected Wt**	**Cumm Wt**	**Cumm Wt %**	**Individual Wt**
2.000	-1	1.90	1.90	1.90	3.8	3.8
1.180	-0.2	3.50	3.50	5.40	10.9	7.1
0.850	0.4	4.97	4.96	10.36	20.9	10.0
0.600	0.7	5.82	5.81	16.17	32.6	11.7
0.300	1.8	16.56	16.54	32.71	66.0	33.4
0.150	2.7	10.46	10.45	43.16	87.1	21.1
0.100	3.5	4.19	4.19	47.35	95.5	8.4
0.063	4	1.24	1.24	48.59	98.0	2.5
pan		0.97	0.97	49.56	100.0	2.0
		49.6	**49.56**			

APPENDIX A

Table A10. Sieve Result of Mamu Formation Samples 5 and 6

MA 5	49.43					
Sieve size (mm)	**Sieve size (Phi)**	**Wt Retained**	**Corrected Wt**	**Cumm Wt**	**Cumm Wt %**	**Individual Wt**
2.000	-1	1.33	1.33	1.33	2.7	2.7
1.180	-0.2	2.77	2.77	4.10	8.3	5.6
0.850	0.4	4.34	4.34	8.44	17.1	8.8
0.600	0.7	5.61	5.61	14.05	28.4	11.3
0.300	1.8	13.43	13.44	27.49	55.6	27.2
0.150	2.7	12.34	12.35	39.84	80.6	25.0
0.100	3.5	6.13	6.13	45.97	93.0	12.4
0.063	4	1.94	1.94	47.91	96.9	3.9
pan		1.54	1.54	49.45	100.0	3.1
		49.4	**49.46**			
MA 6	49.27					
Sieve size (mm)	**Sieve size (Phi)**	**Wt Retained**	**Corrected Wt**	**Cumm Wt**	**Cumm Wt %**	**Individual Wt**
2.000	-1	3.61	3.61	3.61	7.3	7.3
1.180	-0.2	2.22	2.22	5.83	11.8	4.5
0.850	0.4	2.14	2.14	7.97	16.2	4.4
0.600	0.7	2.93	2.93	10.90	22.1	5.9
0.300	1.8	12.30	12.29	23.19	47.1	25.0
0.150	2.7	5.29	5.29	28.48	57.8	10.7
0.100	3.5	18.20	18.19	46.67	94.8	37.0
0.063	4	2.25	2.25	48.92	99.3	4.5
pan		0.33	0.33	49.25	100.0	0.7
		49.3	**49.24**			
MA 7	49.34					

APPENDIX A

Table A11: Sieve Result of Mamu Formation Samples 7 and 8

Sieve size (mm)	**Sieve size (Phi)**	**Wt Retained**	**Corrected Wt**	**Cumm Wt**	**Cumm Wt %**	**Individual Wt**
2.000	-1	7.41	7.42	7.42	15.0	15.0
1.180	-0.2	1.83	1.83	9.25	18.7	3.7
0.850	0.4	3.58	3.58	12.83	26.0	7.3
0.600	0.7	2.25	2.25	15.08	30.5	4.5
0.300	1.8	10.51	10.52	25.60	51.9	21.4
0.150	2.7	16.55	16.56	42.16	85.4	33.5
0.100	3.5	4.62	4.62	46.78	94.8	9.4
0.063	4	1.91	1.91	48.69	98.6	3.8
pan		0.68	0.68	49.37	100.0	1.4
		49.3	**49.38**			
MA 8	49.68					
Sieve size (mm)	**Sieve size (Phi)**	**Wt Retained**	**Corrected Wt**	**Cumm Wt**	**Cumm Wt %**	**Individual Wt**
2.000	-1	1.68	1.68	1.68	3.4	3.4
1.180	-0.2	1.64	1.64	3.32	6.7	3.3
0.850	0.4	2.43	2.43	5.75	11.6	4.9
0.600	0.7	2.08	2.08	7.83	15.8	4.2
0.300	1.8	16.05	16.04	23.87	48.1	32.3
0.150	2.7	15.43	15.42	39.29	79.1	31.0
0.100	3.5	7.41	7.41	46.70	94.0	14.9
0.063	4	2.54	2.54	49.24	99.2	4.5
pan		0.42	0.42	49.66	100.0	0.8
		49.7	**49.66**			

APPENDIX A

Table A12 Sieve Result of Owelli Sandstone Samples 1 and 2

Owelli 1	**Wt of Sample 200**					
Sieve size (mm)	**Sieve size (Phi)**	**Wt Retained**	**corrected wt**	**Cumm wt**	**Cumm wt %**	**indwt**
2.36	-1.20	0.3	0.30	0.30	0.15	0.15
2	-1.00	0.6	0.60	0.90	0.45	0.30
1.18	-0.25	7.4	7.45	8.35	4.18	3.73
0.85	0.30	17.9	18.01	26.36	13.18	9.00
0.6	0.85	33.8	34.01	60.37	30.19	17.01
0.425	1.30	37.8	38.03	98.40	49.20	19.01
0.3	1.85	89.2	89.75	188.15	94.08	44.88
0.15	2.80	10.5	10.56	198.71	99.36	5.28
0.125	3.00	1	1.01	199.72	99.86	0.50
0.075	3.80	0.1	0.10	199.82	99.91	0.05
0.063	4.00	0.01	0.01	199.83	99.92	0.01
PAN	5.00	0.17	0.17	200.00	100.00	0.08
		198.78				
Owelli 2						
Sieve size (mm)	**Sieve size (Phi)**	**Wt Retained**	**Corrected wt**	**Cumm Wt**	**Cumm Wt %**	**Ind Wt**
5.6	-2.4	22.00	22.03	22.03	11.06	11.06
4	-2	6.00	6.01	28.04	14.08	3.02
2.36	-1.20	7.30	7.31	35.35	17.75	3.67
2	-1.00	2.70	2.70	38.05	19.11	1.36
1.18	-0.25	12.20	12.22	50.27	25.25	6.14
0.85	0.30	18.00	18.03	68.30	34.30	9.05
0.6	0.85	34.10	34.15	102.45	51.46	17.16
0.425	1.30	65.80	65.90	168.35	84.56	33.10
0.3	1.85	26.14	26.18	194.53	97.70	13.14
0.15	2.80	3.40	3.40	197.93	99.41	1.71
0.125	3.00	0.20	0.20	198.13	99.51	0.10
0.075	3.80	0.80	0.80	198.93	99.91	0.40
0.063	4.00	0.07	0.07	199.00	99.95	0.04
PAN	5.00	0.10	0.10	199.10	100.00	0.05
		198.81				

APPENDIX A

Table A13 Sieve Result of Owelli Sandstone Samples 3 and 4

Owelli 3	**198.2**					
Sieve size (mm)	**Sieve size (Phi)**	**Wt Retained**	**Corrected Wt**	**Cumm Wt**	**Cumm Wt %**	**Individual Wt**
2.36	-1.20	0.05	0.05	0.05	0.03	0.03
2	-1.00	0.20	0.20	0.25	0.13	0.10
1.18	-0.25	2.00	1.96	2.21	1.12	0.99
0.85	0.30	6.40	6.26	8.47	4.27	3.15
0.6	0.85	19.70	19.26	27.73	13.99	9.72
0.425	1.30	48.30	47.23	74.96	37.82	23.83
0.3	1.85	109.90	107.45	182.41	92.03	54.21
0.15	2.80	15.40	15.06	197.47	99.63	7.60
0.125	3.00	0.20	0.20	197.67	99.73	0.10
0.075	3.80	0.30	0.29	197.96	99.88	0.15
0.063	4.00	0.06	0.06	198.02	99.91	0.06
PAN	5.00	0.20	0.20	198.20	100.00	0.09
		202.71				
Owelli 4	**Wt of sample 199.9**					
Sieve size (mm)	**Sieve size (Phi)**	**Wt Retained**	**Corrected Wt**	**Cumm Wt**	**Cumm Wt %**	**Individual Wt**
2.36	-1.20	0.70	0.71	0.71	0.36	0.36
2	-1.00	1.10	1.11	1.82	0.91	0.55
1.18	-0.25	8.10	8.18	10.00	5.00	4.09
0.85	0.30	18.60	18.78	28.78	14.40	9.40
0.6	0.85	35.70	36.04	64.82	32.43	18.03
0.425	1.30	37.30	37.66	102.48	51.27	18.84
0.3	1.85	71.60	72.29	174.77	87.43	36.16
0.15	2.80	14.20	14.34	189.11	94.60	7.17
0.125	3.00	1.30	1.31	190.42	95.26	0.66
0.075	3.80	5.70	5.75	196.17	98.13	2.86
0.063	4.00	3.20	3.23	199.40	99.75	1.62
PAN	5.00	0.50	0.50	199.90	100.00	0.25
		198.00				

APPENDIX A

Table A14: Sieve Result of Owelli Sandstone Samples 5 and 6

Owelli 5	**Wt of sample 198.7**					
Sieve size (mm)	**Sieve size (Phi)**	**Wt Retained**	**Corrected Wt**	**Cumm Wt**	**Cumm Wt %**	**Individual Wt**
2.36	-1.20	0.06	0.06	0.06	0.03	0.03
2	-1.00	0.10	0.10	0.16	0.08	0.05
1.18	-0.25	1.20	1.21	1.37	0.69	0.61
0.85	0.30	4.60	4.63	6.00	3.02	2.33
0.6	0.85	16.70	16.82	22.82	11.48	8.46
0.425	1.30	26.00	26.19	49.01	24.67	13.19
0.3	1.85	104.20	104.96	153.97	77.49	52.82
0.15	2.80	38.90	39.18	193.15	97.21	19.72
0.125	3.00	1.80	1.81	194.96	98.12	0.91
0.075	3.80	3.20	3.22	198.18	99.74	1.62
0.063	4.00	0.10	0.10	198.28	99.79	0.05
PAN	5.00	0.40	0.40	198.70	100.00	0.21
		197.26				
Owelli 6	**Wt of sample 198.1**					
Sieve size (mm)	**Sieve size (Phi)**	**Wt Retained**	**Corrected Wt**	**Cumm Wt**	**Cumm Wt %**	**Individual Wt**
5.6	-2.4	0.80	0.80	0.8	0.40	0.40
4	-2	0.10	0.10	0.9	0.45	0.05
2.36	-1.20	0.50	0.50	1.40	0.71	0.26
2	-1.00	0.30	0.30	1.70	0.86	0.15
1.18	-0.25	3.20	3.21	4.91	2.48	1.62
0.85	0.30	12.70	12.73	17.64	8.90	6.42
0.6	0.85	29.90	29.97	47.61	24.03	15.13
0.425	1.30	31.70	31.77	79.38	40.07	16.04
0.3	1.85	103.40	103.63	183.01	92.38	52.31
0.15	2.80	13.80	13.83	196.84	99.36	6.98
0.125	3.00	0.20	0.20	197.04	99.46	0.10
0.075	3.80	0.90	0.90	197.94	99.92	0.46
0.063	4.00	0.06	0.06	198.00	99.95	0.03
PAN	5.00	0.10	0.10	198.10	100.00	0.05
		197.66				

APPENDIX A

Table A15 Sieve Result of Owelli Sandstone Sample 7

Owelli 7	**Wt of sample 194.7**					
Sieve size (mm)	**Sieve size (Phi)**	**Wt Retained**	**corrected wt**	**Cumm wt**	**Cumm wt %**	**Ind Wt**
5.6	-2.4	0.4	0.40	0.40	0.21	0.21
4	-2	2.2	2.22	2.62	1.35	1.14
2.36	-1.20	6.6	6.67	9.29	4.77	3.42
2	-1.00	4.8	4.85	14.14	7.26	2.49
1.18	-0.25	20.8	21.00	35.14	18.05	10.79
0.85	0.30	22.9	23.13	58.27	29.93	40.72
0.6	0.85	24.9	25.15	83.42	42.85	1.85
0.425	1.30	20.8	21.00	104.42	53.63	42.85
0.3	1.85	48.3	48.78	153.20	78.69	25.06
0.15	2.80	27	27.27	180.47	92.69	14.00
0.125	3.00	1.4	1.41	181.88	93.42	0.73
0.075	3.80	10.3	10.40	192.28	98.76	5.34
0.063	4.00	0.8	0.81	193.09	99.17	0.41
PAN	5.00	1.6	1.62	194.71	100.01	0.83
		192.8				

APPENDIX B Plate 1

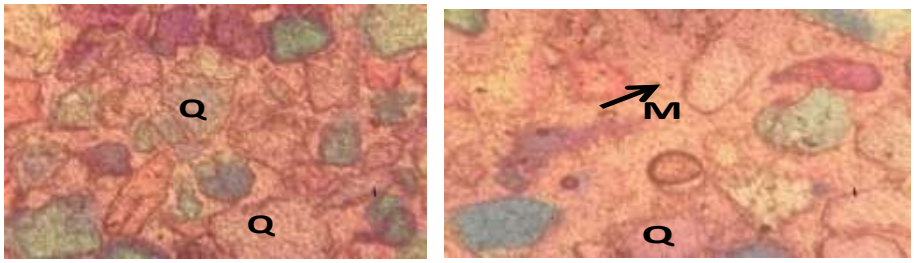

Microscopic View of Petroraphic Analysis of Ajali Sandstoes Exposed at Onyekaba Quarry

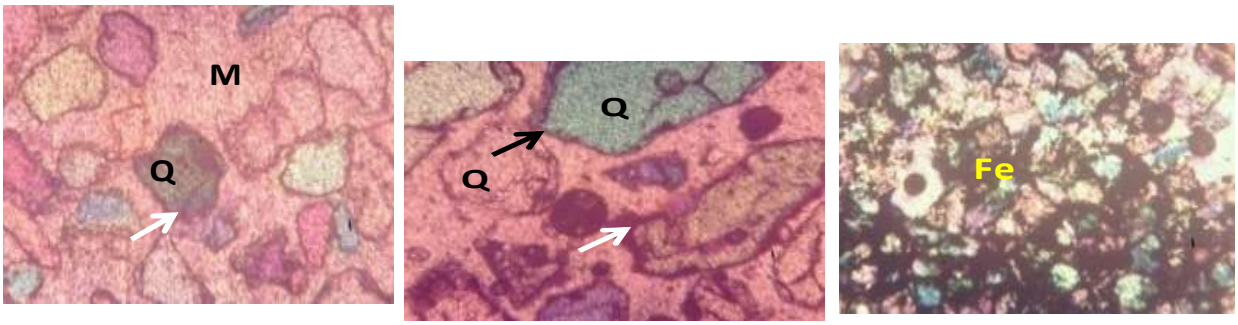

Microscopic View of Petroraphic Analysis of Mamu Formation Exposed at Ihube

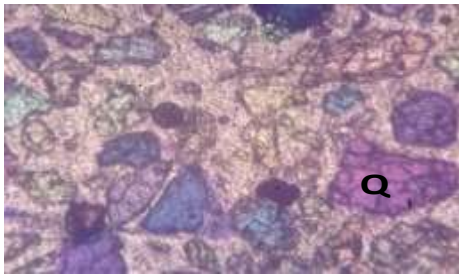

Microscopic View of Petroraphic Analysis of Nsukka Formation Exposed at Isukwato

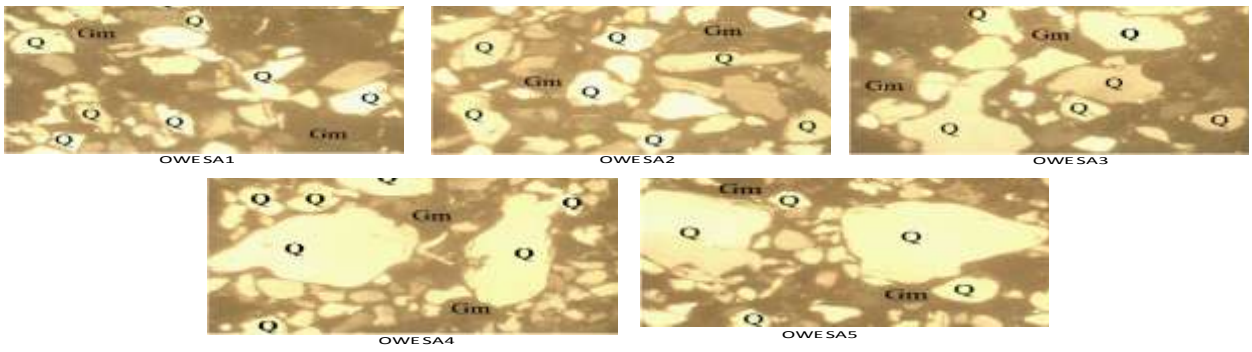

Microscopic View of Petroraphic Analysis of Owelli sandstones exposed at Agbogugu